AD-A057 931 BENDIX CORP NORTH HOLLYWOOD CALIF ELECTRODYNAMICS DIV F/G 13/7
DEVELOPMENT OF A HIGH TEMPERATURE ROTARY ACTUATOR FOR AIRCRAFT --ETC(U)
MAY 78 R K VAN AUSDAL F33615-72-C-1187

UNCLASSIFIED AFAPL-TR-78-26 NL

1 OF 3
AD A057931

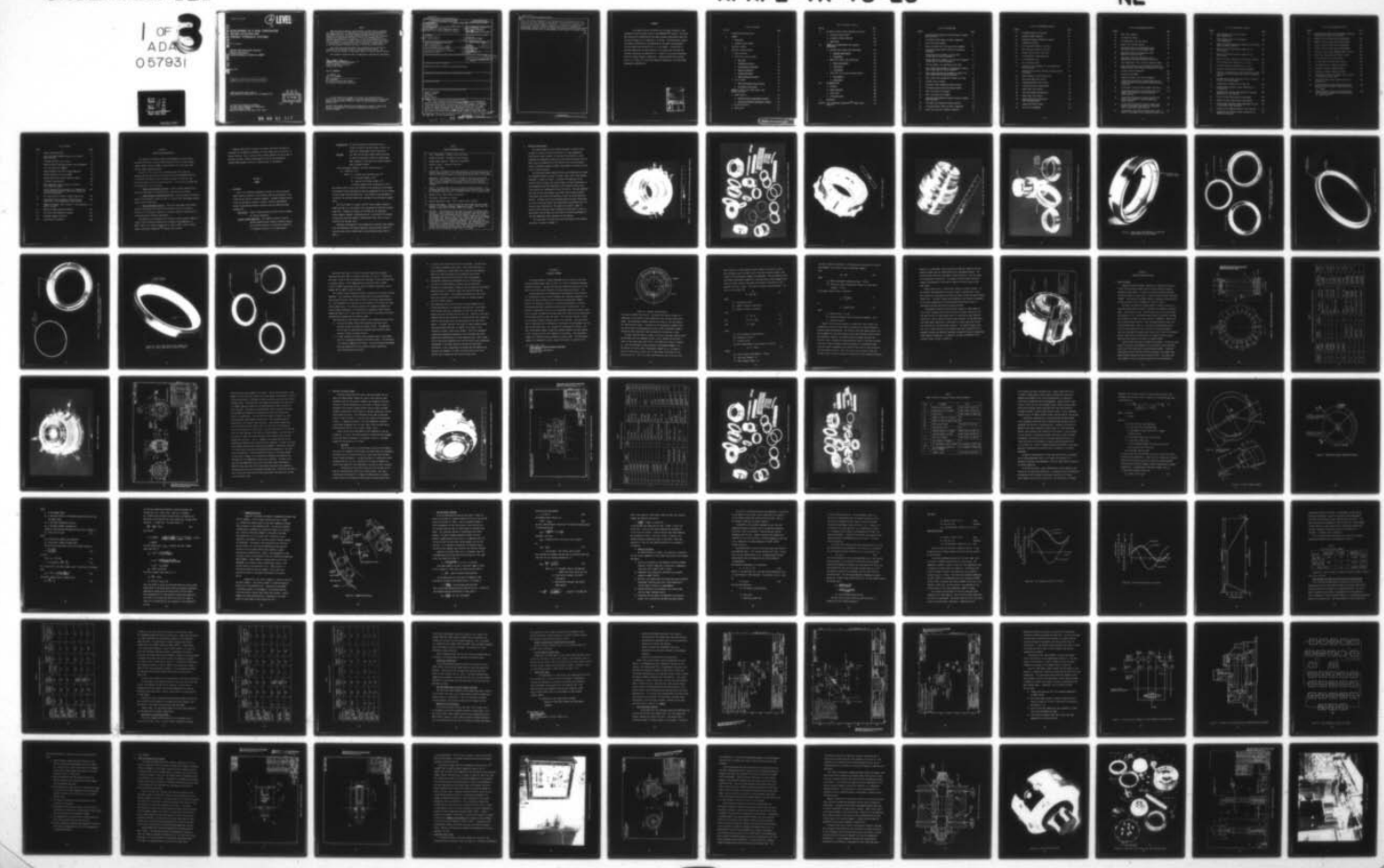

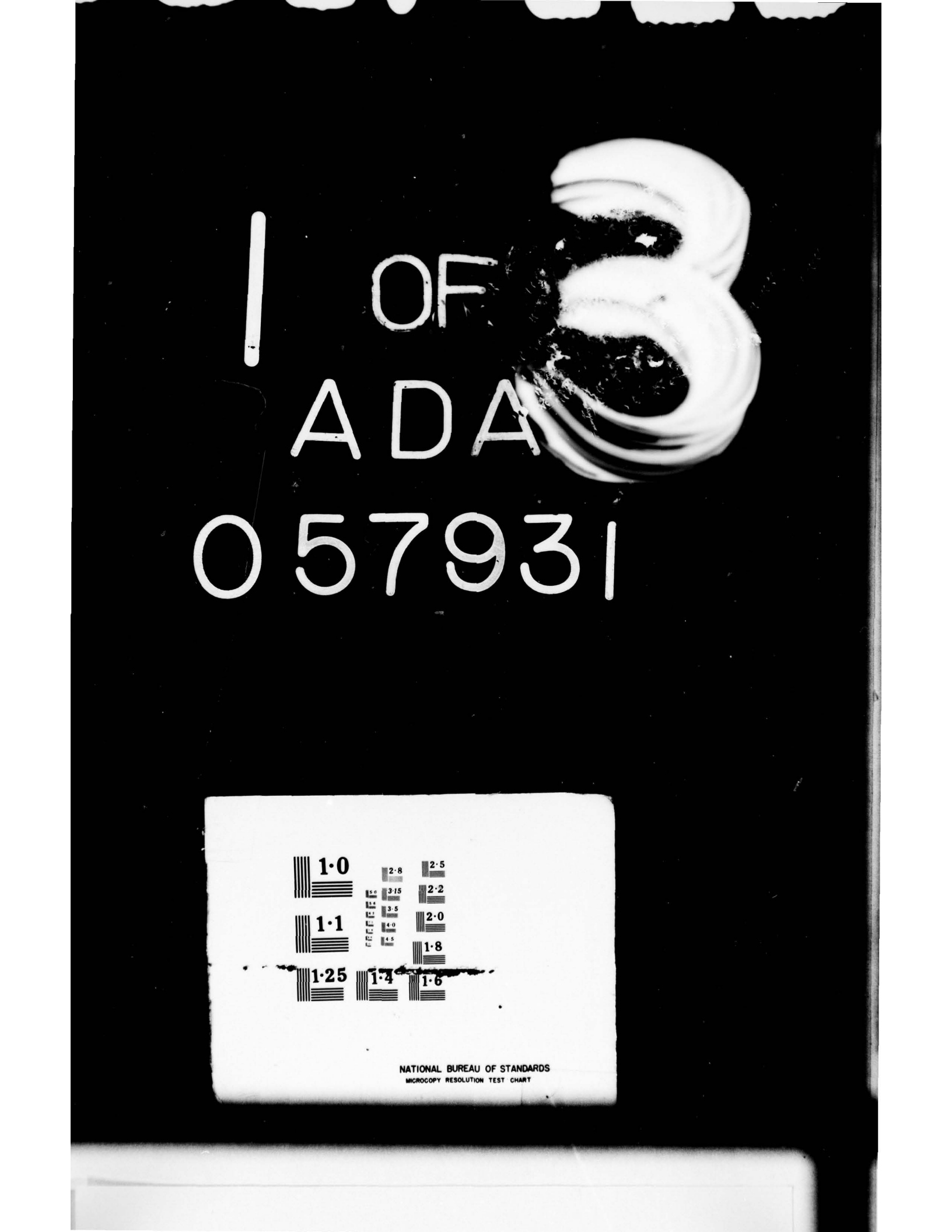
1 OF 3
ADA
057931
1·0
1·1
1·25
2·8
3·15
3·5
4·0
4·5
1·4
2·5
2·2
2·0
1·8
1·6
NATIONAL BUREAU OF STANDARDS
MICROCOPY RESOLUTION TEST CHART

AFAPL-TR-78-26

(2) LEVEL II

DEVELOPMENT OF A HIGH TEMPERATURE ROTARY ACTUATOR FOR AIRCRAFT HYDRAULIC SYSTEMS

R.K. Van Ausdal

Bendix Electrodynamics Division
Bendix Corporation
North Hollywood, California, 91605

MAY 1978

TECHNICAL REPORT AFAPL-TR-78-26
FINAL REPORT FOR PERIOD APRIL 1972 TO DECEMBER 1977

AIR FORCE AERO PROPULSION LABORATORY
AIR FORCE WRIGHT AERONAUTICAL LABORATORIES
AIR FORCE SYSTEMS COMMAND
WRIGHT-PATTERSON AIR FORCE BASE, OHIO 45433

NOTICE

When Government drawings, specifications, or other data are used for any purpose other than in connection with a definitely related Government procurement operation, the United States Government thereby incurs no responsibility nor any obligation whatsoever; and the fact that the government may have formulated, furnished, or in any way supplied the said drawings, specifications, or other data, is not to be regarded by implication or otherwise as in any manner licensing the holder or any other person or corporation, or conveying any rights or permission to manufacture, use, or sell any patented invention that may in any way be related thereto.

This report has been reviewed by the Information Office (OI) and is releasable to the National Technical Information Service (NTIS). At NTIS, it will be available to the general public, including foreign nations.

This technical report has been reviewed and is approved for publication.

Kenneth E. Binns

Kenneth E. Binns, Project Engineer
Fluid and Mechanical Systems
Vehicle Power Branch

FOR THE COMMANDER

B L McFadden

B. L. McFadden
Act'g Chief, Vehicle Power Branch
Air Force Aero Propulsion Laboratory

"If your address has changed, if you wish to be removed from our mailing list, or if the addressee is no longer employed by your organization please notify AFAPL/POP, W-PAFB, OH 45433 to help us maintain a current mailing list".

Copies of this report should not be returned unless return is required by security considerations, contractual obligations, or notice on a specific document.

UNCLASSIFIED

SECURITY CLASSIFICATION OF THIS PAGE (When Data Entered)

REPORT DOCUMENTATION PAGE

READ INSTRUCTIONS BEFORE COMPLETING FORM

1. REPORT NUMBER: AFAPL-TR-78-26
2. GOVT ACCESSION NO.
3. RECIPIENT'S CATALOG NUMBER

4. TITLE (and Subtitle): Development of a High Temperature Rotary Actuator for Aircraft Hydraulic Systems.

5. TYPE OF REPORT & PERIOD COVERED: Final, Apr 1972 - Dec 1977
6. PERFORMING ORG. REPORT NUMBER

7. AUTHOR(s): R. K. Van Ausdal

8. CONTRACT OR GRANT NUMBER(s): Contract F33615-72-C-1187

9. PERFORMING ORGANIZATION NAME AND ADDRESS:
Bendix Electrodynamics Division
Bendix Corporation
North Hollywood, Calif. 91605

10. PROGRAM ELEMENT, PROJECT, TASK AREA & WORK UNIT NUMBERS: 62203F 31453009 30

11. CONTROLLING OFFICE NAME AND ADDRESS:
Air Force Aero-Propulsion Lab/Pop-3
WPAFB, Ohio 45433

12. REPORT DATE: May 1978
13. NUMBER OF PAGES: 190

14. MONITORING AGENCY NAME & ADDRESS (if different from Controlling Office)

15. SECURITY CLASS. (of this report): UNCLASSIFIED
15a. DECLASSIFICATION/DOWNGRADING SCHEDULE

16. DISTRIBUTION STATEMENT (of this Report)

Approved for public release; distribution unlimited

17. DISTRIBUTION STATEMENT (of the abstract entered in Block 20, if different from Report)

18. SUPPLEMENTARY NOTES

19. KEY WORDS (Continue on reverse side if necessary and identify by block number)

Hydraulic Actuator
Hydraulic Motor
Dynavector
Rotary Actuator

20. ABSTRACT (Continue on reverse side if necessary and identify by block number)

This report describes the development program for a high temperature hydraulic rotary actuator based on the DYNAVECTOR® concept. Included are illustrated results based on replies by six airframe companies to a Bendix survey that determined the projected 1975-80 horizontal tail and rudder actuator stiffness requirements for fighter/attack aircraft, as well as the critical design conditions relative to Mach number and altitude. Also reported are the results for the 800°F ambient testing of three different

over

DD FORM 1 JAN 73 1473 EDITION OF 1 NOV 65 IS OBSOLETE

UNCLASSIFIED

SECURITY CLASSIFICATION OF THIS PAGE (When Data Entered)

shaft seal designs (created for the program) that are presented in terms of leakage versus time, temperature and pressure. Actuator test results -- with and without the epicyclic gear transmission -- and analyses included in the report reveal that the limitation imposed by the particular transmission disengagement concept used for load decoupling (actuator redundancy application) prohibitively detracts from the performance of the actuator for analog control.

FOREWORD

This report contains the results of an effort to develop a high temperature rotary actuator based on the DYNAVECTOR ® concept. The design and analyses was accomplished by the Bendix Research Laboratories under the direction of Messrs. R. G. Read and J. H. Tarter. The fabrication, testing and program coordination was accomplished by the Bendix Electrodynamics Division under the direction of Mr. R. K. Van Ausdal. Consultation on aircraft application and participation in the rotary seal selection and stiffness survey was provided by Mr. H. T. Dowell of the Convair Aerospace Division, General Dynamics Corporation. Program direction was provided by Mr. K. E. Binns, Air Force Aero Propulsion Laboratory, Air Force Wright Aeronautical Laboratories.

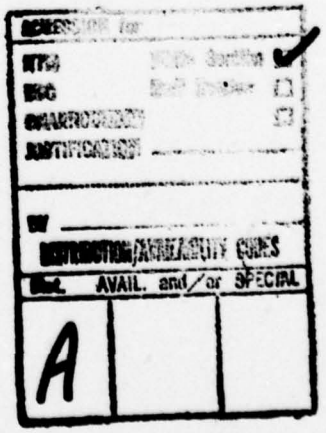

TABLE OF CONTENTS

SECTION		PAGE
I	INTRODUCTION AND OBJECTIVES	1
II	SUMMARY	2
	1. BACKGROUND	2
	2. PROGRAM ACCOMPLISHMENTS	5
III	TECHNICAL APPROACH	19
IV	PROTOTYPE ACTUATOR DESIGN	25
	1. MOTOR CARTRIDGE	25
	2. PROTOTYPE ACTUATOR ASSEMBLY	31
	a. Gear Mesh	31
	b. Commutation Porting	44
	c. Vane and Rotor Clearance	46
	d. Material Selection	48
	e. Rotary Shaft Seals	60
	f. Cooling and Heat Transfer	61
	3. TEST FIXTURES	70
	a. Motor and Actuator Test Fixtures	70
	b. Shaft Seal Test Fixture	73
V	SUMMARY OF SHAFT SEAL SURVEY RESULTS AND DESIGN EVALUATION	85
	1. SURVEY RESULTS	85
	a. USAF and Convair Development Programs	85
	b. Industry and Bendix Development Programs	86
	2. DESIGN EVALUATION	87
	3. CONCLUSIONS	90

TABLE OF CONTENTS (CONT'D)

SECTION		PAGE
VI	ACTUATOR STIFFNESS SURVEY AND ANALYSES RESULTS	95
	1. STIFFNESS SURVEY RESULTS	95
	2. ACTUATOR STIFFNESS ANALYSES	100
	3. CONCLUSIONS	110
VII	SUMMARY OF ACTUATOR/MOTOR TESTS RESULTS/ CONCLUSIONS	113
	1. ACTUATOR TEST RESULTS AND CONCLUSIONS	114
	a. Actuator Test Results	116
	b. Conclusions	121
	2. MOTOR TEST RESULTS AND CONCLUSIONS	125
	a. Motor Test Results	126
	b. Conclusions	139
	c. Limitations	141
	3. SHAFT SEAL TEST RESULTS AND CONCLUSIONS	145
	a. Test Results	145
	b. Conclusions	154
VIII	RECOMMENDATIONS	167
	1. ACTUATOR	167
	2. MOTOR CARTRIDGE	168
	3. SHAFT SEALS	169
	4. STIFFNESS/WEIGHT	169
IX	REFERENCES	171
APPENDIX	HIGH TEMPERATURE DYNAVECTOR ® TORQUE RIPPLE ANALYSIS	173

LIST OF ILLUSTRATIONS

FIGURE		PAGE
1	Prototype High Temperature Rotary Actuator Assembly Model HL-043-U1	6
2	Prototype Actuator Model HL-043-U1 Components	7
3	Motor Cartridge Assembly	8
4	Motor Cartridge Test Unit Output Shaft Assembly	9
5	Prototype Actuator Model HL-043-U1 Transmission Components	10
6	Rotary Shaft Seal Assembly, Lip Type Seal (4.6205 Nominal Sealing Diameter)	11
7	Rotary Shaft Seal Assembly, Lip Type Seal Components (4.6205 Nominal Sealing Diameter)	12
8	Sealing Element, Lip Type Rotary Shaft Seal	13
9	Rotary Shaft Seal Assembly, Circumferential Sealing Type (4.6205 Nominal Sealing Diameter)	14
10	Rotary Shaft Seal Bellows Assembly for Radial Face Type (4.6205 Nominal Sealing Diameter)	15
11	Rotary Shaft Seal Components of Radial Face Type	16
12	Actuator Forces Diagram	20
13	Dynavector High Temperature Rotary Actuator	24
14	Prototype Actuator Motor Cartridge Assembly	26
15	Motor Cartridge Test Assembly	28
16	Motor Cartridge Test Assembly	29
17	Prototype High Temperature Rotary Actuator Assembly Model HL-043-U1	32
18	Prototype High Temperature Rotary Actuator	33
19	Prototype Actuator Model HL-043-U1 Components	35
20	Motor Cartridge Test Assembly Components	36

LIST OF ILLUSTRATIONS (CONT'D)

FIGURE		PAGE
21	Free-Body Diagram of Ring Gear	40
22	Actuator Chamber Geometry	40
23	Dynavector Actuator Commutation Sectors	41
24	Commutation Porting	45
25	Full Load Cycle Profile, Life Test	52
26	Half Load Cycle Profile, Life Test	53
27	Thermal Cycle Profile, Life Test	54
28	Circumferential Type Rotary Seal	62
29	Lip Type Rotary Seal	63
30	Face Type Rotary Seal	64
31	Cooling Circuit Schematic for High Temperature Rotary Actuator	66
32	Actuator Cross Section (Partial) Showing Cooling Flow Paths	67
33	Block Diagram of Cooling Flow Paths	68
34	Motor Cartridge Test Fixture	71
35	Prototype Actuator Test Fixture	72
36	Insulation Box and Infrared Oven	74
37	Rotary Seal Test Fixture	75
38	Shaft and Bushing Configuration	78
39	Rotary Seal Test Fixture	79
40	Rotary Seal Test Fixture Parts (Not Including Seals)	80
41	Rotary Seal Drive Fixture	81
42	Seals Test Arrangement	82

LIST OF ILLUSTRATIONS (CONT'D)

FIGURE		PAGE
43	Seals Test Schematic	84
44	Lip Type Seal Design	92
45	Circumferential Type Seal Design	94
46	Radial Face Type Seal Design	94
47	Horizontal Stabilizer Actuator/Structure Spring Rate Versus Aircraft Gross Weight	97
48	Horizontal Stabilizer Aerodynamic Hinge Moment Versus Gross Weight	98
49	Horizontal Stabilizer Aerodynamic Hinge Moment Versus Actuator/Structure Spring Rate	99
50	High Temperature Linear Actuator Comparison Model	102
51	Normalized Comparison of Calculated Stiffness and Weight Between Linear Model and Dynavector Actuators	107
52	Actuator Spring Designations	109
53	Actuator Spring Model	109
54	Temporary Actuator Load Test Arrangement	115
55	Torque Motor Differential Pressure Required for Constant Speed for Various Hold-in Motor Pressures at No Load	117
56	Torque Motor ΔP Versus Hold-in Motor Pressure P_H	118
57	Torque Motor Differential Pressure Versus Load Angular Displacement at 500 and 1000 psig Supply Pressure	119
58	Torque Motor Differential Pressure Versus Load Angular Displacement at 1500 and 2000 psig Supply Pressure	120
59	Torque Motor Differential Pressure Versus Load Angular Displacement Obtained with a Wide Open Valve and Variable Supply Pressure	122
60	Torque Motor Differential Pressure Versus Load Angular Displacement Using a Relative Viscous Fluid	123

LIST OF ILLUSTRATIONS (CONT'D)

FIGURE		PAGE
61	Test Equipment and Circuit Schematic (Room Temperature)	127
62	Test Equipment and Circuit Schematic (High Temperature)	128
63	Motor Cartridge Torque Versus Speed with P_H Pressure Vented to Return Pressure	130
64	Motor Cartridge Torque Versus Speed with P_H Port Blocked	131
65	Motor Cartridge Torque Versus Speed with P_H Port Blocked	132
66	Motor Cartridge Torque Versus Differential Pressure	133
67	No Load Flow Versus Speed with P_H = 0 psig	134
68	No Load Flow Versus Speed with P_H = 0 psig	135
69	Leakage Flow Measurement Plumbing Arrangements	137
70	Test Unit Case Leakage and Supply Flow Versus Speed with Hold-in Motor Pressure (P_H) Vented to Return or Blocked	138
71	Exploded View of Motor Cartridge Test Unit Showing Failed Teflon Thrust Washer	143
72	Leakage Versus Temperature Lip Type Seal	146
73	Leakage Versus Pressure at Room Temperature for Lip Type Seal	147
74	Leakage Versus Time of High Temperature Endurance Conditions for Lip Type Seal	148
75	Static Friction Torque Versus Displacement	149
76	Dynamic Friction Torque Versus Displacement	150
77	Torque Versus Pressure at Room Temperature for the Lip and Radial Face Type Seals	151
78	Leakage Versus Temperature Radial Face Type Seal	152
79	Leakage Versus Pressure at Room Temperature for Radial Face Type Seal	153

LIST OF ILLUSTRATIONS (CONT'D)

FIGURE		PAGE
80	Leakage Versus Time at High Temperature Endurance Conditions for Radial Face Type Seal	155
81	Dynamic Friction Torque Versus Displacement	156
82	Dynamic Friction Torque Versus Displacement	157
83	Static Friction Torque Versus Displacement	158
84	Dynamic Friction Torque Versus Displacement	159
85	Test Seals and Fixture Components After Testing	163
86	Radial Face Type Rotary Seal After Testing	164
87	Lip Type Rotary Seal After Testing	165
88	Lip Type Sealing Element After Testing	166
A-1	Free Body Design of Dynavector Ring Gear	177
A-2	Dynavector Actuator Chamber Geometry	178
A-3	Dynavector Actuator Commutation Sector	181
A-4	Orientation of Hold-in and Motor Forces Relative to a Fixed Eccentricity Axis	182
A-5	Normalized Torque Versus Angular Position of Eccentricity	185
A-6	Normalized Output Torque Versus Output Shaft Position with an Angularly Linear Spring Load, $P_H = P_{S\ MAX}$.	188
A-7	Normalized Output Torque Versus Output Shaft Position with an Angularly Linear Spring Load, P_H = Torque Motor ΔP	190

LIST OF TABLES

TABLE		PAGE
1	Design Performance Goals	4
2	Motor Cartridge Component Materials and Process Specifications	27
3	Prototype Actuator List of Parts	34
4	Model HL-043-U1 Prototype Actuator Design Parameters	37
5	Life Test Load Cycle Summary	55
6	Design Properties for Use at Room Temperature	57
7	Design Properties for Use at $600^{o}F$	58
8	Dynamic Rotary Seal Inquiry Response Summary	88
9	Stiffness Survey Results	96
10	High Temperature Linear Actuator Preliminary Design Analyses Summary	103
11	Convair Computer Analysis Results of a Hypothetical Dual Tandem Linear Actuator Application Weight and Stiffness Requirements	104
12	Calculated Values of Rotary Actuator Compliances	105
13	Calculated Values of Actuator Spring Rates and Compliances - High Temperature Linear Actuator	108
14	Summary of Computer Stress Analysis - High Temperature Rotary Actuator	111
15	Motor Cartridge Assembly Performance	126
16	Test Seals High Temperature Leakage	161
A-1	Parameter Symbols and Values	176
A-2	Torque Ripple Calculation	184

SECTION I

INTRODUCTION AND OBJECTIVES

This report was prepared by Bendix Electrodynamics Division, North Hollywood, California, for the United States Air Force, Air Force Systems Command, 4950th Test Wing (PMNB), Wright-Patterson Air Force Base, under Contract Number F33615-72-C-1187.

The work on this contract was performed between April 1972 and December 1977 by Bendix Research Laboratories and Electrodynamics Division of the Bendix Aerospace-Electronics Group, The Bendix Corporation, and Convair Aerospace Division of General Dynamics. The division of program work and responsibility was as follows:

1) Bendix Electrodynamics Division: Overall program responsibility, shaft seal development, stiffness analysis, fabrication and testing.

2) Bendix Research Laboratories Division: Actuator design and analyses based on the Dynavector concept, proven in a previous USAF development program under contract F33615-3431.

3) Convair Aerospace Division: Shaft seal development and stiffness analysis participation with Bendix Electrodynamics Division, as well as provision of the necessary expertise in surface actuation, installation and structure/actuator interface requirements.

The objective of the program was to develop a rotary actuator capable of typical flight surface performance with a maximum fluid temperature of 600°F (316°C) in an ambient temperature of -40° to +800°F (-40° to 427°C), based on the Bendix DYNAVECTOR ® actuator drive concept.

A special effort was to be made in reviewing seal design and material technology for recommending candidates for high temperature testing prior to actuator testing. Also, a survey of the airframe companies was to be made to determine actuator stiffness requirements for future high performance fighter/fighter-bomber aircraft as a design guide in the program.

SECTION II

SUMMARY

1. BACKGROUND

One of the significant parameters involved in critical aircraft control design conditions is the stiffness that can be attained in the flight surface hydraulic actuator component. Although consensus points to the multiparametric nature of actuator stiffness requirements, certain trends emerged through a program survey of leading airframe manufacturers.

Scale Factor: Larger surfaces generally require stiffer actuators for flutter prevention.

Transonic Speed Capability: This capability tends to require greater rudder/elevator actuator stiffness requirement primarily because of a significant reduction in aerodynamic damping in this speed regime.

Configuration: All-moving stabilizer configuration may be flutter-critical at the mach number at which the stabilizer leading edge becomes supersonic.

Altitude: The lower the altitude (higher dynamic pressure) at which the horizontal stabilizer leading edge goes supersonic, the higher the stiffness requirement to prevent flutter.

Since the actuator hydraulic stiffness (spring rate), is

$$K_h = 2(A^2B)/Vo, \text{ lb/in}$$

where: A = cylinder cross-sectional area, in^2

B = fluid bulk modulus, lb/in^2

Vo = one-half of cylinder volume, in^3,

it becomes apparent that the decrease in fluid bulk modulus--which occurs with increased fluid temperature (anticipated with greater aircraft performance)--must be compensated for by an increase in the cylinder cross-sectional area. The increase in area portends an increase in the cylinder weight and a decrease in the stiffness-to-weight ratio.

The fluid volume of a typical aircraft linear actuator produces a compliance that is in the range of 70 to 80 percent of the total actuator compliance. Although the typical fluid volume for the Dynavector rotary actuator produces a compliance that is in the order of 95 percent of the total, the fluid volume is significantly less, since it varies inversely with the gear ratio.

Therefore, the purpose of this program was to develop a high temperature configuration of the Bendix Dynavector rotary actuator capable of meeting future aircraft needs based on the performance goals shown in Table 1.

TABLE 1

DESIGN PERFORMANCE GOALS

1. Stall hinge moment - 80,000 in-lbs (9.05 kN-m).

2. Actuator slew rate - 30 deg/sec (0.523 rad/sec).

3. System supply pressure - 4000 psig (27.58 MN/m^2).

4. Actuator travel - ±30 deg (±0.523 rad).

5. Life - 3,000 hours.

6. Lubrication: The working fluid shall be used to provide lubrication to the greatest extent possible. Dry film lubricants may be used provided that such dry film does not need to be reapplied during the life of the actuator.

7. Redundancy: The actuator is to be designed so that two actuators are capable of driving the same load. If power to one of these actuators is lost, it must be automatically decoupled from the load so that the remaining power actuator is not required to back-drive the nonoperative actuator.

8. Weight: The weight goal shall be an actuator weighing 40 pounds. The prototype model built for testing may weigh more, but the ability to meet the 40 pound weight goals with a production device shall be demonstrated.

9. Working Fluids: MIL-H-27601 or equivalent.

10 Efficiency: 80 percent or better.

11. Ambient temperature range: -40° to +800°F (-40°to +427°C).

12. Cooling requirements: Provision shall be made to keep the MIL-H-27601 hydraulic fluid from exceeding a temperature of 600°F (316°C) when the actuator is operating in an 800°F (427°C) environment.

13. Life Test: The following life test duty cycle shall be imposed on the actuator. A total of 250 hours of load and thermal cycling is required. The actuator fluid temperature shall be lowered to -40°F (-40°C) and the actuator shall be in a -40°F (-40°C) ambient temperature environment. The actuator shall then be cycled at 30 ±5 cpm at one half and full load. At the same time, the environmental temperature shall be raised to 800°F (427°C) within a 15-minute time period. This temperature shall be maintained for a one-hour time period and then shall be lowered to -40 F (-40°C) over a one-hour period. This thermal cycling shall be done a minimum of 50 times during the testing. The remaining 137 hours of testing shall be conducted at 800°F (427°C) or higher.

2. PROGRAM ACCOMPLISHMENTS

The accomplishments of this program have been in several areas including (1) design, fabrication and test of a high temperature, fluid-cooled, rotary actuator, (2) design and fabrication of three candidate high temperature rotary shaft seals and the testing of two of these, and (3) documentation of the results of an aircraft industry survey to determine probable stiffness requirements for future aircraft control surface actuators.

The prototype actuator, Model HL-043-U1, was fabricated and tested. The assembled actuator is shown in Figure 1 and a view of the actuator components is shown in Figure 2. The motor cartridge unit of the actuator shown in Figure 3 was tested without the gear transmission at room temperature and high temperature, 275°F maximum (135°C), with mixed results as a consequence of some limitations. The same components were used for both the actuator (low speed, high torque) and motor (high speed, low torque) configurations, except for output shaft and gearing. The motor tests were conducted without the gear transmission by using a shaft and integral cam, duplicating the eccentricity of the epicyclic gear transmission. The special test shaft is shown in Figure 4 and the epicyclic gear transmission can be seen in Figure 5. Both shafts used the same size shaft seals to minimize development of the high temperature seals necessary for the program.

The three types of rotary shaft seals fabricated for the program are shown in Figures 6 through 11.

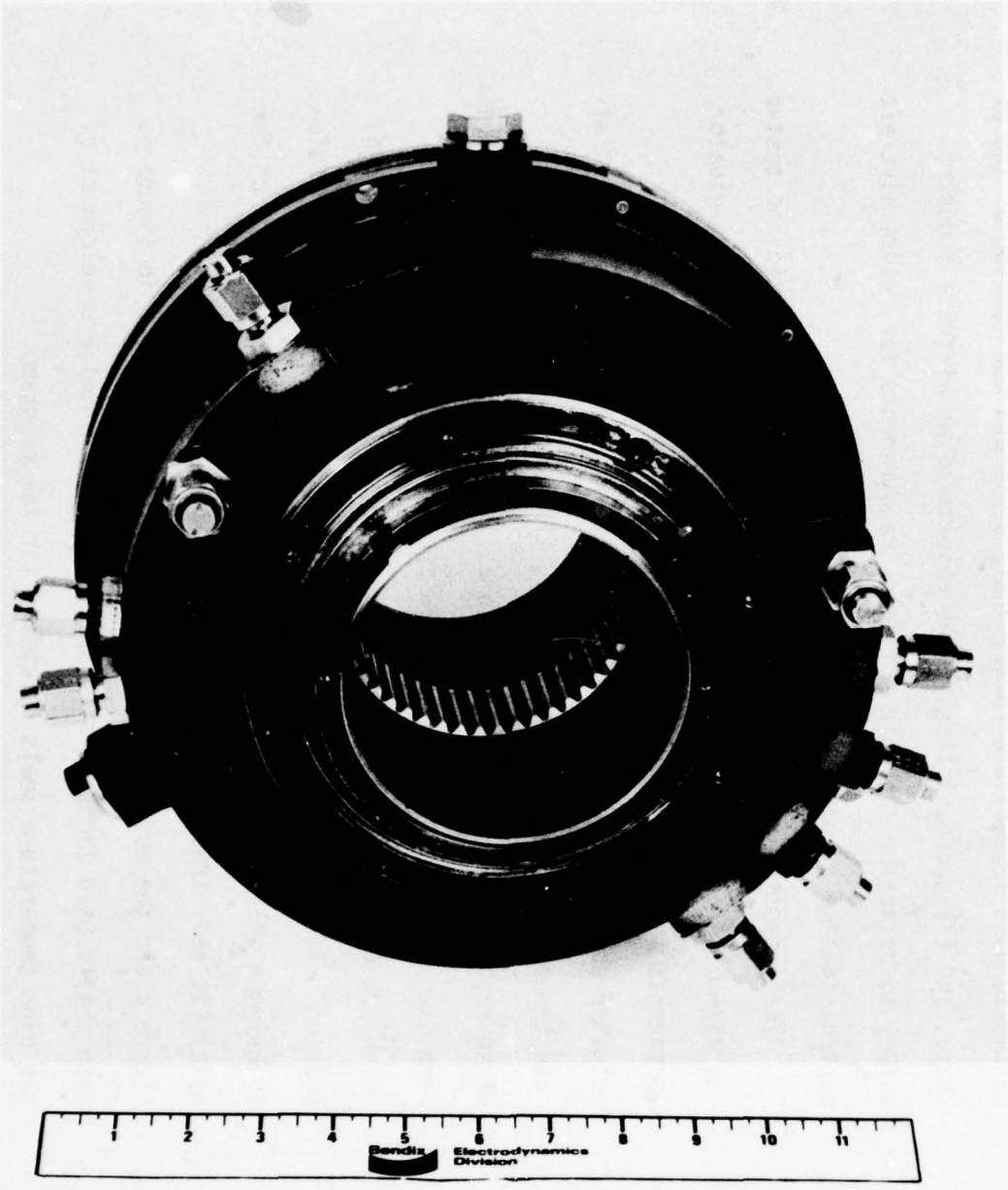

Figure 1. Prototype High Temperature Rotary Actuator Assembly Model HL-043-U1

Figure 2. Prototype Actuator Model HL-043-U1 Components

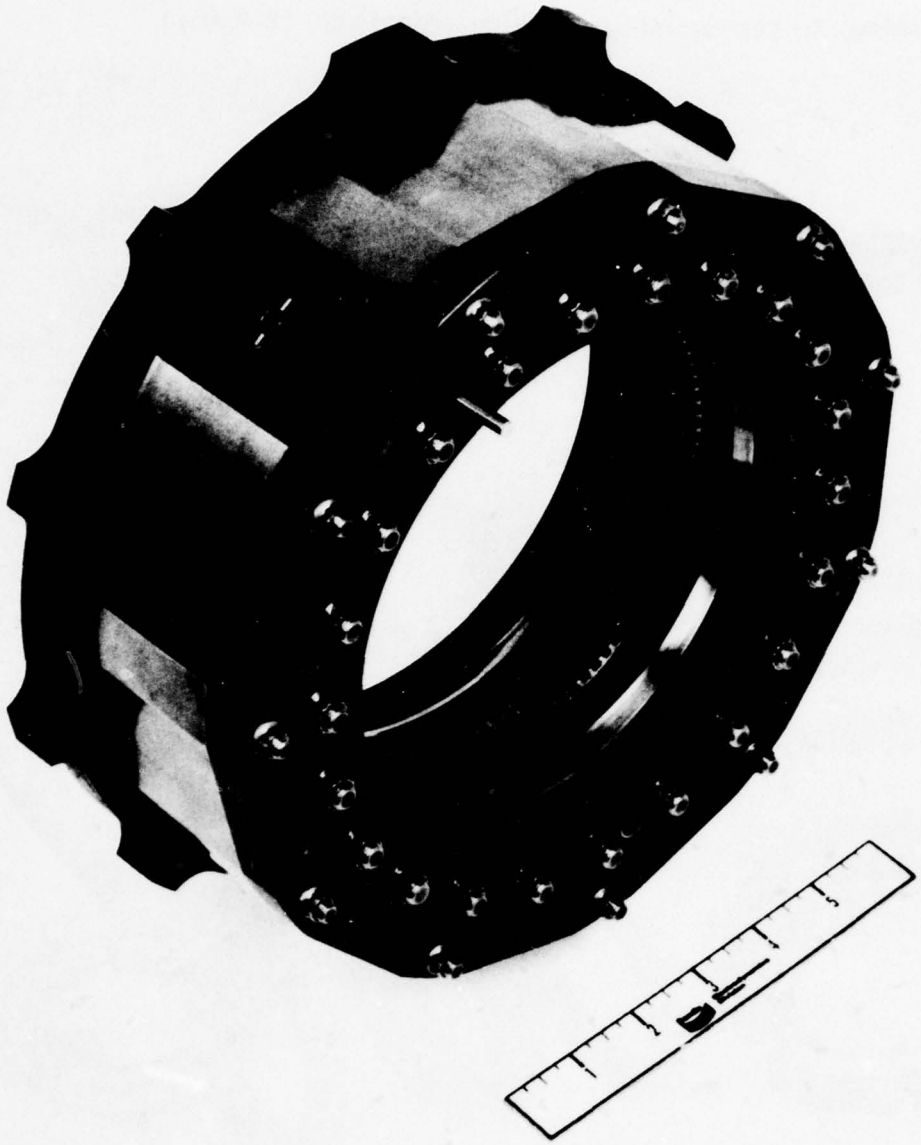

Figure 3. Motor Cartridge Assembly

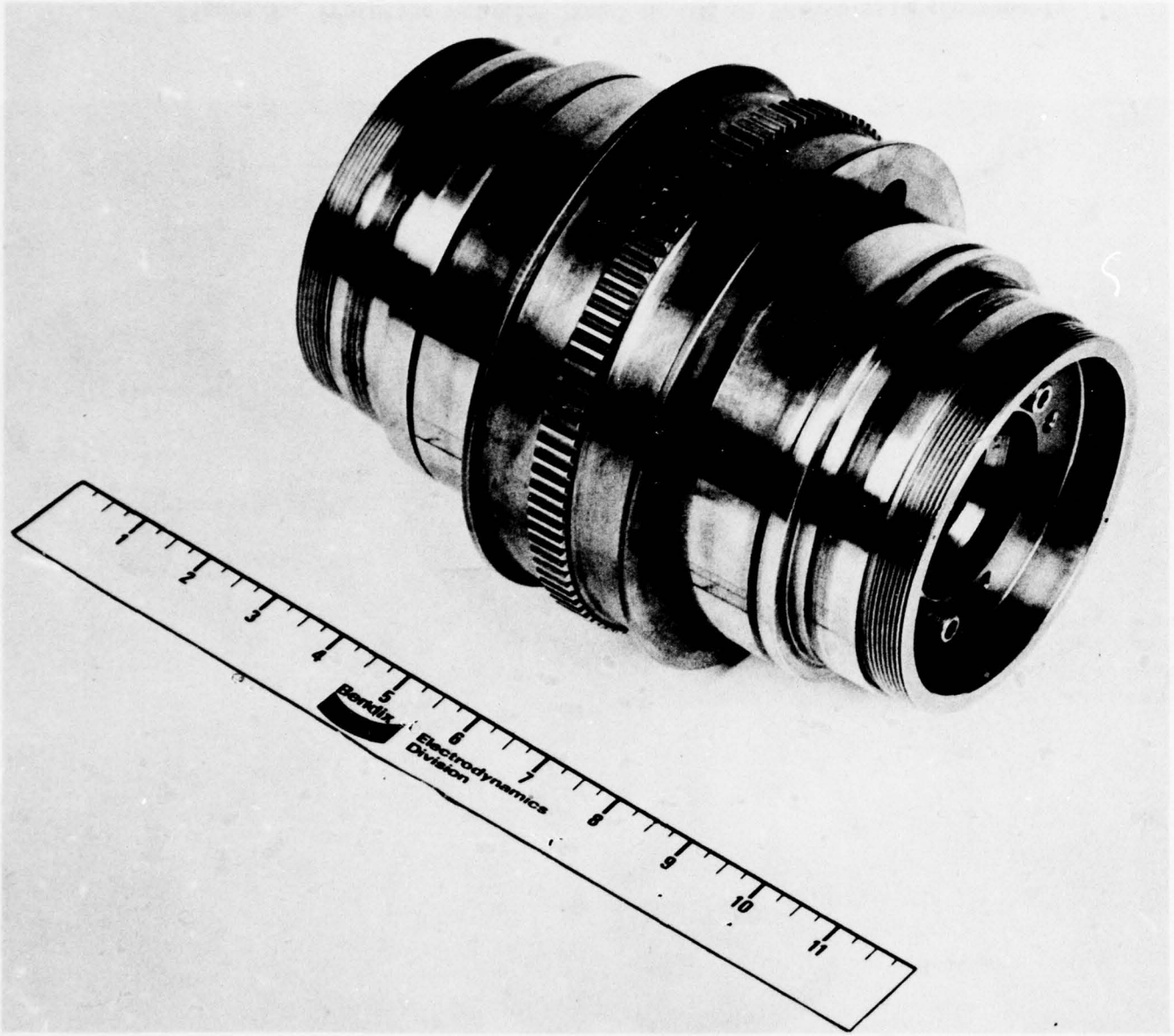

Figure 4. Motor Cartridge Test Unit Output Shaft Assembly

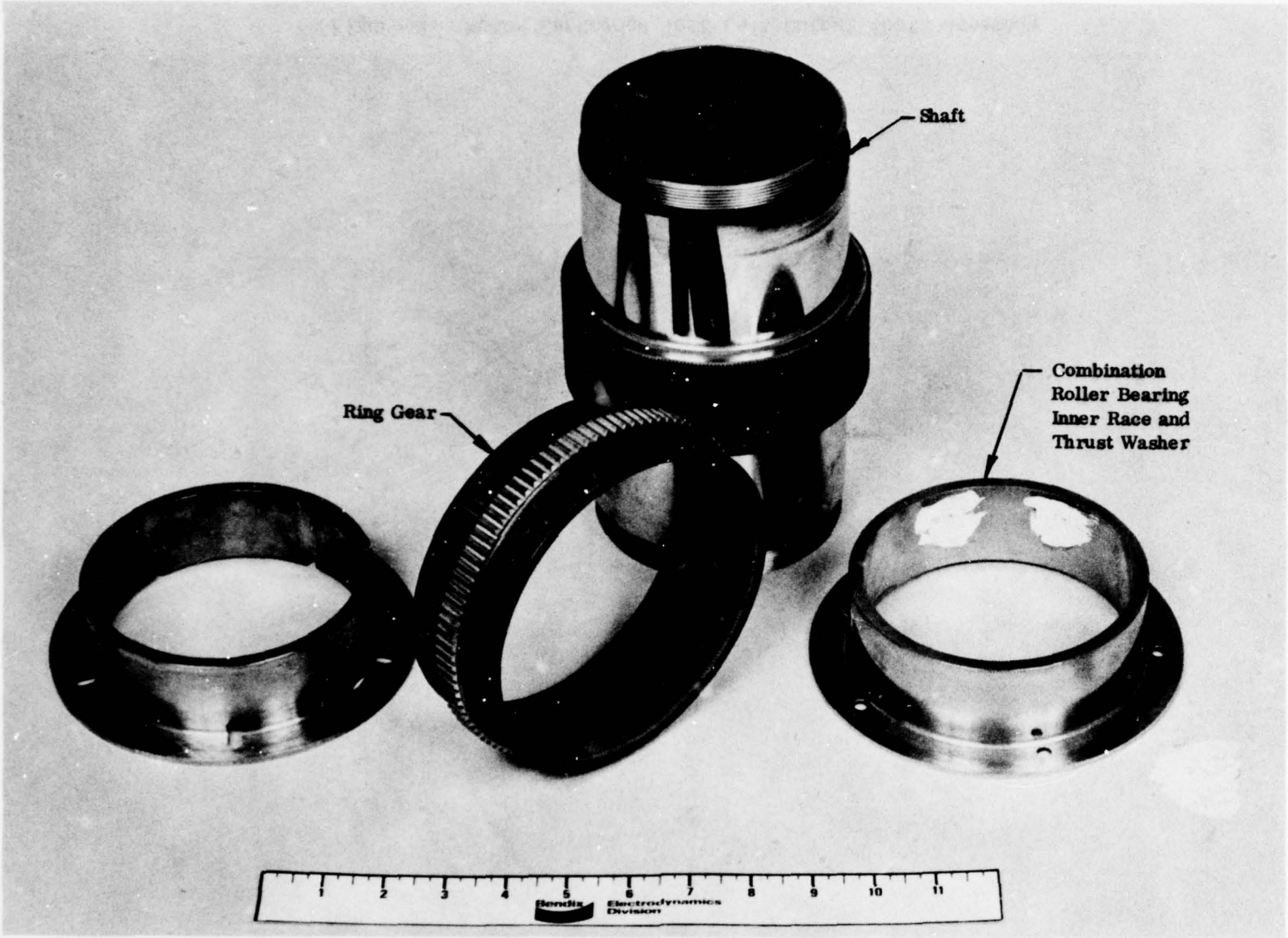

Figure 5. Prototype Actuator Model HL-043-U1 Transmission Components

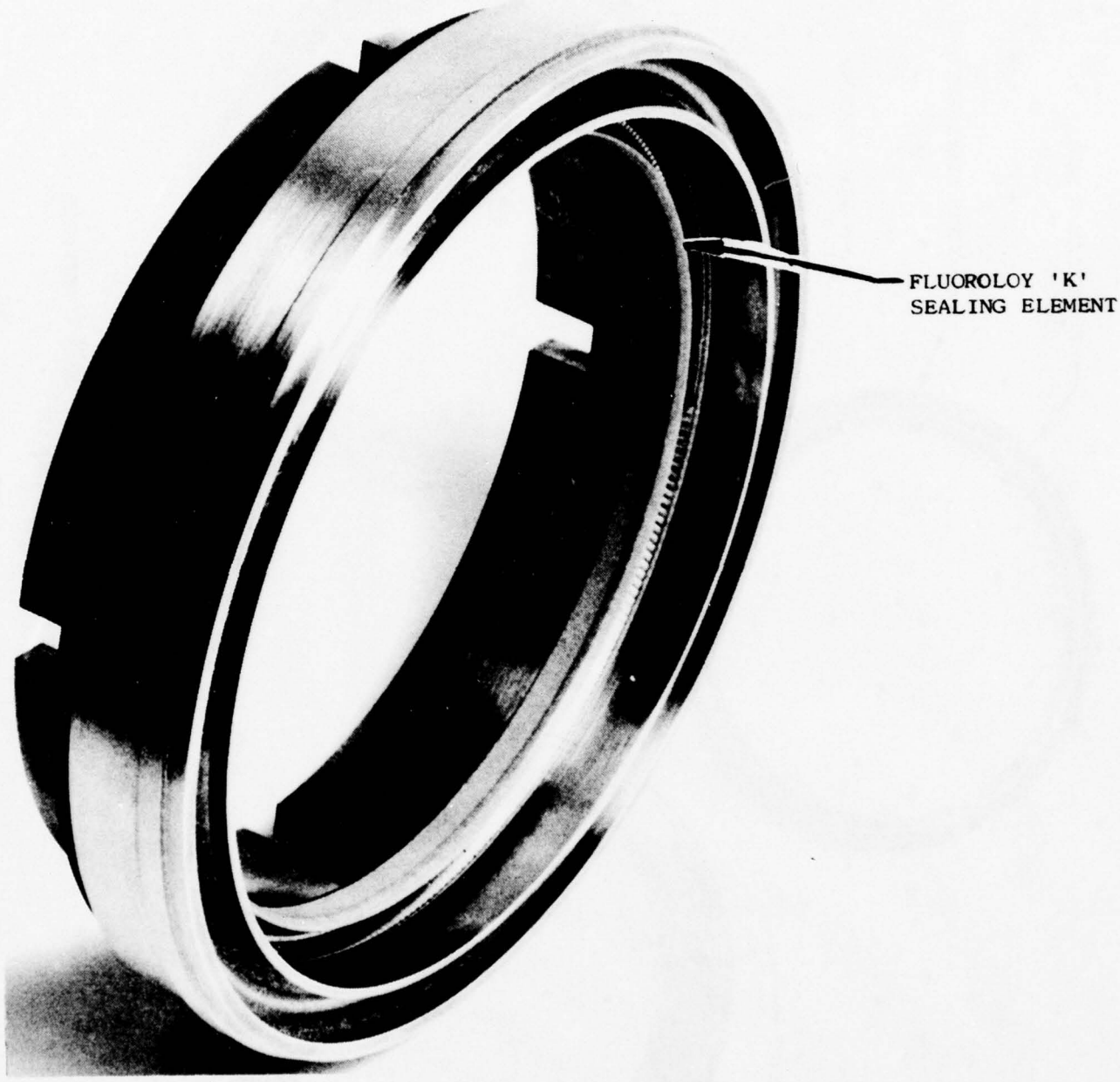

Figure 6. Rotary Shaft Seal Assembly, Lip Type Seal
(4.6205 Nominal Sealing Diameter)

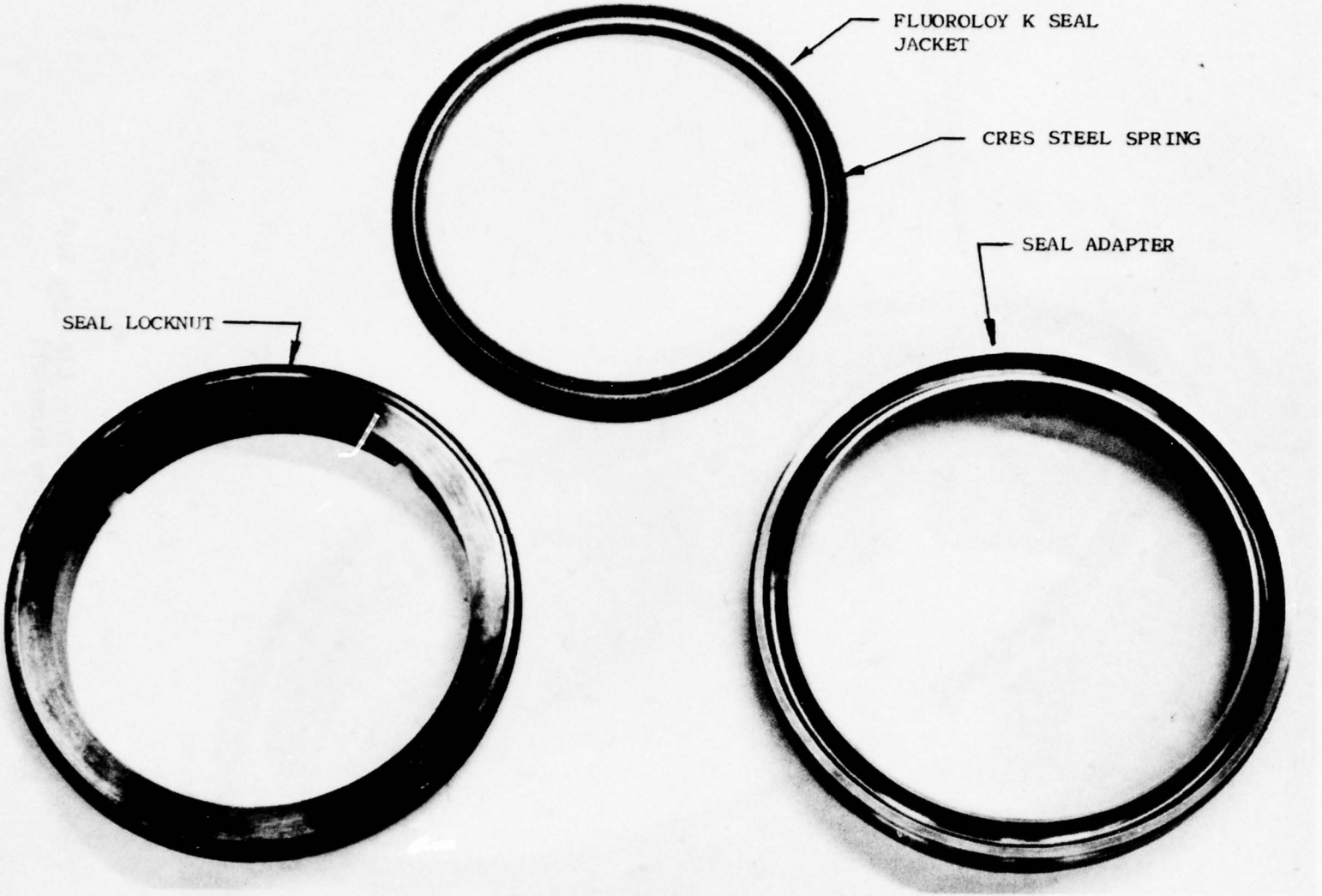

Figure 7. Rotary Shaft Seal Assembly, Lip Type Seal Components
(4.6205 Nominal Sealing Diameter)

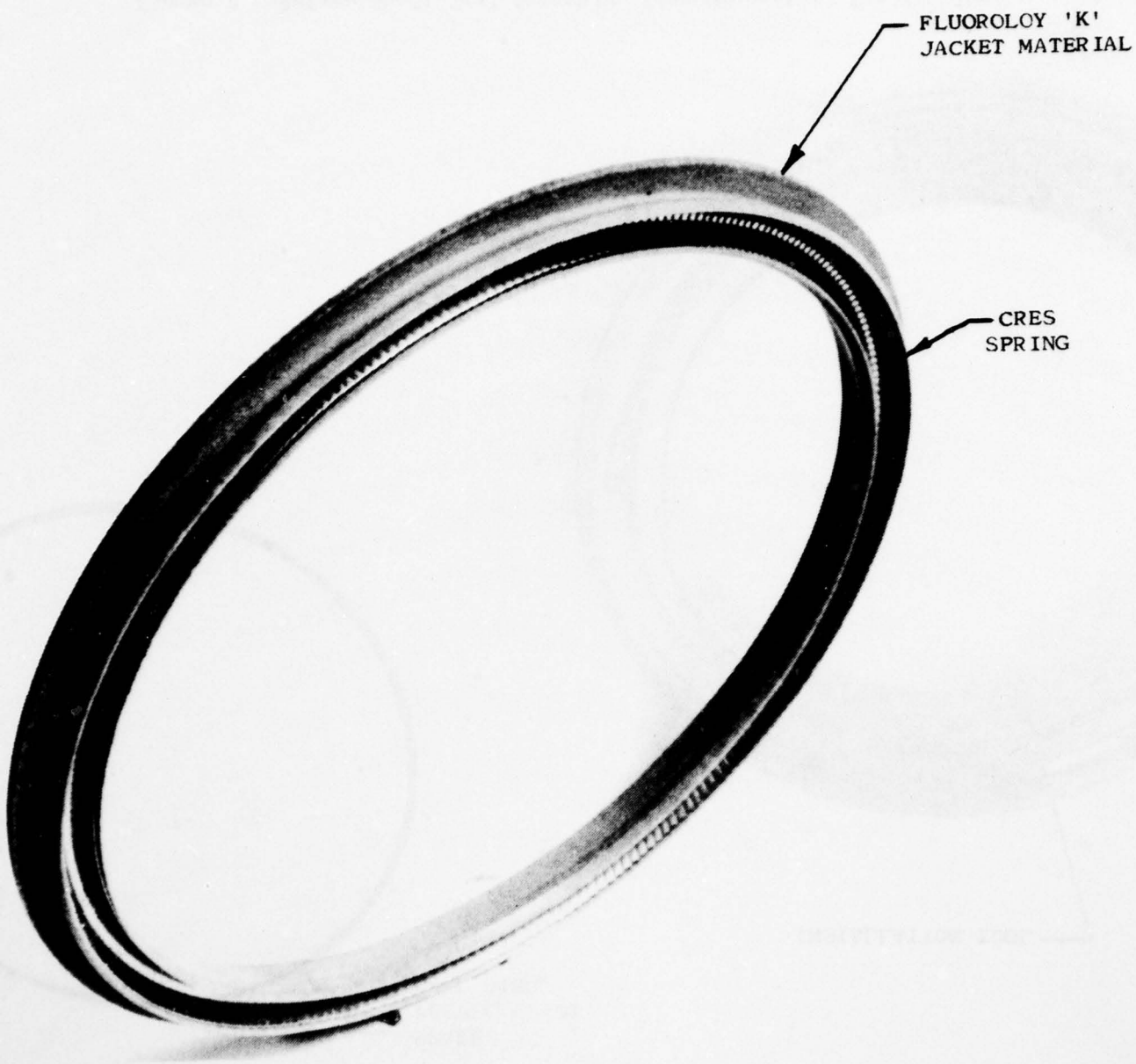

Figure 8. Sealing Element, Lip Type Rotary Shaft Seal

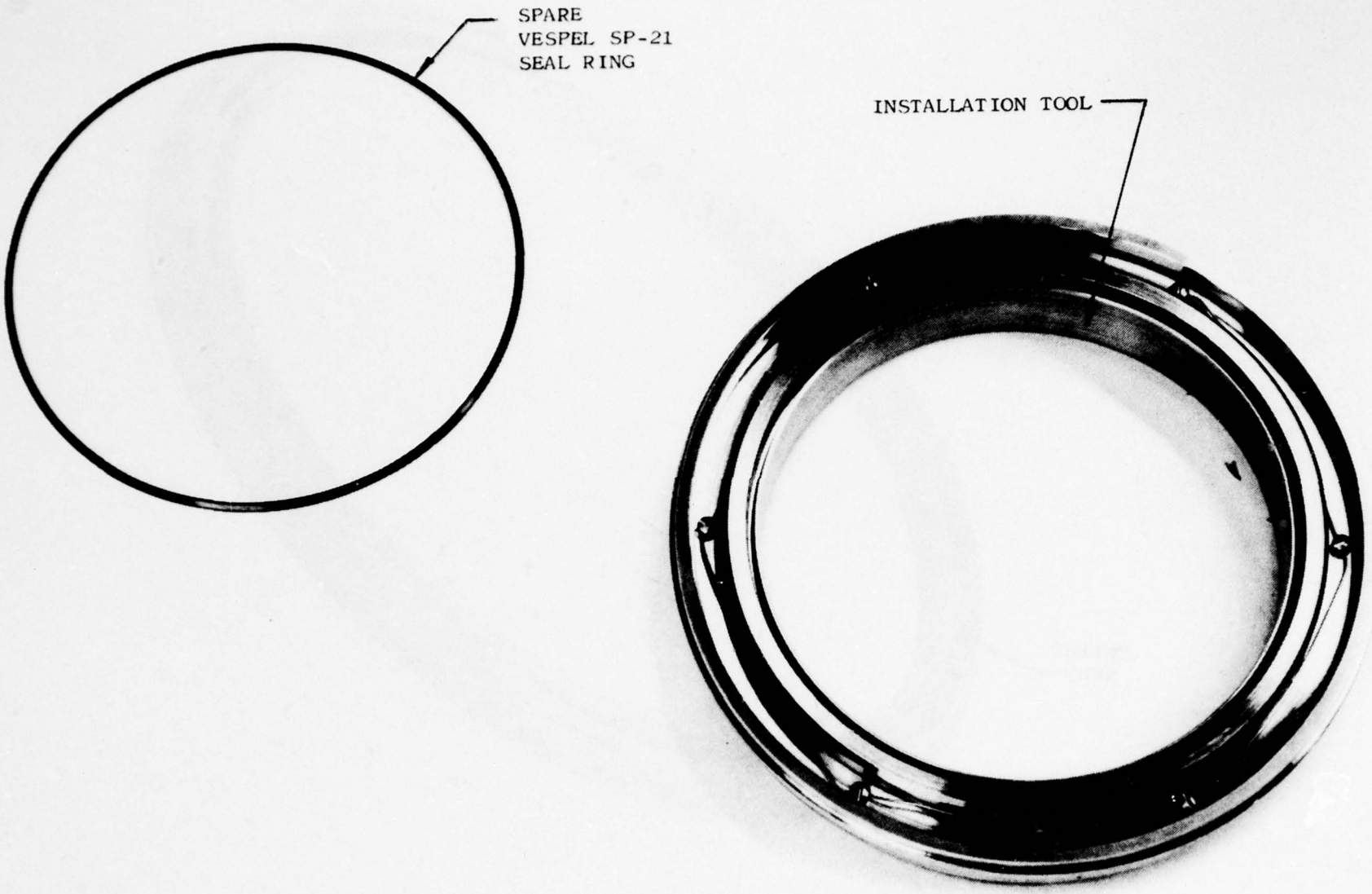

Figure 9. Rotary Shaft Seal Assembly, Circumferential Sealing Type
(4.6205 Nominal Sealing Diameter)

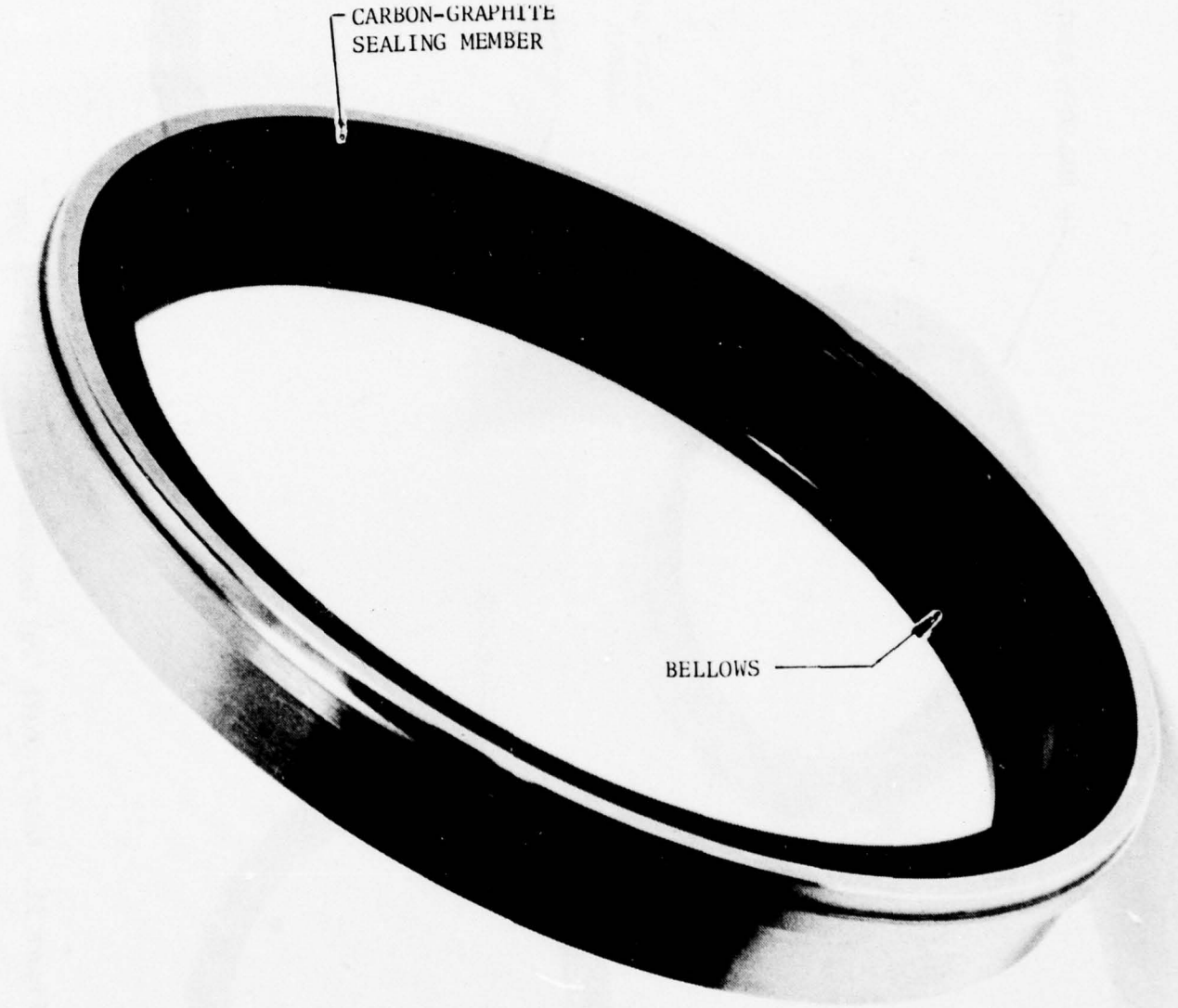

Figure 10. Rotary Shaft Seal Bellows Assembly for Radial Face Type (4.6205 Nominal Sealing Diameter)

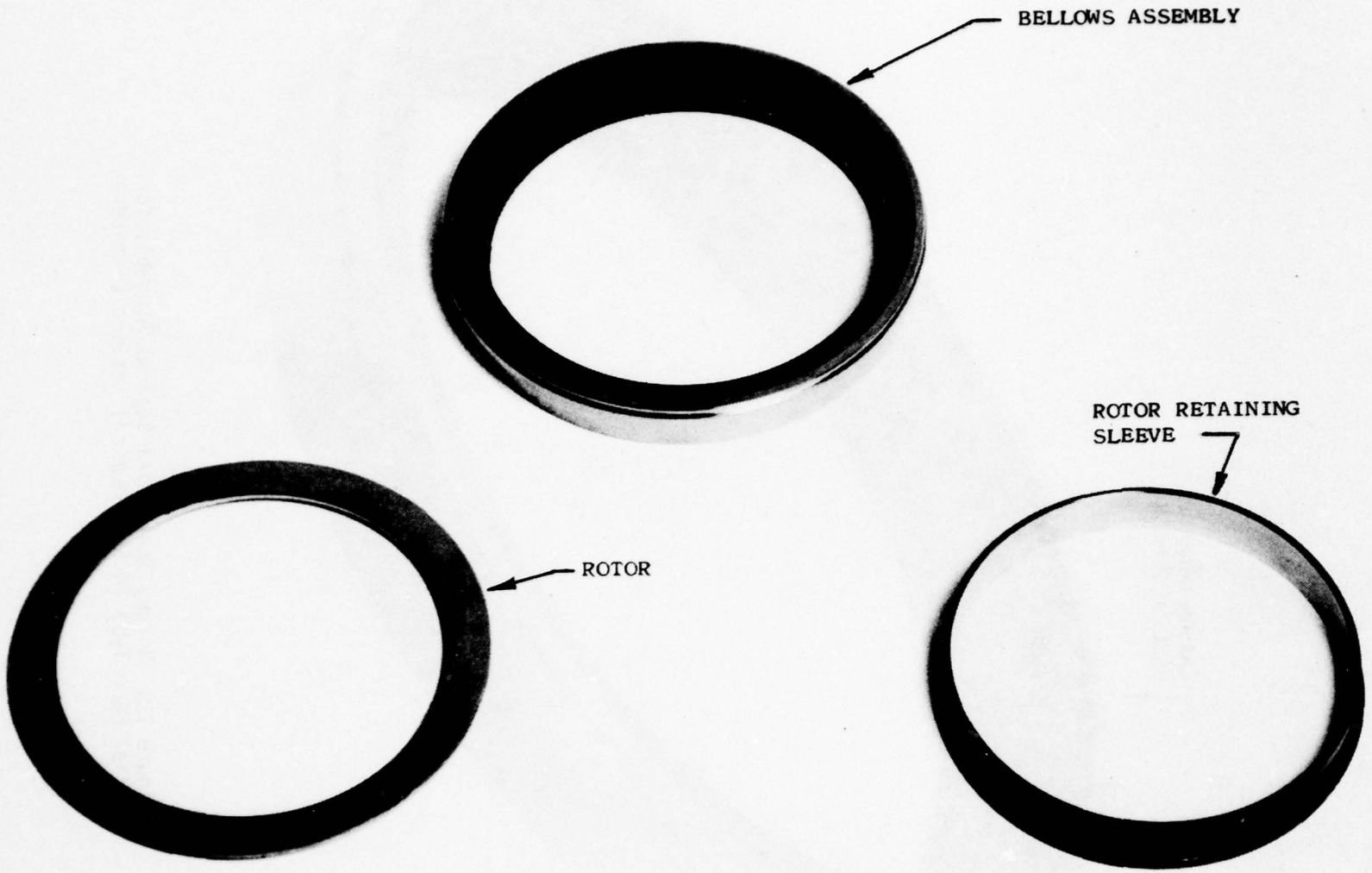

Figure 11. Rotary Shaft Seal Components of Radial Face Type

During the seal tests, only two of the three types were evaluated. These were the seals shown in Figures 6 through 8, 10, and 11. Although the third seal, Figure 9, was not quantitatively evaluated, it was used extensively in actuator testing. Fluid temperature was varied from -50^{o} to $+600^{o}$F (-45.6^{o} to 316^{o}C) during seal testing, while the ambient temperature varied between -50^{o} to $+800^{o}$F (-45.6^{o} to 427^{o}C).

The stiffness survey conducted resulted in replies from six major airframe companies. The information received covered actual and projected actuator spring rates from small fighter type aircraft to the large, high performance SST. The information was restricted to the horizontal tail surface and rudder surface applications. A stiffness-to-weight ratio comparison between the rotary actuator developed in this program and a comparable linear actuator diagram was made as part of the survey task to reflect significantly different characteristics between the two different types.

The limitations of the actuator evolved in this program were found to be:

1) An excessive output torque ripple caused by the force vector required to keep the transmission gears in mesh. The magnitude of the ripple is approximately 40 percent when the hold-in motor pressure is equal to supply pressure.
2) A lower volumetric efficiency than estimated, which is attributed mainly to the pumping effected by the hold-in motor. The efficiency is 70 percent compared to 85 percent. The hold-in motor displacement which was theoretically to be zero was actually measured as 0.36 in^3/revolution (5.9 cc/rev).

3) A slightly lower torque efficiency than estimated. The efficiency is 92 percent compared to 94 percent. This slight deficiency is also accompanied by a lower motor stall torque than the necessary 1860 lb-in (210 N-m) because of the effective loss of motor displacement resulting from the hold-in motor displacement.

4) The measured torque motor displacement of 3.05 in^3/revolution (50 cc/rev) is approximately 2 percent less than specified.

5) The Motor Cartridge Assembly leakage to case at 2000 psig (13.8 MN/m^2) supply pressure is 18 percent larger than required to meet the volumetric efficiency. This leakage was measured with the hold-in motor port blocked to eliminate the impact on leakage caused by the hold-in motor pumping.

6) High temperature testing of the Motor Cartridge Assembly was not accomplished because of an operating characteristic of the output shaft assembly that was incompatible with the tool steel thrust washers that were provided with the Test Unit. Rotation of the shaft produced a thrust that resulted in a clamping action that caused the shaft to stop and galling of the mating parts of the rear thrust washer. To prevent seizing of the shaft at supply pressure greater than approximately 200 psig, (1.4 MN/m^2), at no-load, it was necessary to install teflon thrust washers. While this expediency allowed room temperature performance to be evaluated, the teflon washers were unsatisfactory for high temperature use. After inspection of the various dimensions that can contribute to the longitudinal displacement of the shaft failed to indicate any significant discrepancy, it was inadvertently discovered that the behavior was caused by the temporary (for Motor Cartridge tests only) roller bearing used to couple the rotor and the output shaft.

SECTION III

TECHNICAL APPROACH

The rotary hydraulic actuator developed for this program to meet the design performance goals shown in Table 1 is a form of the Bendix-developed Dynavector actuator. Previous work directed toward the application of this device to aircraft control functions has been reported previously. [1]

A simple depiction of the operation of the Dynavector rotary actuator is illustrated by Figure 12 which indicates the significant geometry of the actuator but does not show the vanes forming the displacement chambers. Briefly, the Dynavector actuator is a positive displacement, low inertia, nonrotating vane motor integrated with an epicyclic transmission. The epicyclic transmission consists of an output gear (keyed to the output shaft) and a ring gear surrounding the output shaft and in mesh with the output gear. The ring gear orbits but does not rotate. The ring gear reaction is taken by pins passing through clearance holes in the ring gear. The transmission ratio is determined by the difference in the number of teeth between the ring gear and the output gear. The ring gear is surrounded by a housing. The motor displacement chambers occupy the clearance between the outer diameter of the ring gear and the inner diameter of the housing. The displacement chambers are separated from one another by captive vanes. The displacement chambers are commutated so that a radial force vector is applied to the

[1] Verge, K.W., et al
Investigation of Rotary Actuator Techniques
AFAPL-TR-70-52
Bendix Research Laboratories
September 1970

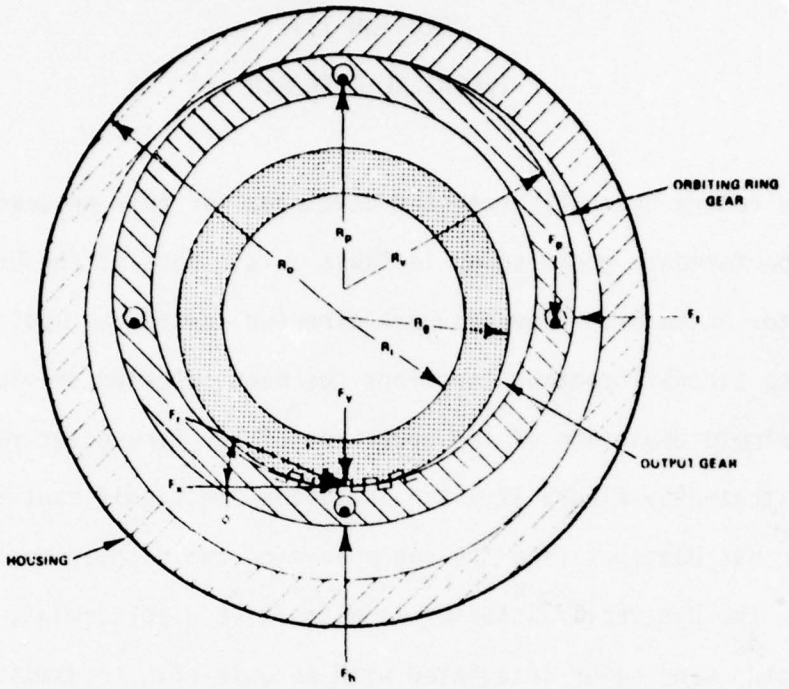

Figure 12. Actuator Forces Diagram

ring gear to produce orbit motion. The radial force vector rotates at a speed equal to the product of the transmission ratio and the output shaft speed. The displacement chambers expand and collapse at the same speed as the rotating force vector. In addition to the displacement chambers which are used to form the torque-producing vector, other displacement chambers produce the force required to keep the epicyclic transmission in mesh.

The gear reaction force F_r, Figure 12, acting at the gear pressure angle may be broken into the component forces F_x and F_y tangent to and along a radius of the output gear pitch circle. The reaction pin force is denoted F_p. The force produced by the torque motor displacement chambers is F_t and that by the hold-in motor displacement chambers is F_h. As shown in Figure 12, the forces F_t and F_h act at right angles and colinear to the eccentricity axis. This is an ideal representation; and in the real case,

where there are a finite number of motor chambers, the forces F_t and F_h swing through an angle to either side of the ideal positions shown in the figure as the displacement chambers are commutated. The distribution of the total motor displacement between the torque and hold-in motor chambers must take this angular swing of the motor force vectors into account if the gearing is to stay in mesh. This facet of design is discussed later. For now, it can be shown that

$$R_t = \frac{N_o}{N_o - N_r} \tag{1}$$

where

R_t = Transmission ratio

N_o = Number of teeth on output gear

N_r = Number of teeth on ring gear

since

$$N_o = D_g \; D_p \tag{2}$$

and

$$N_o - N_r = 2D_p e \tag{3}$$

then

$$R_t = D_g/2e \tag{4}$$

where

D_g = Pitch diameter of output gear-in

D_p = Diametral pitch-in^{-1}

e = Eccentricity-in

The total displacement of the actuator is given by

$$d_t = 2 \pi D_v eb \tag{5}$$

where

d_t = Total actuator displacement - in^3/rev

D_v = Vane seal diameter - in

b = Motor chamber length - in

The total actuator displacement is divided among the torque motor displacement chambers and the hold-in motor displacement chambers.

Also

$$d_m = f_m d_t \tag{6}$$

where

d_m = Motor displacement producing torque - in^3/rev

f_m = Fraction of total displacement allotted to torque motor chambers - in^3/rev

The actuator output torque is therefore:

$$T_o = \frac{d_m \, \Delta P R_t \eta_t}{2\pi} \tag{7}$$

or

$$T_o = D_v D_g b \Delta P \eta_t f_m / 2 \tag{8}$$

where

T_o = Output torque - in.-lbs

ΔP = Pressure difference across torque motor chambers - psid

η_t = Torque efficiency

Several limiting factors present in conventional rotary motors plus transmission systems are significantly improved by the typical Dynavector actuator design and operation. The relative velocities between dynamic and static members are very small because of the small amplitude orbital motion. In a Dynavector actuator, the relative velocity between the gears and housing is only a function of the eccentricity, which is less than one-tenth of an inch, times the angular velocity, whereas in a conventional motor there are usually components with a radius of more than an inch rotating at the same angular velocity. Thus, for a force vector speed of 3,000 rpm, rubbing velocity would not exceed 30 inches/second (76.20 centimeters/second),

whereas in a conventional motor rotating at 3,000 rpm, rubbing velocities would be greater than 300 inches/second (762.0 centimeters/second). The relative tooth velocities correspond to those found only in the last stage of a conventional transmission. The absence of high relative velocities produces high mechanical efficiency by reducing friction losses at high motor speed.

Another factor that is significantly reduced is actuator inertia. In conventional high-speed motors, the motor inertia resulting from a rotor mass rotating at high angular velocities has always limited the motor response capabilities. The small volumes under compression have helped to compensate for the poor response due to inertia and have placed rotary servos in contention, provided high supply pressures are used.

The Dynavector actuator, having no mass rotating at input speed and only a small reflected inertia due to the small eccentric rotation of the ring gear and the low speed output shaft, is equivalent to the reflected inertia of a similar capacity piston/cylinder actuator. On the other hand, the volume under compression is equivalent to a rotary servo and is much less than that of a piston/cylinder actuator. This smaller volume allows the use of a lower pressure or bulk modulus than used in state-of-the-art pneumatic systems, and hydraulic Dynavector systems will have correspondingly higher natural frequencies. An isometric, cut away illustration of the actuator design is shown in Figure 13.

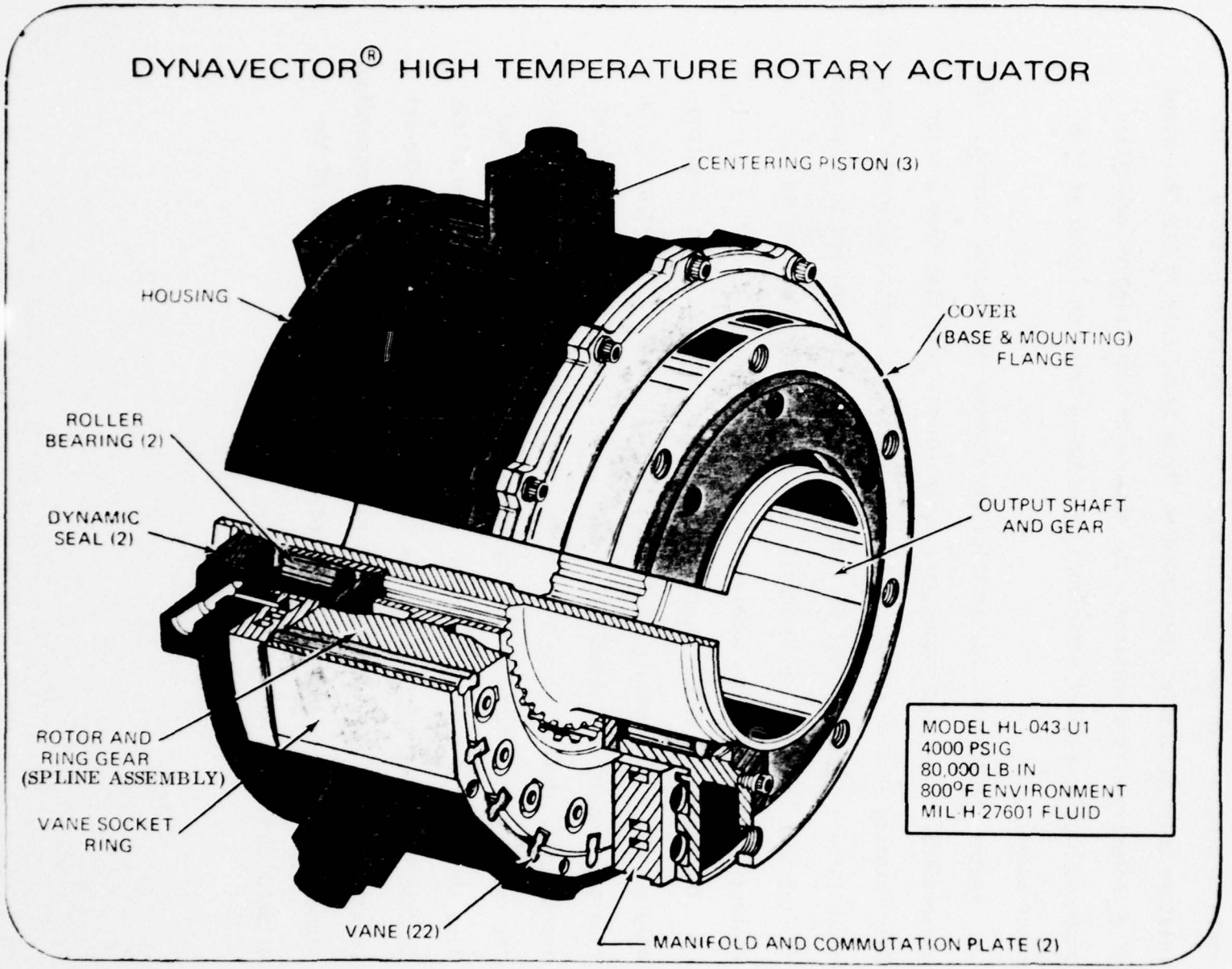

Figure 13. Dynavector High Temperature Rotary Actuator

SECTION IV

PROTOTYPE ACTUATOR DESIGN

1. MOTOR CARTRIDGE

The motor cartridge assembly comprises all internal working parts of the final prototype actuator used to convert hydraulic energy to mechanical rotary motion. It does not include the gearing, bearings, decoupling pistons or output shaft. Figure 14 shows the motor cartridge assembly. The materials and Bendix Research Laboratories specifications used for the parts in this assembly are listed in Table 2.

The motor cartridge test assembly shown in Figure 15 consists of those parts which enable the motor cartridge to be tested as a hydraulic motor. No gear mesh is used. Since the gear ratio of the final prototype actuator is 43:1, the maximum output torque of the motor cartridge test assembly at a 4000 psig supply pressure is 80000/43 = 1860 in.-lbs and the output speed, based on a final prototype actuator output rate of 90 degrees/second is 645 rpm. The greatly reduced output torque level is a more convenient value to absorb in continuous rotation tests than the 80000 inch-pound output torque level of the final actuator design. Hence the basic measurements of volumetric efficiency were made during the running of the motor cartridge assembly.

Figure 16 shows the motor cartridge test assembly. The housing (item number 2) and cover (item number 6) are the identical parts which were used on the final high output torque prototype assembly. These were fabricated from 18 Ni 350 steel and were processed in accordance with Bendix Research Laboratories specification PS-1187. The output shaft (item number 9) acts as a crank and converts the force obtained by

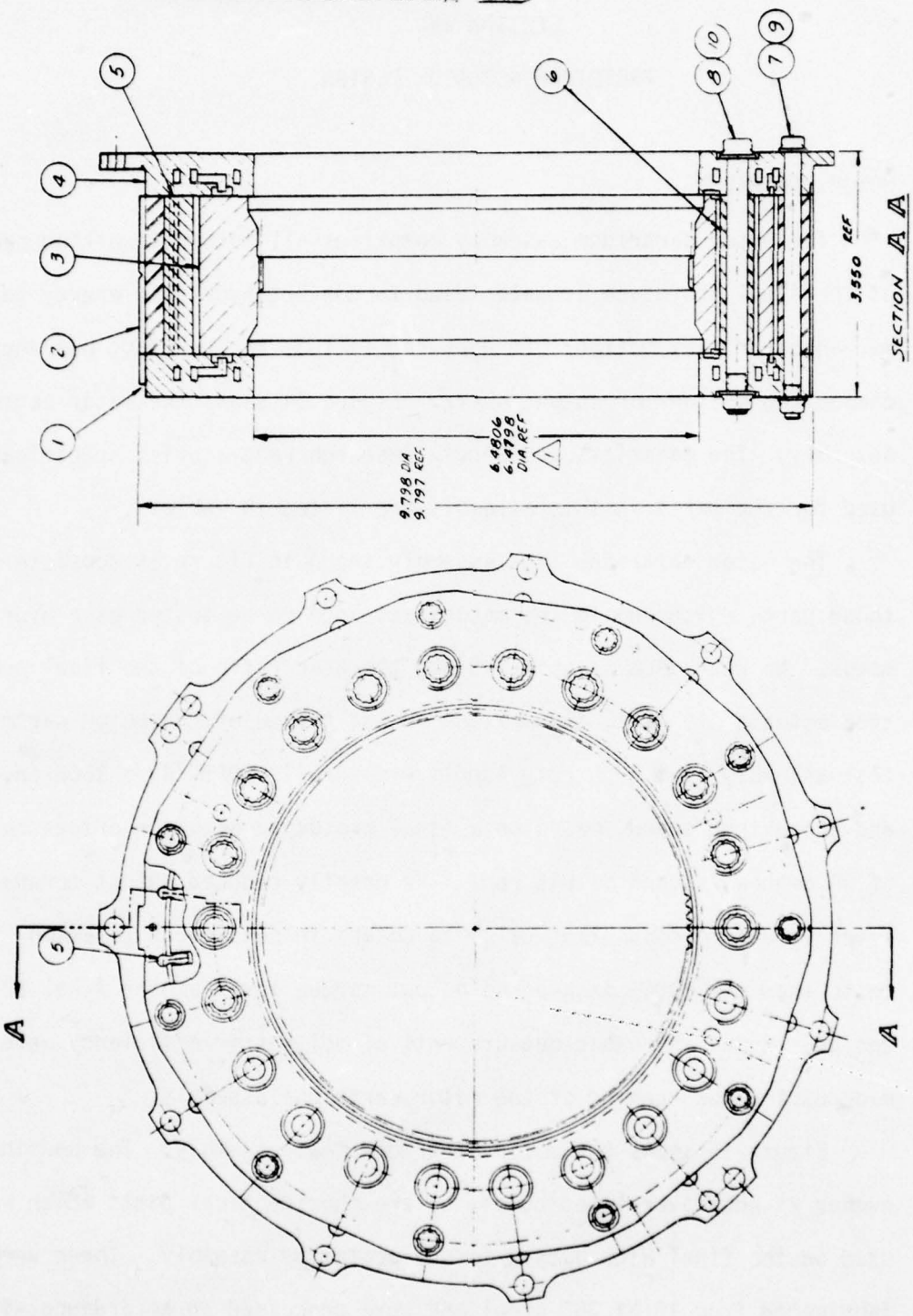

Figure 14. Prototype Actuator Motor Cartridge Assembly

Table 2

Motor Cartridge Component Materials and Process Specifications

Fig. 14 Callout	Bendix Part No.	Other Part No.	Qty. Required	Part Name	Material	Process Specification	Weight Lbs.
1	D2178185	-	1	Rear Commutation Plate	AMS-6485A	PS-1190& PS-1191	5.88
2	D2178099	-	1	Rotor Ring	18 Ni 350	PS-1187	8.22
3	D2178101	-	1	Rotor	18 Ni 350	PS-1188	10.19
4	D2178095	-	1	Front Commutation Plate	AMS-6485A	PS-1190 & PS-1191	8.00
5	D2178102	-	22	Vane	M2 Tool Steel	PS-1189 & PS-1191	0.81
6	D2178103	-	22	Spacer	18 Ni 350	PS-1188	1.50
7	-	EWB TM-9-4-54	11	Bolt 0.250 - 28 x 3.875	AMS-6485 or 6487	Purchased Part (SPS)	0.69
8	-	EWB TM-9-5-50	22	Bolt 0.312 - 24 x 3.718	AMS-6485 or 6487	Purchased Part (SPS)	2.25
9	-	FN922-428	11	Locknut 0.250-28	AMS-6304	Purchased Part (SPS)	
10	-	FN922-524	22	Locknut 0.250-28	AMS-6304	Purchased Part (SPS)	

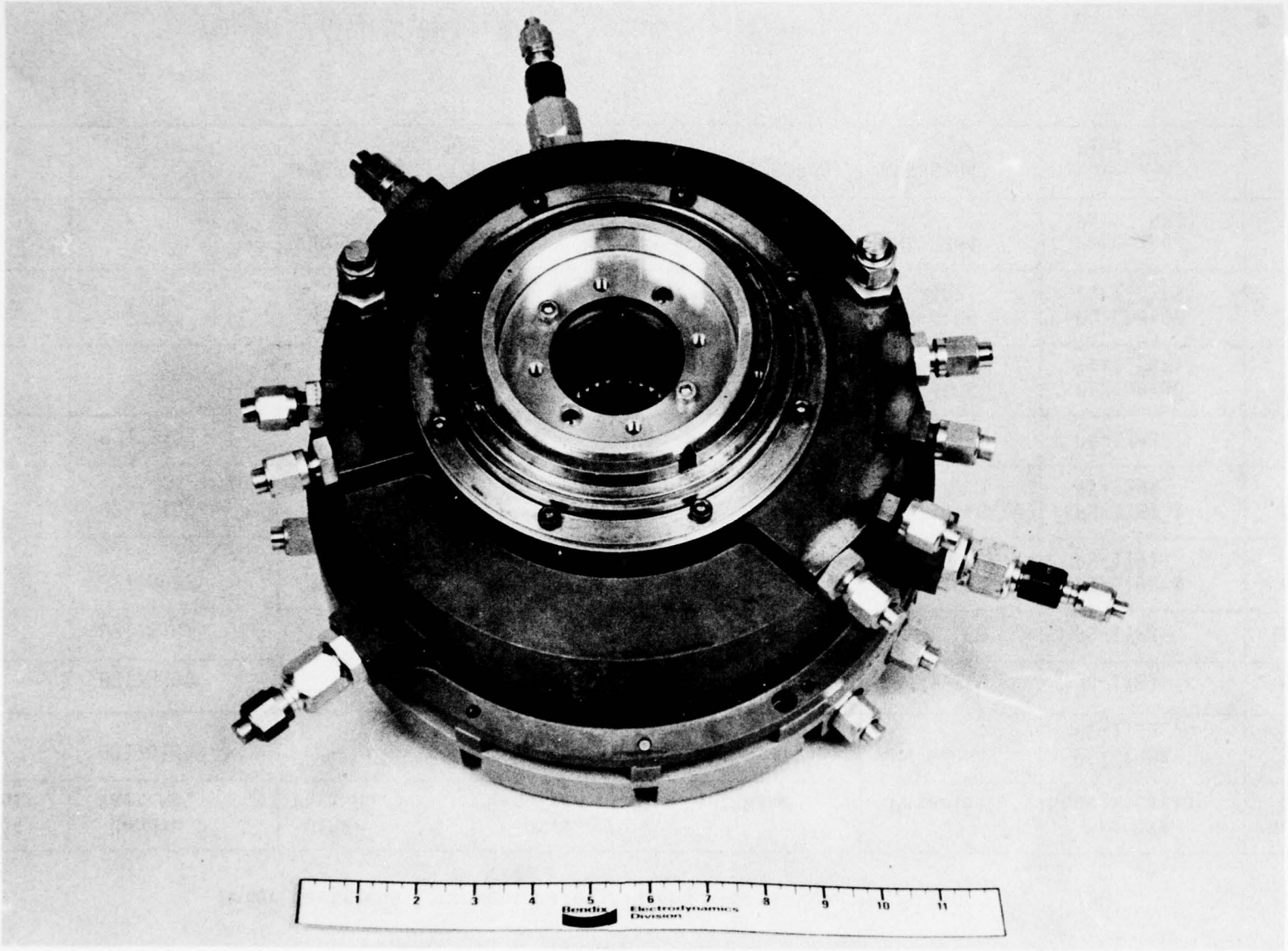

Figure 15. Motor Cartridge Test Assembly

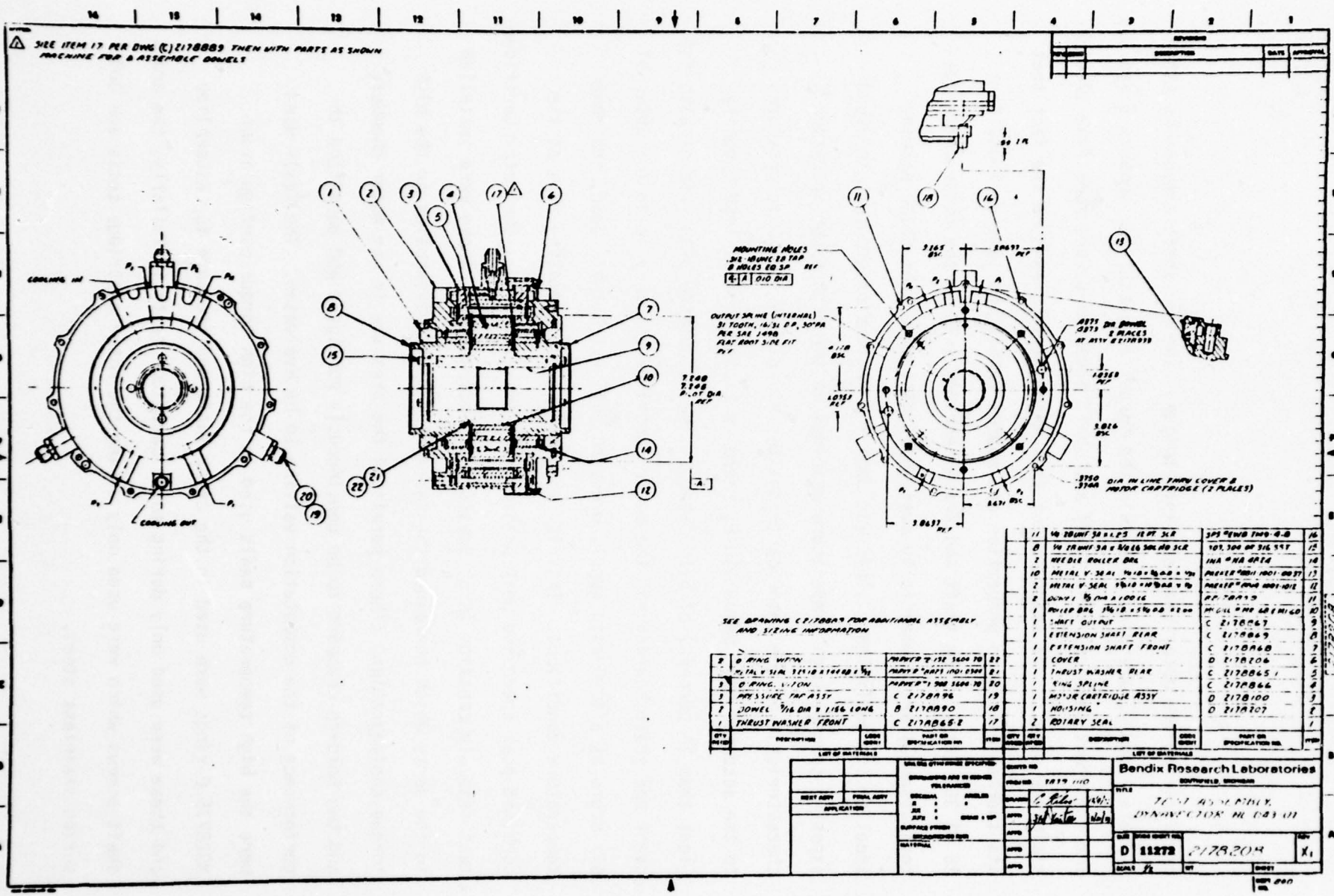

Figure 16. Motor Cartridge Test Assembly

pressurizing the motor chambers into torque. The two shaft extensions (item numbers 7 and 8) are used to retain the thrust washers (item numbers 5 and 17) and the crank bearing. The shaft and shaft extensions were made from 17-4 PH stainless steel. The selection of this material was based on the fact that its thermal expansion properties are approximately the same as those for 18 Ni 350 steel. The shaft and crank bearings used in the motor cartridge test assembly are commercially available units made from 52100 bearing steel or its equivalent. This was done for reasons of economy, to avoid exposing special high temperature bearings to the high speed operation characteristic of the motor cartridge tests. With internal temperatures in the actuator kept below 400^{o}F, there is little loss of load capacity (less than 10 percent) of 52100 steel. The calculated B-10 life of both the crank and shaft bearings of the motor cartridge assembly is on the order of six hours at a 4000 psig supply pressure, 645 rpm output speed, and room temperature conditions. This is adequate, since operating time at the combined peak speed and peak pressure was not extensive. The motor cartridge test assembly contains three pressure tap assemblies. These were installed in the ports which contained the decoupling piston assemblies in the high torque configuration. These permitted the pressure in one motor chamber and two hold-in chambers to be continuously monitored and permitted the performance of the commutation valving to be evaluated. The seals used were the high temperature seals used in the high torque configuration. MS28775 O-rings were used in the crank shaft and pressure tap assemblies and these were used only during motor cartridge tests. Similarly, the crank shaft screws which were used only during the motor cartridge tests are 300 series stainless steel.

2. PROTOTYPE ACTUATOR ASSEMBLY

Since the housing and cover used in the test assembly for the motor cartridge assembly (Figure 16, items 2 and 6) were the same components used for the actuator assembly, the assemblies look much the same in external appearance as can be seen in Figures 15 and 17. Internally, the actuator assembly differs from the motor cartridge assembly principally by the inclusion of the gear transmission and the three centering pistons. This difference can be seen by comparing Figures 16 and 18, which is a partial cross section of the prototype actuator. A complete difference in the two assemblies, including miscellaneous components such as static seals, bolts and nuts can be determined from the two lists of parts, Tables 2 and 3.

Figures 19 and 20 are photographs of the components of the two assemblies. A list of the design parameters evolved from the statement of work and layout requirements is presented in Table 4. The major elements of the design are as follows:

a. Gear Mesh

During the course of layout design, the use of two different ring gear pitch diameters (6.750 inches and 5.500 inches) was considered. The eccentricity of the rotor orbit was in both cases kept at 0.0625 inches (0.1588 centimeters). So that the range of transmission ratios considered was 43:1 to 53:1. Selection of the smaller diameter was based on the reduction of the magnitude of the hold-in forces required.

Minimization of the forces acting to drive the gears out of mesh was accomplished by reducing the pressure angle. Gear tooth profiles were calculated for 20 degree, (0.3488 radian), 35 degree, (0.4361 radian), and 30 degree (0.5233 radian) pressure angles using

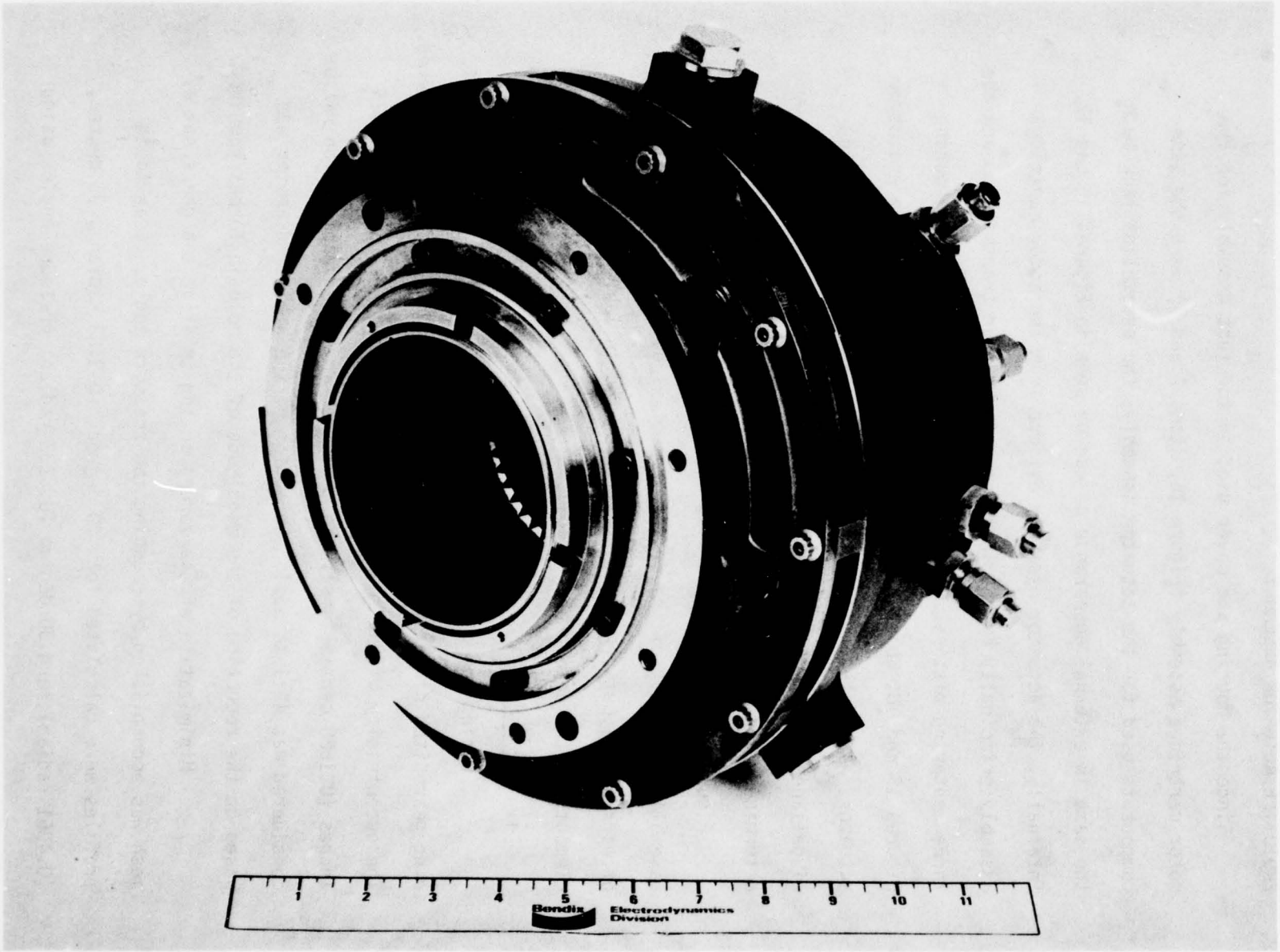

Figure 17. Prototype High Temperature Rotary Actuator Assembly Model HL-043-U1

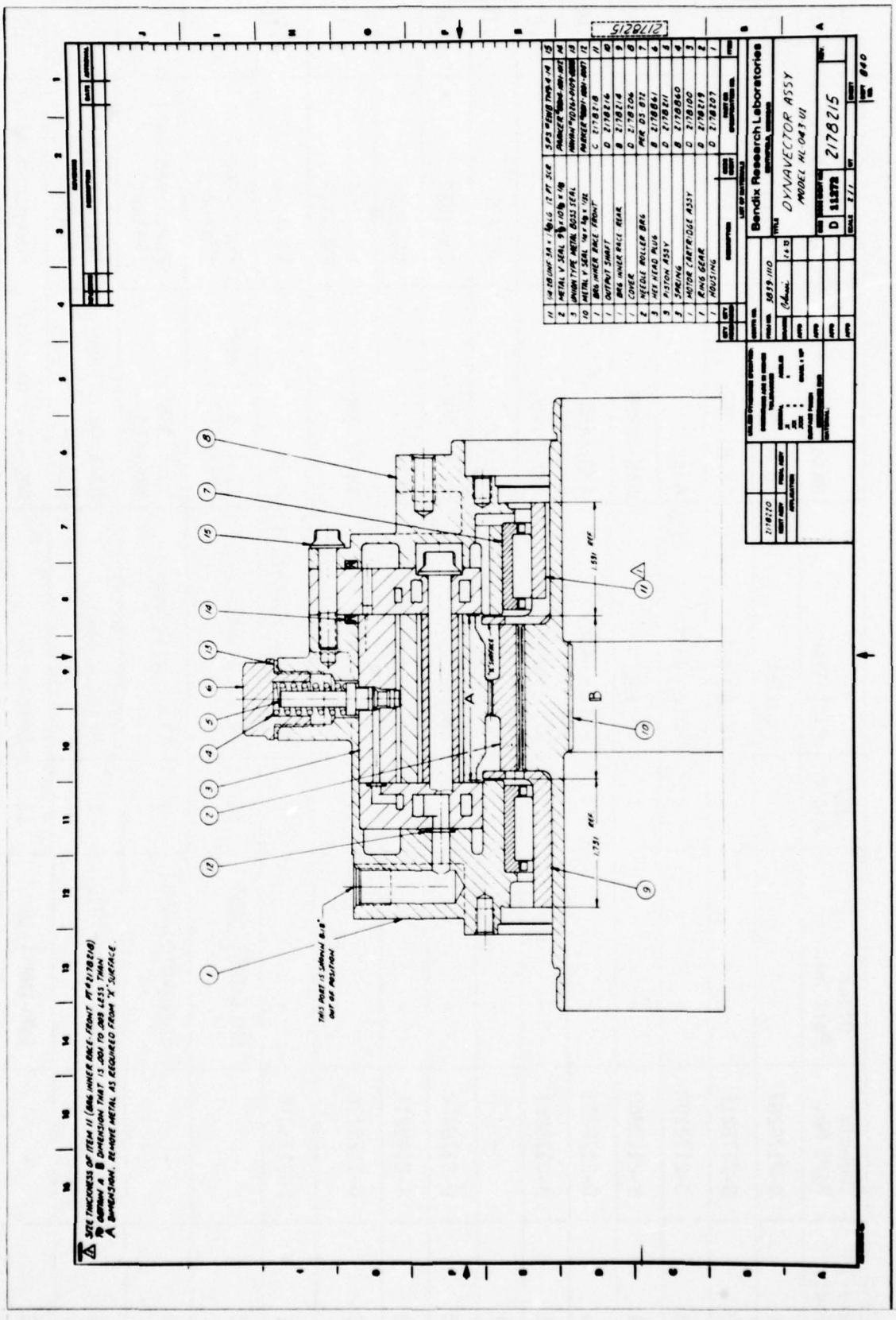

Figure 18. Prototype High Temperature Rotary Actuator

Table 3

Prototype Actuator List of Parts

Figure 18 Callout	Bendix Part No.	Other Part No.	Qty. Req'd	Part Name	Material	Process or Design Spec.	Weight Lbs.
1	D-2178207	-	1	Housing	18 Ni 350	PS-1187	17.75
2	D-2178219	-	1	Ring Gear	18 Ni 350	PS-1188	2.88
3	D-2178100	-	1	Motor Cartridge Assy	Assy	-	37.54
4	B-2178860	-	3	Spring	AMS-5698B	-	0.06
5	D-2178211	-	3	Piston Assy	AMS-6485	PS-525	0.06
6	B-2178861	-	3	Hex Head Plug	AMS-5648C	-	0.03
7	-	-	2	Needle Roller Brg	M-50	DS-872	3.25
8	D-2178206	-	1	Cover	18 Ni 350	PS-1187	16.38
9	B-2178214	-	1	Brg Inner Race-Rear	M-50	PS-1166	2.25
10	D-2178216	-	1	Output Shaft	18 Ni 350	PS-1188 PS-1192	9.30
11	C-2178218	-	1	Brg Inner Race-Front	M-50	PS-1166	2.13
12	-	8811-1001-0037	10	Metal V Seal	17-4 PH Silver Plated	Purchased Part (Parker)	
13	-	VD261-0109-0008	3	Metal Boss Seal	Type 303 Stainless	Purchased Part (Natorq)	
14	-	8814-1001-1012	2	Metal V Seal	17-4 PH Silver Plated	Purchased Part (Parker)	
15	-	EWB-TM9-4-14	11	Bolt	AMS-6485 or 6487	Purchased Part (SPS)	0.38

Figure 19. Prototype Actuator Model HL-043-U1 Components

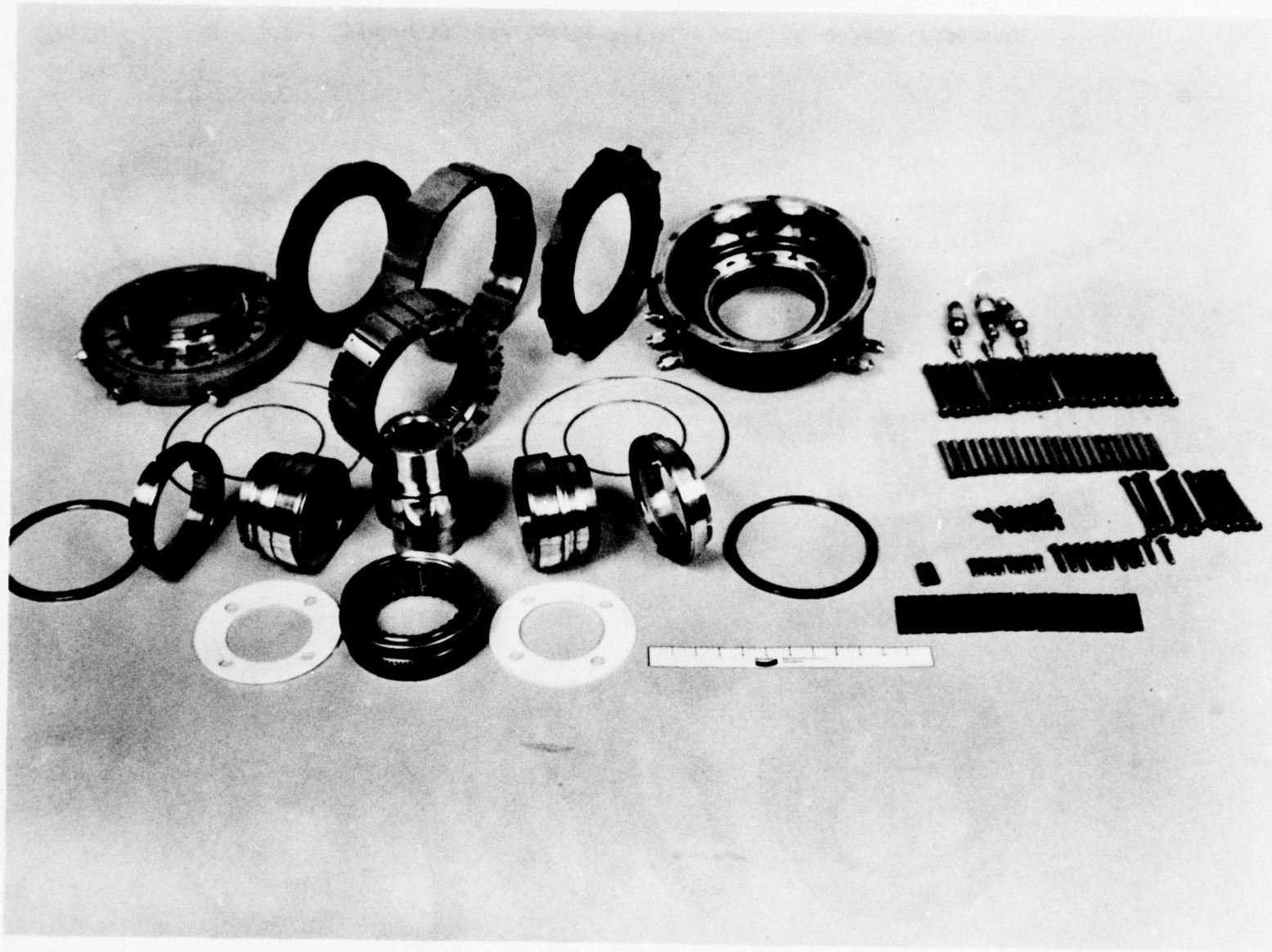

Figure 20. Motor Cartridge Test Assembly Components

Table 4

Model HL-043-U1, Prototype Actuator Design Parameters

Sym.	Parameter	Value
D_g	Ring gear pitch diameter	5.500 inches (13.970 cm)
D_o	Output gear pitch diameter	5.375 inches (13.653 cm)
e	Eccentricity	0.0625 inches (0.1588 cm)
N_r	Number of teeth on ring gear	264
N_o	Number of teeth on output gear	258
ϕ_p	Gear pressure angle	25 degrees (0.436 rad)
R_t	Transmission ratio	43:1
-	Outside diameter of chamber	8.800 inches (22.352 cm)
-	Outside diameter of rotor	8.675 inches (22.035 cm)
D_v	Vane seal diameter	8.400 inches (21.336 cm)
-	Total number of chambers	22
γ_M	Arc subtended by motor chamber	13.33 degrees (0.2325 rad)
$\gamma_M + \gamma_H$	Arc subtended by motor and hold-in chamber	32.72 degrees (0.5708 rad)
b	Chamber length	2.300 inches (5.842 cm)

the procedure outlined in Reference [1]. Layouts showed that with a 20 degree (0.3488 radian) pressure angle, considerable reduction of addendum and dedendum of the ring and output gears is required to avoid tooth interference during disengagement. Potential tooth interference is much less for the 25 degree (0.4361 radian) pressure angle which also has better lead-in characteristics than the originally-selected 30 degree (0.5233 radian) pressure angle. It was, therefore, decided to use a 25 degree (0.4361 radian) pressure angle on the gearing.

A significant consideration in the gear design was necessitated by the redundancy requirement which stipulated that the gears must be decoupled with the loss of system pressure. Instead of being able to depend on the normal wraparound of gear teeth, as in most Dynavector designs, that prevents radial separation of the gears, it was necessary to size the gears so they would separate upon loss of supply pressure. Consequently, the reaction force to the gear separating force (F_v in Figure 12) had to be furnished by a supply pressure generated force (F_h in Figure 12). The self commutating porting necessary to use supply pressure in developing the reaction force is covered in a following paragraph.

In addition to being able to orient the reaction force (90 degrees to the torque developing force, F_t in Figure 12) correctly, it is necessary to maintain the magnitude of the force under adverse conditions to prevent separation.

To achieve this goal, a basic understanding of the kinematics and kinetics of the device was imperative. The Dynavector motor configuration developed has hold-in chambers alternately spaced with its torque motor chambers and also has reaction pins. By considering a free-body

diagram of the ring gear (Figure 21) and the angular swing of the developed fluid pressure force, a condition for maintaining gear mesh is derived and is:

$$K \leq \cos\left(\frac{90}{\eta}\right) \frac{1}{\left(\frac{R_o + e}{R_o + e + \varepsilon} + \tan \phi_p\right)} - \sin\left(\frac{90}{\eta}\right) \qquad (9)$$

where K is defined

$$K = F_M / F_H \qquad (10)$$

and where

F_M is the net motor force magnitude

F_H is the net hold-in force magnitude

η is the number of motor (and hold-in) chambers and must be odd

R_o is the output shaft pitch circle radius

e is the basic eccentricity

ε is the difference between the reaction pin circle and ring gear pitch circle radii

ϕ_p is the gear pressure angle

It can be shown that the net motor and hold-in forces each remain constant during commutation. These forces act through the ring gear center and are found by vectorially adding the force developed by each pressurized motor chamber and each charged hold-in chamber, respectively. The magnitude of each motor chamber force F_m is found from (reference Figure 22):

$$F_m = 2d\, R_V\, \Delta P \sin(\gamma_M/2) \qquad (11)$$

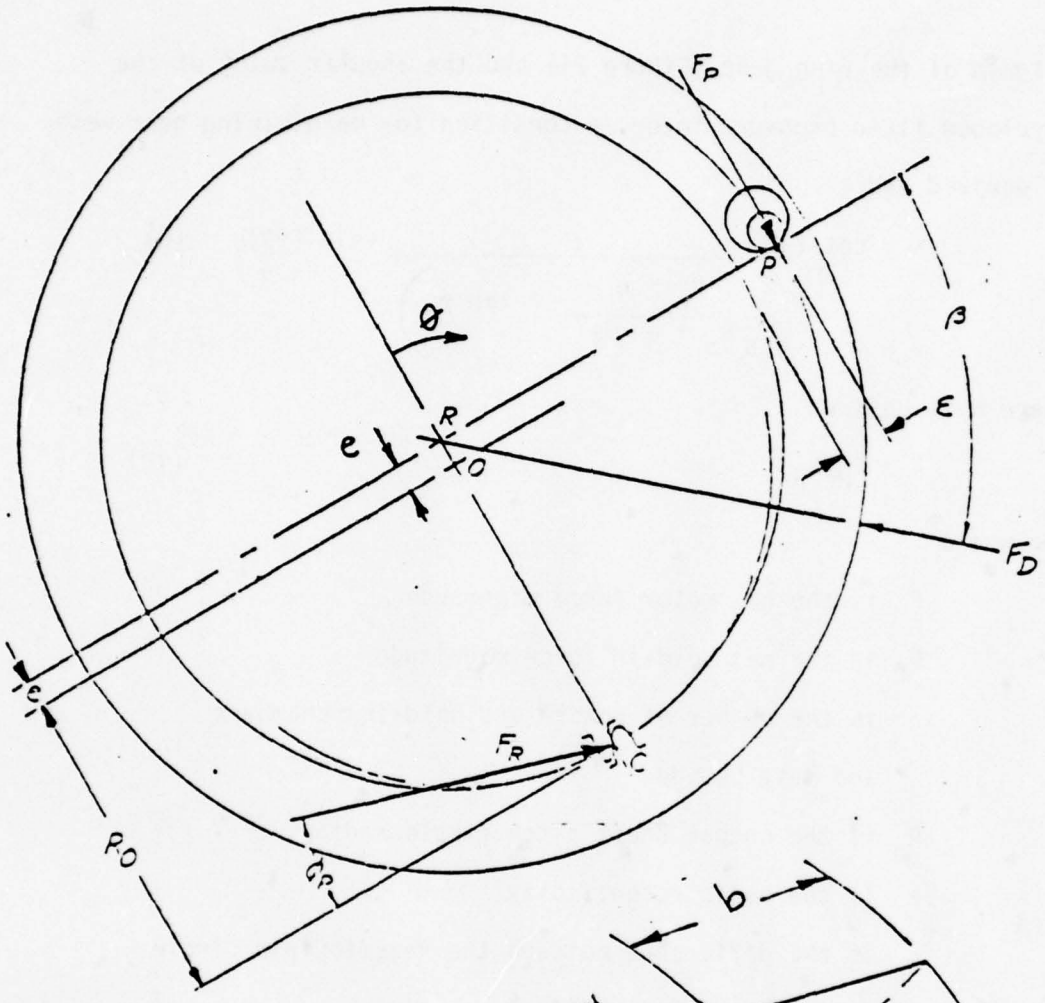

Figure 21. Free-Body Diagram of Ring Gear

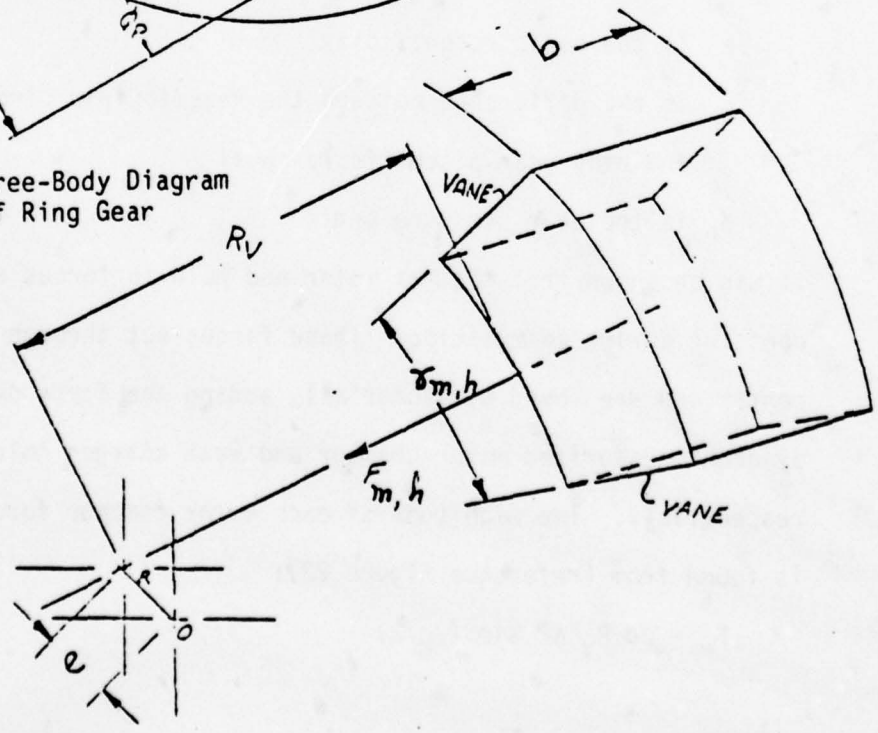

Figure 22. Actuator Chamber Geometry

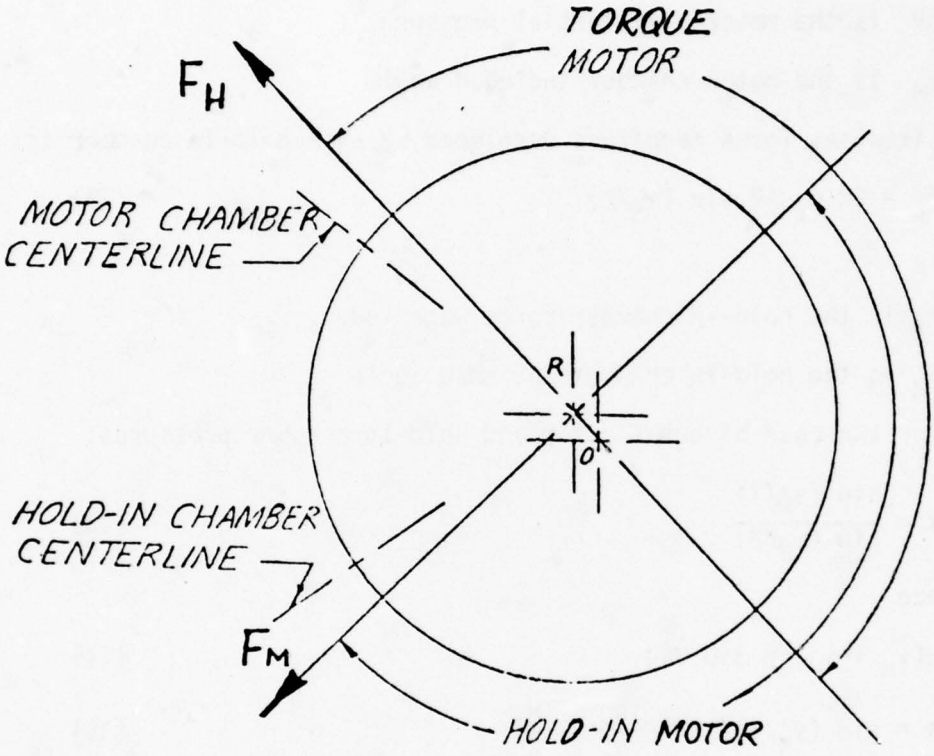

Figure 23. Dynavector Actuator Commutation Sectors

where

d is the chamber depth

R_V is the minor radius of the chamber measured relative to the ring gear center

ΔP is the motor differential pressure

γ_M is the motor chamber included angle

Likewise, force magnitude developed by each hold-in chamber is:

$$F_h = 2d\, R_V\, \Delta P \sin(\gamma_H/2) \tag{12}$$

where

F_h is the hold-in chamber force magnitude

γ_H is the hold-in chamber included angle

For the case of equal motor and hold-in chamber pressures:

$$K = \frac{\sin(\gamma_M/2)}{\sin(\gamma_H/2)} \tag{13}$$

or since

$$\eta(\gamma_M + \gamma_H) = 360 \text{ deg}, \tag{14}$$

$$K = \sin(\gamma_M/2)/\sin\left(\frac{180}{\eta} - \frac{\gamma_M}{2}\right) \tag{15}$$

For a calculated K, the motor chamber angle is specified in accordance with:

$$\gamma_M = 2 \tan^{-1} \frac{K \sin(180/\eta)}{1 + K \cos(180/\eta)} \tag{16}$$

The hold-in chamber angle is computed from:

$$\gamma_H = \frac{360}{\eta} - \gamma_M \tag{17}$$

For the high temperature Dynavector actuator developed, the eccentricity is e = 0.0625 inch. There are 11 chambers, R_o = 2.6875 inches, the gear pressure angle is 25 degrees and the radius of the reaction pin circle exceeds the ring gear pitch radius by = 1.1250 inch. The angle (90/η) is:

$$\left(\frac{90}{\eta}\right) = \left(\frac{90}{11}\right) = 8^{o}11' \qquad (18)$$

and from (9)

$$K \leq (0.98982) \left(\frac{1}{\left(\frac{2.6875 + 0.0625}{2.6875 + 0.0625 + 1.1250} + 0.46631\right)}\right) - 0.14231$$

$$\leq 0.69935$$

For the limiting case of K_{Max} = 0.69935, the motor chamber angle from (16) is:

$$\gamma_M = 2 \tan^{-1} \frac{K \sin (180/\eta)}{1 + K \cos (180/\eta)}$$

$$= 2 \tan^{-1} \frac{0.69935 \sin (16.364)}{1 + (0.69935) \cos (16.364)}$$

$$= 2 \tan^{-1} (0.1178956)$$

$$\gamma_M = 13^{o}26' \text{ (0.234 rad)}$$

The hold-in chamber angle from (17) is:

$$\gamma_H = \frac{360}{} - 13^{o}26'$$

$$\gamma_H = 19^{o}17.6' \text{ (0.337 rad)}$$

Thus, the values of γ_M and γ_H calculated based on F_t and F_h being proportional to the system supply pressure (assuming a negligible magnitude of system return pressure) assure that the hold-in force developed will be large enough to prevent gear separation. The sectors of the motor over which the forces act, shown in Figure 23, are determined by the orientation of the commutation porting.

b. Commutation Porting

Figure 24 illustrates the method of commutating the motor and hold-in chambers. In this figure, eccentricity axis is noted i_e. Pressure and exhaust ports for the motor chambers are oblong slots located in a fixed manifold plate. The slots are radially oriented and are symmetrically spaced with respect to a reaction pin. Porting of the motor chambers is designed so that when the eccentricity axis is colinear with a reaction pin hole centerline, the chamber is at a neutral pressure (neither charged nor exhausted). Any change in the eccentricity axis from this position results in a port being commutated with the reaction pin hole in the ring gear and the motor chamber is either pressurized or depressurized. Arrows in the passageways in the ring gear indicate the direction of flow for charging and exhausting motor chambers. Motor chambers are pressurized in one of the 180-degree (3.14 radian) sectors (labeled motor sector in the figure) formed by the eccentricity axis. Motor reversal is achieved by depressurizing the chambers in this sector and pressurizing those in the opposite 180-degree (3.14 radian) sector.

Commutation of the hold-in chambers is similar to that for the motor chambers. Each hold-in chamber is supplied through an oblong slot in the manifold plate. Exhausting of the chamber is achieved by means of a passageway in the manifold with the fluid sink being an annular space within the ring gear. Hold-in chambers are always pressured over a 180-degree (3.14 radian) sector at right angles to the eccentricity axis.

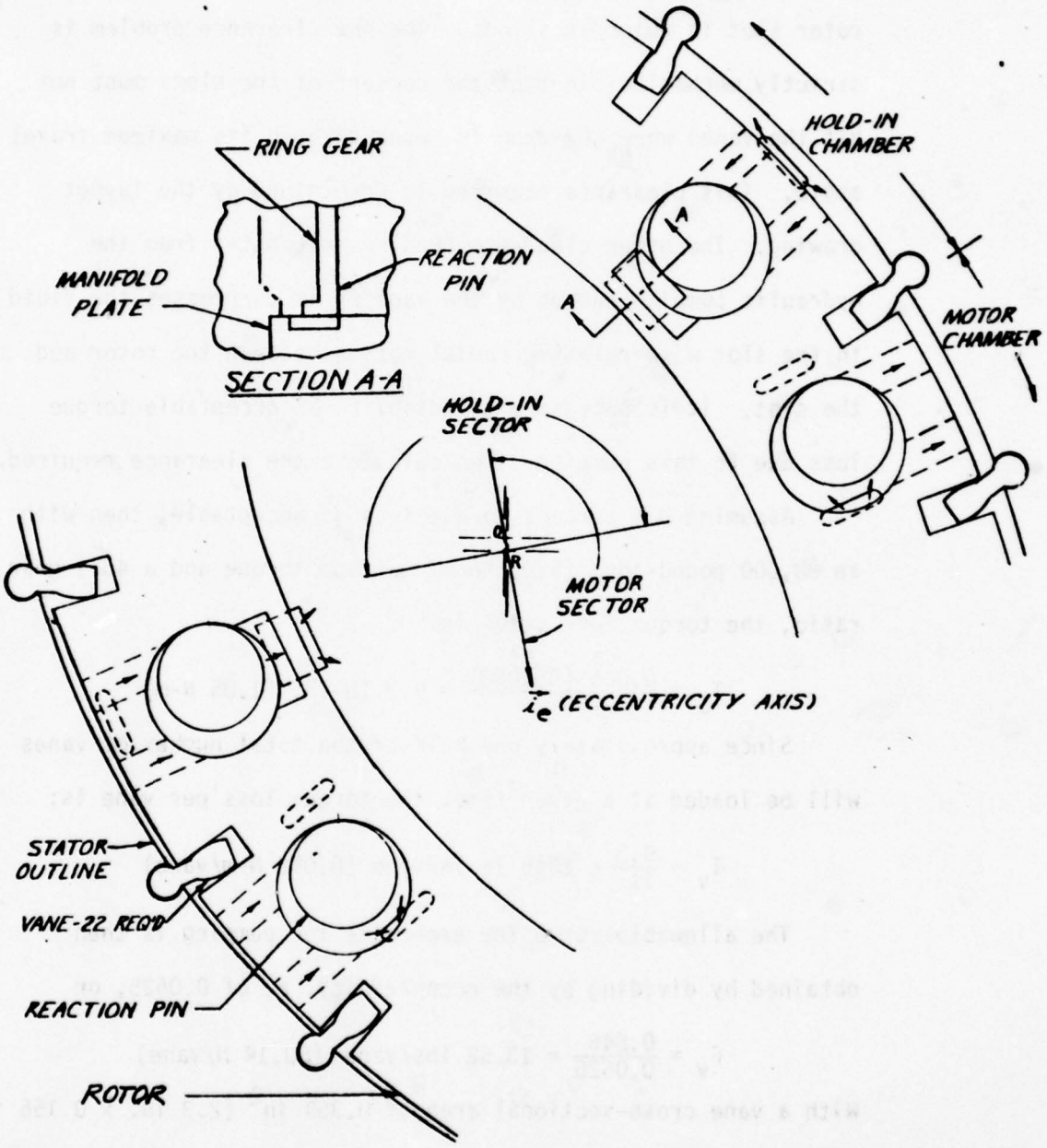

Figure 24. Commutation Porting

c. Vane and Rotor Clearance

As can be understood by observing the vanes in Figure 24, there are two types of clearance problems involving a vane and the rotor slot in which it slides. The one clearance problem is strictly mechanical in that the corners of the slots must not hit the vanes when the vane is swung through its maximum travel angle. This clearance required is determined by the layout drawing. The other clearance problem originates from the hydraulic pumping caused by the vane as it compresses the fluid in the slot with relative radial motion between the rotor and the slot. It is necessary to establish an acceptable torque loss due to this pumping, then calculate the clearance required.

Assuming 0.5 percent torque loss is acceptable, then with an 80,000 pound-inch (9.05 KN-m) maximum torque and a 43:1 gear ratio, the torque loss value is:

$$T_L = \frac{0.005\ (80{,}000)}{43} = 9.3 \text{ lb-in. } (1.05 \text{ N-m})$$

Since approximately one half of the total number of vanes will be loaded at a given time, the torque loss per vane is:

$$T_v = \frac{9.3}{11} = .845 \text{ lb-in/vane } (0.095 \text{ N-m/vane})$$

The allowable force for each vane for pumping is then obtained by dividing by the eccentricity, e, of 0.0625, or

$$F_v = \frac{0.845}{0.0625} = 13.52 \text{ lbs/vane } (60.14 \text{ N/vane})$$

With a vane cross-sectional area of 0.359 in^2 (2.3 in. x 0.156 in.), the allowable pressure differential on each vane is:

$$\Delta P_v = \frac{13.52}{0.359} = 37.7 \text{ psi } (0.26 \text{ MN/m}^2)$$

Since the vane displacement,

$$X = e \sin \omega t \tag{19}$$

the maximum linear velocity is:

$$\dot{X}_{max} = e\, \omega_{max}. \tag{20}$$

So with a maximum angular velocity of 43 times the maximum output of 90 degrees/second,

$$\omega_{max} = \frac{2\ \pi 43(90)}{360} = 67.54\ \frac{rad}{sec}$$

Therefore, from (20)

$$\dot{X}_{max} = (0.0625)\ 67.54 = 4.22\ in/sec\ (10.72\ cm/sec)$$

So,

$$q_{max} = \dot{X}_{max} A \tag{21}$$

$$= 4.22\ (0.359) = 1.52\ in^3/sec\ (24.91\ cc/sec)$$

The clearance area between vane and slot to allow this much flow with only 37.7 psi pressure differential is:

$$A_{max} = \frac{q_{max}}{C_d} \sqrt{\frac{w}{2\ g\ \Delta P}} \tag{22}$$

where: C_d = 0.1 (assumed, since at low Reynolds numbers the value can be very low)

w = Fluid specific weight, .03 lb/in^3 (0.83 gm/cc)

g = Gravitational constant, 386 in/sec^2 (980 cm/sec^2)

$$A = \frac{1.52}{0.1} \sqrt{\frac{0.03}{2(386)37.7}} = 0.0154\ in^2\ (0.099\ cm^2)$$

With a vane length of 2.300 inches (5.842 cm) then, the clearance between the vane and slot must be

$$C = \frac{0.0154}{2.300} = 0.0067 \text{ in } (0.0170 \text{ cm})$$

or the minimum slot width must be 0.156 + 0.0067 = 0.1627 inch (0.4133 cm). Since the slot width dimension was designed for 0.174 -0.178 inch (0.442 - 0.452 cm) and the vane width dimension was designed for 0.154 - 0.156 inch, (0.391 - 0.396 cm), the minimum clearance allowed was 0.020, or more than 3 times that necessary to limit the vane pumping torque loss to a maximum of 0.5 percent.

d. Material Selection

As shown previously in Table 3, the selection of materials for the various components in the actuator was based on the following philosophy:

1) System to be operable in and compatible with MIL-H-27601A hydraulic fluid for 3000 hours or more over a temperature range from -40° to 600°F (-40° to 316°C).
2) Components to be essentially unaffected by occasional exposure to 800°F (427°C).
3) Materials to be fabricated with established state-of-the-art technology to provide parts with a high expectancy of initial success (little or no development).
4) Thermal distortion to be avoided by use of one single alloy for major structural parts.
5) Consistent with the above, consideration to be given to weight, cost, availability and other pertinent factors.

As an aid in evaluating materials and components, a calculation of the number of cycles under various conditions to be imposed on the actuator during the life test had to be made. Bearing and fastener loads were of primary interest.

As detailed in the original statement of work, the high temperature Dynavector actuator was to be loaded and thermally cycled for a total of 250 hours. Load cycling was required throughout the life test. Thermal cycling of the actuator was required for 112.5 hours (Phase I), with the remainder of the test to be conducted at a steady temperature of 800°C (427°C) minimum (Phase II).

Two maximum levels of cyclic load testing were specified for the Dynavector motor - full load and one-half full load. At each level, the rate amplitude was to be 30 degrees/second (0.5233 radian/second) and the frequency was 30 cycles/minimum or π radian/second.

The actuator displacement, θ is expressed:

$$\theta = A \sin \omega t + \theta_0 \tag{23}$$

where A is the amplitude, θ_0 is the mean (offset deflection, and ω is the frequency (radian/second). The actuator rate $\dot{\theta}$ is given by

$$\dot{\theta} = A\omega \cos \omega t \tag{24}$$

From the specified rate,

$$A\omega = 30 \text{ deg/sec } (0.5233 \text{ rad/sec})$$

or

$$A = (30/\pi) \text{ deg}$$

$$= 9.554 \text{ deg } (0.1667 \text{ rad})$$

for both loading conditions. The displacement offset, 0_o, for the full load maximum level is found from Equation (23) by letting θ = 30 degrees (0.5233 radian) (at which the 80,000 inch/pound hinge moment occurs) and $\sin\omega t = 1.0$. Likewise, for the one-half full load condition, 0_o is determined by letting 0 = 15 degrees (0.2617 radian) (corresponding to a 40,000 inch pound hinge moment). Equations (23) and (24) then determined the required actuator displacement and rate for the two life test loading conditions.

For output shaft bearing selection, the bearing force for the two loading levels was determined. This force, F_B, is related to the instantaneous actuator deflection by a spring constant, K_S,

$$K_B = K_S \theta \qquad (25)$$

The spring constant has units of pounds/degree and is the torsional spring constant of the torsilastic load fixture spring (80,000 pound-inch/30 degrees) divided by the output gear pitch radius, R_0, and multiplied by the sine of the gear pressure angle ϕ_p, since the bearing is required to counteract only the radial force on the output shaft. For this high temperature Dynavector actuator design, R_0 = 2.6875 inches (6.826 cm) and ϕ_p, = 25 deg (0.4633 radian). The spring rate is

$$K_S = \frac{80{,}000 \sin (25)}{(30)\ (2.6875)}$$

$$= \frac{(26666.7)\ (0.42262)}{2.6875}$$

$$K_S = 419.34 \text{ lb/deg } (106.87 \text{ kN/rad})$$

The load cycle for each of the two specified levels is summarized by the following equations:

Full Load

$$\theta = 20.446 + 9.554 \sin(\pi t) \quad \text{(deg)}$$

$$\dot{\theta} = 30.0 \cos(\pi t) \quad \text{(deg/sec)}$$

$$F_B = 419.34\,[20.446 + 9.554 \sin(\pi t)] \quad \text{(lb)}$$

One-Half Full Load

$$\theta = 5.446 + 9.554 \sin(\pi t) \quad \text{(deg)}$$

$$\dot{\theta} = 30.0 \cos(\pi t) \quad \text{(deg/sec)}$$

$$F_B = 419.34\,[5.446 + 9.554 \sin(\pi t)] \quad \text{(lb)}$$

The load cycles are plotted in Figures 25 and 26. It was assumed that each loading condition was to be used for one-half of the 250 hours.

In the high temperature Dynavector life test, Phase I was to consist of thermal cycling as well as load cycling. The temperature schedule is shown in Figure 27; the temperature rates of change are assumed linear for simplicity. According to the original statement of work, the actuator was to be thermally cycled 50 times as follows: Starting with an ambient temperature of -40°F (-40°C), this temperature was to be increased to 800°F (427°C) within 15 minutes, maintained at 800°F for one hour, then lowered to -40°F over a one hour period. The remainder of the testing, Phase II, was to be conducted at 800°F or higher.

For estimating the fatigue life of bolts and other motor components, the total number of cycles for which these items must last had to be determined. The output shaft cycle life (30 cycles/minute) (60 minutes/hour) (250 hours) = 450,000 cycles of

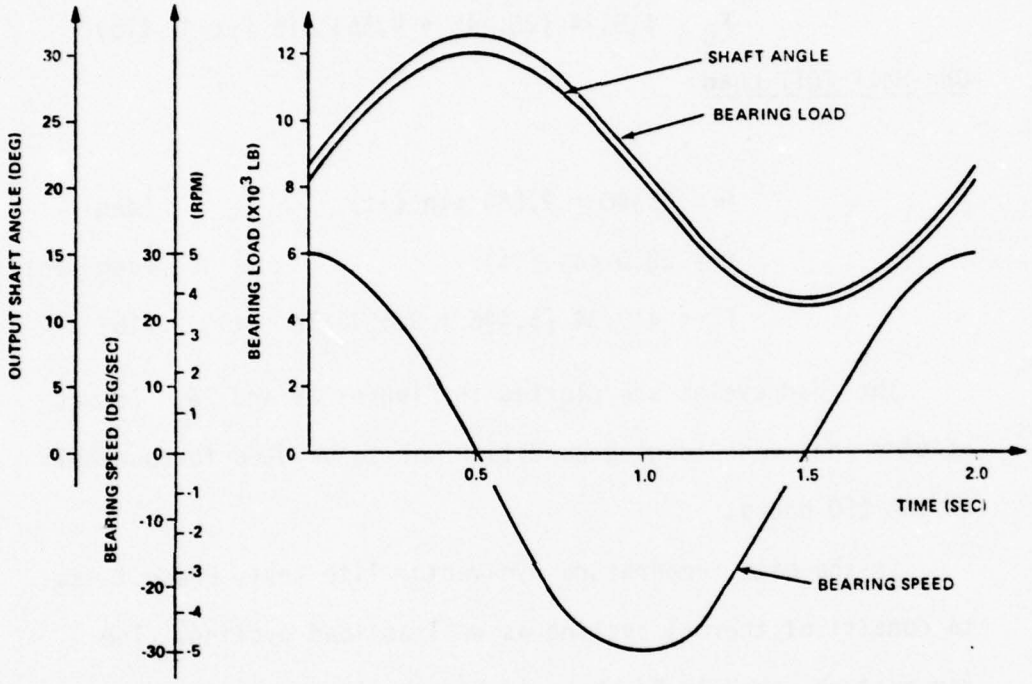

Figure 25. Full Load Cycle Profile, Life Test

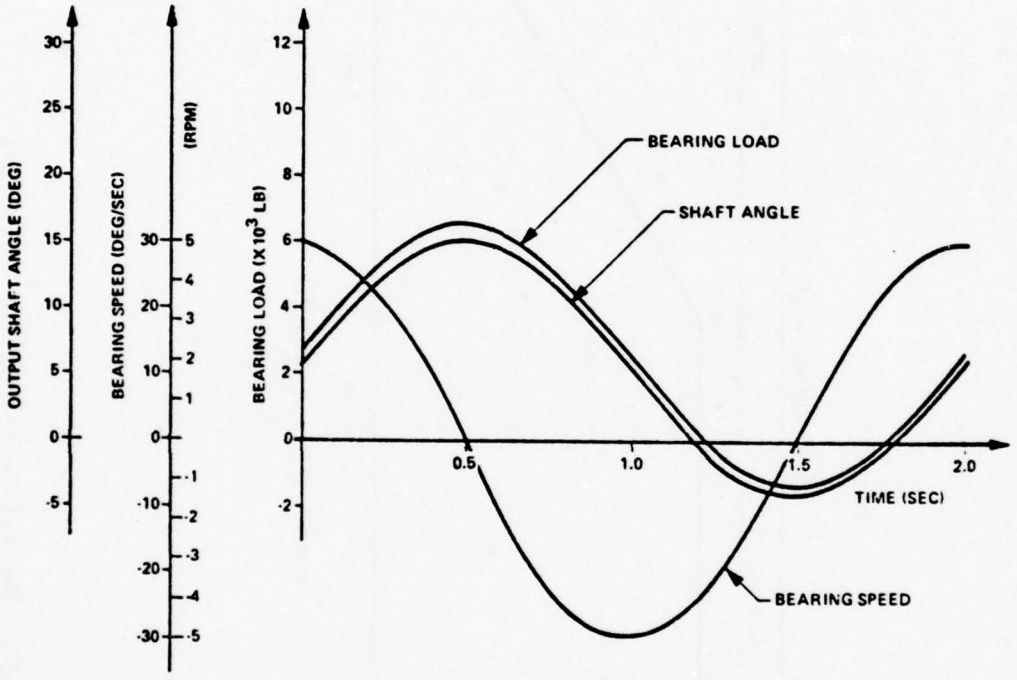

Figure 26. Half Load Cycle Profile, Life Test

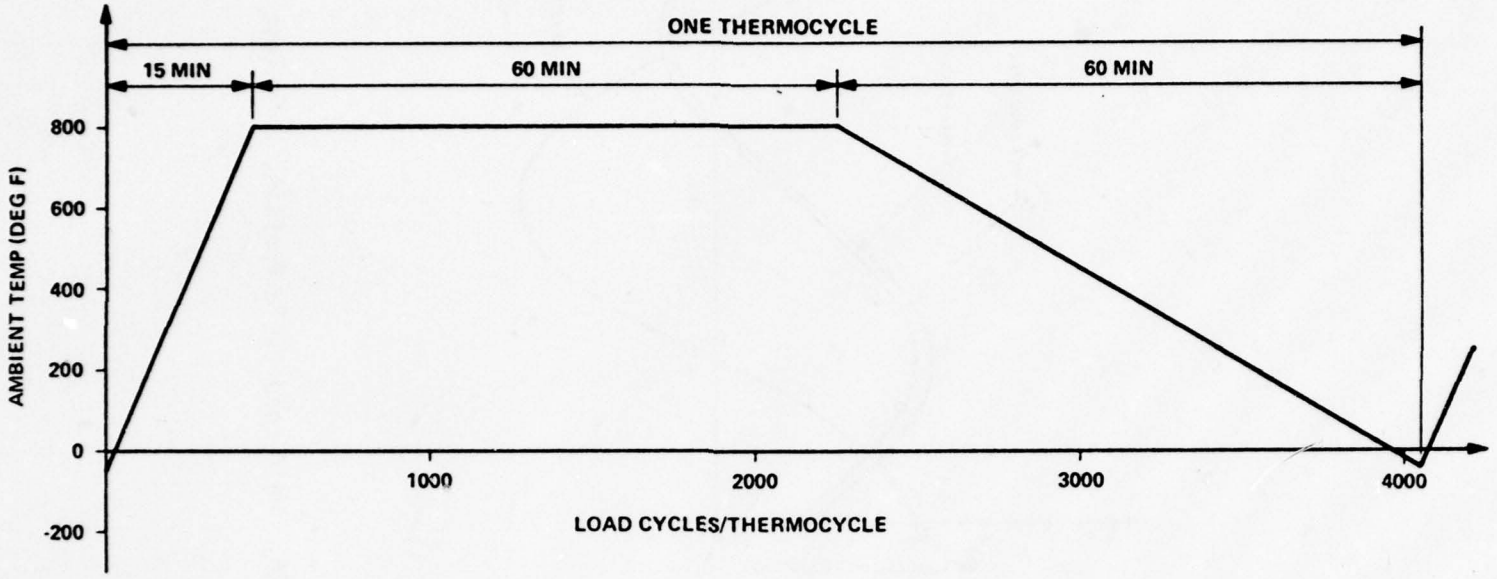

Figure 27. Thermal Cycle Profile, Life Test

peak-to-peak deflection 2(9.554) = 19.108 degrees (0.3335 radian). The motor displacement is equal to the output shaft displacement multiplied by the Dynavector motor transmission ratio (43:1). The motor peak-to-peak displacement is then (19.109) (43) = 821.6 degrees (14.340 radian) or 2.282 cycles/cycle of output shaft rotation and the motor components consequently had to be stressed for (3) (450,000) = 1,350,000 cycles of operation.

All of the foregoing considerations for life test of the high temperature Dynavector motor are summarized in Table 5.

Table 5

Life Test Load Cycle Summary

Max Load	Load Cycles/ Thermocycle	No. Thermo Cycles	Cumulative Load Cycles	Hours
Full Load (Ref. Fig. 25)	4050	25	101,250	56.25
1/2 Full Load (Ref. Fig. 26)	4050	25	101,250	56.25
Phase I Totals		50	202,500	112.50

Discussion of factors leading to materials selection shown in Tables 2 and 3 are as follows:

18 Ni Maraging 350 Steel for Housing Cover and Rotating Parts

Of all the high strength materials available at the time, the Maraging 350 alloy had the highest strength and hardness combined with sufficient ductility to render it an "engineering alloy." For use in heavily loaded aircraft devices, an engineering alloy should have a tensile elongation of about 10 percent before it is considered sufficiently ductile for structural use. The extra hardness to resist galling and

Table 6

Design Properties for Use at Room Temperature

Material Designation	Minimum Hardness at Room Temp (Rc)	Ultimate Tensile Strength (ksi)	Tensile Yield Strength (ksi)	Elongation (% in 4 dia.)	Ultimate Shear Strength (ksi)	E, Modulus of Elasticity, (10^6 psi)	Average Coefficient of Thermal Expansion (10^{-6} in./in. ^{o}F) (0 to 600^{o}F)
350 Maraging (925 F/6 Hrs Age)	56.5	335	325	5.0 Long 3.0 Trans.	190	27	6.3
H-11 Modified (AMS 6487 or 6488)	50-56	280	240	7.0	170	30	6.8
Inconel X-750 (AMS 5698B, Wire under 7/16" Dia.)	-	155	100	20	100	31	7.8
M-2 HSS	64	~450	420 (Bend Test)	~0.01	~250	29.5	6.5
M-50-HSS (AMS 6490)	62	~400	360 (Bend Test)	~0.1	~210	30	7.4
17-4 PH(H-900) (AMS 5643) MIL-C-2411	-	190	170	8	123	28.5	6.1

brinelling, rather than the extra strength was the principle reason for recommending Maraging 350 over the 300 alloy. Among other advantages, it is deep hardening, has a high elastic modulus to limit deflection under load, has a low coefficient of thermal expansion and retains hardness well up to 600°F (316°C) and 800°F (427°C). It age hardens with a simple heat treatment, 3 hours at 950°F (510°C) in air and slow cool, that minimizes distortion and has a predictable shrinkage of 1 mil per inch (0.001 cm/cm) during hardening. Because of the predictable shrinkage, finish machining can be virtually eliminated or converted to a "dust" grind or light lap for final fit. An alternative combination heat treatment (48 hours at 875°F) (468°C) both hardens and nitrides a case with the same predictable shrinkage. It can be welded and brazed. Nitrided gear teeth achieve maximum surface wear resistance with a tough core.

No other alloy offered all of these benefits at the time of selection.

On the negative side, Maraging 350 was a new alloy, not at the time listed in MIL-HDBK-5B, and was fairly expensive. Earlier lots of Maraging steels were troubled with banding segregation, but that was believed to have been cured. Finally, the 350 alloy is notch sensitive to some degree.

Alternative alloys included the other maraging grades, 300 and 250, which differ from 350 primarily in hardness and yield strength, and a Modified H-11 tool steel such as Vascojet 1000 (AMS 6488).

Tables 6 and 7 list the design properties of the various materials at room temperature and 600°F, respectively.

Modified H-11 for Manifold Plates

This alloy competes with Maraging 350 in hot hardness, but is not quite as strong. Also, it can be further hardened by nitriding.

Table 6

Design Properties for Use at Room Temperature

Material Designation	Minimum Hardness at Room Temp (Rc)	Ultimate Tensile Strength (ksi)	Tensile Yield Strength (ksi)	Elongation (% in 4 dia.)	Ultimate Shear Strength (ksi)	E, Modulus of Elasticity, (10^6 psi)	Average Coefficient of Thermal Expansion (10^{-6} in./in. °F) (0 to 600°F)
350 Maraging (925 F/6 Hrs Age)	56.5	335	325	5.0 Long 3.0 Trans.	190	27	6.3
H-11 Modified (AMS 6487 or 6488)	50-56	280	240	7.0	170	30	6.8
Inconel X-750 (AMS 5698B, Wire under 7/16" Dia.)	-	155	100	20	100	31	7.8
M-2 HSS	64	~450	420 (Bend Test)	~0.01	~250	29.5	6.5
M-50-HSS (AMS 6490)	62	~400	360 (Bend Test)	~0.1	~210	30	7.4
17-4 PH(H-900) (AMS 5643) MIL-C-2411	-	190	170	8	123	28.5	6.1

Table 7

Design Properties for Use at 600°F

Material Designation	Minimum Hardness at Room Temp. (Rc)	Ultimate Tensile Strength (Ksi)	Tensile Yield Strength (ksi)	Elongation (% in 4 dia.)	Ultimate Shear Strength (ksi)	E, Modulus of Elasticity, (10^6 psi)	Average Coefficient of Thermal Expansion (10^{-6} in./in, °F) (0 to 600°F)
350 Maraging Steel (925 F Age, 6 Hours)	56.5	300	290	5.0	170	24.3	6.3
H-11 Modified (AMS 6487 or 6488)	50-56	238	206	7.0	154	27.3	6.8
Inconel X-750 Wire under 7/16" Dia.)	-	141	86	20	90	28.2	7.8
M-2 High Speed Steel	64	360	336	~0.01	~196	~27	6.6
M-50 High Speed Steel	62	335	302	~0.1	~184	~27	7.4
17-4 PH (H900)	-	160	140	8	94	24.8	6.1

A principle disadvantage is that H-11 requires an air quench from between 1800° and 1900°F (982° and 1038°C) with accompanying size changes and scaling to achieve through hardening. This is followed by a tempering cycle between 1000° and 1080°F (538° and 582°C) depending upon the strength and ductility needed. An allowance for finish machining is always required.

Both the Maraging steels and the H-11 steel are weldable and can be brazed or diffusion bonded to fabricate the manifold plate.

M-50 Alloy for Bearings

Of the high temperature bearing materials suitable for use at 600°F (316°C), M-50 semi-high speed steel has about the highest hot hardness. Alternative alloys include 440 C stainless steel and BG-42 or other improved forms of 440 C. The bearing manufacturers seemed to be comfortable in working with M-50 and it was more readily available in vacuum-melted form than some other alloys that may have been about as good.

M-2 High Speed Steel for Thrust Washers and Vanes

The very high surface hardness of high speed steel made it attractive for small wear parts such as these which are heavily loaded, but almost entirely in compression. A dry film lubricant (nitriding-sulfiding process) was applied to these parts to reduce friction.

Modified H-11 for Fasteners

The aircraft fastener industry (Voi Shan, SPS, Hi Shear, etc.) has developed qualified Mil-standard fasteners in many alloys. H-11 was the best choice among common fastener alloys suitable for use at 800°F (427°C), because it most closely matches the thermal expansion rate of the Maraging 350 alloy used for actuator structure and spacers.

The comparatively small diameter fasteners were preloaded so that neither differential thermal expansion nor thermal gradients removed the preload nor overloaded the bolts and studs.

Inconel X-750 Alloy for Decoupling Piston Springs

Inconel X-750 was selected since it is a superior spring alloy at 800°F (427°C) and above.

17-4 PH Alloy for Static Seals

Commercially available metallic seals (Parker 8800 and 8900 series, as well as other makes) uses 17-4 PH, Inconel X-750 and other alloys to maintain spring tension. Soft silver plate on the mating surface conforms to minor surface irregularities and reduces leakage. Elastomeric seals were considered marginal at 500°F (260°C) and above in oil.

e. Rotary Shaft Seals

The development of a satisfactory high temperature shaft seal was considered as a critical item for the program. Consequently, a survey was undertaken to evaluate the available seal technology and to recommend a seal design and a seal material for a seal test that would limit leakage to one drop per minute for 1,000 hours in MIL-H-27601 fluid in an environment of -40° to 800°F (-40° to 427°C).

As reported [2], the survey effort included:

- Review of recent USAF and NASA seal development programs.

[2] Van Ausdal, R.K.
Seal Survey Report
Report 7-3133
Bendix Electrodynamics Division, Bendix Corp.
July, 1972

- Review of past Bendix and Convair seal projects.
- Solicitation of seal manufacturers applicable designs.
- Determination of applicable seal cost and availability.
- Generation of special seal designs.
- Review of recent seal development literature.
- Determination of applicable elastomeric and polymeric materials.
- Selection of promising seal configurations.

Based on the survey results, three configurations for seal design, as recommended [2], were selected for fabrication and testing. One configuration was a circumferential type seal using polymide resin Vespel 21 (graphite filled) shown in Figure 28. The second configuration was lip type seal using an alloy of teflon and Ekonol (aromatic polyester) called Fluoroloy K. This second configuration is shown in Figure 29. The last seal configuration, shown in Figure 30, was a face-type seal, using carbon graphite sealing against a chrome-plated 18 Ni 350 maraging steel. The bellows used to load the face-type seal was also made of 18 Ni 350 maraging steel. In all three seal configurations, the static seals required were silver plated, 17-4 PH corrosion resistant steel. Photographs of the three seals (Figures 6 through 11) have been previously shown in Section II, Summary.

f. Cooling and Heat Transfer

During operation, the prototype actuator was designed to be cooled with the servo valve exhaust flow. This flow enters the actuator through the coolant inlet port. The coolant flow is conducted through all internal spaces in the actuator. Particular

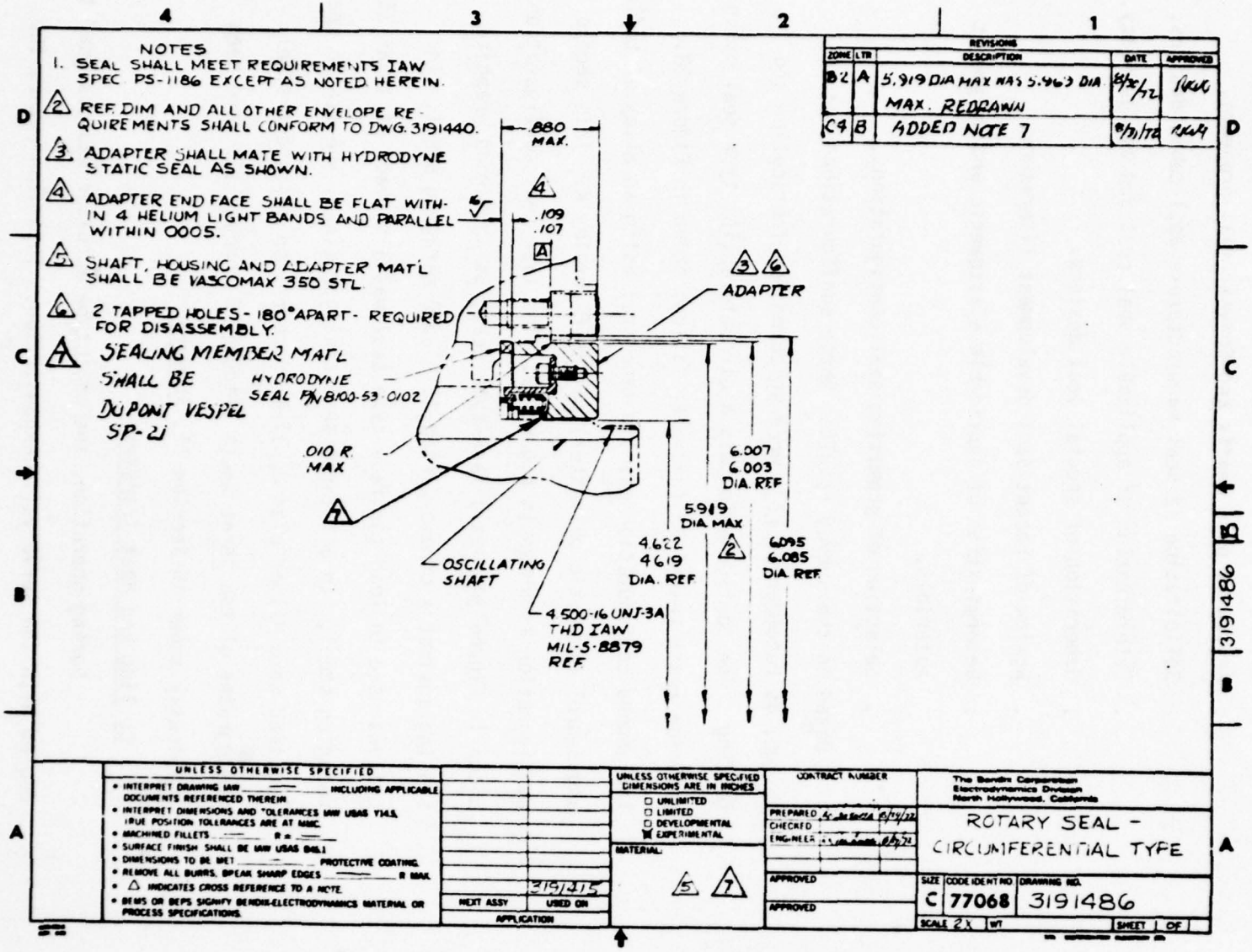

Figure 28. Circumferential Type Rotary Seal

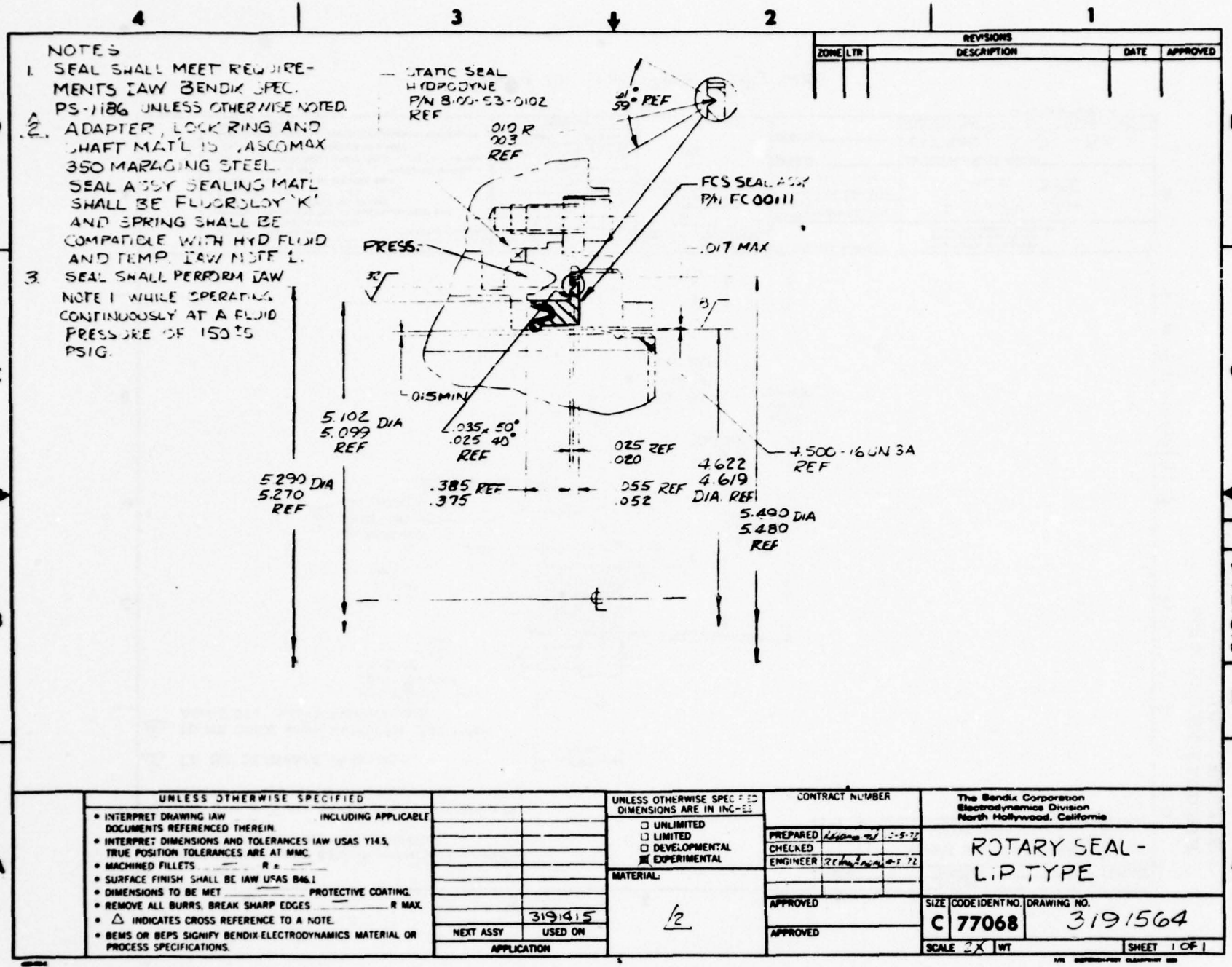

Figure 29. Lip Type Rotary Seal

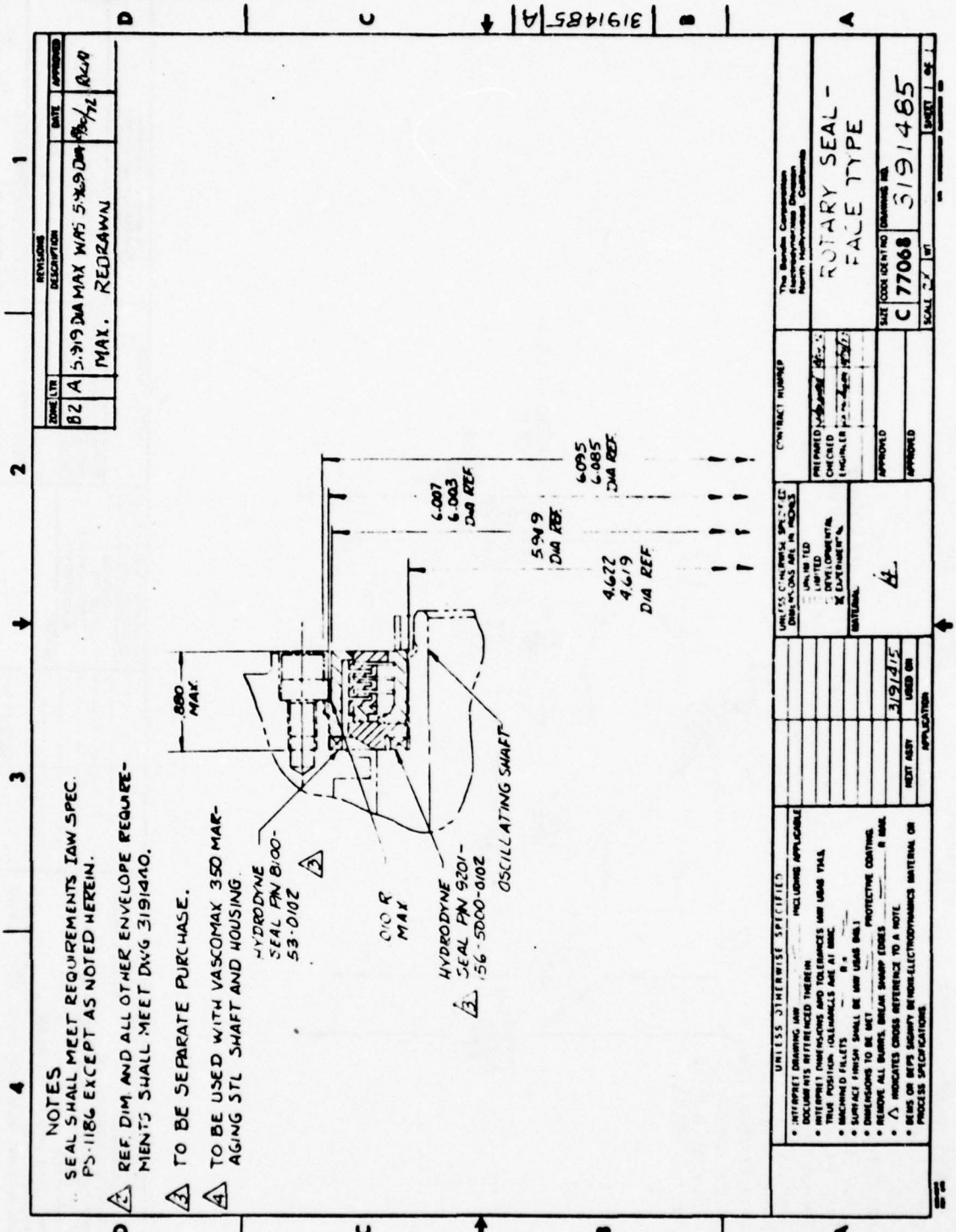

Figure 30. Face Type Rotary Seal

emphasis was placed on assuring a positive flow of the coolant through the bearings and around the shaft seal. Care was also taken to ensure that coolant would flow through all actuator internal volume to minimize the residence time of the working fluid in the actuator. To the greatest extent possible, the coolant is used to minimize the flow of heat into the actuator from the high temperature environment.

The hydraulic fluid (MIL-H-27601A) is used as the coolant fluid in the cooling circuit represented by Figure 31. The cross section of the actuator is shown in Figure 32, with flow paths numbered to correspond to the element blocks of Figure 33.

Since all three modes of heat transfer will be present in the actuator, a mathematical network was established and solved for nodal temperatures. The temperatures were obtained for boundary conditions defined by either fixed temperature or heat inputs and based on geometrical factors and thermal resistances established by the heat transfer modes. Assumptions used in the heat transfer analysis were:

1) Steady state operation with an environment temperature of $800^{o}F$ ($427^{o}C$).
2) All surface nodes exposed to thermal radiation have an emissivity equal to 1.0 and a view factor to the environment equal to 1.0.
3) Cooling fluid node temperatures were assumed at a single fixed value throughout the model.
4) Fixed internal actuator nodes were fixed at the same temperature as the cooling fluid.

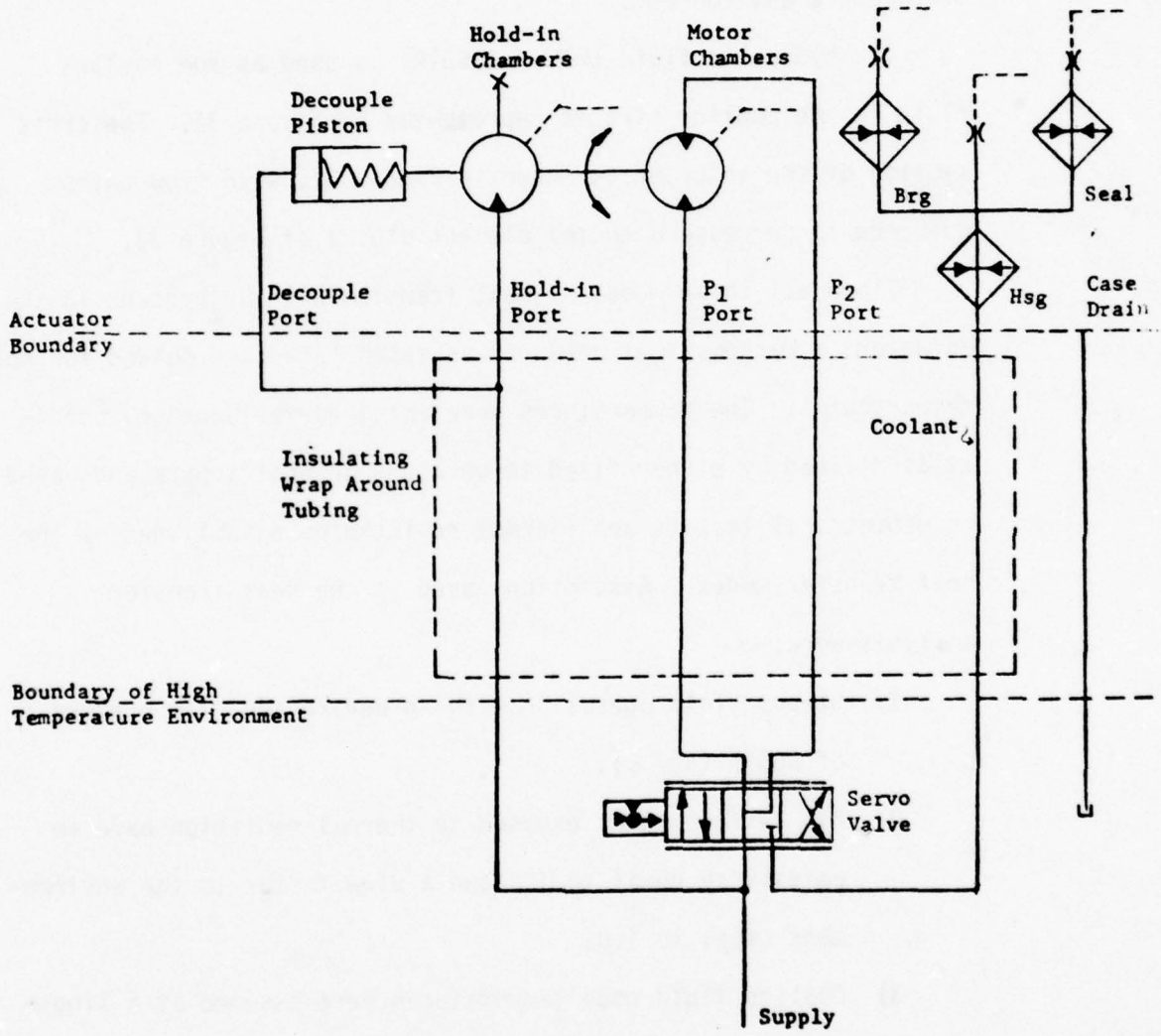

Figure 31. Cooling Circuit Schematic for High Temperature Rotary Actuator

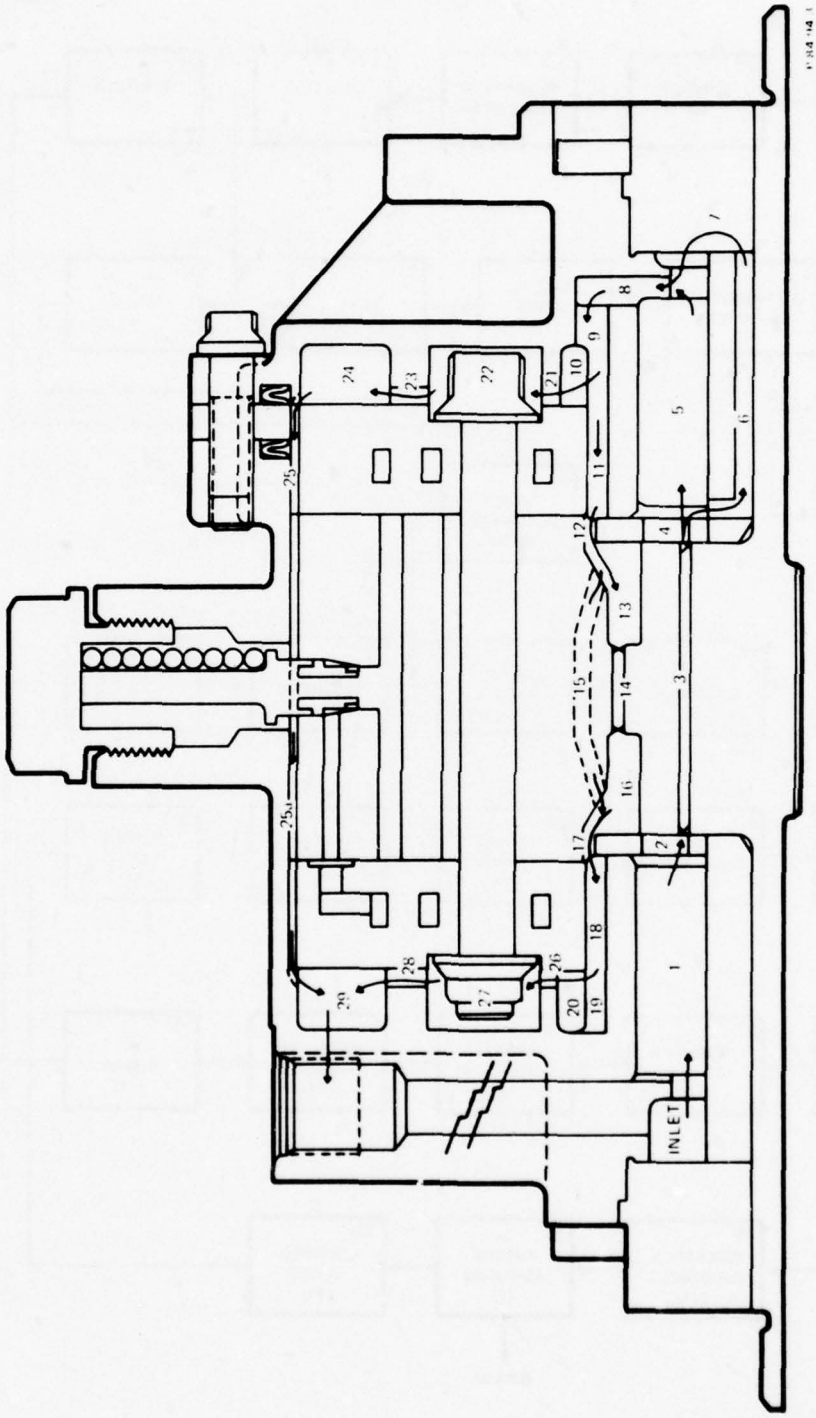

Figure 32. Actuator Cross Section (Partial) Showing Cooling Flow Paths

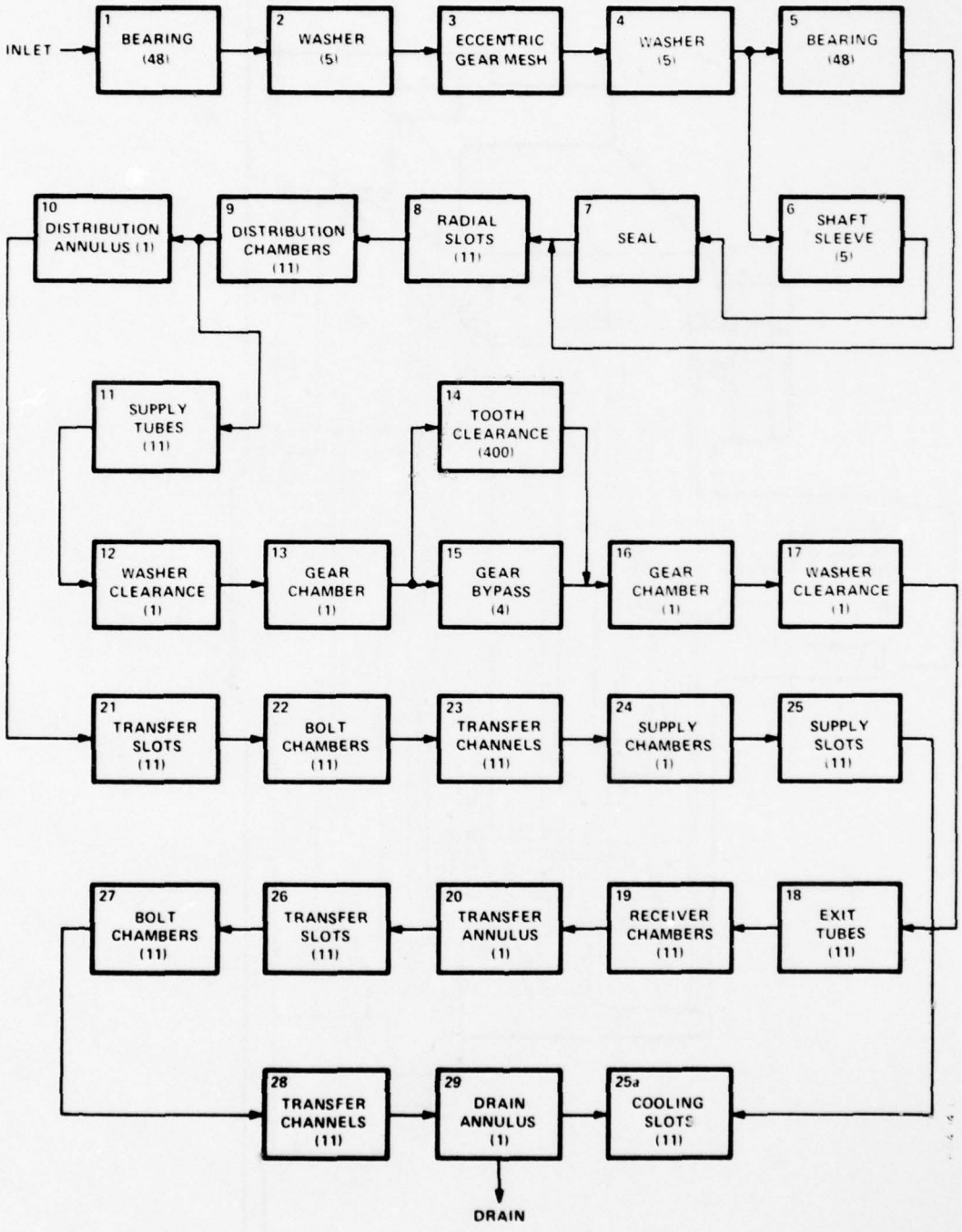

Figure 33. Block Diagram of Cooling Flow Paths

Conclusions reached as a result of the heat transfer analysis were:

1) Overall pressure drop through the actuator for the cooling flow would be approximately 1 psi (6.9 KN/m^2) for a flow rate of 3 gpm (11,356 cc/mm) for 30 degrees/second (0.52 rad/sec) output speed based on the Hagan-Poiseville law ($Q = \pi D^4 \Delta P/128 \mu L$).
2) About 61 percent of the flow would occur near the exterior surfaces of the actuator and directly remove the environmental heat load.
3) Environmental heat loads would be absorbed by this 3 gpm flow with a 16^oF (8.9^oC) temperature rise for the 200^oF (93.3^oC) fluid and a 11^oF (6.1^oC) rise for the 450^oF (232^oC) fluid.
4) The remaining 39 percent of the flow would cool the interior of the actuator.
5) Environmental heat would go directly into the fluid, as the addition of insulation or modifications of the actuator design only causes local temperature changes.
6) The temperature of actuator exterior structure would be only slightly higher than the cooling fluid.
7) No major temperature problems were expected if sufficient fluid flow is provided and the inlet fluid temperature is below 450^oF (232^oC).

3. TEST FIXTURES

a. Motor and Actuator Test Fixtures

The motor cartridge test fixture, shown in Figure 34, is in the form of a pedestal on which the motor cartridge test assembly is mounted. Within the pedestal is contained a torque cell with a speed pickup and a hydraulic motor (Char Lynn 3006) which is operated as a pump and used to load the actuator. With this test fixture, motor torque-speed curves were plotted on an X-Y recorder. Installation of flowmeters and pressure pickups on the motor cartridge test assembly permitted the taking of data on flow-speed and other important motor performance characteristics under steady-state conditions.

The test fixtures for the motor cartridge test assembly and the prototype actuator, referenced in Figure 35, were designed to have the maximum commonality of parts. The output torque of the prototype actuator was taken up by a Torsilastic spring which replaced the torque cell and the load motor in the motor cartridge test fixture. In the motor cartridge test fixture, the reaction path was through the outer housing; in the prototype actuator test fixture, the reaction torque was taken up by a tube concentric to the outer housing in which the Torsilastic spring was inserted. The function of the outer housing when the test fixture was in the high torque configuration was to contain the water used to cool the Torsilastic spring during high temperature testing.

A potentiometer was installed underneath the prototype actuator test fixture. This permitted actuator displacement to be measured. Since the torque-displacement characteristics of the Torsilastic spring were known, this also permitted an instantaneous torque measurement to be made. An adjustable cam was driven from the same shaft

THIS PAGE IS BEST QUALITY PRACTICABLE
FROM COPY FURNISHED TO DDC

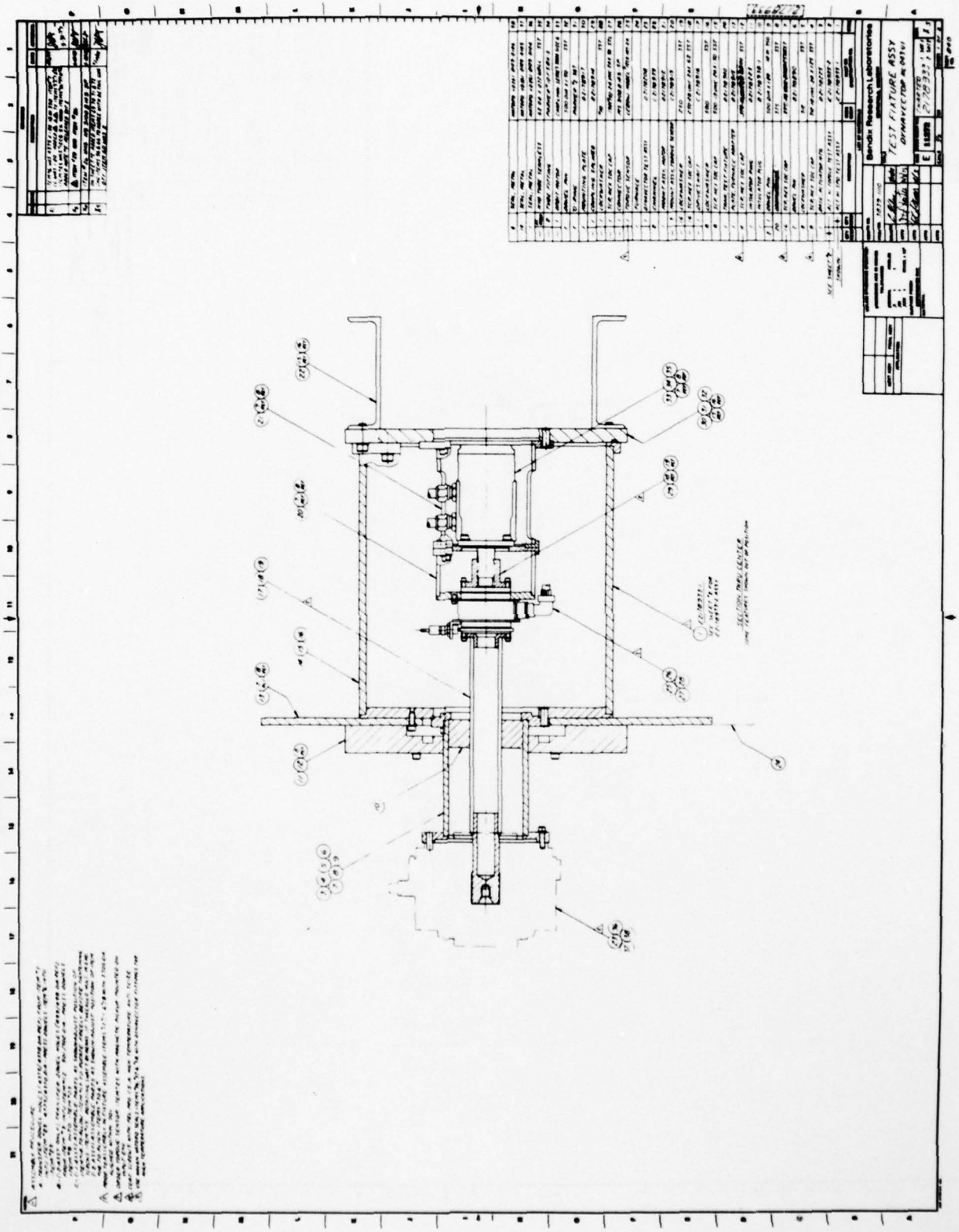

Figure 34. Motor Cartridge Test Fixture

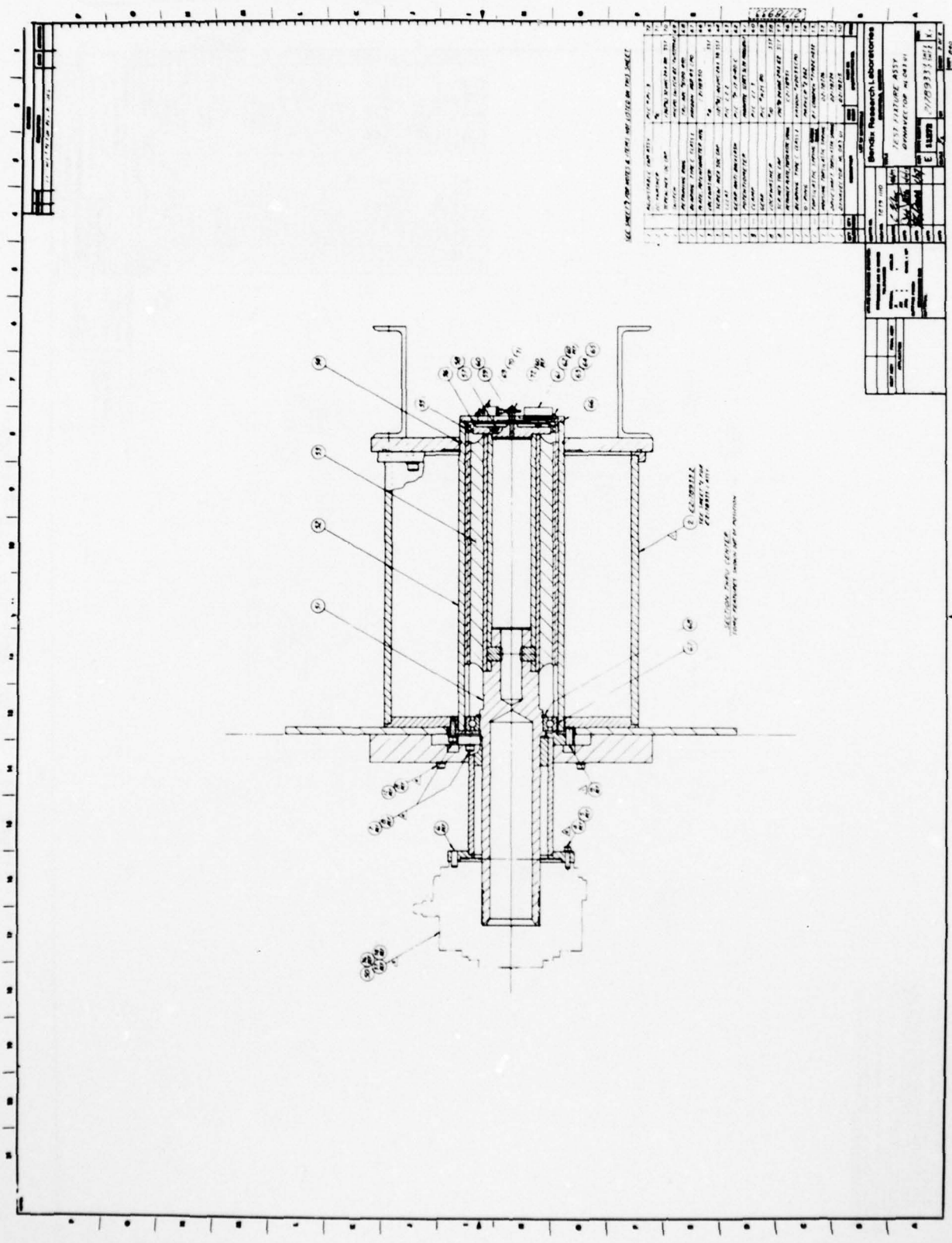

Figure 35. Prototype Actuator Test Fixture

as the potentiometer. This was set to actuate a limit switch and thus shut the system down, if a greater than desired actuator displacement occurred in either direction.

To provide the heat input and environmental control for the -40° to 800°F (-40° to +427°C) ambient temperature and the -40° to +600°F (-40° to 316°C) fluid temperature, the infrared oven and insulating chamber used for the seal tests, as shown in Figure 36, were to be used. The sliding glass panels on the insulating chamber were to be replaced with insulating panels during application of CO_2 for cold temperature. For high temperature the solid panels were to be removed, the glass panels inserted, and the mobile oven moved to envelop the chamber, as done in the seal tests. Automatic on-and-off control of the oven was to be effected through the use of a thermocouple suspended in the chamber to determine the amount of heat transmitted to the actuator through the glass and ambient air. Heat transmission through the actuator was to be the only source of heating for the fluid. A cooler in the hydraulic fluid circuit was included in the best arrangement to prevent the fluid temperature exceeding +600°F (316°C). However, because of performance limitations of the motor and actuator (discussed in Section VII SUMMARY OF TEST RESULTS) the maximum operating temperature of the fluid was reduced to +275°F (+135°C). Consequently, the environmental chamber and infrared oven were not used for the motor tests. Instead the laboratory MIL-H-5606, high temperature fluid test equipment was used.

b. Shaft Seal Test Fixture

To simulate the seal installation envelope for testing, a test fixture design was evolved, as shown by Figure 37. The design configuration

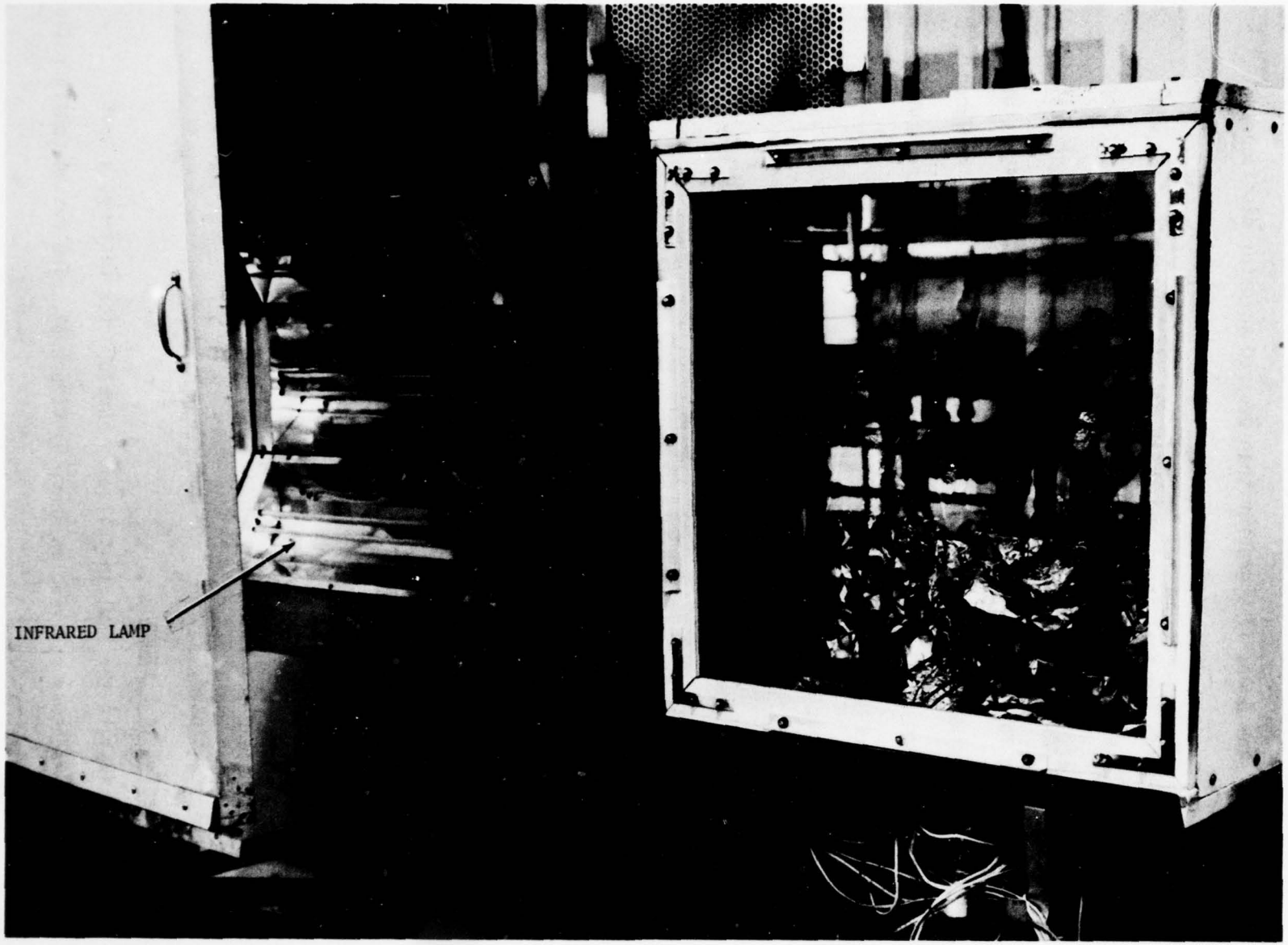

Figure 36. Insulation Box and Infrared Oven

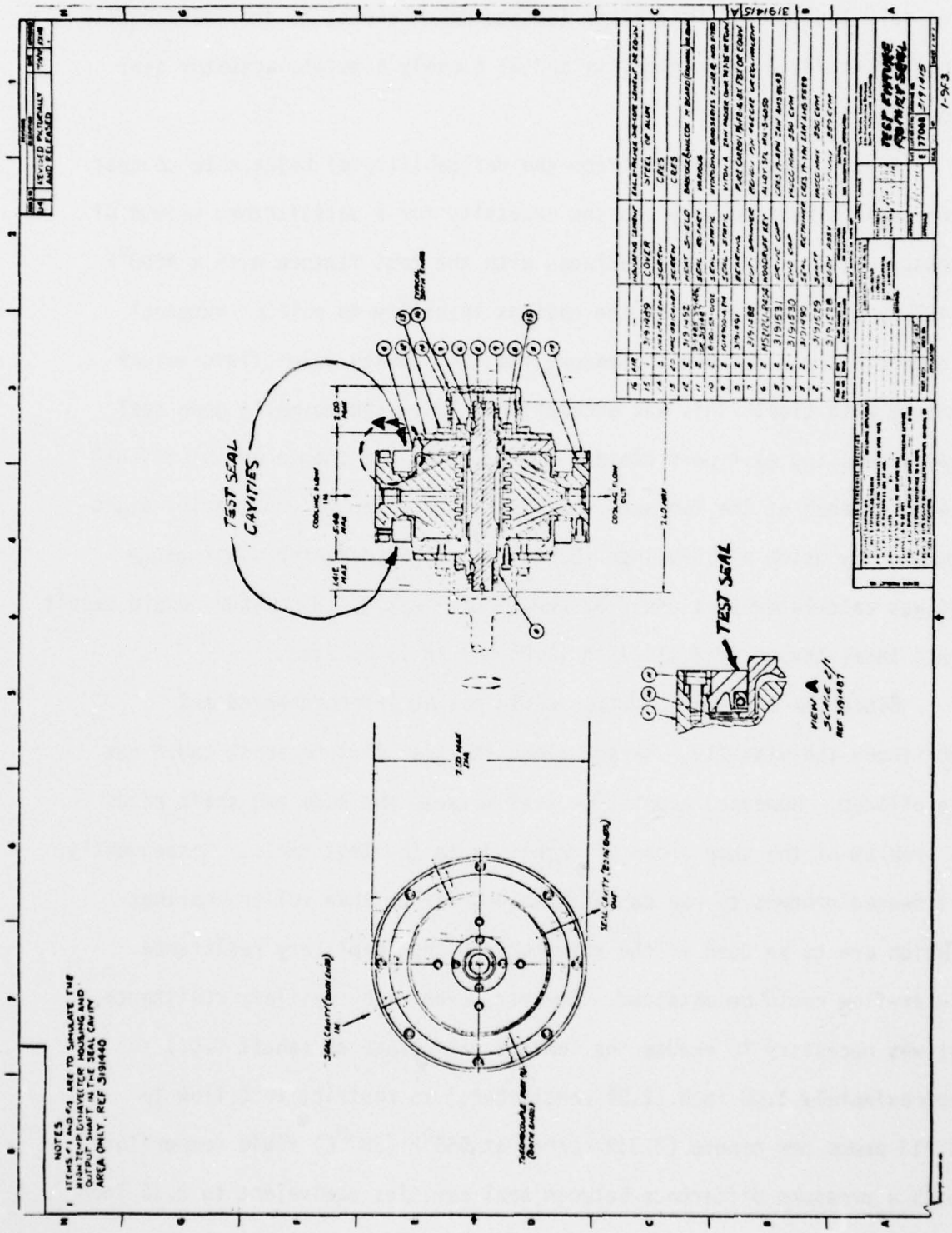

Figure 37. Rotary Seal Test Fixture

was selected to: 1) Facilitate leakage measurement; 2) provide adequate cooling fluid; 3) reduce costs; and 4) closely simulate actuator seal envelope.

Fixture design evolved from the desirability of being able to test two seals simultaneously and the necessity for a satisfactory method of measuring very small seal leakages with the test fixture with a +800°F (427°C) environment. With the obvious inability to collect external leakage, it was decided to measure the seal cavity inlet fluid volume change with time. This was accomplished (with the normally open seal cavity cooling exit port closed) by recording the change of inlet fluid level in each of the two seal cavities as observed in each cavity sight gauge. By using a 0.375 inch (0.953 cm) inside diameter sight gauge it was calculated that one drop per minute leakage (3 cc/hour) would result in a level change of 0.415 inch (1.05 cm) in 15 minutes.

Since the two seal cavities could not be interconnected and monitored individually, leakage along the test fixture shaft could not be allowed. However, a positive seal between the body and shaft posed a problem of the same order of magnitude as the test seals. Consequently, it seemed prudent to use carbon bushings rather than roller bearings (which are to be used in the actuator) so that capillary resistance inter-flow could be obtained. However, even with capillary resistance, it was necessary to reduce the leakage path diameter (shaft O.D.) to approximately 1.00 inch (2.54 centimeters) to restrict interflow to 0.113 drops per minute (0.339 cc/hr) at 550°F (287°C) fluid temperature with a pressure difference between seal cavities equivalent to 0.10 inch (0.254 centimeters) head difference. To further reduce this leakage, standard flanged bushings were selected as the shaft bearings. This

configuration provided two additional capillary resistance path in series with the paths along the shaft diameter; see Figure 38. With reasonable form tolerances and end loading between the end cap and flanged bushing thrust surfaces, inter-cavity leakage was expected to be negligible.

The fixture configuration adopted provided another advantage in that the end cap, which simulated the actuator output shaft and seal interface, was a separate part for each seal which was assembled and locked to the shaft. This provided the capability of easy replacement if the end cap sustained damage at the sealing interface, or a dimensional change was desired. This construction, along with availability of relatively low cost standard bushings, contributed to reducing fixture fabrication costs.

Material selection for the critical parts of the fixture that could affect the seal envelope and performance was the same as planned for the actuator - 18 percent nickel-cobalt-molybdenum maraging steel with a 350 KSI (2413 MN/m^2) ultimate tensile strength. These critical parts are the body assembly, shaft, and end caps. Materials for the remaining parts were selected for availability, cost and compatibility with the critical parts, fluid, and environment. Figures 39 and 40 show the assembled fixture and the components, respectively.

The Rotary Seal Drive Fixture (illustrated by Figure 41) provided the oscillatory input motion for seal testing and is shown in Figure 42. In this photograph, the insulating box on top of the fixture (in which the seals and test fixture are located) is in the cold temperature configuration. For high temperature testing, the insulating box configuration was modified by replacement of the sliding side panels

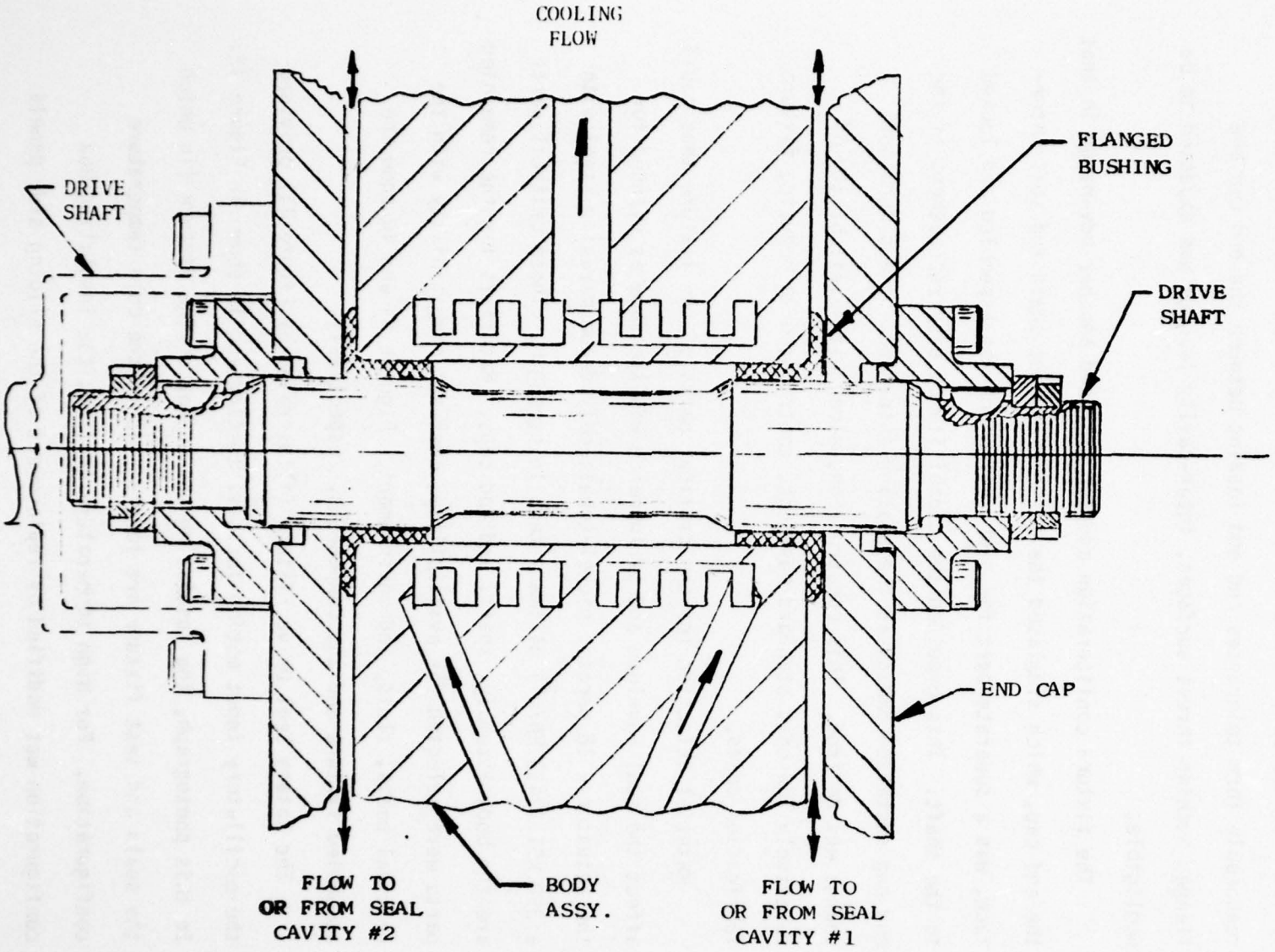

Figure 38. Shaft and Bushing Configuration

Figure 39. Rotary Seal Test Fixture

Figure 40. Rotary Seal Test Fixture Parts (Not Including Seals)

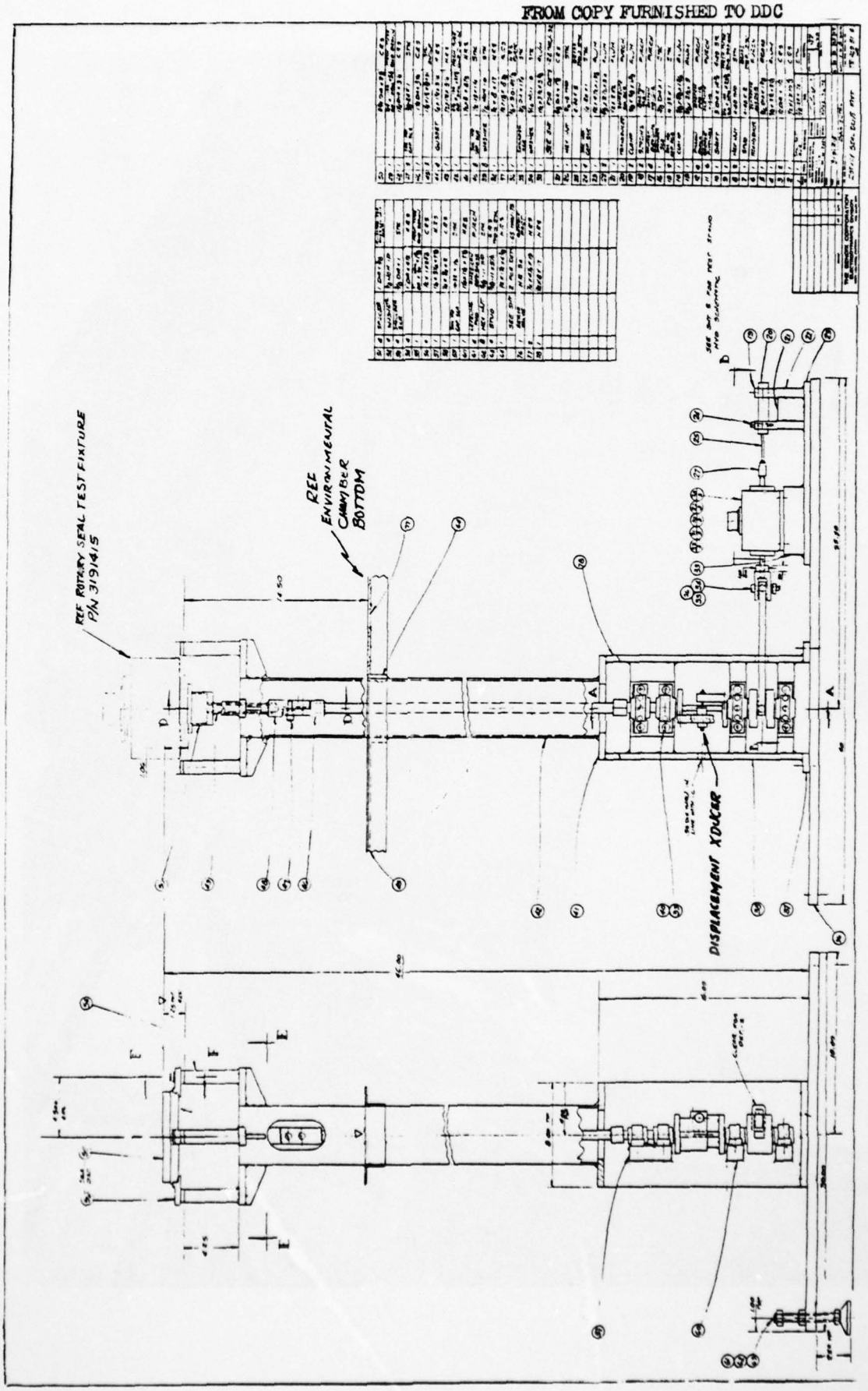

Figure 41. Rotary Seal Drive Fixture

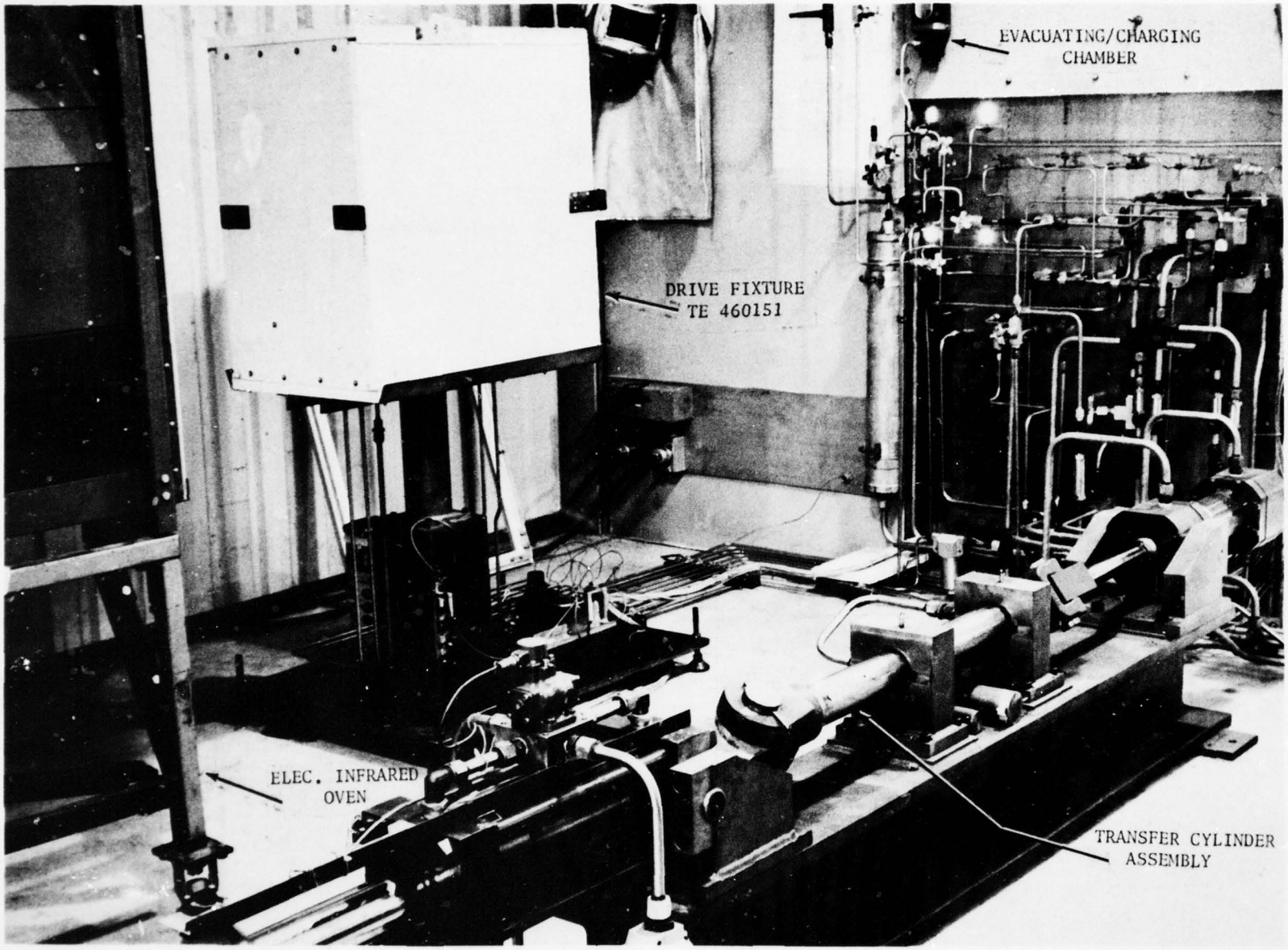

Figure 42. Seals Test Arrangement

AD-A057 931 BENDIX CORP NORTH HOLLYWOOD CALIF ELECTRODYNAMICS DIV F/G 13/7
DEVELOPMENT OF A HIGH TEMPERATURE ROTARY ACTUATOR FOR AIRCRAFT --ETC(U)
MAY 78 R K VAN AUSDAL F33615-72-C-1187

UNCLASSIFIED AFAPL-TR-78-26 NL

2 OF 3
ADA
057931

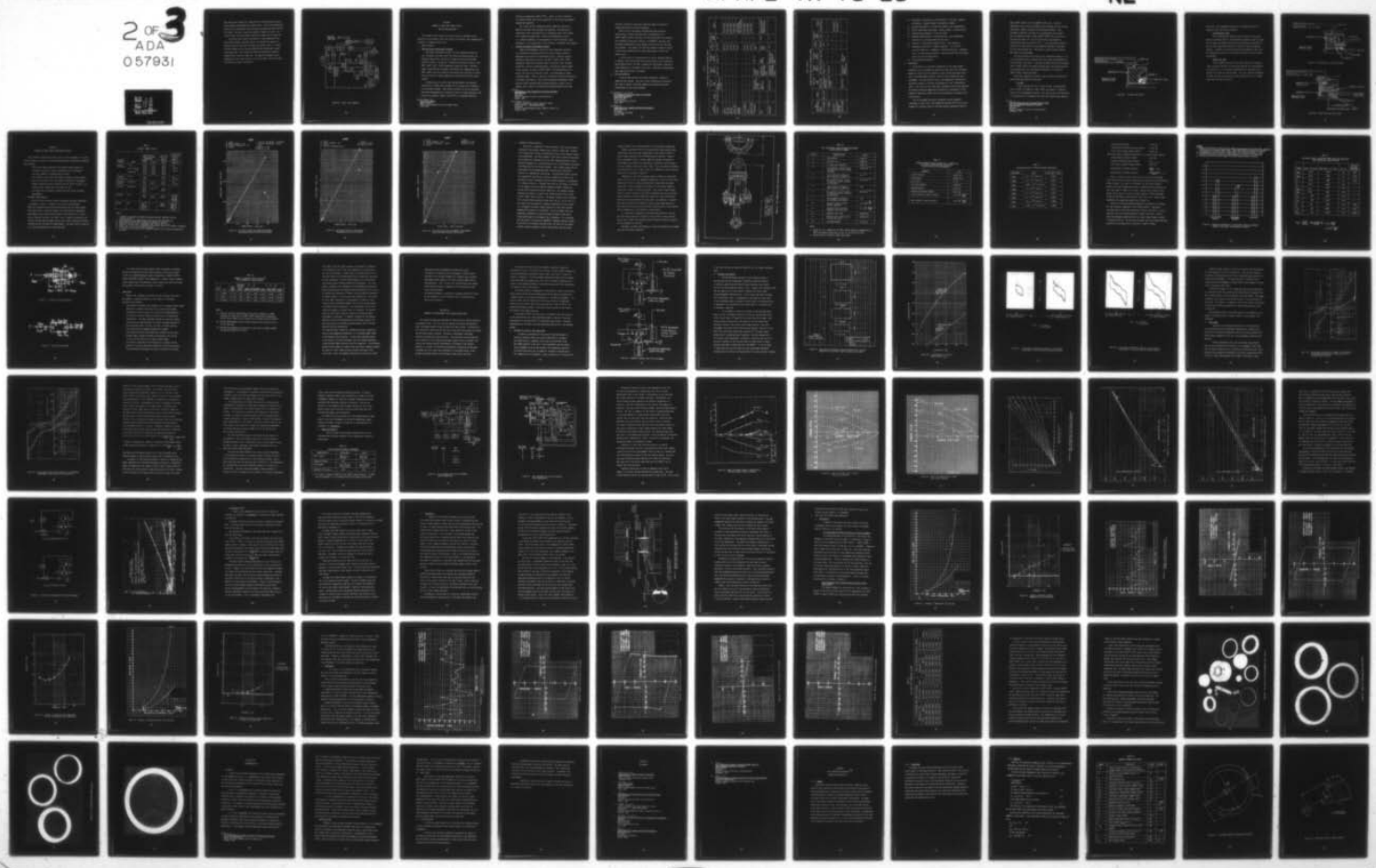

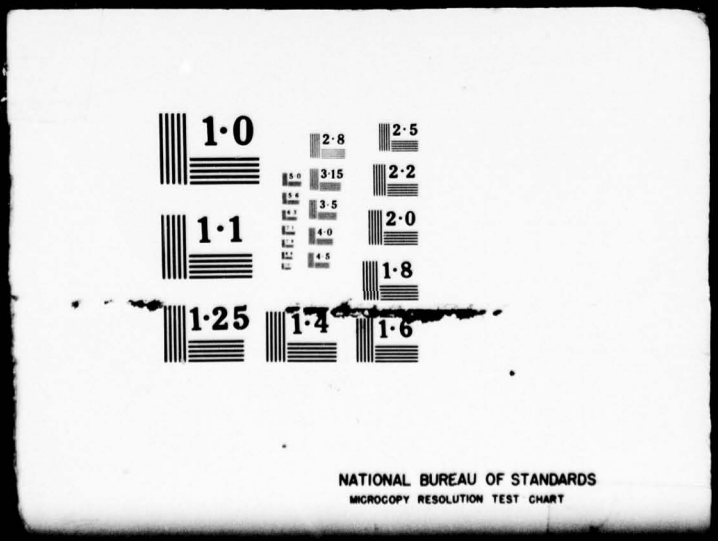

with double pane windows for transmission of infrared energy supplied by the movable high temperature electric oven. During high temperature testing, the insulating box was continuously purged with carbon dioxide for safety. The oven is partially shown in Figures 42 and 36. The insulating box with the windows installed is shown also in Figure 36.

To minimize and conserve the quantity of high temperature test fluid (MIL-H-27601A) required, as well as eliminate the need for a 4000 psig pump for the motor cartridge and actuator tests, a transfer cylinder assembly and an existing 3000 psig MIL-H-5606 power supply system were used. The transfer cylinder was designed to intensify pressure and is shown in Figure 42. The piping arrangement using a combination of four check valves to allow continuous flow to the seals test fixture is shown in Figure 43.

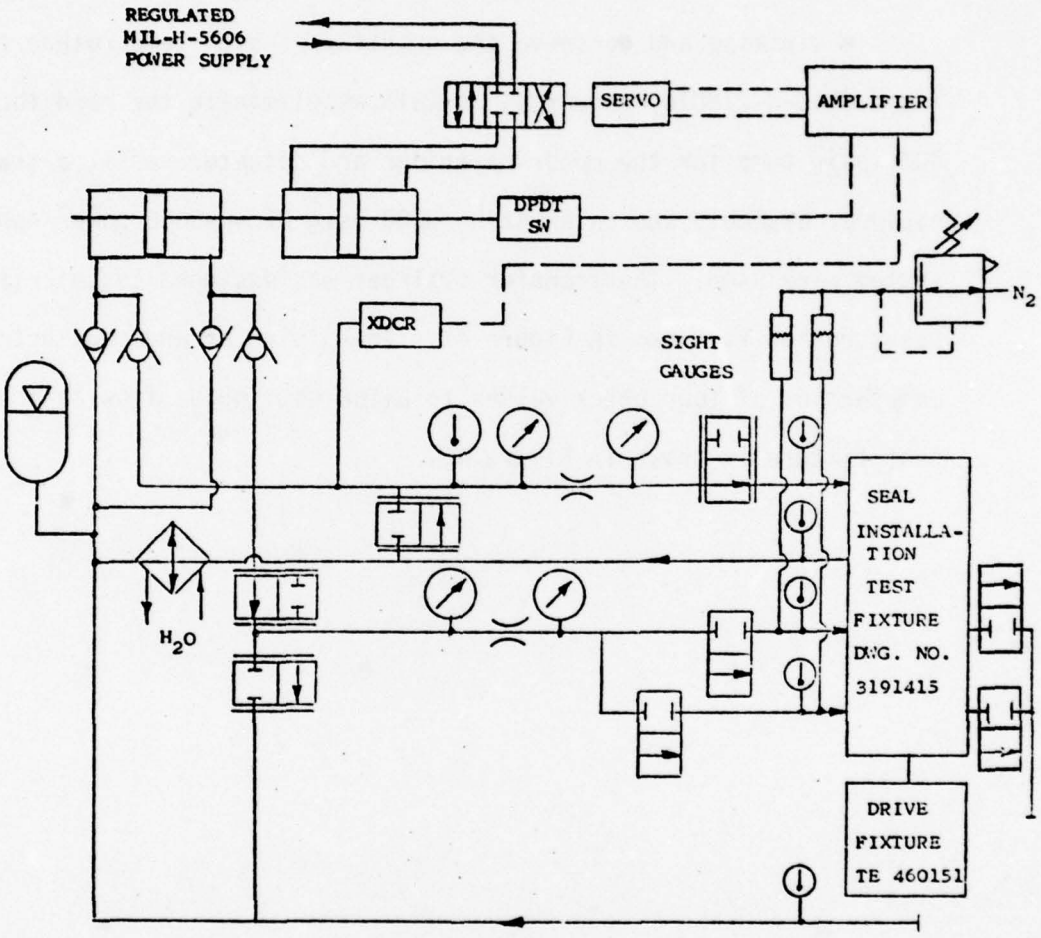

Figure 43. Seals Test Schematic

SECTION V

SUMMARY OF SHAFT SEAL SURVEY RESULTS AND DESIGN EVALUATION

This summary of the shaft seal survey, which was conducted in the beginning of the program, covers the results, conclusions, and recommendations included in a separate report, [2].

1. SURVEY RESULTS

a. USAF and Convair Development Programs

The search conducted by Convair for high temperature hydraulic seal information was made within the Production Design Section, The Research Laboratories, the Division Research Library and the VSMF Microfilm Library. No specific information applicable to seals in the 600^{o} - 800^{o}F (316^{o} - 427^{o}C) temperature range was found. Available reports indicated that elastomers are effective at temperatures up to 450^{o}F (232^{o}C), and that materials and designs were available in radial-face type seals for higher temperatures than required for the current program.

Information was also solicited from the Material and Research Laboratories at WPAFB, NASC and NASA but it provided little substance for the present program. NASA reports available at Convair Aerospace described development work on hydraulic seals for linear actuators, both primary and secondary stages, with 400 PSI (27.58 MN/m^2) operating

[2] Van Ausdal, R.K
Seal Survey Report
Report 7-3133
Bendix Electrodynamics Division, Bendix Corp.
July, 1972

pressure at temperature 350°F (177°C). Again, no plastic materials or suitable designs specifically applicable to the current development program were apparent.

As a result of the information search, potential sources for materials and seals were obtained and contacted. Manufacturers of conventional seals were generally not interested unless their product line included face type seals. Materials manufacturers, such as E. I. DuPont de Nemours, The Carborundum Co. and Olin Chemical, were interested in the application of their products to potential seal designs.

b. Industry and Bendix Development Programs

Bendix Electrodynamics' search for high temperature hydraulic seal information was made within the Division's Dynamic Controls Department and the Division Engineering Library. While no specific information applicable to seals in the 600° - 800°F (316° - 426°C) temperature range was discovered, report literature, [3], indicates successful testing of polyimide plastic, low pressure (second stage) linear actuator rod seals at 500°F (260°C) fluid temperature for as long as 937 hours and 18 million cycles. A bibliography of recent literature (1965 - 1971) on seals was included [2], along with abstracts of eleven of the reports. While the bibliography represented a small portion of the literature that has been generated on seals, one of reports, [4], contains an extensive bibliography compiled from 1100

[3] Lee, J.
Development of High Temperature Polyimide Rod Seals
NASA CR-72563
N70-10905
Republic Aviation Division, Fairchild-Hiller
August, 1969

[4] Findlay, J.A. et al
"Study of Dynamic and Static Seals for Liquid Rocket Engines", Seals Design Guide
N70-26148
Research and Development Center, General Electric Co.
January, 1970

abstracts from ASTIA literature, classified under 18 descriptor headings pertinent to sealing technology.

While a few of the reports reviewed described successful applications of radial face-type seals at temperature up to 1200°F (649°C), relative velocity up to 450 feet/second (137.2 M/Sec), and differential pressure to 250 psi (1.722 MN/m^2), only one, [5], presented exceptionally concise design directives for the face type seal designer. Two reports, [4] and [6], present a wealth of design criteria and considerations for most common types of static and dynamic seals.

A solicitation of 18 manufacturers of seals, reference Table 8, to propose a seal design meeting the "Rotary Dynamic Seal Preliminary Design Specification, PS-1186", prepared for the program, resulted in eight submittals as indicated in the table. Additional configurations were submitted by Convair and Bendix.

2. DESIGN EVALUATION

To derive three designs from those considered, a method of comparison was evolved. The list of seal characteristics following were used to obtain a predicted comparative performance and cost effectiveness of the various designs:

[5] Povinelli, V.P., et al
Development of Main Shaft Seals for Advanced Air Breathing Systems
Report No. 3933
N71-12035-039
Pratt and Whitney Aircraft
June, 1970

[6] Bayer, P.
Investigation of Leakage and Sealing Parameters
AFRPL-TR-65-153
AD 470462
ITT Research Institute
August, 1965

Table 8

Dynamic Rotary Seal Inquiry Response Summary

Seal Manufacturer	Vendor	Seal Type or Name	Primary Seal Material	Secondary Seal Material	Cost Per Seal $	Delivery Time Weeks	Remarks
Aeroquip	Accratronics	Omniseal - Circumferential Lip Type	Vespel Sp-1	Vespel SP-1	60 & 48	16	
Koppers	-	-	-	-	No Bid	-	Letter Reply
Bal Seal	-	-	-	-	No Bid	-	Letter Reply
NOK-USA	-	-	-	-	No Bid	-	Verbal Reply
Parker Seal	-	-	-	-	No Bid	-	Letter Reply
Chicago Rawhide	-	-	-	-	No Bid	-	Letter Reply Sold Face Seal Line to GITS Mfg.
E. B. Wiggins	-	-	-	-	No Bid	-	Letter Reply
Crane	-	-	-	-	No Bid	-	Letter Reply
Magnetic Seals	-	-	-	-	No Bid	-	Letter Reply
Fluorocarbon	-	Modified RP-Circumferential Lip Type	Floroloy K (Teflon Alloy)	Press Fit	30 & 70 Tool.	4	
GITS	-	Type 74 Radial-Face	Carbon and Maraging 350 Steel-Chrome Plate	AM350 Bellows	850 & 1000 Tool.	14-16	Does not include Mating Ring or Clamping Sleeve
Hydrodyne	-	Radial-Face	Carbon-Graph and Maraging Steel-Chrome Plate	Maraging Steel Bellows and 8100 Series Seal	465	16	

Table 8 (Contd.)

Dynamic Rotary Seal Inquiry Response Summary

Seal Manufacturer	Vendor	Seal Type or Name	Primary Seal Material	Secondary Seal Material	Cost Per Seal $	Delivery Time Weeks	Remarks
Sealol	-	Radial-Face	Not Specified	Not Specified	300-500	10-12	Letter Reply
R. E. Krueger	Rubly Engr.	Circumferential Wedge Type	Vespel SP-21	-	497	5	
W. S. Shamban	-	Circumferential Lip Type	Polyimide	-	67	10	
Cartriseal	-	-	-	-	-	-	No Response
International Packings	-	-	-	-	-	-	No Response
Cook Airtromic	-	Radial-Face	Steel Hard Coated/ Carbon-Graph	CRES and Vespel	-	-	

1) Predictable, controllable, uniform loading - low static leakage performance - pressure loaded - mechanically loaded.

2) Low wear performance - low pressure loading - wear compensation.

3) Similar application experience - proven concept - proven material.

4) State-of-the-art-design, or low risk level.

5) Adequate safety margins - low failure rate - low contamination sensitivity - low catastrophic failure risk.

6) Few parts - few different types of parts - few interfaces.

7) Compatible coefficient of thermal expansion - low friction - no exotic materials - redundancy - pressure balancing - integrated unit - no shaft plating required - good protection from environment - good fluid cooling possibility.

8) Easy assembly/disassembly.

3. CONCLUSIONS

On the basis of a qualitative comparison of the eight designs submitted it was concluded that radial-face type seals were considered better for the low pressure hydraulic rotary oscillating output shaft seal in the development actuator, than the lip and wedge type seals considered. This was primarily due to the temperature limitations of the plastic materials available and proposed for the circumferential seals. Also, the face type seals were considered to have more potential for meeting increased temperature and endurance requirements (at the expense of their more complex and critical parameters and higher fabrication costs).

The lip and wedge type seals considered, offered immediate advantages of lower costs, less complexity and more reliability at the expense of a possibly shorter life under maximum temperature require-

ments [600°F (316°C) fluid and +800°F (427°C) air]. The high temperature would strain the capability of available plastic materials (polyimides, aromatic polyester and perfluoroelastomer). Most elastomeric materials available for circumferential seal designs were considered even more limited +450°F (232°C) than the plastics. Hard and soft metals for lip seal applications have generally exhibited more wear and shorter life, 7 , than the program target of 1000 hours of high thermal cycling operation expected in high mach aircraft and therefore were considered to require greater development effort than programmed.

Positive cooling flow circulation was considered mandatory if any of the available plastic materials were to be used, and desirable for the radial-face seal types. A maximum sustained cooling fluid temperature of +500°F (260°C) was highly desirable when using these materials for prolonged life, but satisfactory performance at a maximum of +600°F (316°C) seemed attainable.

Three seals appeared to be more worthy of detail evaluation and testing than the others and they were:

. Lip Type

It was concluded that the lip type of seal, using polyimide plastic Vespel 21 (graphite filled) rather than Vespel 1, offered a good risk for developmental testing. This type of seal (see Figure 44), if satisfactory, was considered to be the least complex type expected

[7] Lee, J.
High Temperature Hydraulic System Actuator Seals for use in Advanced Supersonic Aircraft
NASA CR-72354
N69-22222
Republic Aviation Division, Fairchild-Hiller
September, 1967

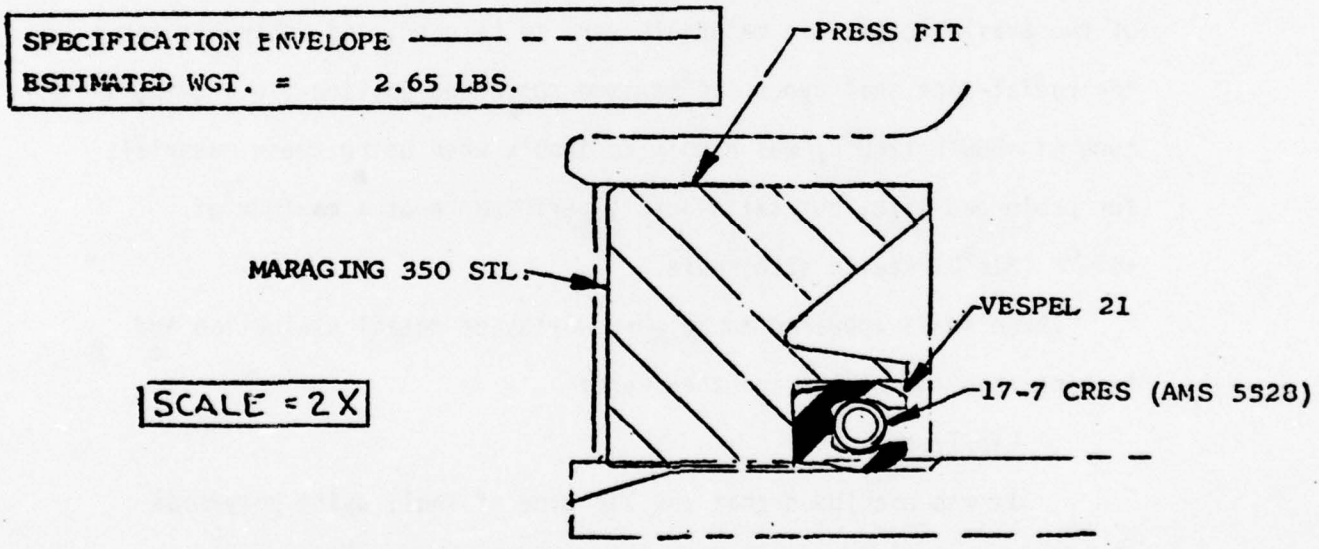

Figure 44. Lip Type Seal Design

to qualify. This suggested assurance of low production costs in comparison with other types considered.

. Circumferential Type

This circumferential type seal (see Figure 45), also using Vespel 21 polyimide plastic, represented more complexity and cost than the lip type, but offered better wear and compensation potential and more uniform, predictable mechanical loading for good low pressure sealing. In addition, the design permitted replacement of seal rings for the possible evaluation of additional materials, such as; Ekonol and ECD-006.

. Radial Face Type

Since consensus favored a radial face type seal as the most likely successful approach to the sealing problem, this configuration (see Figure 46), was considered representative of those that use a bellows for loading the sealing faces. This seal type was considered to offer the best low pressure and life characteristics, at a higher cost, than the other two types.

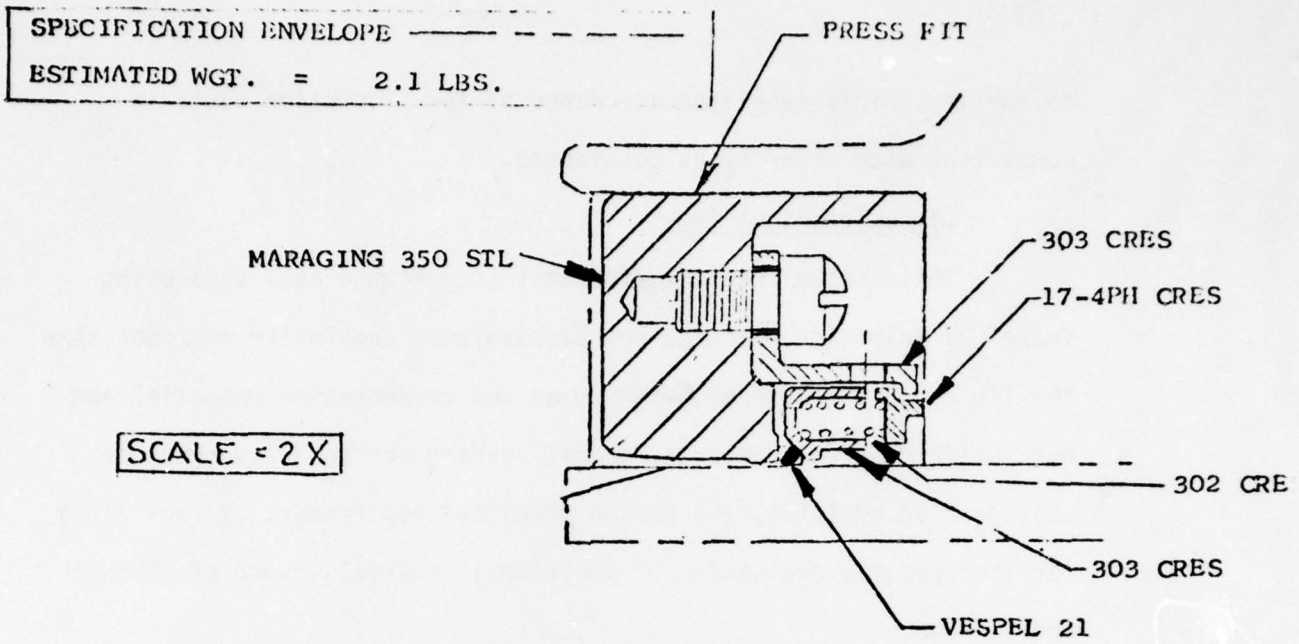

Figure 45. Circumferential Type Seal Design

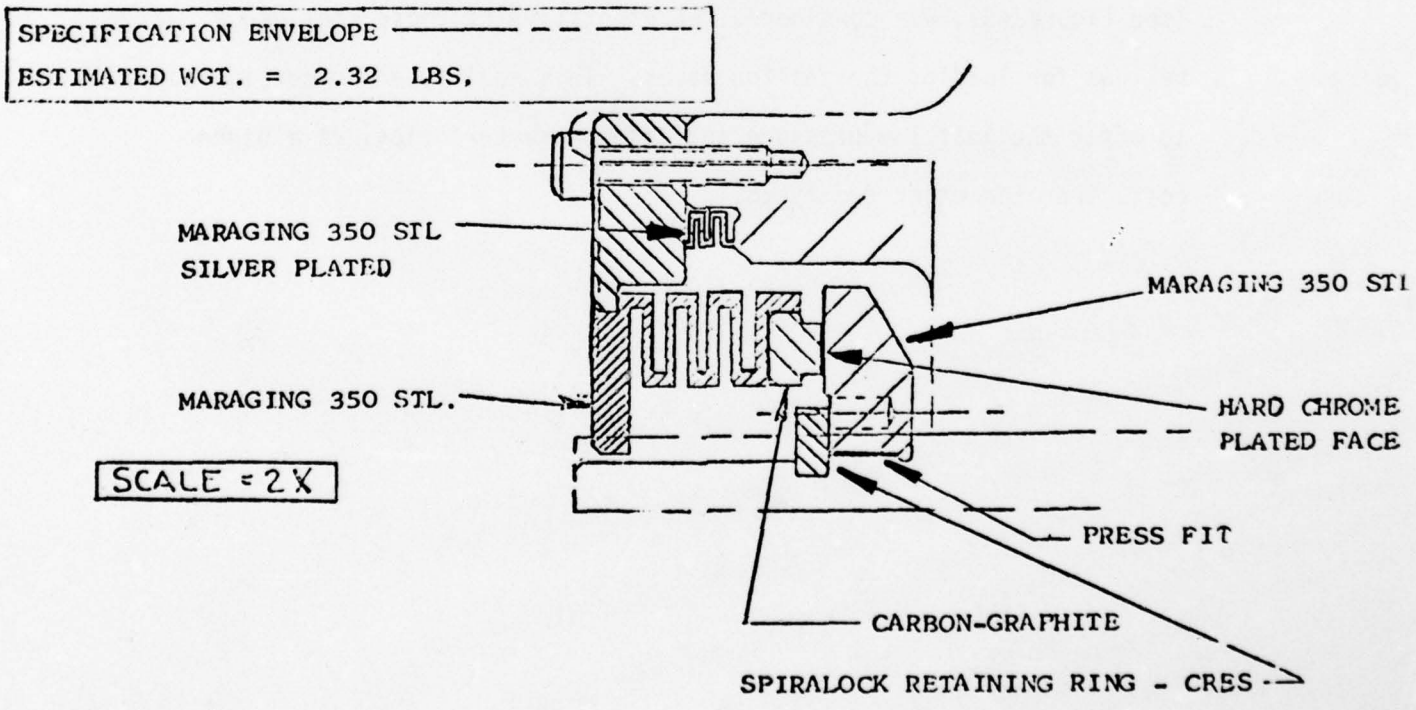

Figure 46. Radial Face Type Seal Design

SECTION VI

ACTUATOR STIFFNESS SURVEY AND ANALYSES RESULTS

Since actuator stiffness was known to be a critical parameter in aircraft control systems, a survey of airframe manufacturers was undertaken to determine the following:

- The critical design condition with respect to Mach number and altitude, for control surface requirements for the horizontal tails and rudders for fighter/attack aircraft.
- The stiffness value (pound-inch/radian) necessary to meet requirements for horizontal tails and rudders, including all components between actuator/structure interface and the control surface, i.e., actuator, horn, torque tube, structure tie, etc.
- The application considered to present the most severe stiffness requirements.

1. STIFFNESS SURVEY RESULTS

Results of the stiffness survey to determine the above information is presented in Table 9. Figure 47 is a plot of the Horizontal Stabilizer Actuator/Structure Spring Rate Versus Aircraft Gross Weight from Table 9 data. Figure 48 displays the relationship of Aerodynamic Hinge Moment versus Aircraft Gross Weight, while Figure 49 is a cross-plot of Figures 47 and 48. The "dash" line in Figure 49 is based on the response from The Boeing Company stating that studies indicated stiffness increased by the 2.25 power of hinge moments. The solid line of Figure 49 is a linear interpretation of the survey data.

TABLE 9

STIFFNESS SURVEY RESULTS

Airframe Company	Model	Spring Rate [1] Mega Lb-In/Rad (Mn-m/Rad)		Aircraft Gross T.O. Weight Kilo Lbs. (Mgm)	Horizontal Stabilizer Hinge Moment Kilo Lb-In (Mgm-m)
		Horiz. Stab.	Rudder		
Convair Aerospace	F-111 Small Fighter Projected [2]	30.0 (3.4) 6.3 (0.7) 15.0 (1.7)	4.0 (0.5) 1.5 (0.17) 2.0 (0.23)	70.0 (31.8) 20.0 (9.1) 45.0 (20.0)	625 (7.21) 78 (0.90)
Lockheed California	F-104	7.0 (0.8)		20.0 (9.1)	180 (2.08)
McDonnell/ Douglas	Projected	20.0 (2.3)	1.0 (0.1)	54.0 (24.5)	275 (3.19)
Northrop	Projected	10.0- (1.1) 20.0 (2.3)	Low [3]	25.0 (10.4)	-
Grumman	F-14	30.0 (3.4)	1.2 (0.14)	53.0 (24.1)	776 Min. (8.74) 864 Nom. (9.96)
Boeing	SST	315 [4] (35.6) 144 [5] (16.3)	-	750.0 (340.5)	7000 [6] (80.7) 5000 [7] (57.7)

NOTES:

1. Includes all components between actuator/structure interface and the control surface.
2. Projected refers to Fighter/Attack Aircraft of the 1975-1980 era.
3. Approximately 50-100 times surface mass moment of inertia.
4. Based on a 30 inch (76.2 centimeter) horn radius and 5.5 Hz.
5. Based on a 30 inch (76.2 centimeter) horn radius and 2.4 Hz (Flutter Frequency).
6. Normal H.M. with 3 of 4 actuators operable.
7. For actuator sizing with 2 of 4 actuators operable and a restricted operating envelope.

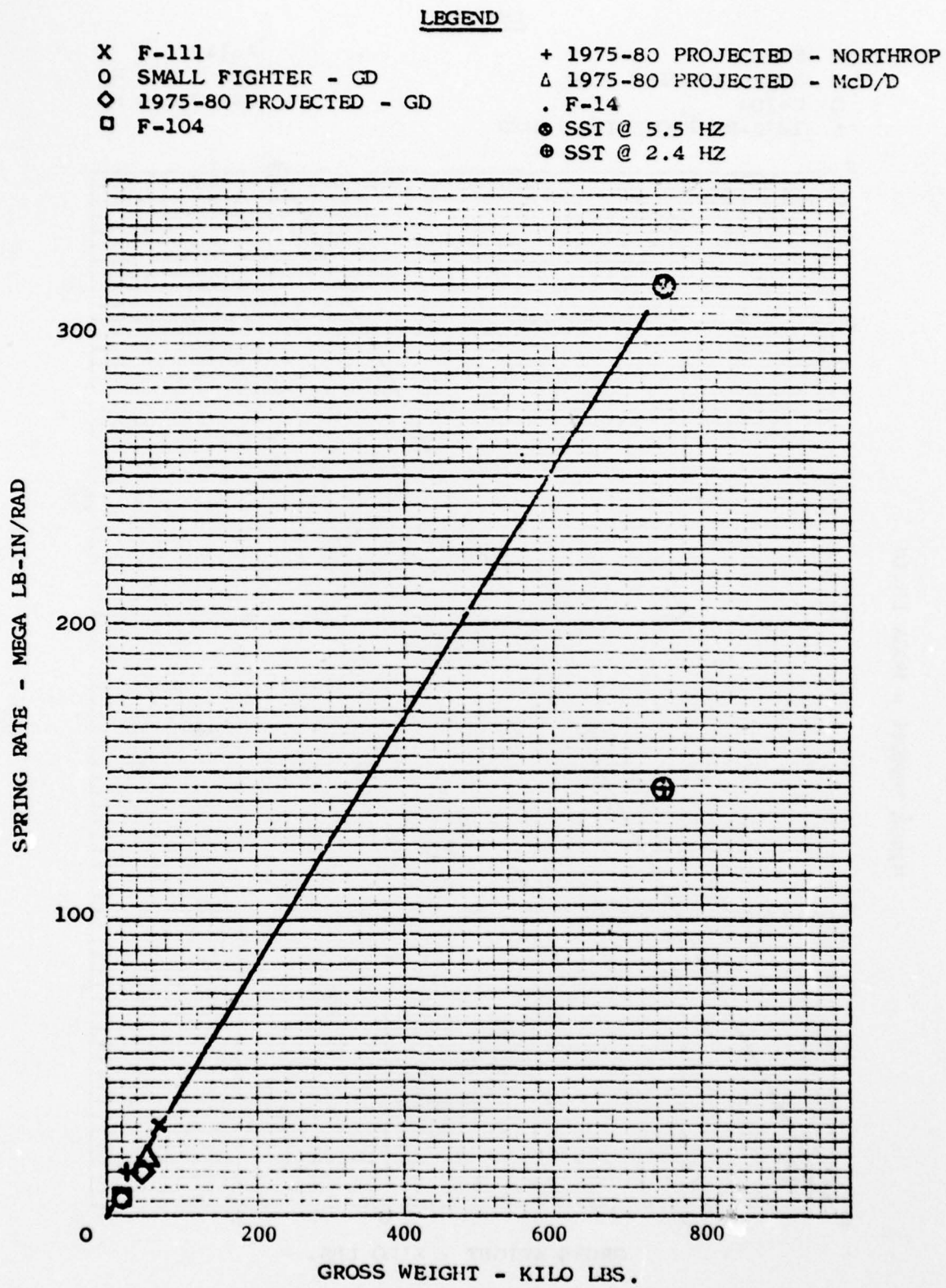

Figure 47. Horizontal Stabilizer Actuator/Structure Spring Rate Versus Aircraft Gross Weight

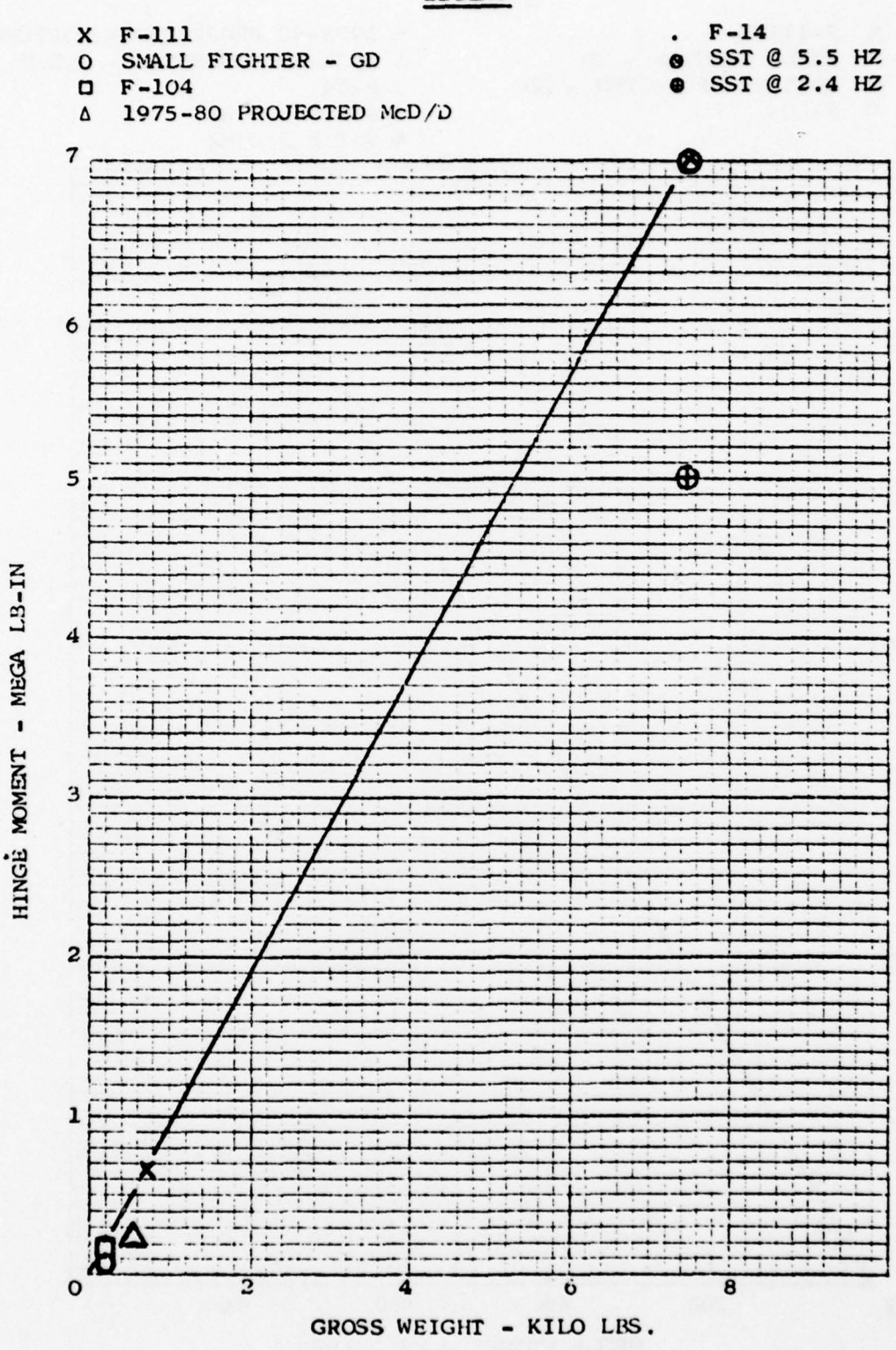

Figure 48. Horizontal Stabilizer Aerodynamic Hinge Moment Versus Gross Weight

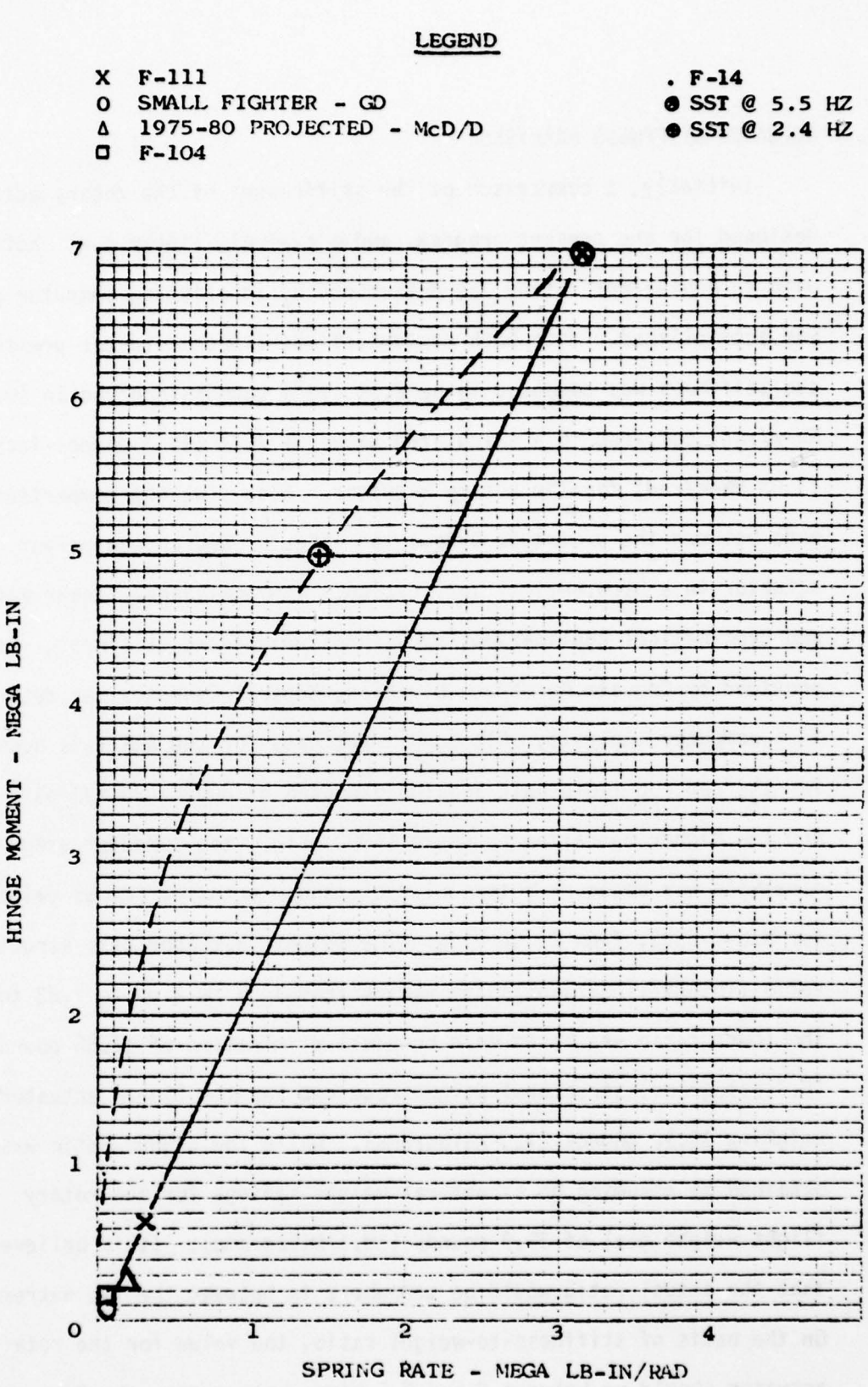

Figure 49. Horizontal Stabilizer Aerodynamic Hinge Moment Versus Actuator/Structure Spring Rate

2. ACTUATOR STIFFNESS ANALYSES

Initially, a comparison of the stiffnesses of the rotary actuator, designed for the present program, and a typical, linear dual actuator with an equivalent rating, as determined by an existing computer program, was accomplished. With both systems of the linear actuator pressurized, the stiffness was computed to be 2.54 (10^6) pounds-inch/radian (0.287 MN-m/rad) compared to a calculated value of 9.11 (10^6) pounds-inch/radian (1.03 MN-m/rad) for the rotary actuator. Also a weight comparison was made between the prototype Dynavector actuator and an equivalent actuator in a hypothetical application. The equivalent linear actuator and hypothetical application, structural weight and stiffness, was provided by Convair Aerospace Division, General Dynamics, as determined in a computer analysis. Although input data for the analysis accounted for the reduced fluid bulk modulus expected at 600^{o}F (70,000 psi) and the higher operating pressure (4000 psig), the computer program otherwise was based on a typical dual tandem actuator (minus valve) for MIL-C-5503, Type II service. The weight (actuator plus structure) ratio (rotary/linear) obtained varied from 1.39 to 1 up to 1.83 to 1. The lower ratio was based on a complete elimination of 12.55 pounds (5.7 kilograms) structural weight required for the linear actuator weighing 16.12 pounds (7.3 kilograms). While the higher ratio was obtained by assuming no structural weight savings for the rotary flight weight goal of 39.9 pounds (18.1 kilograms). It is believed that the actual ratio would be somewhere in between the two extremes. On the basis of stiffness-to-weight ratio, the value for the rotary actuator should be between 2 and 2.5 times better than the linear

actuator based on the values generated in the preliminary comparison.

Without substantial effort in an application layout design study, nothing more could have been accomplished in the program to effect a better weight comparison that included mounting structure. However, with a reasonable effort, a better comparison between the weight of the actuators was obtained by conducting a preliminary linear actuator sizing, stiffness, weight and stress study. From the analyses performed, the characteristics of a single system, high temperature linear actuator, Figure 50, are recorded in Table 10.

Comparison of the linear actuator rotary stiffness and the weight shown in Table 10 with the comparable parameters in Table 11 (which were determined by Convair analyses and previously presented) shows good correlation. Both the weight and stiffness of the actuator shown in Figure 50 is higher as might be expected. The slightly higher weight might be expected because of the penalty imposed by the heavy end gland design required to provide sufficient rigidity to insure satisfactory sealing of the face-type metallic seal used. The stiffness is greater than that attributed to the Convair linear actuator model because of the larger piston area resulting from the single hydraulic system design and the predominance of the hydraulic spring effect.

It is believed a comparison of the prototype Dynavector actuator with the linear actuator of Figure 50 is more realistic than with the Convair dual tandem linear actuator model although the previous comparison was expedient at the time.

Therefore, excluding the weight of a valve, manifolding, and linkage, using the following assumptions:

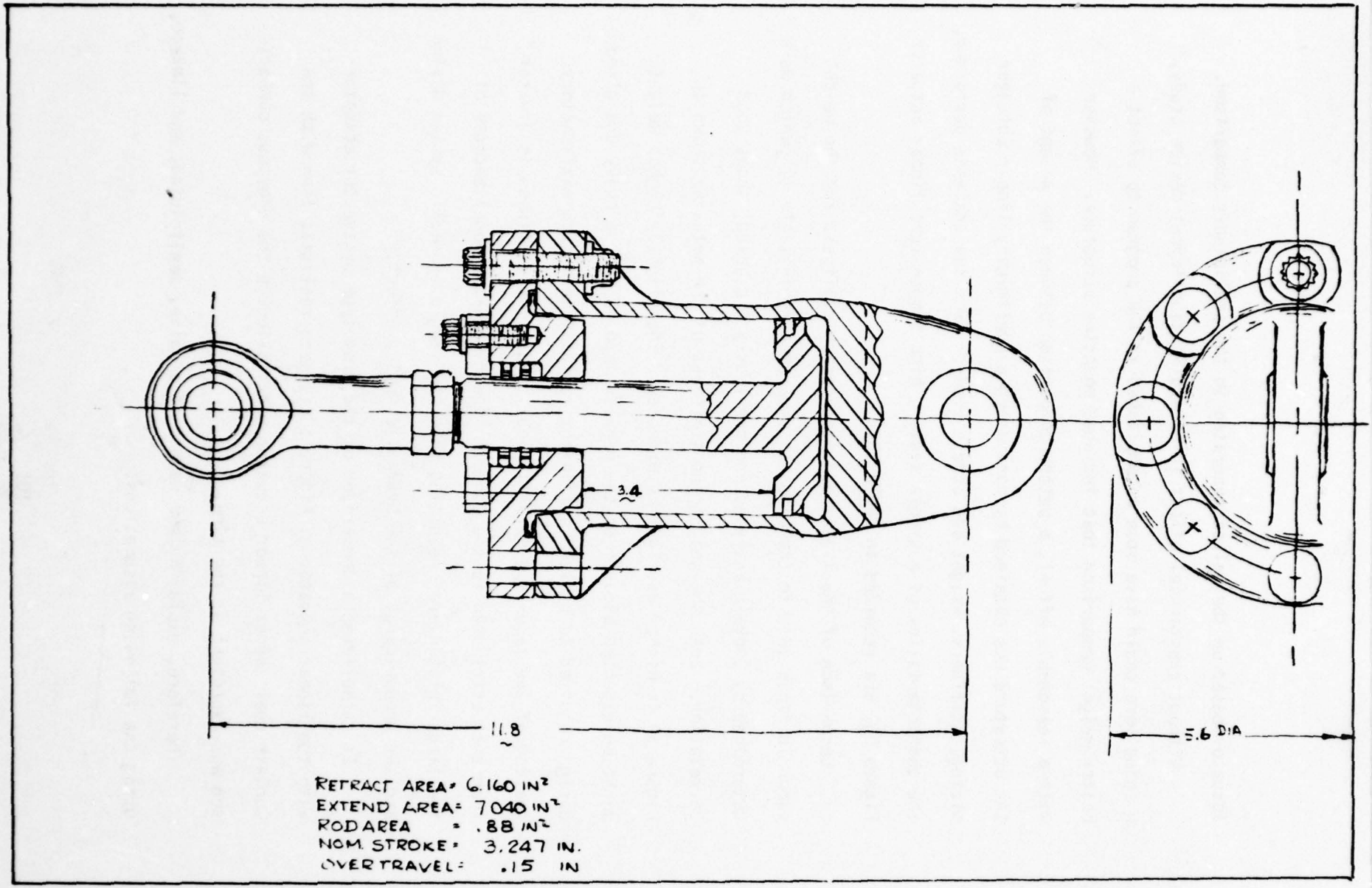

Figure 50. High Temperature Linear Actuator Comparison Model

TABLE 10

HIGH TEMPERATURE LINEAR ACTUATOR PRELIMINARY
DESIGN ANALYSES SUMMARY

ITEM NO.	PARAMETER/ITEM	VALUE
1	Rod diameter	1.059 in.
2	Cylinder I.D.	2.994 in.
3	Cylinder wall thickness	0.205 in.
4	End gland Max. flange stress (at 4000 PSI, Piston bottomed extended)	19,963 PSI (1)
5	Item 4 margin of safety at burst pressure (10,000 PSI)	+4.3 (2)
6	Max. effective shell stress at 4000 PSI (piston extended not bottomed)	56,154 PSI (1)
7	Item 6 margin of safety at burst pressure (10,000 PSI)	+.85
8	Max. stress level of piston at 4000 PSI (piston retracted-not bottomed)	90,178 PSI (1)
9	Item 8 margin of safety at 1.5 ultimate load factor	+.92
10	Actuator linear stiffness (piston centered)	$4.25\ (10^5)\ \frac{lb.}{in.}$
11	Actuator rotary stiffness (based on 3.25 horn rad.)	$4.5\ (10^6)\ \frac{lb\text{-}in}{Rad}$
12	4000 PSI stall load	24,640 lbs.
13	4000 PSI stall torque (based on 3.25 horn rad.)	80,000 lb-in
14	Estimated weight	17.07 lbs.

NOTES:

1. Based on a ref. temperature of 70^oF, maximum operating temperature of 600^oF and thermal coefficient of exp. of 5.6 (10^{-6}) in/in/^oF.
2. Design based on stiffness rather than stress.

TABLE 11

CONVAIR COMPUTER ANALYSIS RESULTS OF A HYPOTHETICAL
DUAL TANDEM LINEAR ACTUATOR APPLICATION
WEIGHT AND STIFFNESS REQUIREMENTS

PARAMETER	VALUE
System Pressure	4,000 PSIG
Hinge moment	80,000 lb-in
Horn radius	3.3 in.
Fluid bulk modulus	70,000 PSI
Actuator weight	16.12 lbs.
Aircraft structural weight	12.55 lbs.
Single hydraulic system stiffness	1.79 (10^6) $\frac{\text{lb-in}}{\text{Rad}}$
Dual hydraulic system stiffness	2.54 (10^6) $\frac{\text{lb-in}}{\text{Rad}}$

TABLE 12

CALCULATED VALUES OF ROTARY ACTUATOR COMPLIANCES

COMPLIANCE	VALUE	FRACTION OF TOTAL
C_{COVR}	1.04×10^{-9} rad/in-lb	0.0094
C_{COMM}	1.10×10^{-9} rad/in-lb	0.0100
C_{HYDR}	1.0601×10^{-7} rad/in-lb	0.9611
C_{CHBR}	1.4×10^{-10} rad/in-lb	0.0013
C_{ROTR}	2.2×10^{-10} rad/in-lb	0.0020
C_{GEAR}	7.0×10^{-10} rad/in-lb	0.0063
C_{SHFT}	1.09×10^{-9} rad/in-lb	0.0099
C_{ACTR}	1.1030×10^{-7} rad/in-lb	1.0000

Linear Actuator Weight = 17.07 lbs.

*Hypothetical Airframe Structural Weight = 12.55 lbs.

Total Linear Actuator Weight Penalty = 29.62 lbs.

*Previously Convair computed requirement for a linear actuator design.

Flight Weight Dynavector Weight = 39.9 lbs.

Assumed Airframe Structural Weight = 0

Total Rotary Actuator Weight Penalty = 39.9 lbs.

Minimum Ratio of Weight Penalties $= \frac{39.9}{29.62} = 1.35$

Maximum Ratio of Weight Penalties $= \frac{39.9 + 12.55}{29.62} = 1.77$

Again, it seems the ratio could well be within the two extremes since some structural weight savings should be possible with the Dynavector rotary actuator. The ratio of stiffnesses for the rotary actuator based on 9.11 (10^6) pounds-inch/radian (1.03 MN-m/rad) and the value for the linear model in Table 10 is 2.02:1. Based on this value, and the weight ratios above, the ratio of rotary actuator stiffness-to-weight to that of the linear actuator varies from 1.14 to 1.50. These various comparisons are summarized graphically in Figure 51.

Table 12 lists the calculated compliances (reciprocal of stiffness) for the individual components of the rotary actuator. Noting the fractional parts of the total compliance listed in the table, it can be seen that the fluid volume compliance is 96% of the total. Table 13 shows the component compliances for the linear actuator model as shown in Figures 52 and 53. For the linear actuator the fluid volume compliance accounts for only about 75% of the total, as table 13 shows.

NOTES:

1. Maximum value based on 100% structural weight savings assumed for DYNAVECTOR. Minimum value based on 0% assumed weight savings. Actual value should be between Min. and Max.
2. Crosshatched bars represent linear model actuator with a calculated weight of 17.4 lbs.
3. DYNAVECTOR Values are based on a flight weight goal of 40 lbs for the actuator only.
4. Calculated airframe structural weight for the linear model actuator is 12.6 lbs.

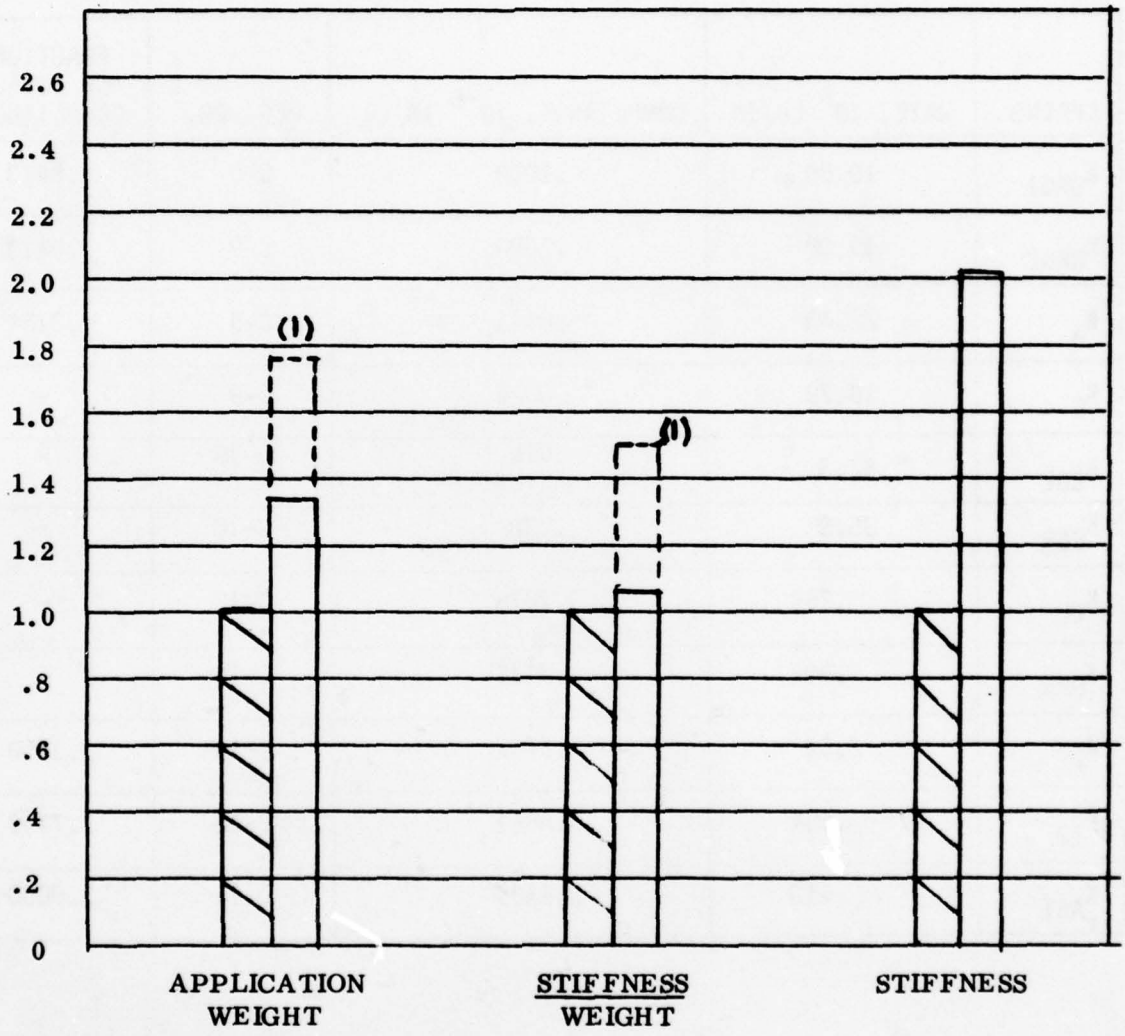

Figure 51. Normalized Comparison of Calculated Stiffness and Weight Between Linear Model and Dynavector Actuators

TABLE 13

CALCULATED VALUES OF ACTUATOR SPRING RATES AND COMPLIANCES
HIGH TEMPERATURE LINEAR ACTUATOR

SPRING	RATE, 10^6 LB/IN	COMPLIANCE, 10^{-6} IN/LB	REF. PG.	FRACTION OF TOTAL COMPLIANCE
K_{BRG1}	10.00	.1000	C-9	.0413
K_{BRG2}	10.00	.1000	C-9	.0413
K_a	22.43	.0446	C-9	.0184
K_C	10.79	.0926	C-9	-
K_{CBL}	52.3	.019	C-10	-
K_{CBR}	35.8	.028	C-10	-
K_{OL}	.264	3.7878	C-10	-
K_{OR}	.302	3.3112	C-10	-
K_P	2.52	.3702	C-10	.1530
K_{12}	.554	1.8051	C-10	.7459
K_{ACT}	.413	2.4199	C-11	1.0000

$$K_{\theta ACT} = \frac{K_{ACT} R^2}{57.325} = \frac{.413\ (3.25)^2\ 10^6}{57.325} = 76{,}250\ \frac{\text{LB-IN}}{\text{DEG}}$$

$$= 4.33(10^6)\ \frac{\text{LB-IN}}{\text{RAD}}$$

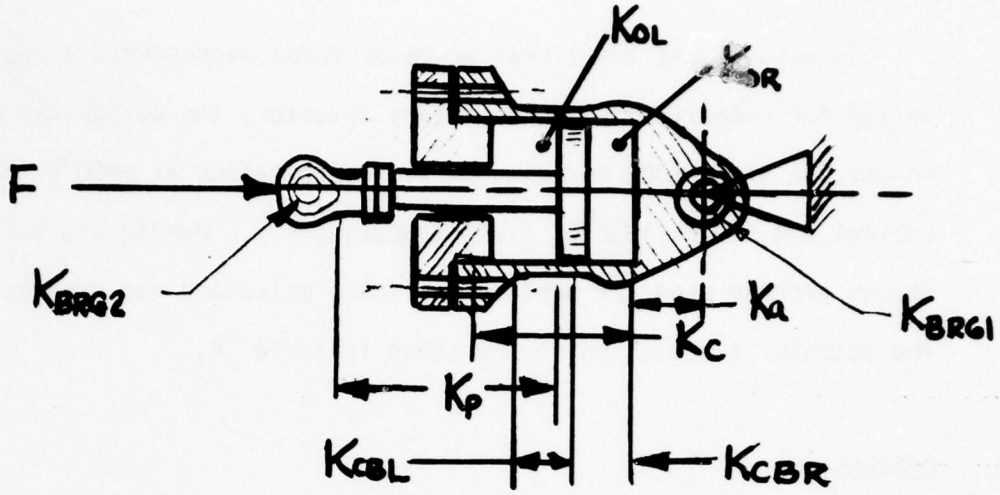

Figure 52. Actuator Spring Designations

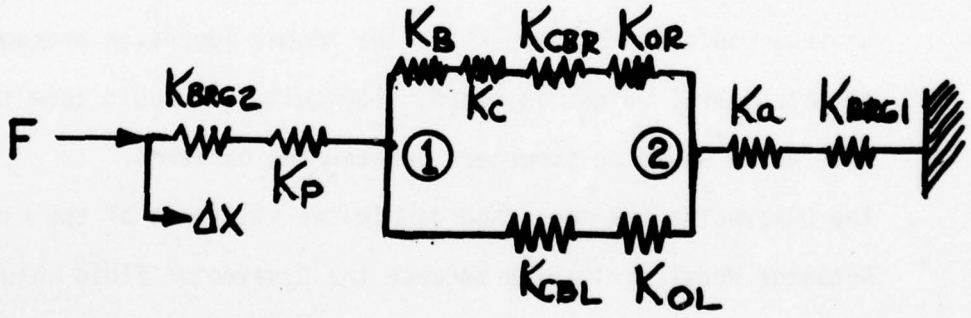

Figure 53. Actuator Spring Model

To assure that the linear actuator model represented a reasonable design for comparison with the rotary actuator, the design was based on the use of 18Ni300 maraging steel for operation at +800°F (+427°C) ambient and 600°F (+316°C) fluid temperature. A Bendix digital computer stress program used for production linear actuators was used to evaluate the actuator stresses which are shown in Table 14.

3. CONCLUSIONS

Based on the information received from the stiffness survey and the summary of analyses presented in this report, the following conclusions are offered.

- The stiffness-to-weight ratio parameter of the proposed flight weight Dynavector is greater than that of the Linear Actuator Model. The Dynavector has 14 percent to 50 percent advantage depending on how much structural weight savings accrue to the Dynavector installation. The lower advantage presumes no structural weight savings would be realized while the higher advantage presumes all the structural weight is saved. Logically, it would seem the true value would be somewhere between the extremes.
- The Dynavector has more than double the stiffness of the Linear Actuator Model, primarily because the Dynavector fluid volume is less than half that of the Linear Actuator Model.
- The hydraulic compliance of the Dynavector is greater than 96 percent of the total compliance, whereas for the Linear Actuator, fluid compliance contributes only about 75 percent of the total.

TABLE 14

SUMMARY OF COMPUTER STRESS ANALYSIS(1)
HIGH TEMPERATURE LINEAR ACTUATOR

ITEM NO.	ITEM	REF. FIGURE NUMBER	MAXIMUM APPLIED LOAD POUNDS	(2) (3) MAX. DISPLACEMENT - IN.			(2) (3) MAX. STRESS - KSI	
				BENDING	VERTICAL	HORIZ.	EFFECTIVE	SHEAR
1	FLANGE	C-2 (A)	4577	.0012	.0090	.0013	19.963	9.543
2	SHELL	C-2 (B)	4003	.0020	.0087	.0166	56.154	28.027
3	PISTON	C-2 (C)	1704	.0025	.0030	.0131	90.176	43.361

NOTES:

(1) Based on 18 Nickel 300 Maraging Steel Solution annealed at 1500^{o}F and aged for three hours at 900^{o}F, 600^{o}F maximum metal temperature, 240 KSI yield stress at 0.2% offset and an ultimate stress of 260 KSI.

(2) Maximum Displacements and/or Stresses shown do not necessarily occur at the same node.

(3) Maximum Displacements and Stresses are the result of thermal (600^{o}F) and pressure (4000 PSIG) effects.

This implies that the elastic modulus of the metallic components of the Dynavector are of much less importance to stiffness than for the Linear Actuator. Substitution of aluminum alloys for all the steel portions of the Dynavector would increase the compliance by only 11 percent. For the Linear Actuator, this same material substitution would increase compliance by 49 percent. The light metals, therefore, are candidates for high temperature Dynavector design providing wear and thermal expansion problems can be solved.

- To maximize the Dynavector stiffness, the most effective parameter to change (reduce) is fluid volume under compression. The volume of fluid under compression in the Dynavector is made up of the volume of the displacement chambers and the fluid volume between the chambers and the servovalve. The requirements for the first volume are reduced as the gear ratio is increased. The requirements for the second volume are reduced as the maximum speed requirement is decreased. In general, selection of the maximum speed will not be the prerogative of the designer; however, the gear ratio, which also affects actuator weight, offers fruitful possibilities for optimization.
- The Linear Actuator created for stiffness and weight comparisons with the high temperature Dynavector is a reasonable model based on preliminary stress analyses. It also seems reasonable based on the Convair (Ft. Worth) Aerospace Division computer generated Linear Actuator Model previously used for comparison. The difference between the two models is logical since the Convair computer program was based on a dual tandem actuator concept resulting in less piston area. Also, the computer program did not account for high

temperature design accommodations required for seals.

- The addition of servovalve and displacement linkages usually required for an actuator assembly will probably have a greater percentage weight impact on the Linear Actuator Model than on the Dynavector. This, in turn, will further improve the weight and stiffness-to-weight comparison of the Dynavector to the Linear Actuator Model.
- The weight advantage in installation plumbing should be in favor of the Dynavector in that flexible lines or rotating unions would not be required.

SECTION VII

SUMMARY OF ACTUATOR/MOTOR TESTS RESULTS/CONCLUSIONS

The original program plan provided for testing of the actuator design in two separate tasks. The first testing task was to evaluate the hydraulic motor cartridge assembly without the epicyclic gear mission. Elimination of the transmission simplified the test task, since the torque output was reduced and the output speed increased. Therefore, simultaneous, continuous rotation and loading was more practical. The second test task provided for cyclic operation of the complete prototype actuator using a torsional load spring and a maximum angular displacement of 30 degrees (.524 radius). However, as a result of difficulties encountered in operation of the motor cartridge test unit, which was attributed to a discrepant rotor, it was decided to proceed directly to the actuator tests with a new rotor.

The results of actuator testing, however, revealed an operating characteristic that is the result of the impact of hold-in motor commutation, that was manifested by excessive torque ripple, resulting in a step-like output or "cogging". Since the probable deleterious effect of the "cogging" would have made the planned cyclic life test of the gears unrealistically severe, it was deemed advisable to discontinue testing with the transmission and revert to motor testing again.

An analysis showing a development of the hydraulic forces from both the hold-in motor and the torque producing motor which combine to produce the "cogging" nature of the output displacement is included as an Appendix. The analysis shows that the amplitude of the torque variation is dependent primarily on the hold-in motor inlet pressure and is equal to 40% of the maximum rated output torque, if the hold-in motor pressure is the same as the control valve supply pressure.

If the hold-in motor inlet pressure is the same as the inlet pressure to the torque motor, the ripple amplitude becomes a function of the load magnitude up to a maximum of 40% of the maximum rated torque. Therefore, theoretically at 10% load, the ripple amplitude would be 4% of the required torque.

1. ACTUATOR TEST RESULTS AND CONCLUSIONS

To obtain an evaluation of the actuator load performance as quickly as possible after the original termination of the Motor Cartridge testing, a temporary test setup was established using MIL-H-5606 hydraulic fluid until it was determined that the special test arrangement using the MIL-H-27601, high temperature hydraulic fluid would definitely not be needed for the Motor Cartridge tests. This temporary test arrangement is shown schematically in Figure 54 (a).

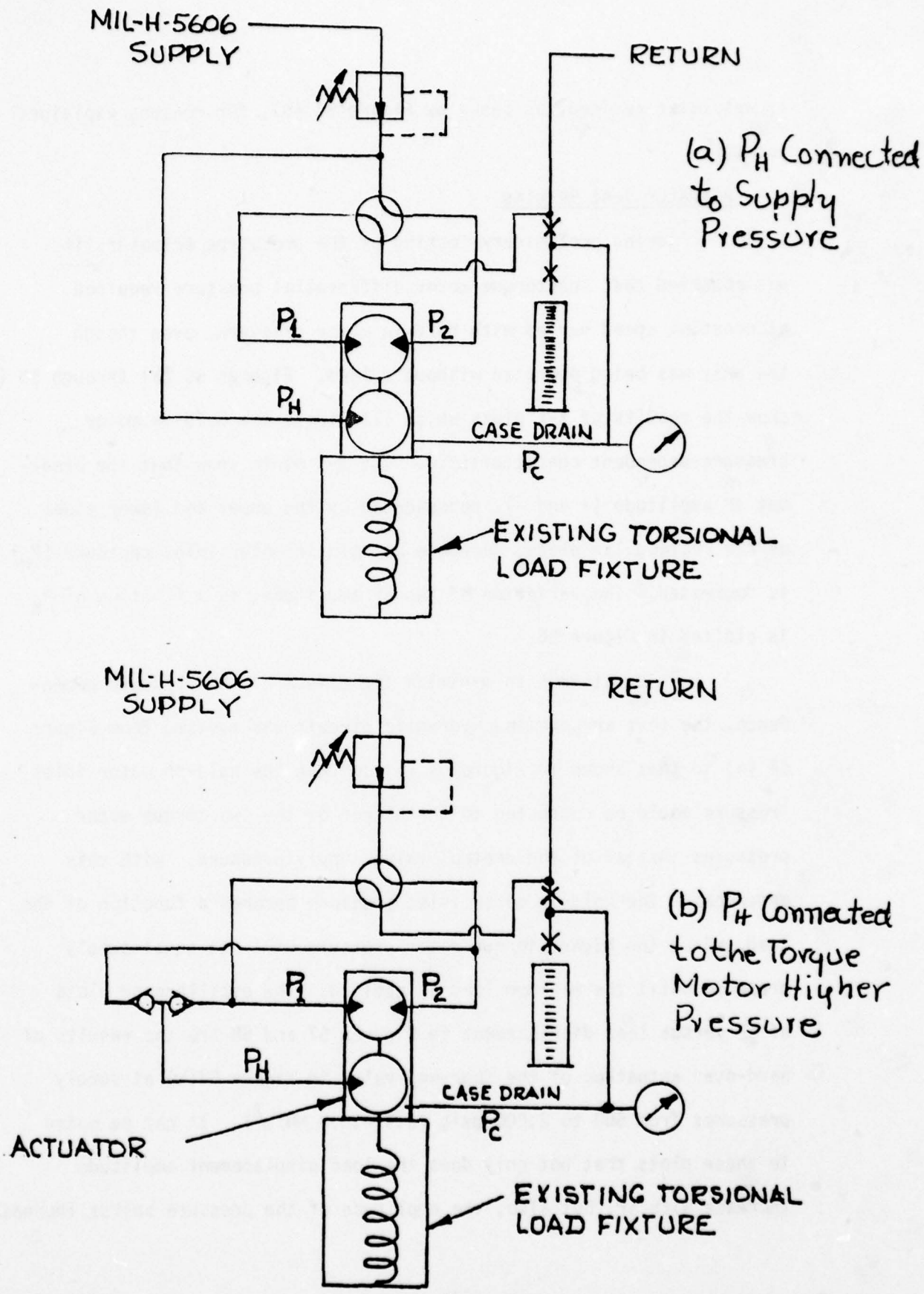

Figure 54. Temporary Actuator Lead Test Arrangement

It was later revised, as shown by Figure 54 (b), for reasons explained later.

a. Actuator Test Results

During preliminary testing of the prototype actuator, it was observed that the torque motor differential pressure required at constant speed varied with hold-in motor pressure, even though the unit was being operated without a load. Figures 55 (a) through 55 (d) show the results of X-Y plots which illustrate the hold-in motor pressure-dependent characteristic. The X-Y plots show that the break-out ΔP amplitude (+ and -), represented by the upper and lower sides of the rectangular plots, decrease as hold-in motor inlet pressure (P_H) is decreased. The variation of the ΔP amplitude, as a function of P_H is plotted in Figure 56.

In an attempt to minimize the effect of the pressure dependence, the test arrangement hydraulic circuit was revised from Figure 54 (a) to that shown in Figure 54 (b) so that the hold-in motor inlet pressure would be connected to the higher of the two torque motor pressures instead of the control valve supply pressure. With this arrangement the hold-in motor inlet pressure becomes a function of the load, since the higher torque motor pressure will not equal supply pressure until the maximum load is applied. The oscilloscope plots of ΔP versus load displacement in Figures 57 and 58 are the results of hard-over actuation of the four-way valve in Figure 54(b) at supply pressures from 500 to 2,000 psig (6.9 -13.8 MN/m^2). It can be noted in these plots that not only does the load displacement amplitude increase with ΔP, but also, the amplitude of the pressure spikes increase.

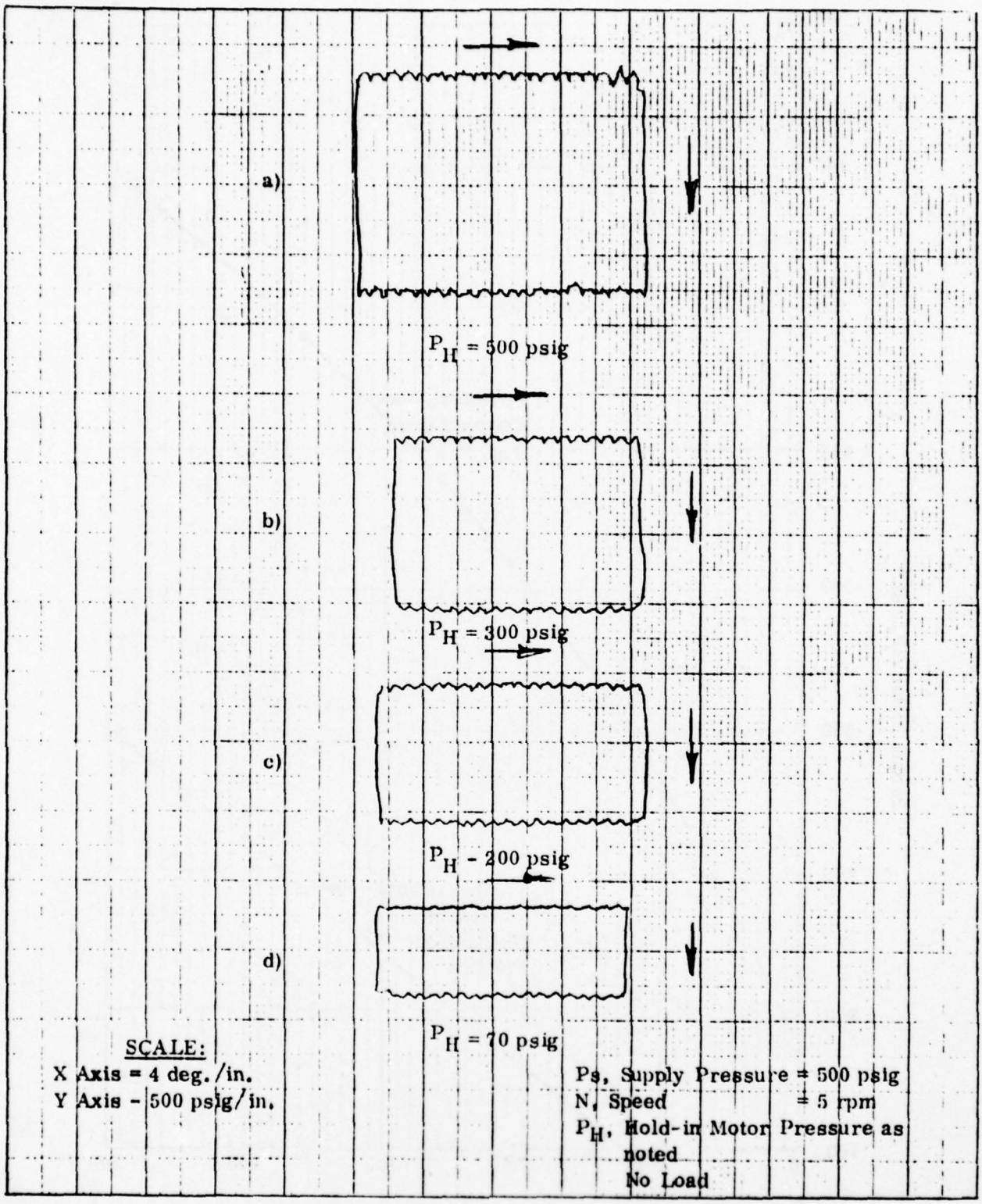

Figure 55. Torque Motor Differential Pressure Required for Constant Speed for Various Hold-in Motor Pressures at No Load

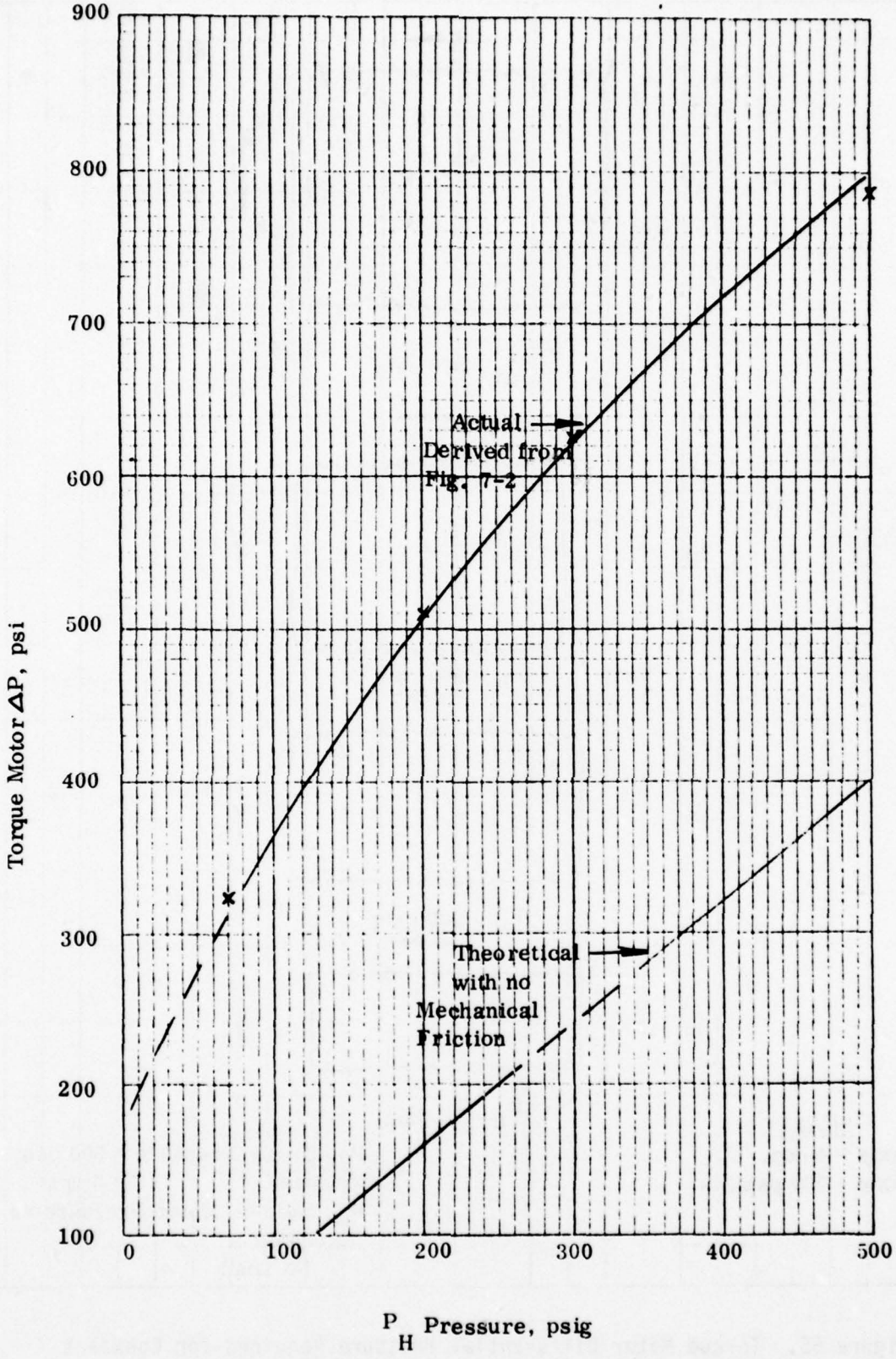

Figure 56. Torque Motor ΔP vs Hold-in Motor Pressure (P_H)

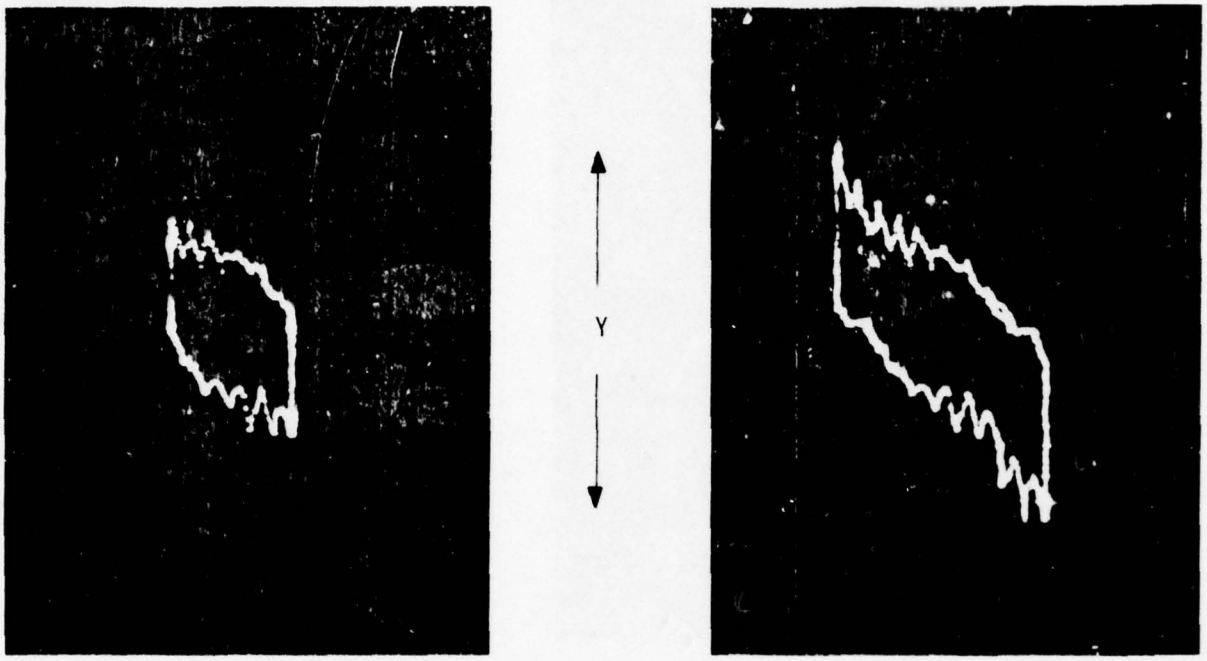

Scale: X = 2 deg/CM
Y = 400 psid/CM

Figure 57. Torque Motor Differential Pressure vs Load Angular Displacement of 500 and 1000 psig Supply Pressure

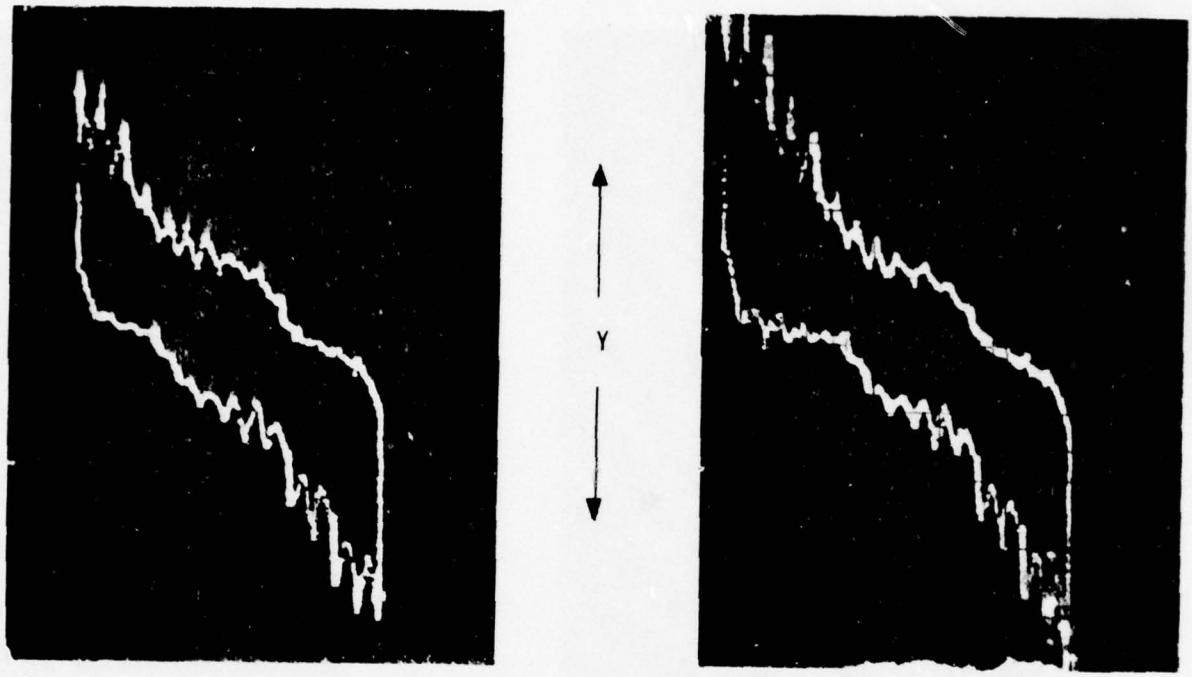

Scale: X = 2 deg/CM
Y = 400 psid/CM

Figure 58. Torque Motor Differential Pressure vs Load Angular Displacement at 1500 and 2000 psig Supply Pressure

Figure 59 shows a typical X-Y plot of ΔP versus load displacement, with the hydraulic circuit of Figure 54(a). This plot was achieved by opening the four-way valve and slowly increasing supply pressure to obtain load displacement. This operating mode is similar to that achieved with the arrangement of Figure 54(b), except breakout friction must be overcome at each spike.

Figure 60 is another X-Y plot conducted under the same conditions as Figure 59, except using steam turbine lubricating oil pursuant with MIL-L-17331B (ships) in lieu of hydraulic fluid MIL-H-5606. The biggest difference in the results with the two fluids is in the uniformity of the spikes. The spikes, or "cogging", with the more viscous lubricating fluid are more uniform and generally of smaller amplitude than those of Figure 59.

The prototype actuator total weight based on the summation of the weight of individual parts as shown in Table 3 is 92.2 pounds (41.9 kilograms).

b. Conclusions

Testing of the prototype actuator was so limited because of the severe non-linear displacement characteristic created by the variation of the effective hydraulic force on the rotor resulting from hold-in motor commutation that very little performance evaluation was possible.

Output displacement tests with and without load produced results that correlate with the analysis in the Appendix, which shows that the torque output varies as a function of the hold-in motor inlet pressure and the angular displacement of the rotor eccentricity during its orbit. While the magnitude of the impact of the hold-in motor

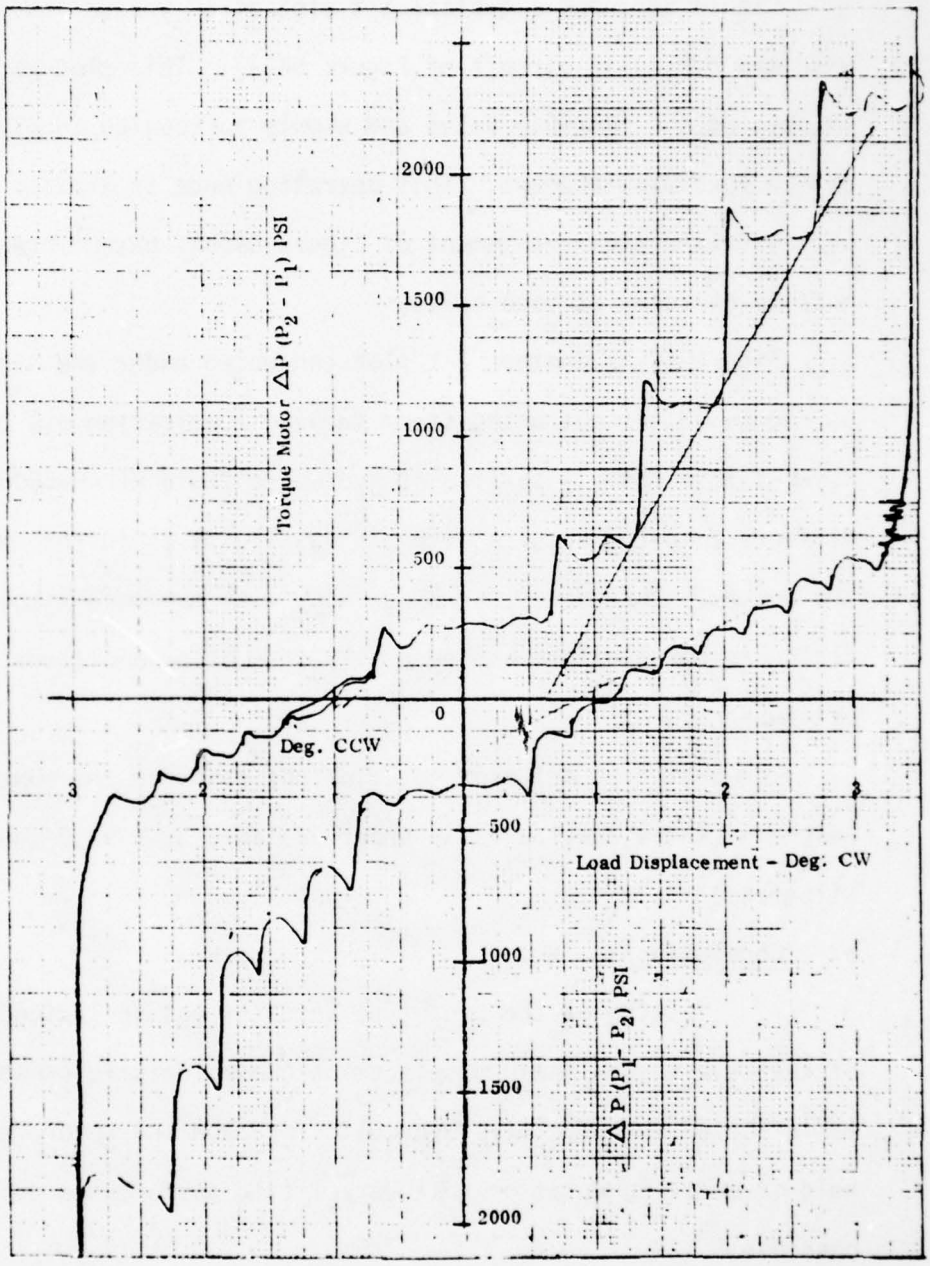

Figure 59. Torque Motor Differential Pressure vs Load Angular Displacement Obtained with a Wide-open Valve & Variable Supply Pressure

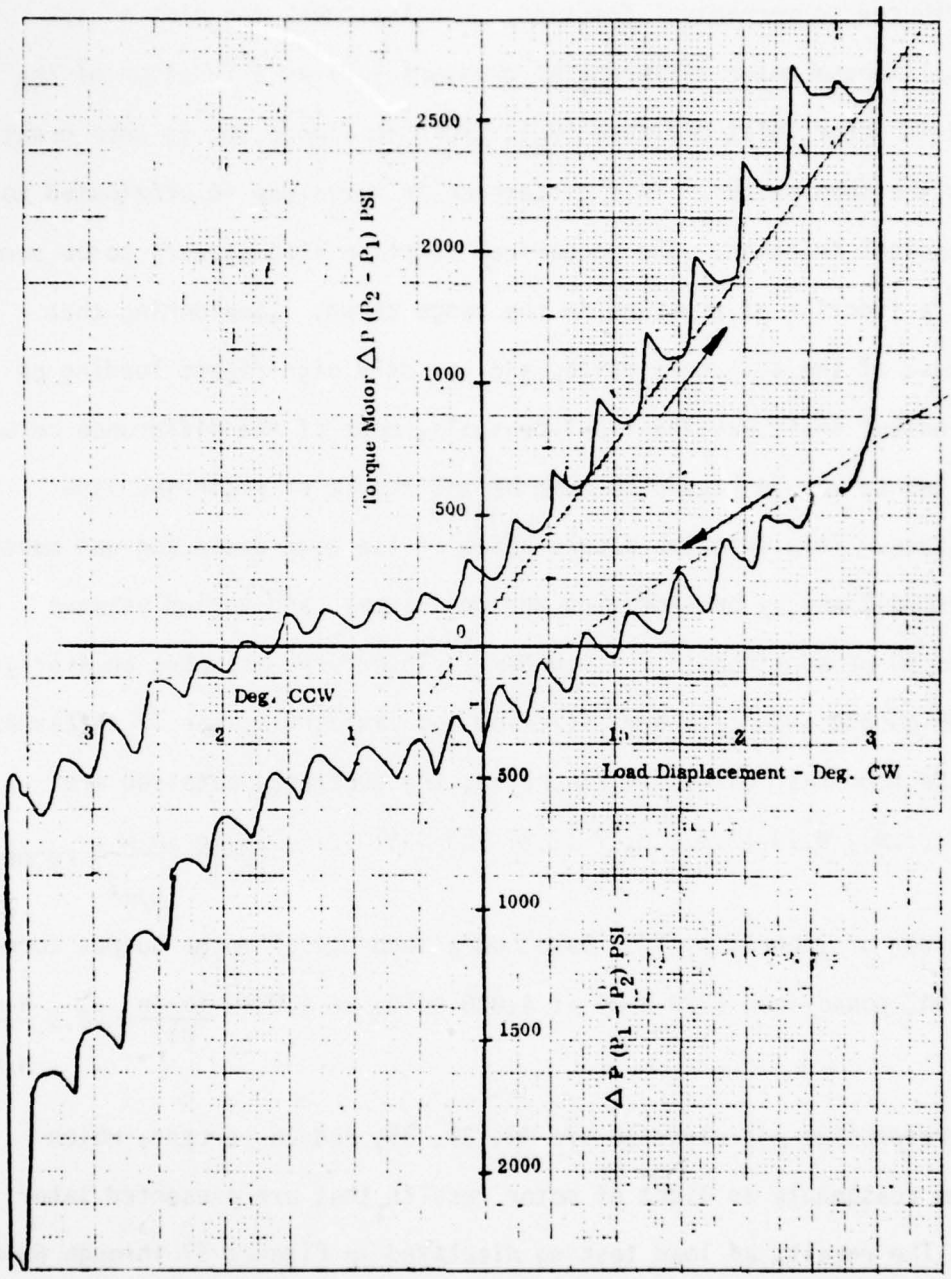

Figure 60. Torque Motor Differential Pressure vs Load Angular Displacement Using a Relative Viscous Fluid

pressure in the test data appears not to correlate very well, this is attributed to mechanical friction. For instance, the plot of the actual torque motor differential pressure (ΔP) as a function of the hold-in motor inlet pressure (P_H), shown in Figure 56, is much greater than the theoretical. This difference in magnitude is attributed to mechanical friction. The mechanical friction also appears to be somewhat a function of pressure in the range shown. Considering that because of the 43:1 gear ratio, and the only significant loading on the output shaft was the lip-type seals, most of the difference between the two curves in Figure 56 must be the result of rotor and vane friction. This friction occurs ahead of the gear ratio and was measured numerous times by back-driving during assembly and varied between 50 to 80 pounds-inch (5.7 - 9.0 N-m). Therefore, assuming an average of 65 pounds-inch (7.4 N-m) friction and dividing by the ΔP difference at the four test points in Figure 56, the quotients obtained are 0.24 (3.9), 0.19 (3.1), 0.17 (2.8) and 0.17 (2.8) $\frac{\text{lb-in}}{\text{psi}}$ ($\frac{\text{N-m}}{\text{N/m}^2}$) respectively, in order of increasing P_H. Based on a theoretical motor output torque of 1942 pound-inch (220 N-m) at 4,000 psid, or a 0.49 $\frac{\text{lb-in}}{\text{psi}}$ (8.1 $\frac{\text{N-m}}{\text{N/m}^2}$) the respective efficiencies are 49, 39, 35, and 35 percent, which seems reasonable in light of motor results that are presented later.

. The results of load testing displayed in Figures 57 through 60 also appear compatible with predicted performance presented in the Appendix. Again, the magnitude of the impact of hold-in motor pressure does not correlate well with prediction, because of mechanical friction. However, visual observation does indicate that the pressure spikes do increase

with increasing P_H and the general shape of the curves agrees with the Appendix. The frequency of the spikes correlate with the predicted frequency of one cycle each 16.36 degrees of the rotor orbit, or 0.38 degrees (0.0066 radian) of output shaft rotation.

. The irregularity of the spikes occurring with increasing load displacement of Figure 59 is attributed to mechanical friction and its impact on acceleration of the output from one spike, or position, to another. This conclusion is based on the regularity of the spikes, or steps, as evident in Figure 60, when the unit was operated with a viscous lubricating oil, MIL-L-17331B (Ships). Based on the measured motor displacement of 3.05 in^3/rev. (50 cc/rev) and the slopes of the plots taken at the bottom of the spikes for increasing displacement, the torque efficiency with MIL-H-5606 fluid is 15% and 19% with MIL-L-17331 lubricating oil.

. The final conclusion based on the results and the analysis of the Appendix is that the automatic (upon loss of supply pressure) decoupling feature, which necessitates using a hold-in motor to keep the gears in mesh, compromises the actuator performance too much.

2. MOTOR TEST RESULTS AND CONCLUSIONS

The motor cartridge assembly of the rotary actuator developed in the program was tested in an assembly (Motor Cartridge Test Unit) that included all the same parts as the prototype actuator, except those associated with the epicyclic gear transmission. The transmission was replaced with a cam shaft (reference Figure 4) to effect a 1:1 transmission. The motor cartridge assembly, shown previously in Figures 3 and 14, is compared to the actuator, a low-torque, high-speed

device, which can be loaded and tested more easily. By using a commercial hydraulic motor as the load device, as shown in the test arrangement schematic of Figure 61, the motor characteristics were evaluated with continuous rotation of the motor. This was not practical in the testing of the actuator, because of its 43 times greater output, which dictated a torsional spring type load, and limited displacement, cyclic operation.

The reason for the substitution of a MIL-H-5606 hydraulic power supply in the test arrangement for the MIL-H-27601A power supply, originally planned, as shown in Figure 62, is explained later in Paragraph 2.C, Limitations.

a. Motor Test Results

Table 15 shows the performance characteristics of the prototype motor cartridge assembly at room temperature, along with design goals.

TABLE 15

MOTOR CARTRIDGE ASSEMBLY PERFORMANCE

CHARACTERISTIC	DESIGN GOAL	RESULT
Stall Torque	1860 lb-in. (210 N-m)	1740 lb-in (197 N-m)
Torque Efficiency	94%	92%
Displacement	3.10 in^3/rev. (50.8 cc/rev)	3.05 in^3/rev. (50 cc/rev)
Volumetric Efficiency	85%	70%*

* This value is based on 3000 psig (20.7 MN/m^2) supply pressure. At 4000 psig (27.58 MN/m^2) it is estimated that the efficiency would be 68%.

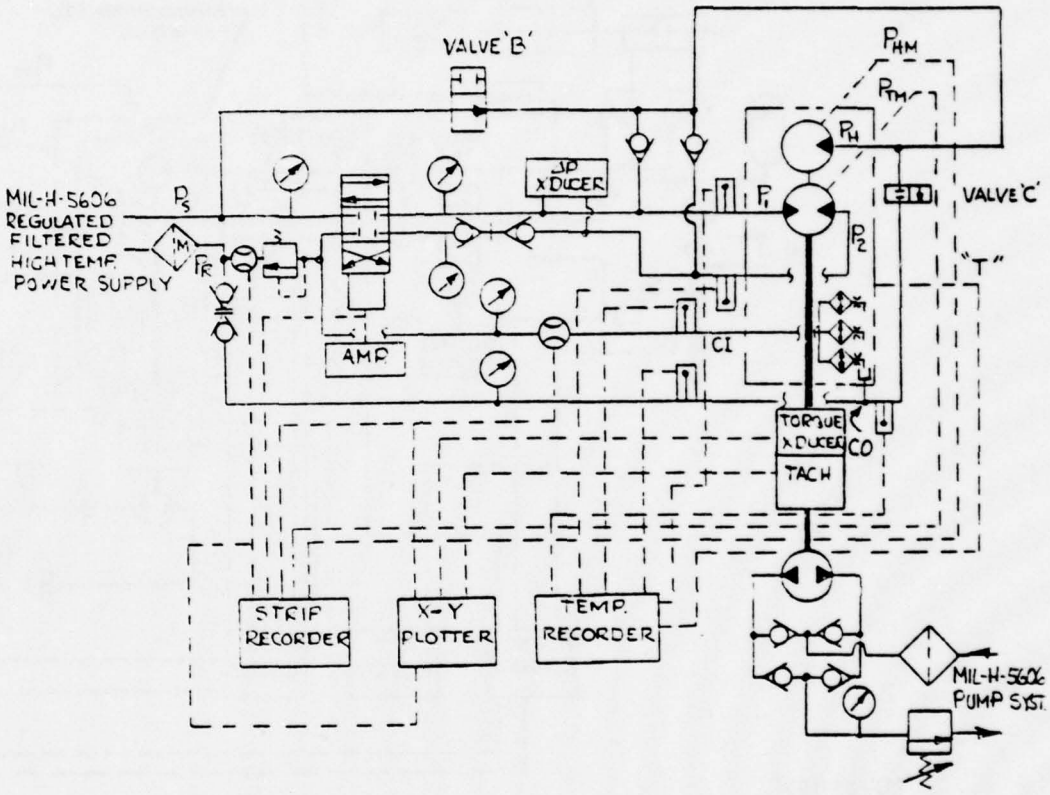

No. of Test Unit Ports	Symbol	Size
4	P_1	AND10050-5
4	P_2	↓
1	P_H	↓
2	CI	AND10050-6
2	CO	AND10050-6

Figure 61. Test Equipment and Circuit Schematic (Room Temperature)

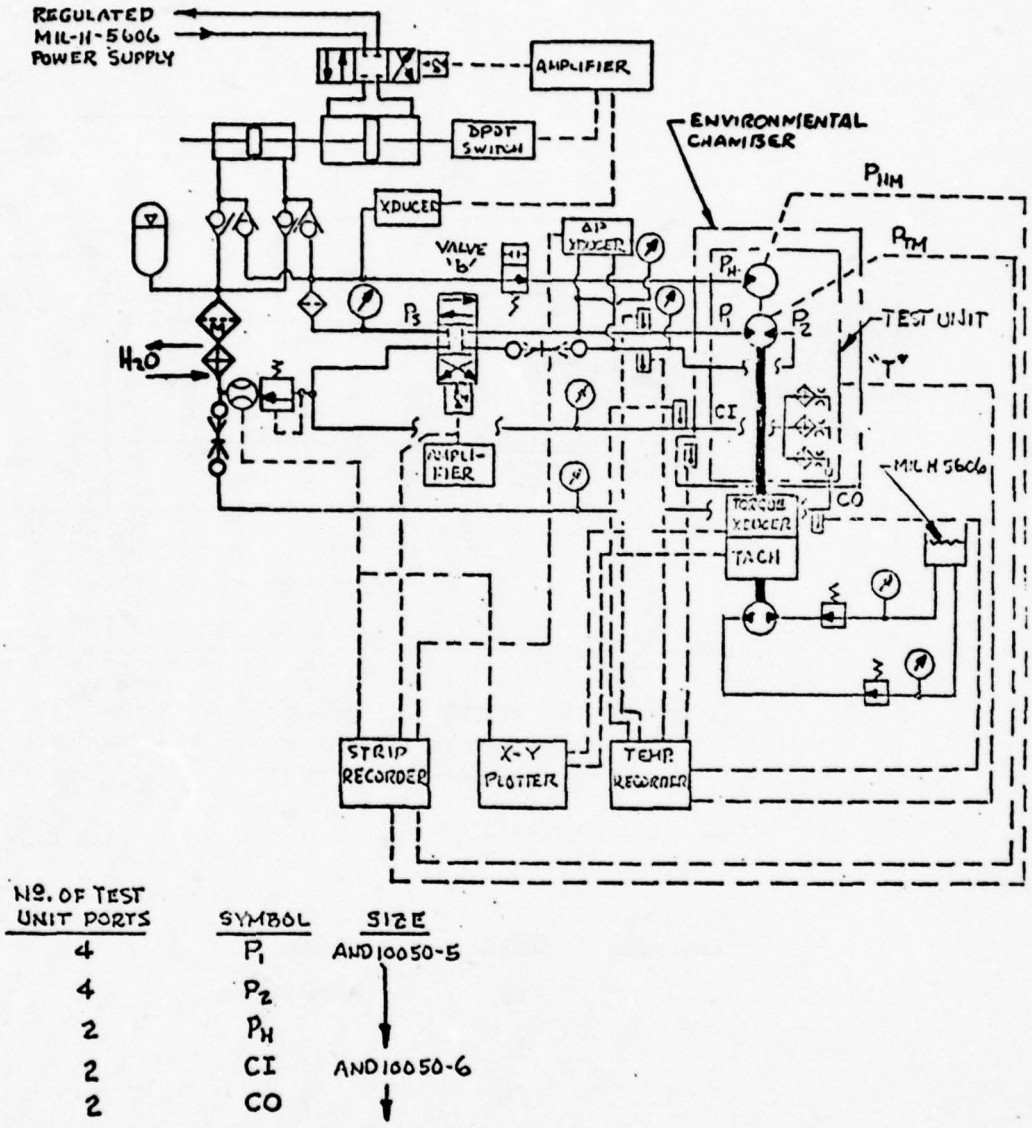

Figure 62. Test Equipment and Circuit Schematic (High Temperature)

The measured running friction of the combined test unit and fixture was approximately 12 pounds-foot (16.3 N-m) of torque. Approximately half of this amount is attributable to the load motor and fixture, and half to the motor cartridge. Consequently, the running torque has been imposed on the Torque Vs Speed plots of Figure 63. With this compensation in the scaling, the symmetry of operation in the CW and CCW directions appears good above approximately 100 rpm. The lack of symmetry for the Torque Vs Speed Characteristic is even more apparent in Figure 64 which was plotted from strip recorder data for other test runs than Figure 63. Figure 65 shows additional test data obtained from strip chart records displaced on Torque Vs Speed plots that show the fairly wide spread location of test points, especially at lower supply pressures and lower speeds. At 3900 psig (26.9 MN/m^2) supply pressure, the maximum torque value near stall is 145 pounds-foot (197 N-m). Using the 3900 psi differential pressure with a measured 3.05 in^3/rev (50 cc/rev) displacement, the torque efficiency is calculated to be 86%.

Figure 66 is a plot from strip chart data as a Torque Vs Differential Pressure plot with calculated efficiencies super imposed (using the 3.05 in^3/rev displacement) from an origin of -6 pounds-foot (-8.1 N-m) torque to account for the tare running torque. As can be seen, most test points above 2000 psid fall above 60% efficiency. More than half of the points above 2000 psid (13.8 MN/m^2) are at greater than 75% efficiency.

Figures 67 and 68 are X-Y plots of Apparent Total Flow Vs Speed at no load for CCW and CW directions respectively. The slope of both plots are nearly the same and equal to 3.86 in^3/rev (63.3 cc/rev).

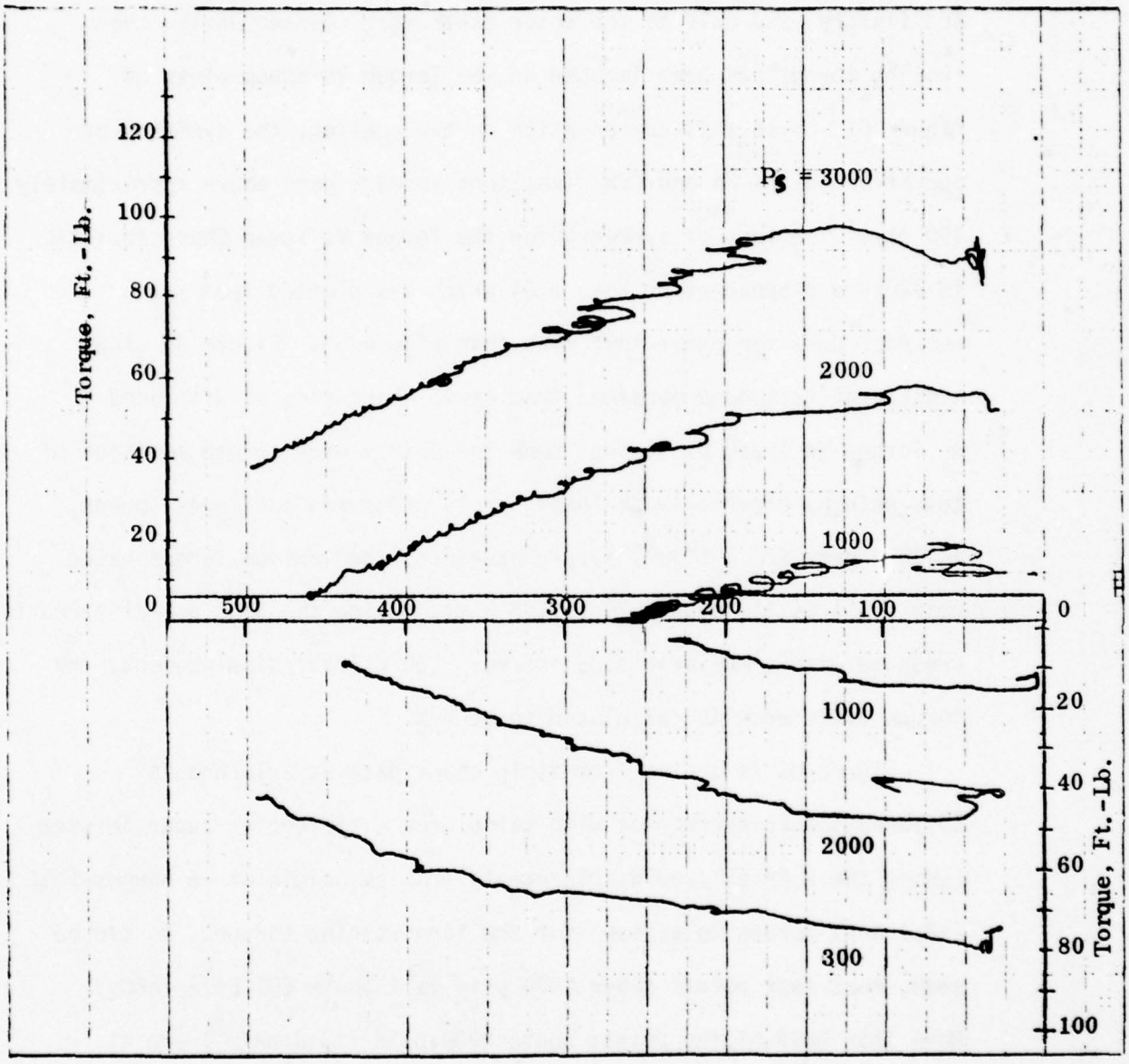

Figure 63. Motor Cartridge Torque vs Speed with P_H Pressure Vented to Return Pressure

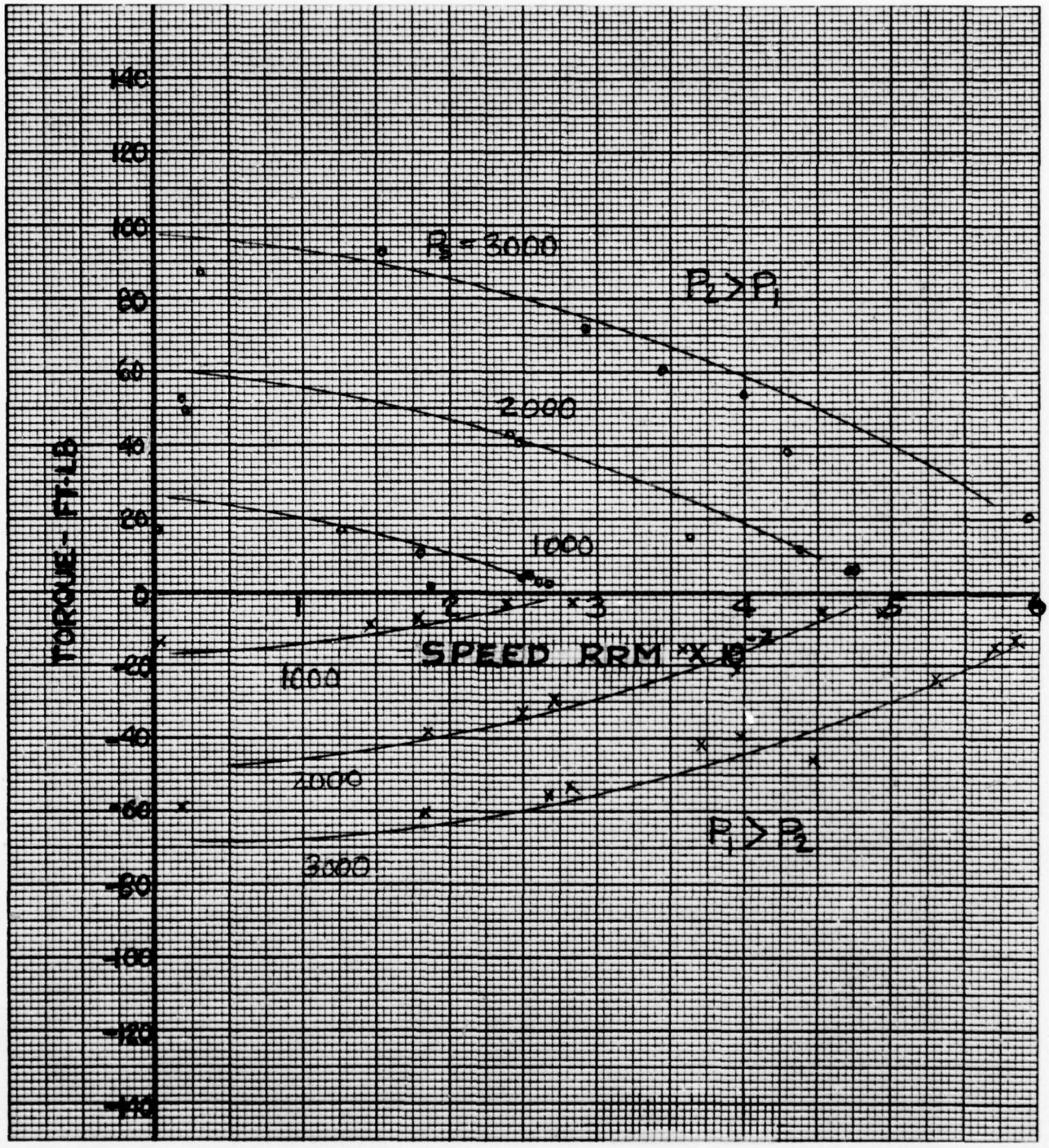

Figure 64. Motor Cartridge Torque vs Speed with P_H Port Blocked

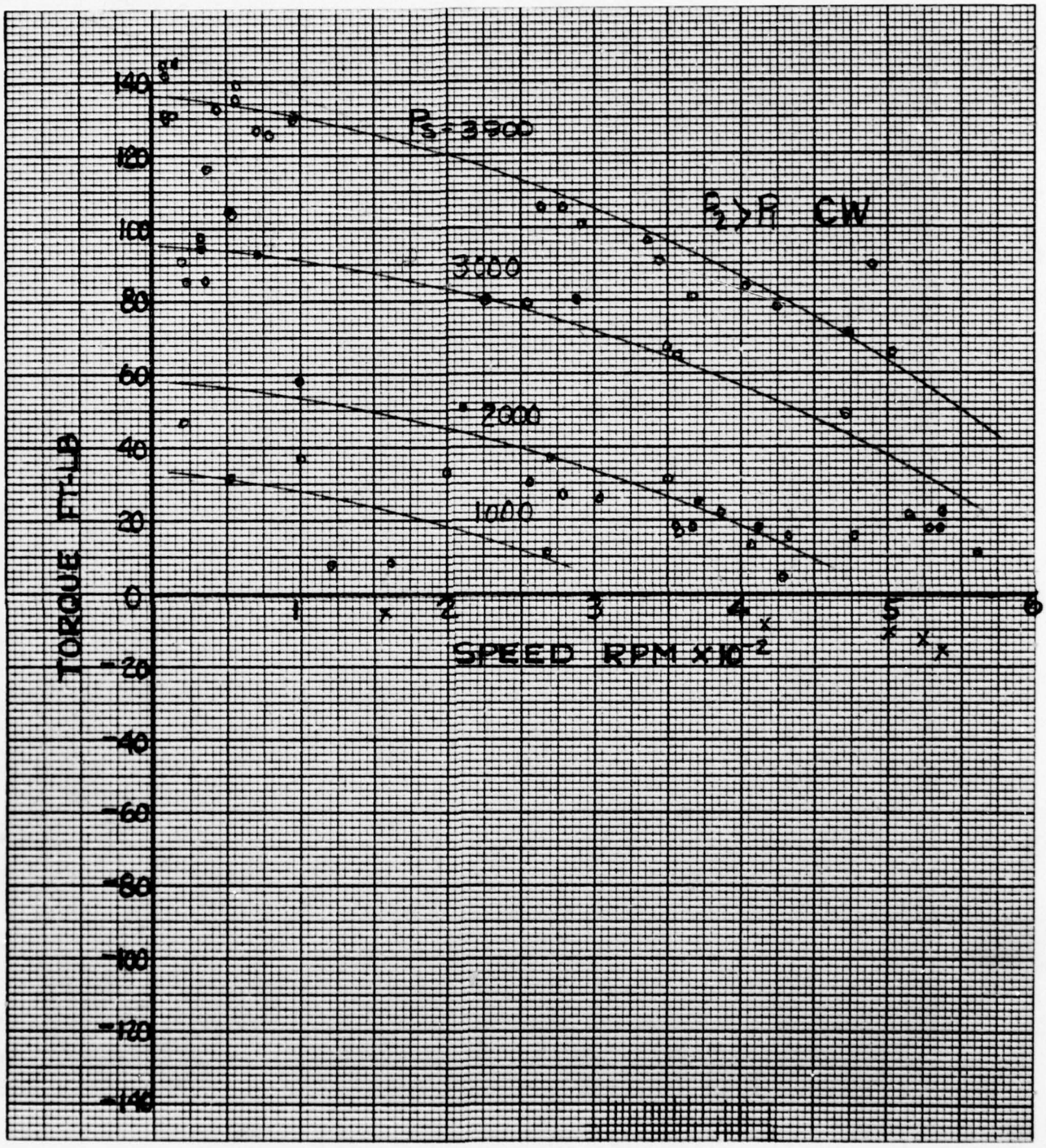

Figure 65. Motor Cartridge Torque vs Speed with P_H Port Blocked

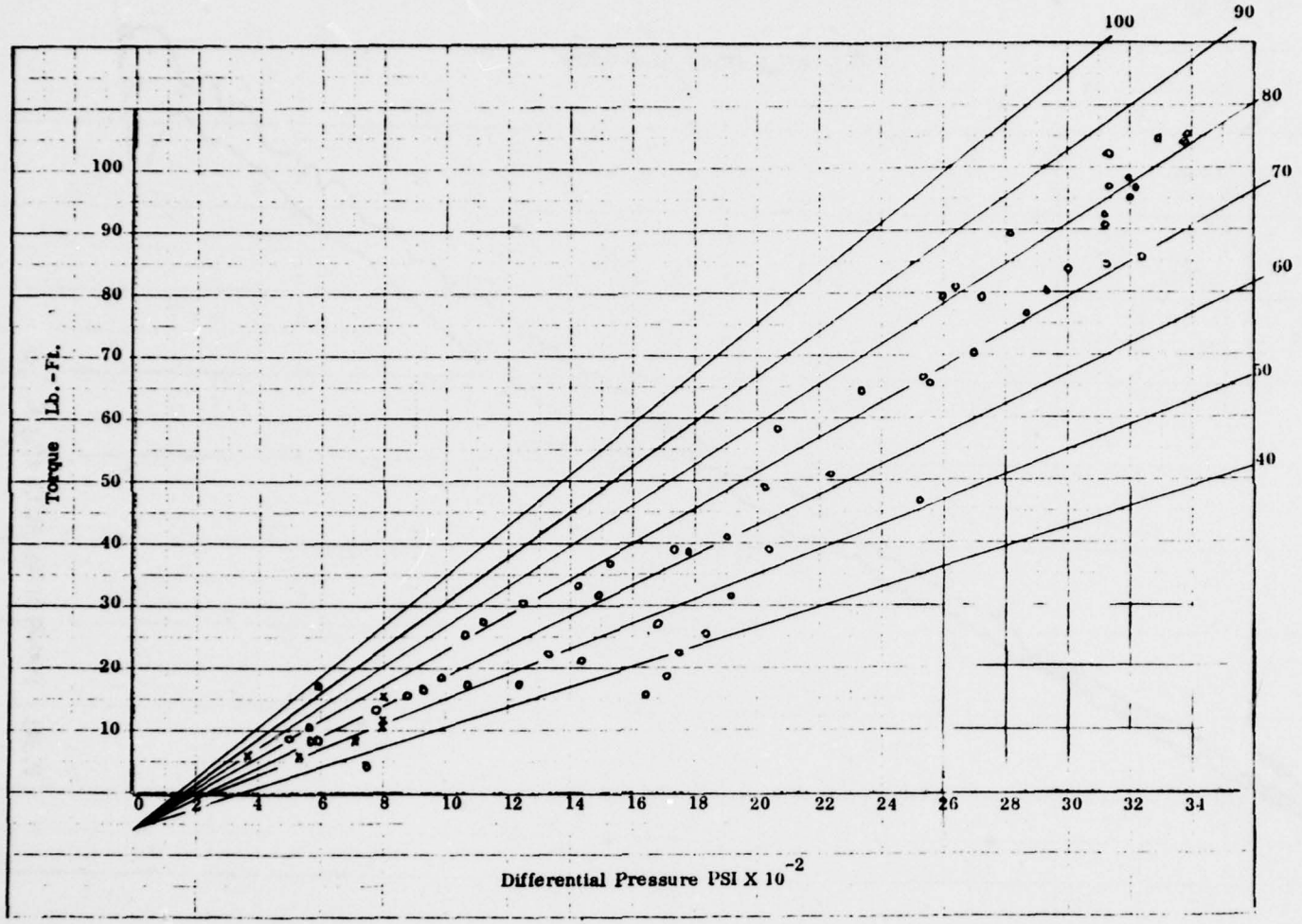

Figure 66. Motor Cartridge Test Unit Torque vs Differential Pressure (Data Taken from Strip Chart Records)

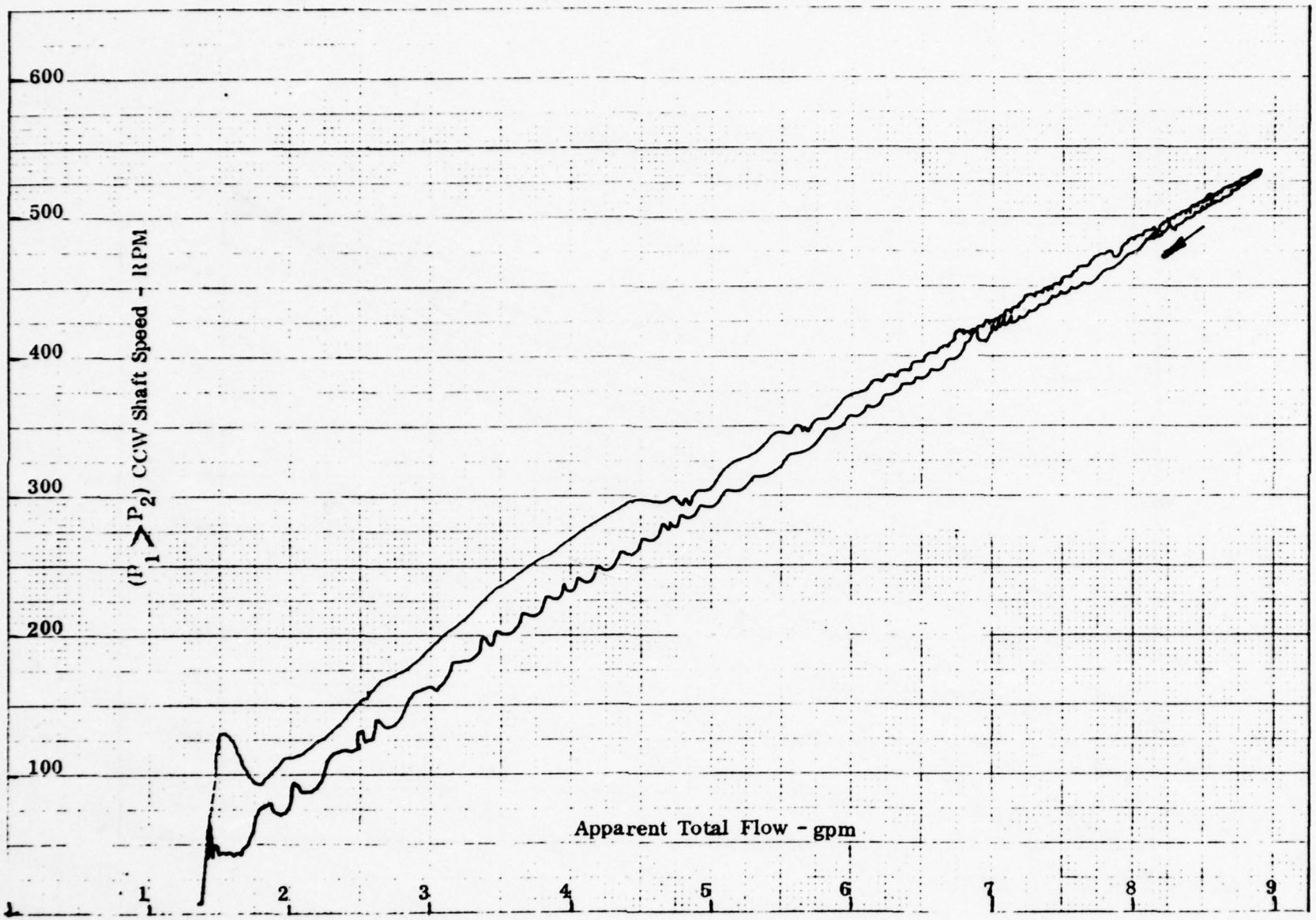

Figure 67. No Load Flow vs Speed with P_H = 0 psig

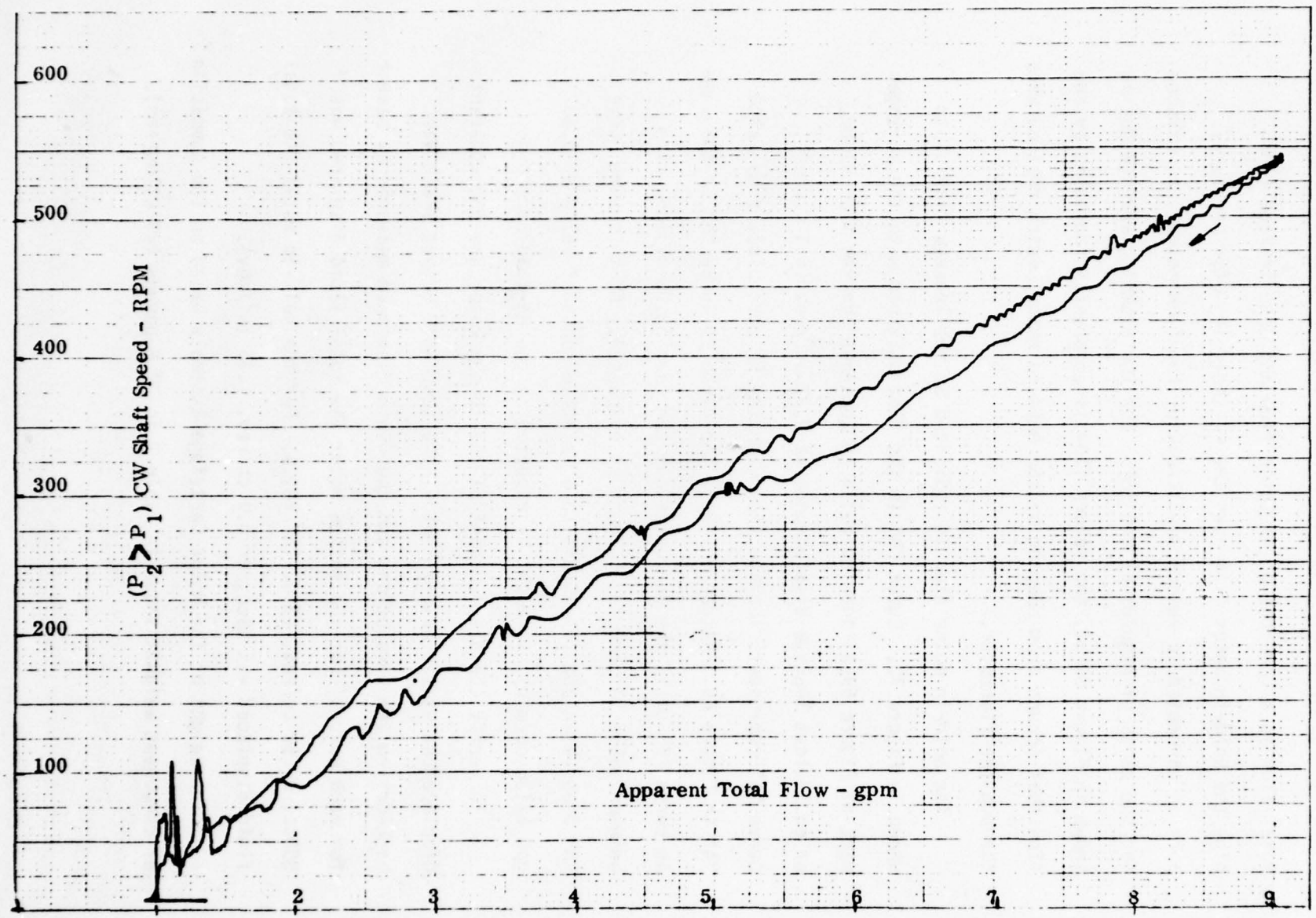

Figure 68. No Load Flow vs Speed with P_H = 0 psig

Total flow is a combination of motor flow and case leakage flow, plus the hold-in motor flow when the P_H (hold-in motor pressure) port is connected to return downstream of the flow meter, (as existed for the plots of Figures 67 and 68). For the plumbing arrangement as shown in Figure 69(a), the return flow is apparently increased by the flow that occurs from pumping by the hold-in motor, which recirculates through the flowmeter.

The hold-in motor flow is indicated by the leakage flow plots shown in Figure 70. Curve "B" is the flow obtained with the arrangement of Figure 69(a) and indicates an apparent leakage flow slope, or equivalent leakage displacement of 0.37 in^3/rev (6.1 cc/rev). Curve "A" represents leakage flow with the P_H port blocked by valve "A" in Figure 69. As can be seen, the slope of Curve "A" is the same as curve "B" until the approximately ten feet (3.05 m) long line between valve "A" and the P_H port is evacuated. At this time Curve "A" drops down and levels off to a relative constant value of 0.30 gpm (1136 cc/min), as might be expected at the no-load condition.

To verify the displacement of the torque motor and the apparent displacement of the hold-in motor, the test unit output shaft was back-driven ten revolutions and the fluid displaced measured by beaker for each motor. For the torque motor the total fluid displaced was 500cc, or 50 cc/rev. (3.05 in^3/rev.). For the hold-in motor the total fluid displaced was 59cc, or 5.9 cc/rev. (.36 in^3/rev).

The weight of the Motor Cartridge Assembly based on the summation of component weights shown in Table 2 is 37.5 pounds (17 kilograms).

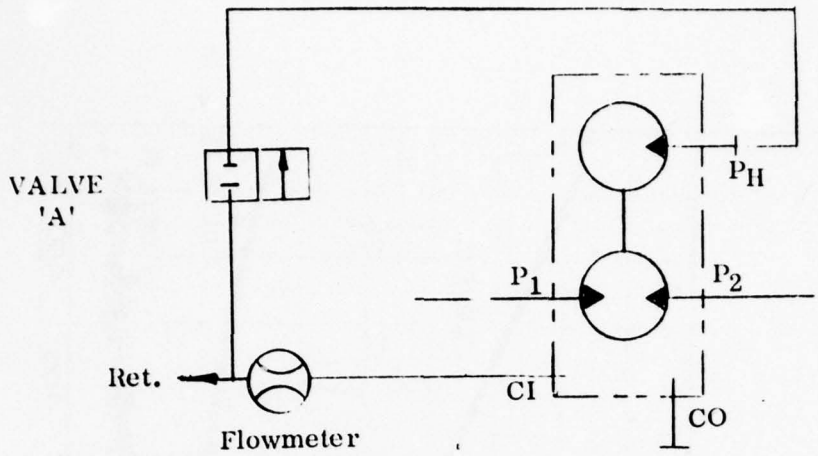

(b) P_H line blocked with valve 'A'.

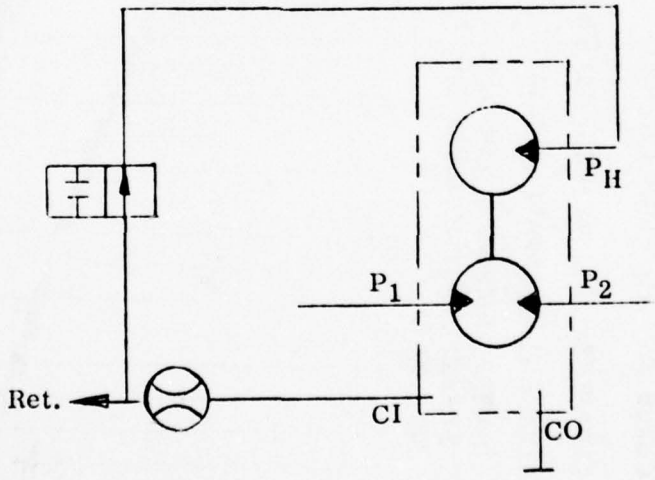

(a) P_H line vented to return.

Figure 69. Leakage Flow Measurement Plumbing Arrangements

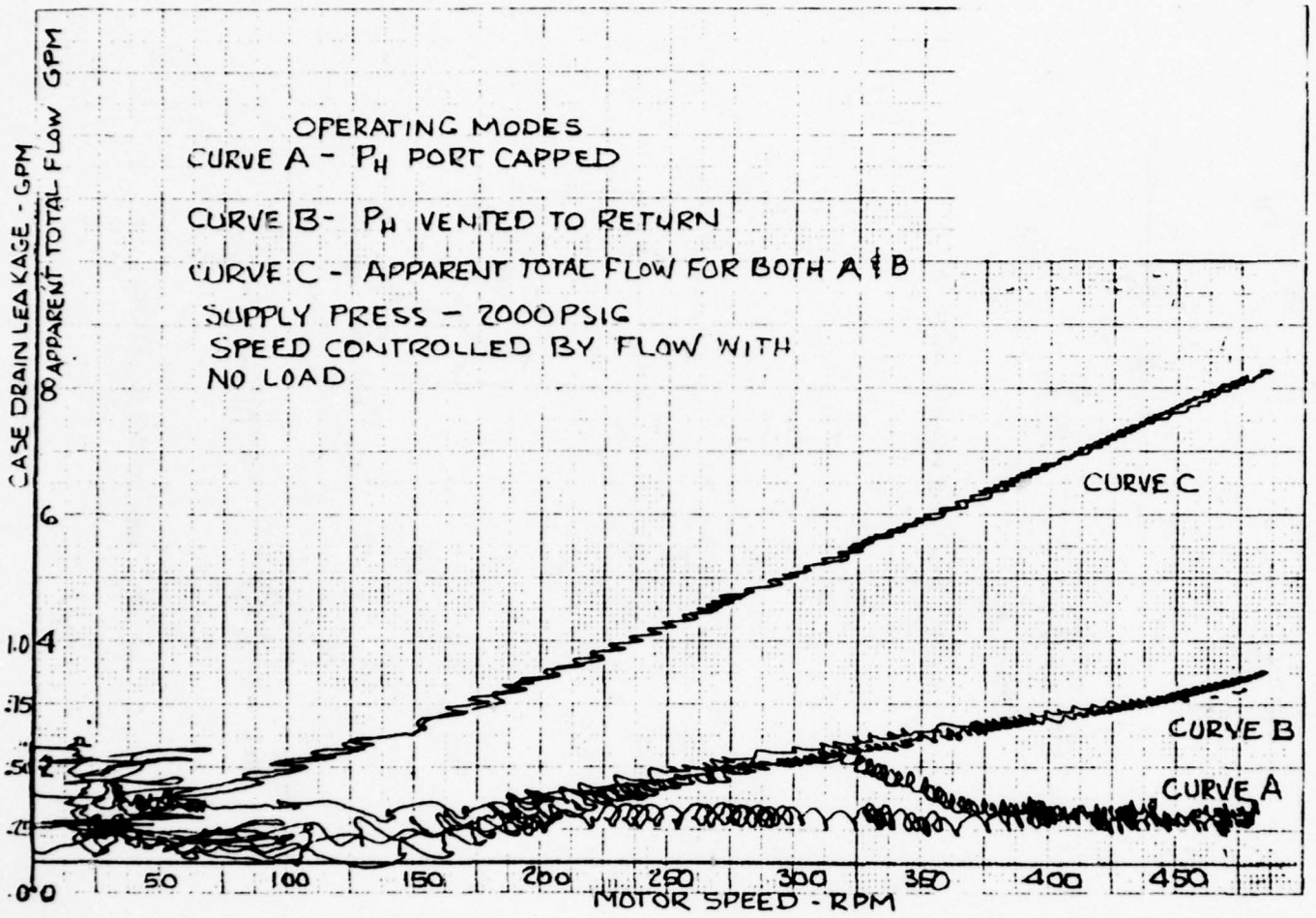

Figure 70. Case Leakage and Supply Flow vs Speed with Hold-in Motor Pressure, P_H Vented to Return or Blocked

b. Conclusions (Motor)

Based on room temperature testing only, for reasons as explained in paragraph 2.C Limitations, the conclusions about the Motor Cartridge are:

. The torque efficiency at stall was within 2 percent of the design goal. Efficiency above half the stall pressure differential varied from 70 to 90 percent.

. The measured displacement of the torque motor was 2 percent less than the design goal.

. The volumetric efficiency varied from 79 percent (3.05 in^3/ rev ÷ 3.86 in^3/rev. X 100) at no load to 70 percent at 3000 psig (20.7 MN/m^2) supply pressure. However, correcting for the 0.36 in^3/rev (5.9 cc/rev) measured displacement of the hold-in motor the no load efficiency would increase to 88 percent ($79 \times \frac{3.05 + .36}{3.05}$) or slightly greater than the design goal, and the efficiency at 3000 psig supply pressure would increase to 78 percent ($70 \times \frac{3.05 + .36}{3.05}$).

. The hold-in motor measured displacement of 0.36 in^3/rev was an unexpected characteristic, since theoretically it was considered to be zero. However, the hold-in motor was also not supposed to produce any torque, but the Appendix and test results refute this. Although there does not seem to be a direct correlation between the effect of the hold-in motor force on the output torque, as developed in the Appendix, and the measured displacement. Based on the displacement, the hold-in motor pumping probably diminished the torque motor output by approximately only 4.6 pounds-inch (0,52 N-m), assuming a 100 psid (690 KN/m^2) pressure rise across the hold-in motor from P_H to the case pressure. This is considered a negligible loss.

. The visible condition of the Motor Cartridge assembly after testing did not indicate any unusual wear or tear of the components. The thrust washers used to locate the output camshaft, in the motor cartridge. test unit, did indirectly contribute to wear of the mating parts as explained in paragraph 2.c.

. The Motor Cartridge leakage of 0.3 gpm (1136 cc/min) at 2000 psig (13.8 MN/m^2) supply pressure and no-load seems reasonable assuming that it would increase approximately proportionally with supply pressure. Based on a design displacement of 3.1 in^3/rev. (50.8 cc/rev) and a maximum speed of 215 rpm, the total flow should have been 3.39 gpm (3.1 x 215/.85x231). Therefore the leakage flow should have been 0.51 gpm (.15 x 3.39) at 4000 psig supply pressure, and 0.25 gpm at 2000 psig. Therefore, the actual leakage of 0.30 gpm with the P_H pressure port blocked, is only 18% too high.

. Below approximately 200 rpm, speed control was difficult to maintain in the test arrangement with a manually controlled pressure regulator in the load motor outlet line. This difficulty was accentuated with small loads because of the inherent friction in test unit and load fixture.

. The Motor Cartridge Assembly weight 37.5 pounds (17 kilograms) is 41% of the prototype actuator weight. The motor assembly along with the transmission components weigh only 57.35 pounds (26 kilograms). The rest of the weight (34.85 pounds) is mainly in the housing and cover. Although these parts incorporate features necessary for the assembly to function (ports, bearing retention, seal cavities, etc.) they mainly are configured to provide the cooling flow paths to protect the motor cartridge.

c. Limitations

Operation of the Motor Cartridge Test Unit with the M-2 tool steel thrust washers could not be achieved. Characteristically, the unit would operate at supply pressure up to approximately 200 psig and no load. At higher pressure the output shaft would abruptly stop. This occurred with rotation either way. Also, galling of the end of the spline ring occurred. This ring which is positioned between the two thrust washers and is pressed onto the middle roller bearing (cam portion of the shaft) was galled on the end next to the rear thrust washer. After repeated attempts to obviate the condition, including thin dense chrome plating the affected end surface, the two steel thrust washers were replaced with ones made of Teflon just to see if this would eliminate the difficulty. After it was determined that the unit operated very well with the Teflon washers, it was decided to use them as an expediency, since their use, combined with the cam shaft, was only a means to test the Motor Cartridge without the gear transmission.

Some concern existed as to whether the front thrust washer made of Teflon would endure under the 35 pound (15.8 kilograms) weight of the test unit output shaft, when the unit was positioned with the shaft in the vertical position on the test fixture. After a few hours of operation in the test position, the washer exhibited little signs of wear. In fact, the upper washer exhibited more wear, or cold extrusion, which in itself seemed tolerable.

Consequently, several days of testing was accomplished to obtain the room temperature characteristics of the Motor Cartridge at the

end of which it was observed that the operation seemed a little different. After a disassembly of the Test Unit Assembly, but not the Motor Cartridge Assembly, it was found that the rear washer (on top as tested) had been severed as shown in Figure 71. The bottom washer, which presumably supported the weight of the shaft assembly, at least in the non-operating mode, was only deformed downward approximately 0.125 inch (0.318 centimeters).

So that the 275°F (135°C) high temperature test could be conducted, it was decided to replace the two washers with new ones, also of Teflon. During the test, with a fluid temperature of 300°F (149°C), it was observed that the shaft was slowly rising approximately one quarter of an inch (0.64 centimeter), then suddenly dropped to rise again with a fairly regular period of about nine seconds.

For fear of incurring damage to the components, it was decided to stop testing. A subsequent dimensional check of the shaft and associated parts failed to reveal any misalignment, taper, etc. that was any more than a few thousandths of an inch. It was noted, however, that spinning of the spline ring and the pressed-in roller bearing by hand resulted in translation of the assembly, with the shaft supported horizontally with its end bearings in two "V" blocks. Spinning the assembly either way resulted in translation in the same direction, which coincided with the end thrust that plagued Motor Cartridge operation. The translational behavior of the spline ring-bearing assembly persisted even when the shaft was tilted about 1.5 degrees (0.026 radian). While this seems somewhat inconsequential, it is believed that this behavior was exaggerated by hydraulic torsion

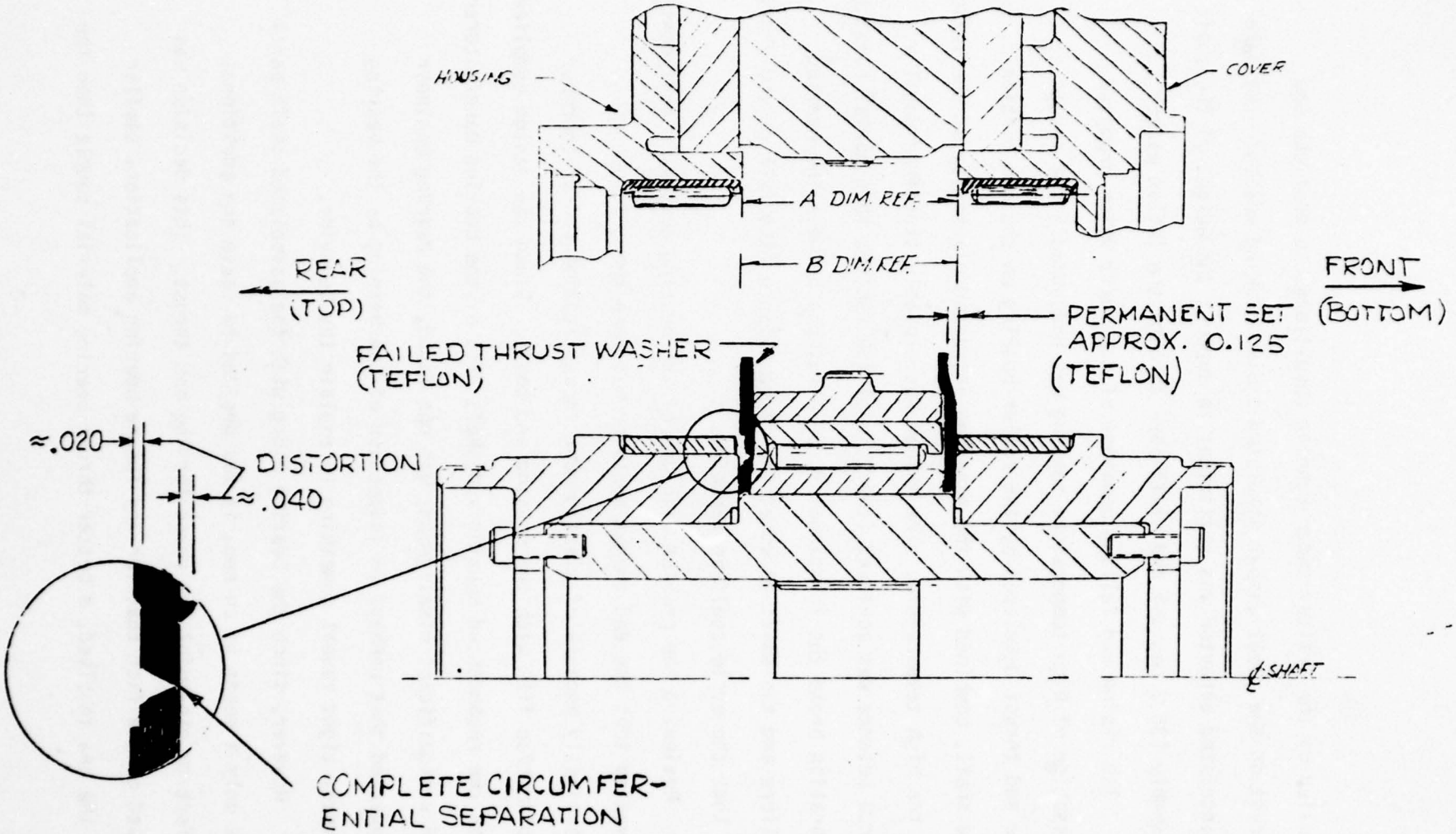

Figure 71. Exploded View of Motor Cartridge Test Unit Showing Failed Teflon Thrust Washer

applied by the orbiter under running conditions, so that the end thrust on the steel washer simulated a disc braking action. The same exaggerated behavior was sufficient to support the weight of the shaft assembly (35.3 pounds) and still bore through the Teflon washer.

The rising and falling behavior of the shaft which prompted cessation of high temperature testing was undoubtedly the result of the end thrust developed by the roller bearing on the cam portion of the shaft, combined with the expected increased plasticity of the Teflon at the high temperature. The washer was probably stretched until a force balance was achieved (the rise of the shaft), then normal running vibration broke the frictional force developed between the bearing rollers and the shaft to upset the force balance (the fall of the shaft), so that the cycle could be repeated.

Reviewing the problem with one of the bearing company's engineers revealed that the end thrust behavior has been known to occur, principally because of misalignment in application and/or improper application fits with the housing and shaft. Since the design complied with the recommended housing and shaft fits by the bearing manufacturer and a significant misalignment was not found, the bearing engineer suggested that perhaps an inspection of the bearing by the bearing company might reveal something to explain the behavior.

However, since the bearing along with the associated shaft parts was only a means to an end, it was decided to cease any additional effort to pin-point the cause for the end thrust. This decision was based on the fact that for any future bearing application, similar to the one involved, a better thrust bearing material couple than the

one used (17-4 PH condition H-900 steel and M2 tool steel, heat treated to R_c60 hardness) is recommended.

3. SHAFT SEAL TEST RESULTS AND CONCLUSIONS

a. Test Results

A summary of the rotary shaft seal testing in the test arrangement shown by the schematic of Figure 43 and in the photograph of Figure 42 is as follows:

Lip Type Rotary Seal (With Fluoroloy 'K' Sealing Element)

The leakage measured for the Serial No. 2 seal (S/N 1 was damaged at installation and not tested) is illustrated in Figures 72 and 73 for fluid temperature from -40°F (-40°C) to +600°F (316°C) and fluid pressures from 25 to 200 psig (.17 to 1.38 MN/m^2). Leakage vs. Time is shown for the same seal in Figure 74. This latter data was obtained during the 24 hours of high temperature endurance testing. Figures 75 and 76 are Torque vs. Displacement plots obtained at room and high temperatures. The Plots represent the torque required to drive both seals, the lip-type seal and the face-type seal, since one of each was tested simultaneously in the test fixture, Figure 38. Approximately 90% (400 pounds-inch) of the room temperature torque value shown is attributable to the bellows loaded face-type seal, (as determined by manual, tare measurements). Torque vs. Pressure characteristics are shown in Figure 77.

Face Type Rotary Seal (Carbon-Graphite Against Chrome Plated Steel)

The measured leakage for the serial No. 1 seal is shown in Figures 78 and 79 for various values of fluid temperature from -40°F (-40°C) to +600°F (316°C) and fluid pressures from 25 to 200 psig

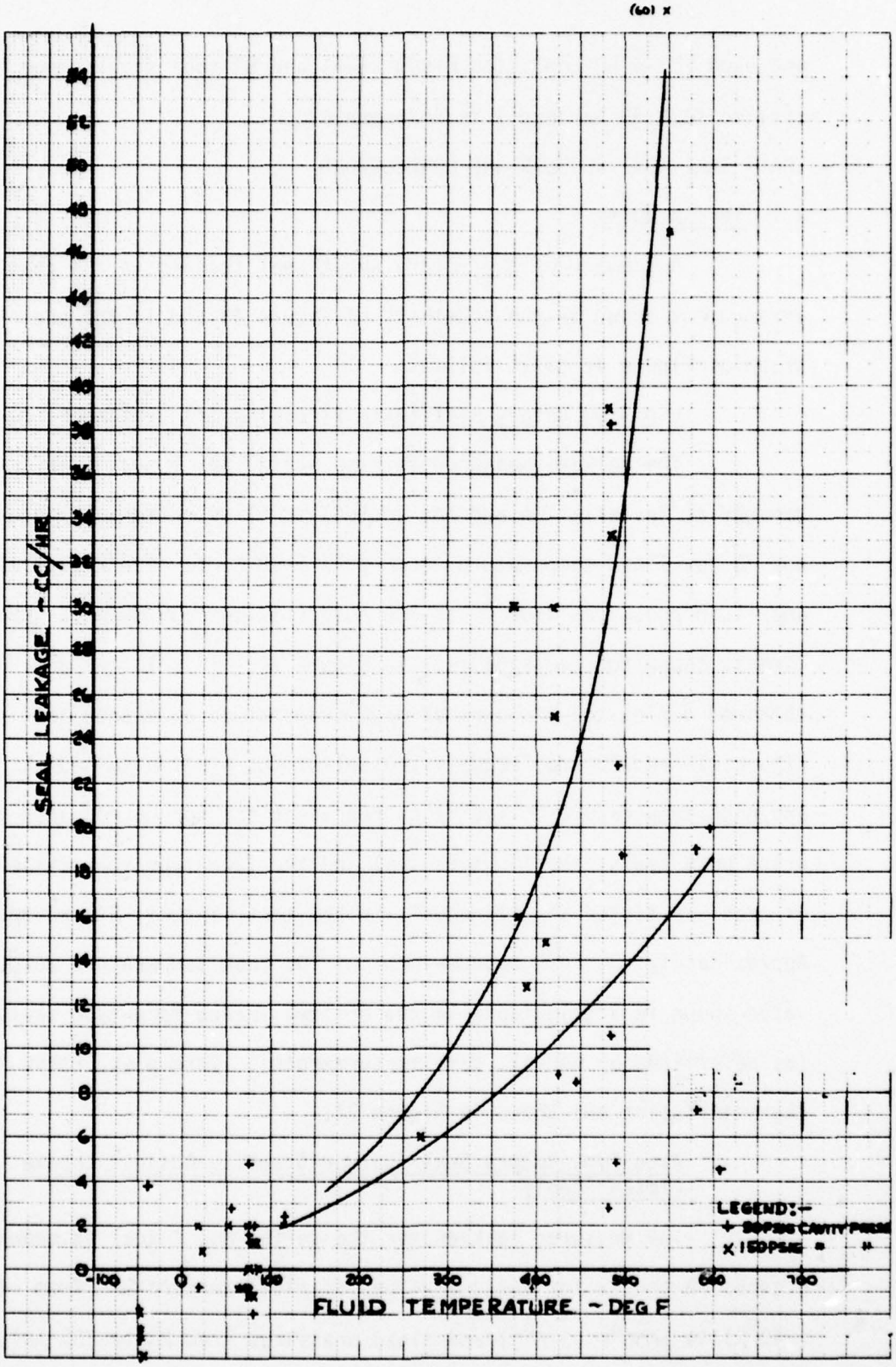

Figure 72. Leakage vs Temperature Lip Type Seal

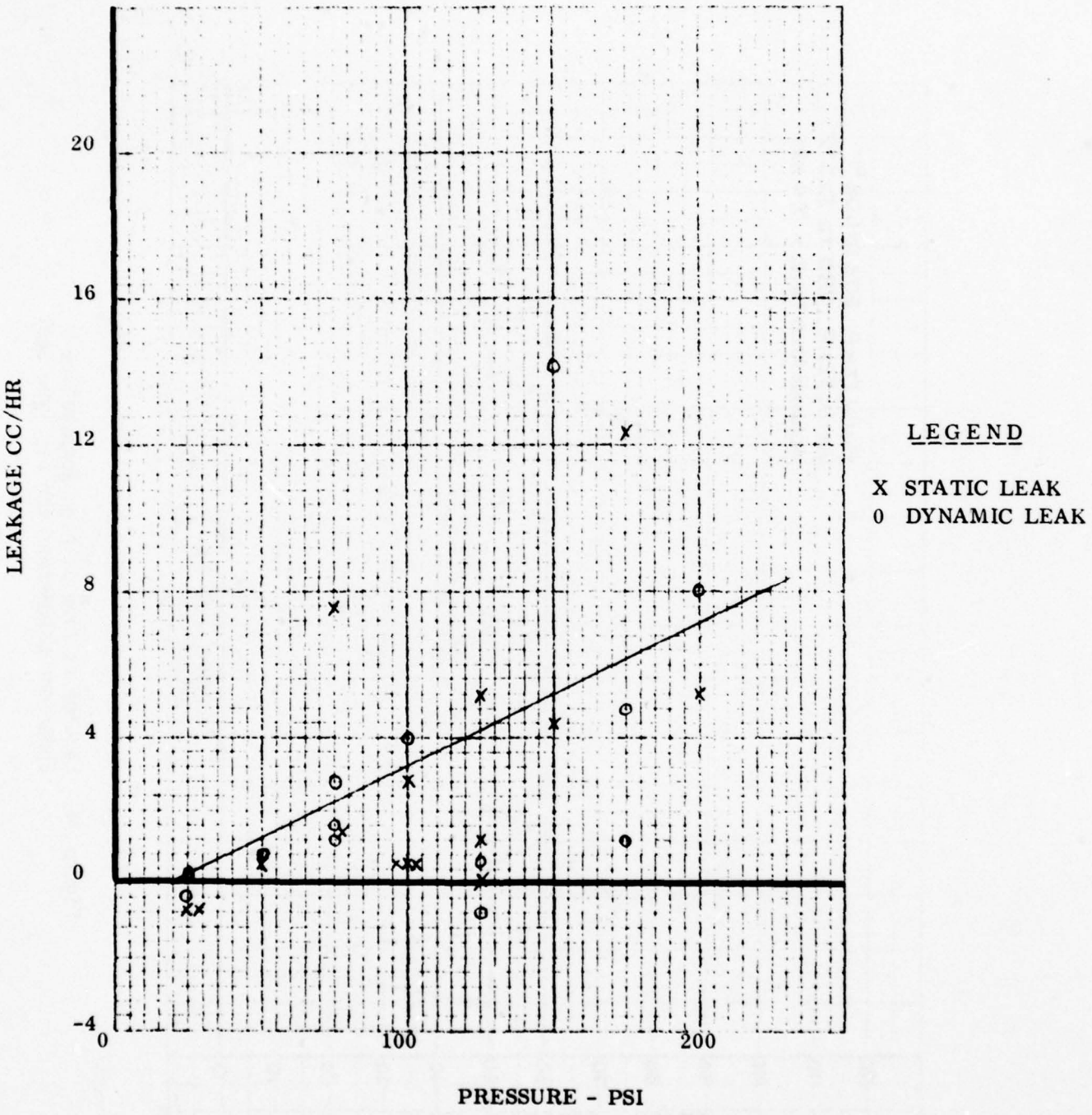

Figure 73. Leakage vs Pressure at Room Temperature for Lip Type Seal

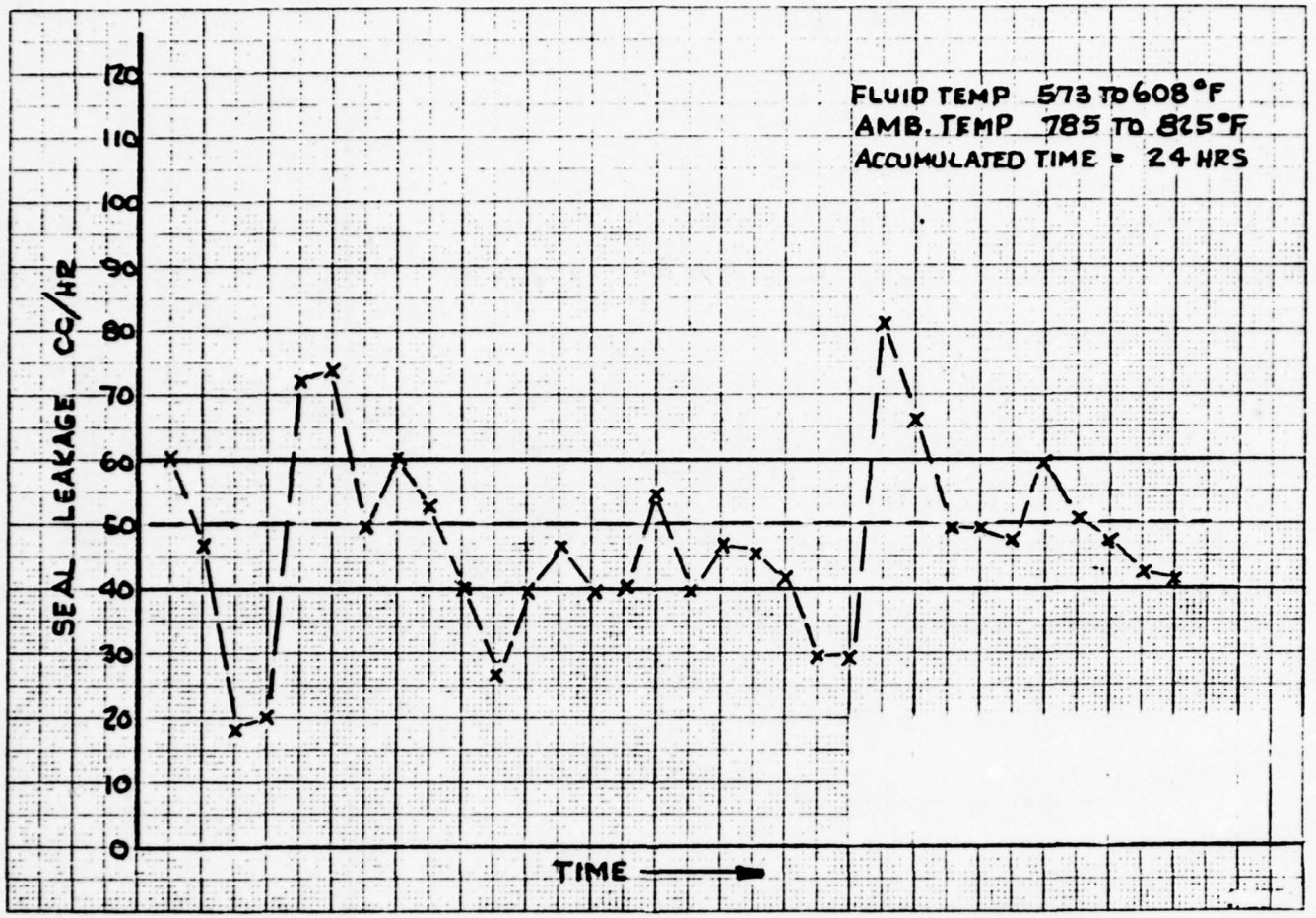

Figure 74. Leakage vs Time at High Temperature Endurance Conditions for Lip Type Seal

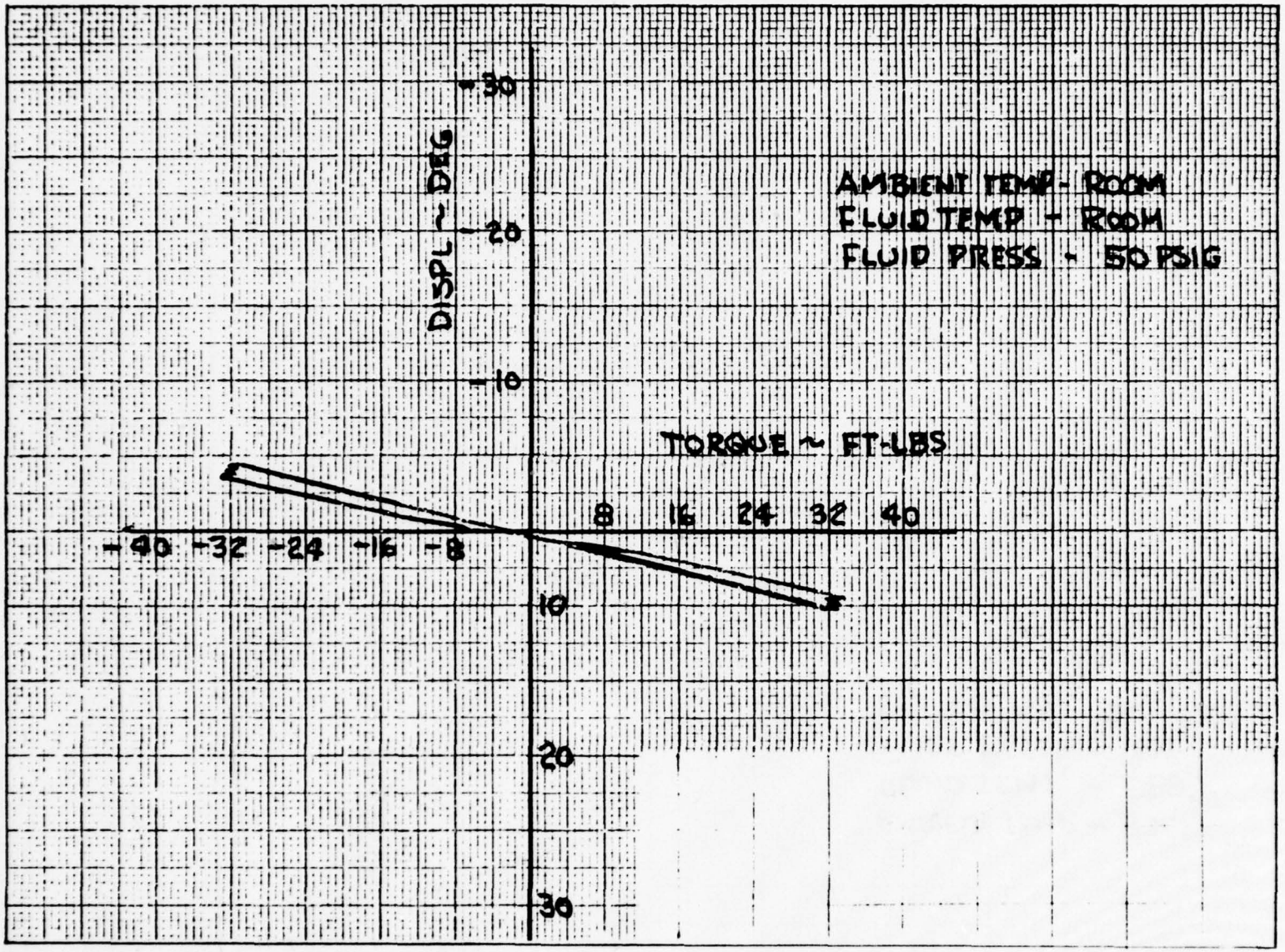

Figure 75. Static Friction Torque vs Displacement

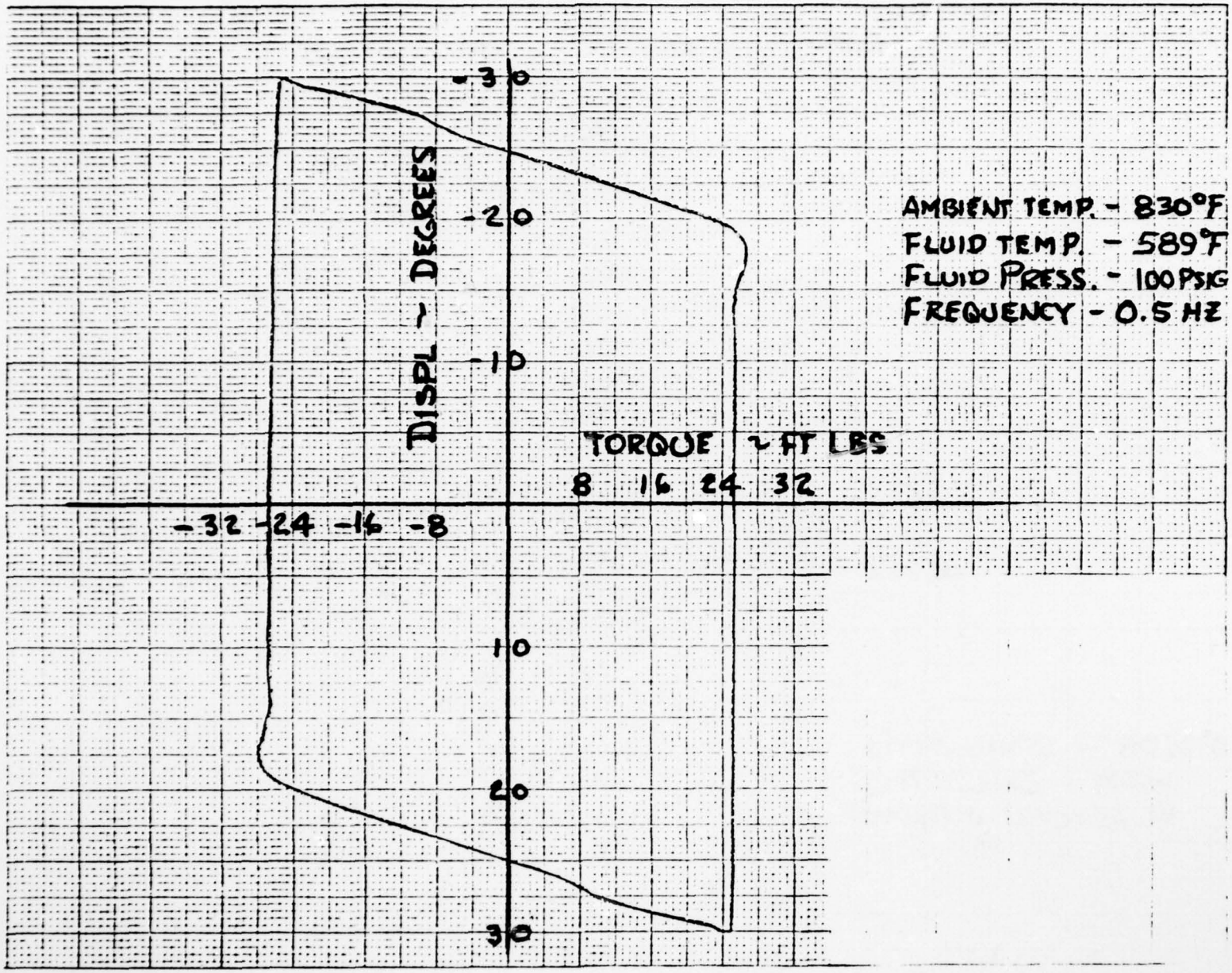

Figure 76. Dynamic Friction Torque vs Displacement

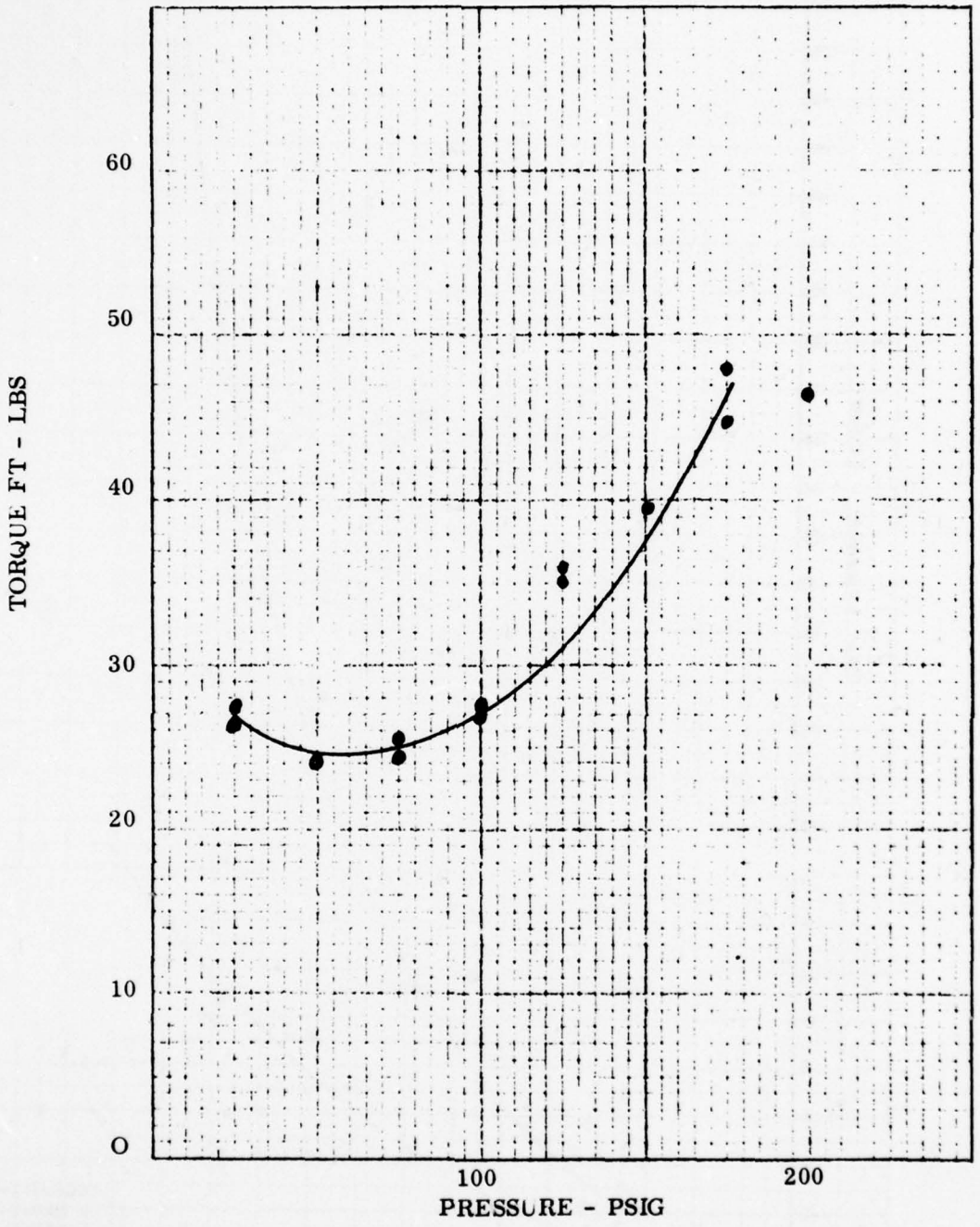

Figure 77. Torque vs Pressure at Room Temperature for the Lip and Radial Face Type Seals

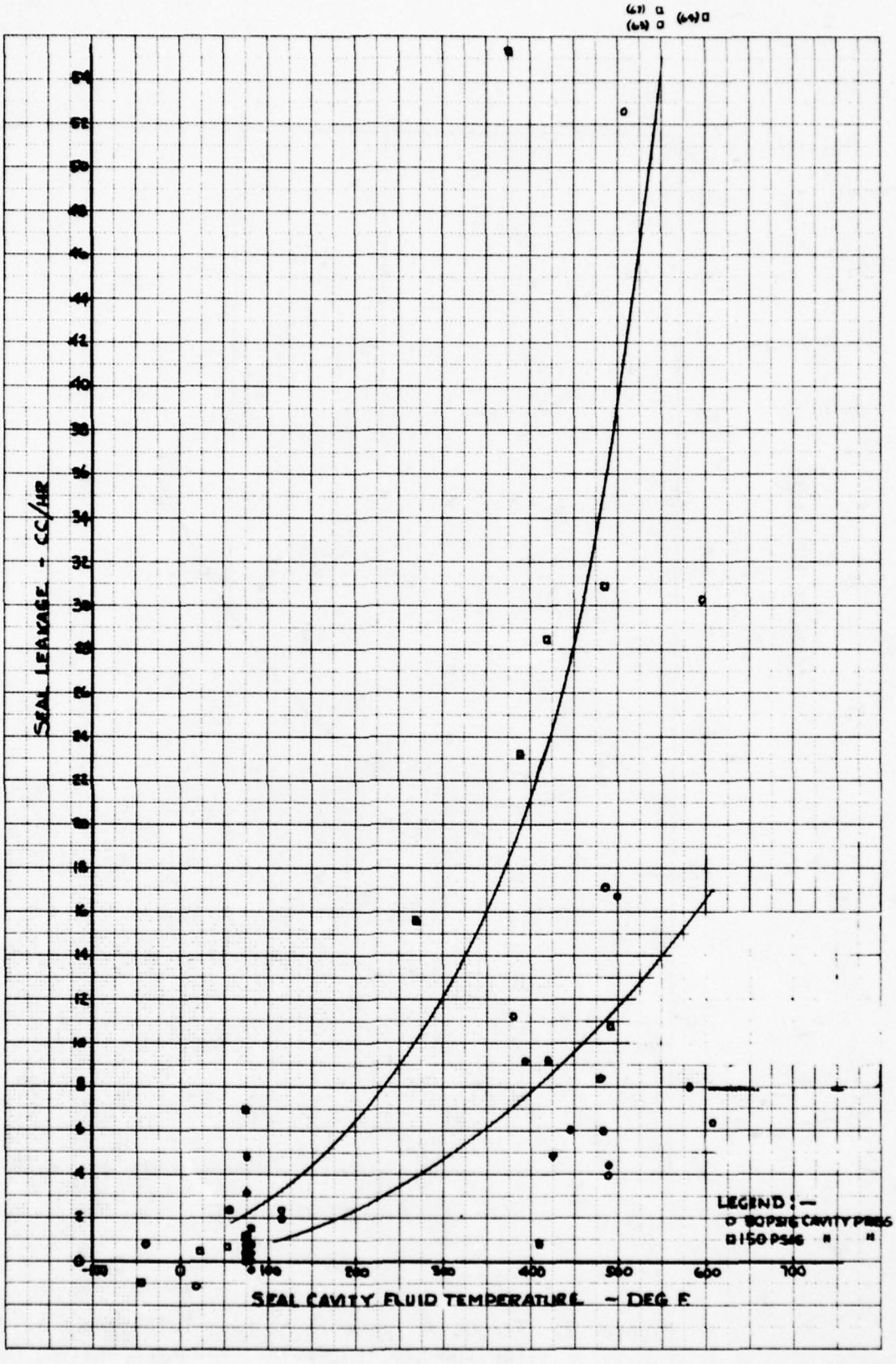

Figure 78. Leakage vs Temperature Radial Face Type Seal

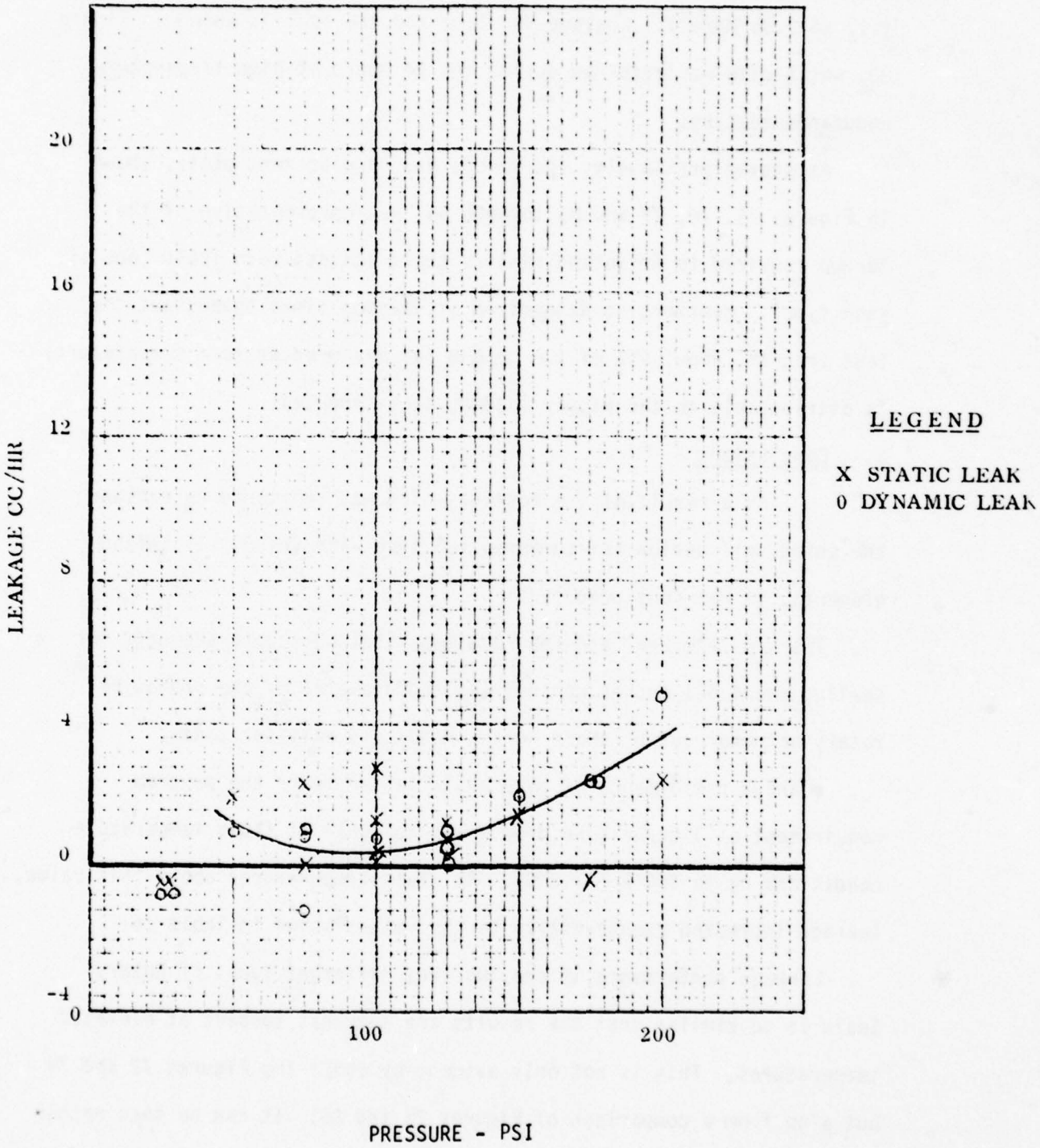

Figure 79. Leakage vs Pressure at Room Temperature for Radial Face Type Seal

(.17 to 1.38 MN/m^2). Leakage Vs. Time for the seal is shown in Figure 80, which also was attained during the 24 hours of high temperature endurance testing.

As stated previously, the Torque Vs. Displacement plots, shown in Figures 75, 76, 77 and 81 through 84 are representative of the torque required to drive the fixture shaft against both seals (one of each type). However, as determined at various times throughout the test program, about 90% of the torque (as measured at room temperature) is attributable to the highly loaded, face-type seal.

b. Conclusions

As a result of the testing which was shortened to exclude the third seal design (circumferential type with Vespel 21 sealing element), it was concluded that:

. The Lip Type Seal and the Face Type Seal were both adequate for sealing the 4.621 inches nominal sealing diameter of the prototype rotary actuator output shaft during motor and actuator tests.

. Leakage performance of both seals tested meets the program requirement of 3 cc/hr (one drop a minute) only at fluid temperature conditions up to $100^{o}F$ ($37.8^{o}C$). At fluid temperatures above this value, leakage increased exponentially to the values shown in Table 16.

. Leakage performance of the two very different types of Rotary Seals is so similar that the results are somewhat suspect at elevated temperatures. This is not only evident by comparing Figures 72 and 78 but also from a comparison of Figures 74 and 80. It can be seen rather dramatically that the leakage changes of the seals were synchronous during the 24-hour endurance test. This appears to indicate that a common factor such as temperature control or leakage measurement could

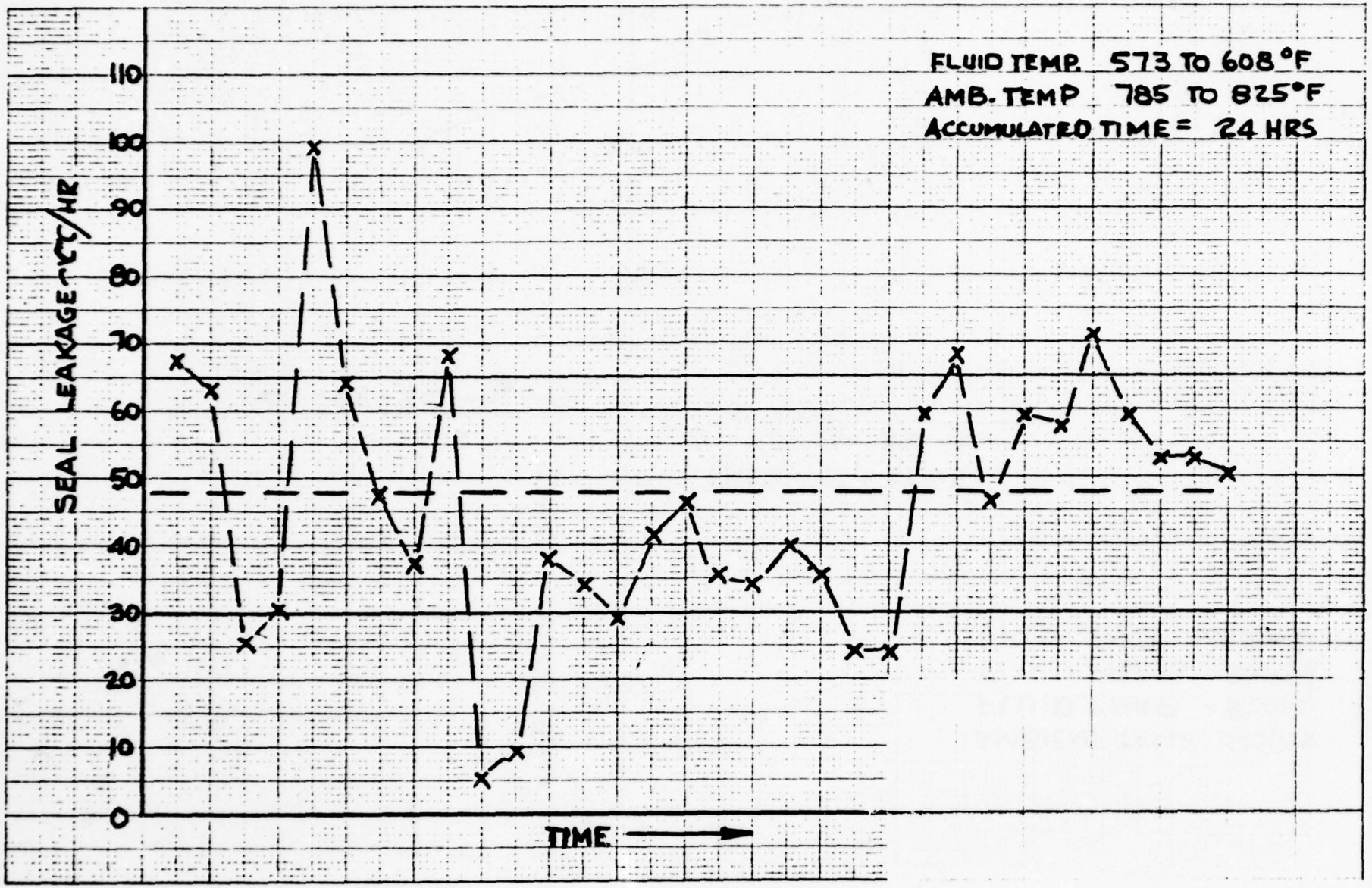

Figure 80. Leakage vs Time at High Temperature Endurance Conditions for Radial Face Type Seal

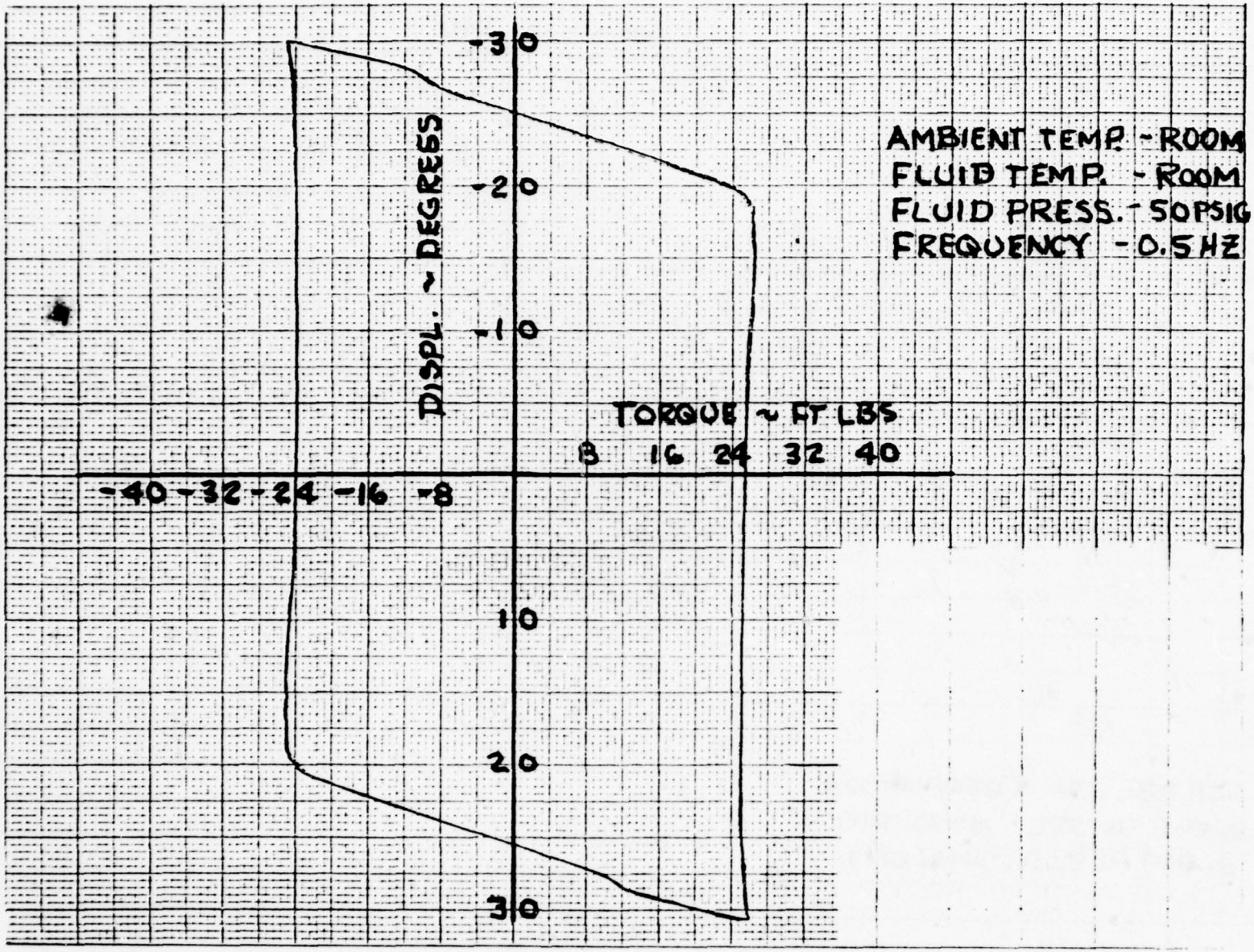

Figure 81. Dynamic Friction Torque vs Displacement

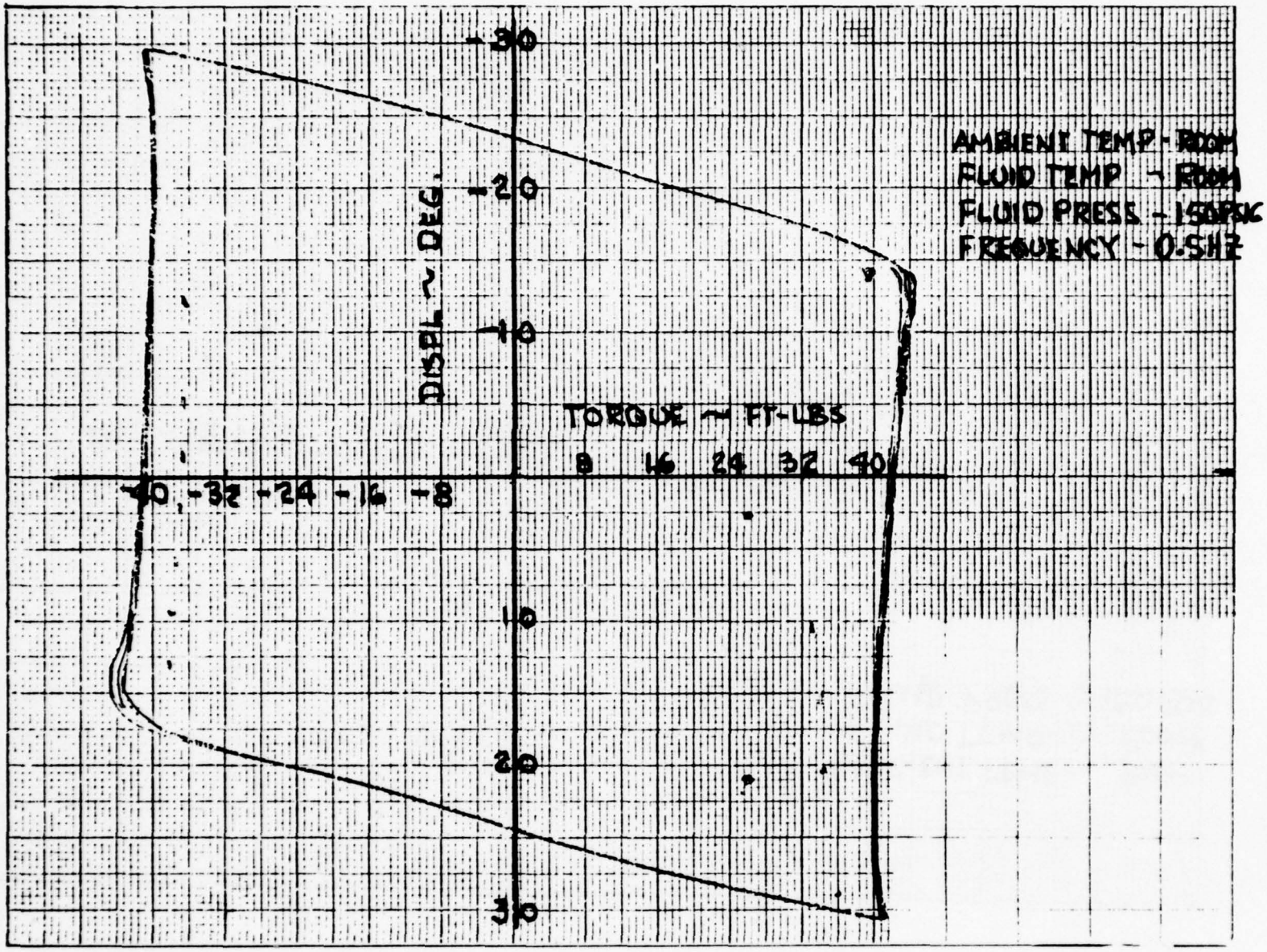

Figure 82. Dynamic Friction Torque vs Displacement

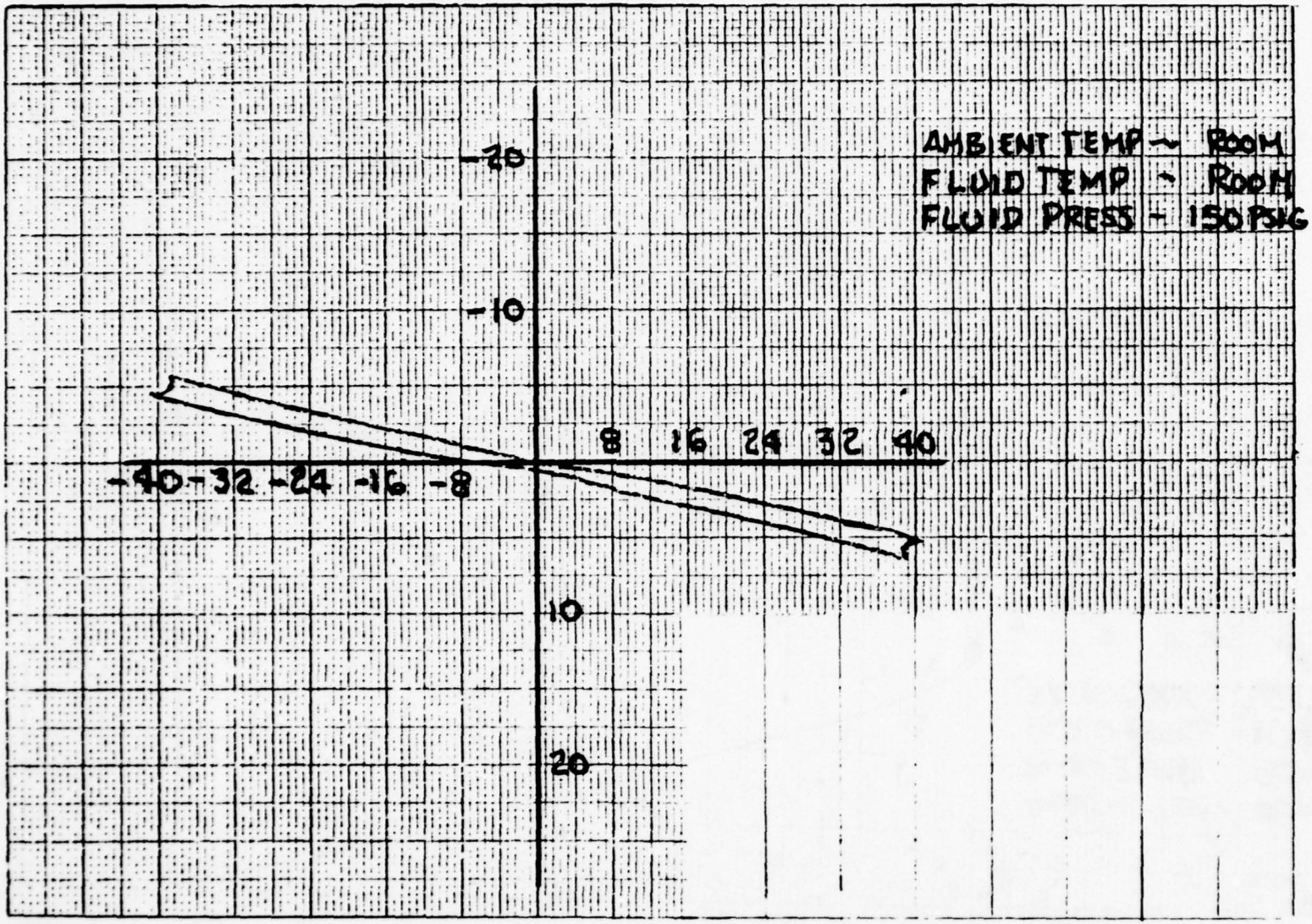

Figure 83. Static Friction Torque vs Displacement

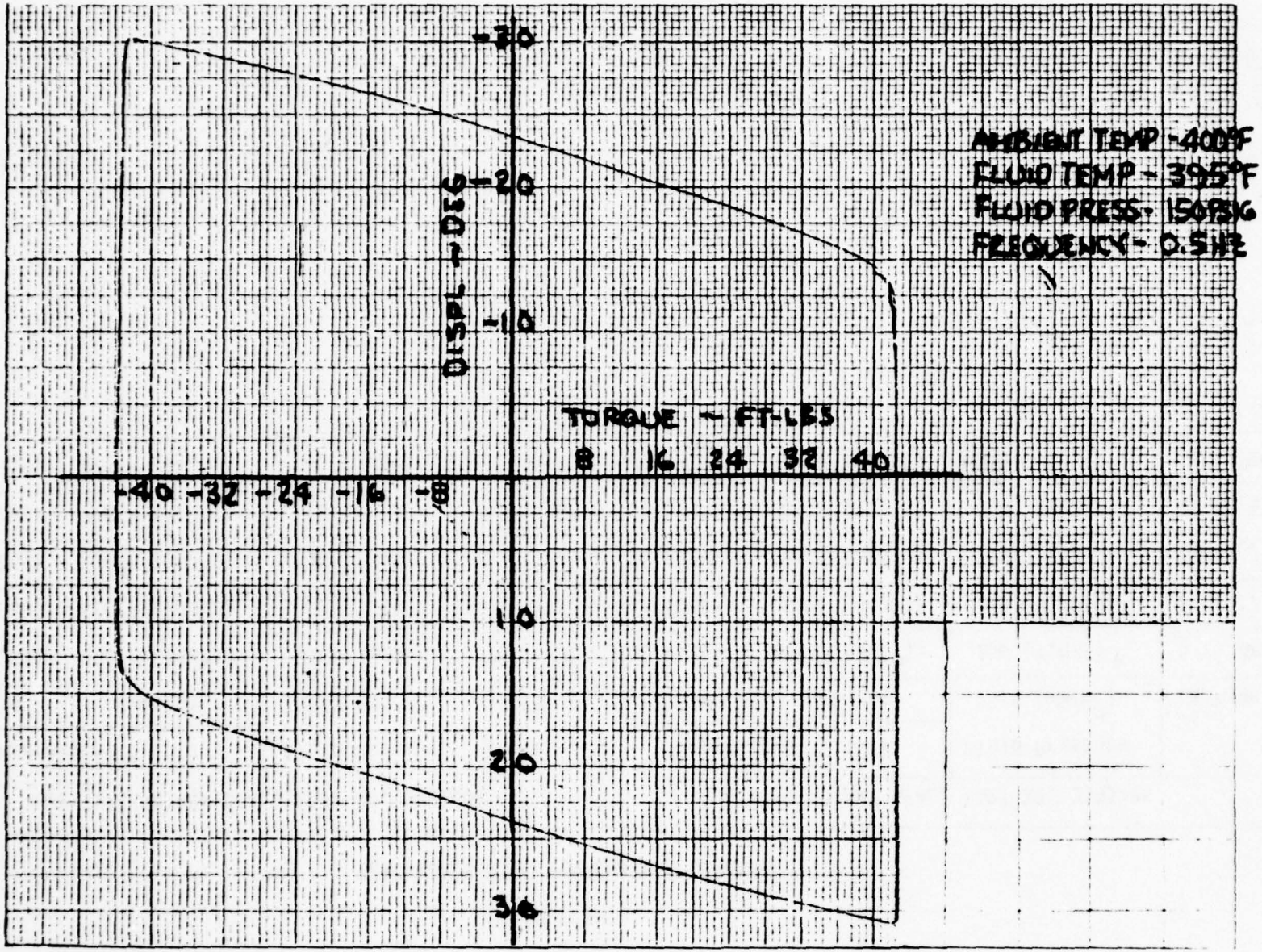

Figure 84. Dynamic Friction Torque vs Displacement

TABLE 16

TEST SEALS HIGH TEMPERATURE LEAKAGE

LIP TYPE ROTARY SEAL, PART NO. 3191564				FACE TYPE ROTARY SEAL, PART NO. 3191485			
Temperature ^{o}F (^{o}C)		Fluid Pressure	Leakage	Temperature ^{o}F (^{o}C)		Fluid Pressure	
Fluid	Ambient	PSIG (MN/m^2)	CC/Hr.	Fluid	Ambient	PSIG (MN/m^2)	Leakage
400 (204)	$600^{o}F$ ($316^{o}C$)	150 (1.035)	13 to 30	400 (204)	$600^{o}F$ ($316^{o}C$)	150 (1.035)	5 to 28
500 (260)	$680^{o}F$ ($360^{o}C$)	50 (0.345)	5 to 23	500 (260)	$680^{o}F$ ($360^{o}C$)	50 (0.345)	4 to 17
500 (260)	$680^{o}F$ ($360^{o}C$)	150 (1.035)	33 to 39	500 (260)	$680^{o}F$ ($360^{o}C$)	150 (1.035)	10 to 31
500 (288)	$775^{o}F$ ($413^{o}C$)	150 (1.035)	47 to 60	550 (288)	$775^{o}F$ ($413^{o}C$)	150 (1.035)	63 to 67
600 (316)	$825^{o}F$ ($441^{o}C$)	50 (0.345)	7 to 20	600 (316)	$825^{o}F$ ($441^{o}C$)	50 (0.345)	8 to 30

be responsible for the wide scattering of measured leakage values.

. Part of the data scatter can be attributed to the significant volumes of hydraulic fluid contained in each seal cavity and the lack of precise temperature control. However, the entrapped fluid volumes measured only 4.76 in^3 (78 cc) for the face-type seal and 5.98 in^3 (98 cc) for the lip-type seal. These combined with fluid volumetric expansion coefficient of 3.8 (10^{-4}) in^3/in^3 per ^oF. (2.1 per ^oC) at 400^oF (204^oC) and a ±25^oF (±14^oC) variation in fluid temperature, will produce a volume change of only ±.045 to ±.057 in^3 (±.72 to ±.91 cc). Based on this magnitude of volume change occurring during the regular 15 minute long leakage measurement by sight gauge, the error would be increased by a factor of four. This would provide a 5.8 cc/hour to 7.2 cc/hour total variation in leakage for a ±25^oF (±14^oC) change in temperature. These latter values are about 16% and 36% of the average data spread shown in Figures 74 and 80 respectively.

During the constant temperature, +600^oF (316^oC) fluid and +800^oF (427^oC) ambient endurance test, it is believed that the fluid temperature was maintained well within the ±25^oF (±14^oC) range (for other tests, variations exceeding this spread did occur). Therefore, the cause of much of the recorded variations in measured leakage (at least during endurance) is unknown.

. The similarity of leakage rates as a function of temperature for the two different seal designs could be the result of the common test fixture although this seems unlikely. The compromise use of 17-4 PH corrosion resistant steel for the fixture housing instead of the 18 Ni 350 Maraging steel used for the shaft should have had a negligible

effect on seal performance based on the small difference in thermal coefficients of linear expansion.

. Since visual observation of seal leakage was prevented by the installation and test arrangement, part of each seal leakage could be the result of the static metallic seals used in each cavity (one for the lip-type seal and two for the face-type seal) and the metallic AN-boss seals used for the inlet and outlet lines. Some leakage from the boss seals was evident from a build-up of varnish and carbon around them (Figure 85); however, most of this occurred in early shake-down runs. The same evidence formed on the rotary seals (Figures 86 and 87) and shaft from external leakage but there was no way of determining whether it emanated from the cavities static or dynamic seals.

. Visual examination of both test seals (Figures 86 and 88) revealed no excessive wear or tear after the 100 hours and 180,000 cycles of operation.

. Inconsistent leakage measurements tend to obscure the Leakage vs. Pressure characteristics (Figure 73) of the Lip-Type Seal. For the Face-Type seal, leakage measurements (Figure 79) were more consistent and indicate an optimum operating pressure range of about 75 to 100 psig. (.52 to .69 MN/m^2).

. Torque as a function of pressure (Figure 77) also indicates the existence of an optimum operating pressure range of 50 to 75 psig (.34 to .52 MN/m^2).

. Since most of the torque (90%) is attributable to the Face-Type seal, it is presumed that this optimum range applies to this seal type only.

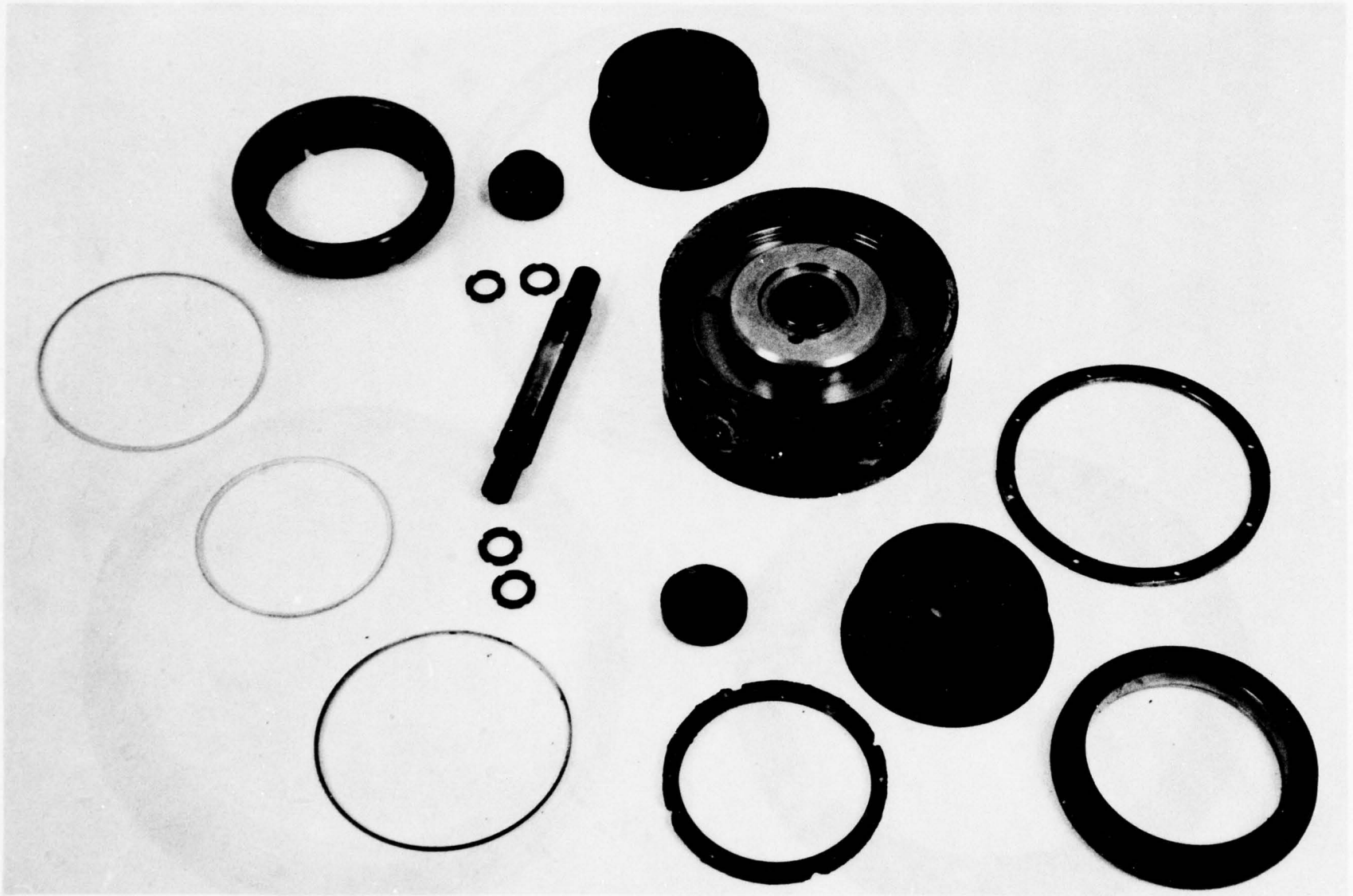

Figure 85. Test Seals and Fixture Components After Testing

Figure 86. Radial Face Type Rotary Seal After Testing

Figure 87. Lip Type Rotary Seal After Testing

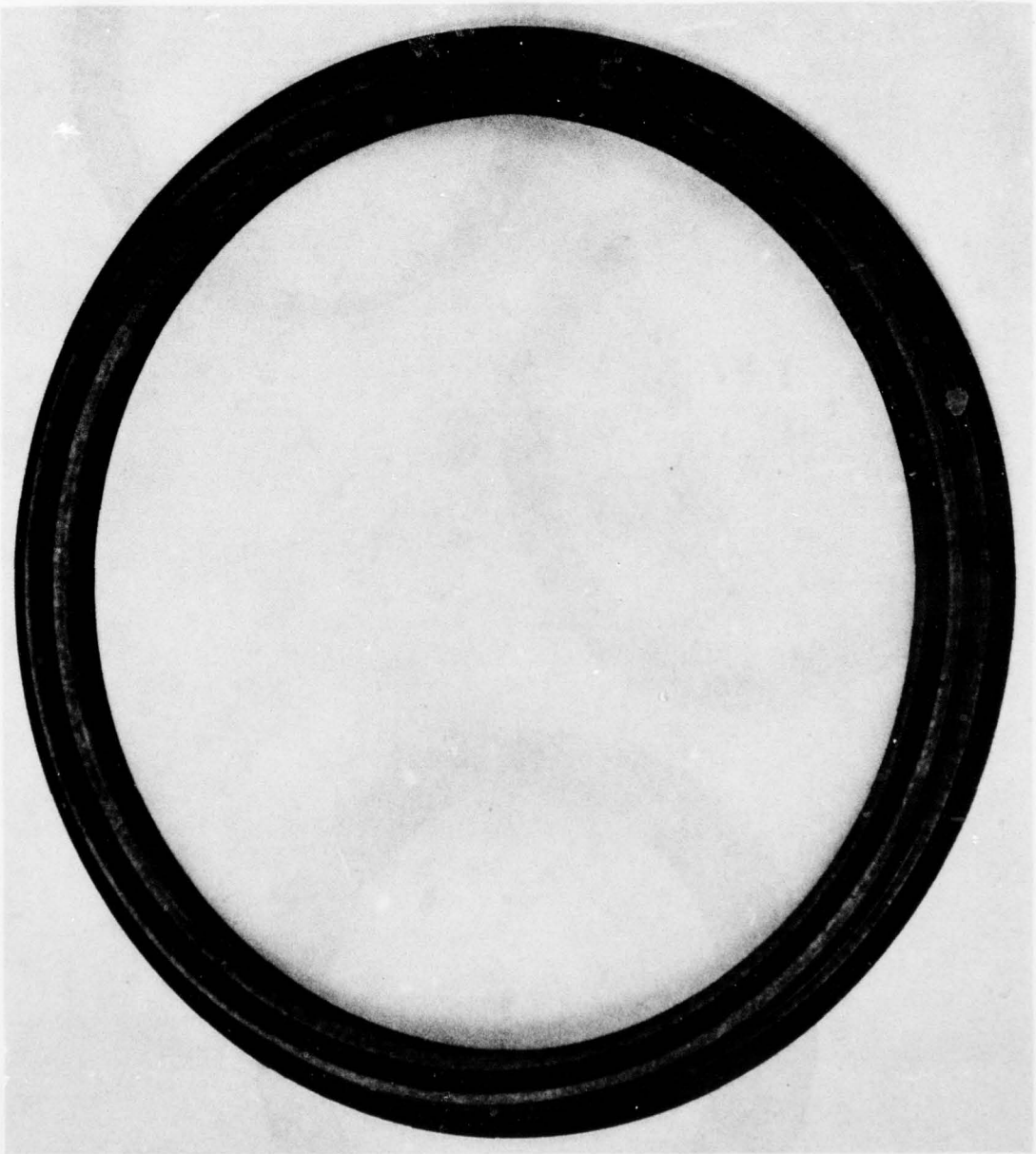

Figure 88. Lip Type Sealing Element After Testing

SECTION VIII

RECOMMENDATIONS

1. ACTUATOR

. Based on the problems encountered in the limited testing performed at room temperature only, it is recommended that the hold-in motor concept for maintaining the transmission gears in mesh during normal operation to provide automatic decoupling from the load with loss of supply pressure be reviewed and re-evaluated.

. Also it is recommended that alternative methods for effecting load decoupling be reviewed and evaluated. In addition, consideration should be given to determine the feasibility of relying on the redundant actuator(s) to back drive the failed unit and estimating the loading and reliability. The decrease in actuator weight and size effected by elimination of the hold-in motor (59% of total displacement) would aid significantly in weight reduction.

. It is also recommended that the hold-in motor concept be considered in view of the digital application of the Dynavector in which the self commutating feature of the typical analog configuration is replaced by a digitally controlled valve, or valves [8]. By using the external method of commutation, it would appear that the unfavorable torque characteristic

[8] Mayer, L.F.
An Electrohydraulic Stepper Actuator for Missile Applications
Report No. BASD-M 6561
Bendix Aerospace Systems Division, Bendix Corp.
October, 1976

as illustrated in the Appendix, Figure A-5, may be tolerated since the digital mode is point-to-point operation. The variation of torque between points would be manifested in varying acceleration, however, which may complicate control. Since an eight chamber digital Dynavector is sized to develop stall torque at 45 degrees (0.79 radius) displacement of the eccentricity, there is a horizontal vector of the hydraulic force that develops the required stall torque and an equal vertical vector that will tend to hold the gears in mesh. Therefore, with a penalty in size and weight the stall torque could be developed at an angle sufficiently less than the 45 degrees so that the vertical vector would be enough greater than the horizontal vector to assure the gears would be held in mesh by the hydraulic force. This would then allow the gears to be designed to decouple at a loss of pressure.

. It is also recommended that consideration be given to other design configurations to provide the cooling flow paths that would reduce actuator volume and weight. One configuration that is suggested would depend on eliminating the motor cartridge, as such, and instead, using two laminated housing-manifolds. These would be fabricated by brazing together a stack of machined plates containing a circuitous case drain flow path around the outer portion of the housing to remove the heat influx.

2. MOTOR CARTRIDGE

Although no data has been included in substantiation, it is recommended that the design of any new motor cartridge should strive to maximize the ratio of the lengths of the spacer bolts and the spacers, through which they pass (items 8 and 6, Figure 14, respectively). Accomplishment of this would stiffen the assembly and lessen the tendency of warping the manifolds (items 1 and 4) resulting in internal friction and variable running clearance

(leakage path). This can best be accomplished by integrating the manifolds into the housings as recommended in paragraph 8.1 ACTUATOR. Use of integrated manifolds would also eliminate the need for the small, low squeeze, metallic face seals (items 12, Figure 18) which could compromise actuator reliability.

3. SHAFT SEALS

On the basis of the high temperature testing of the seals at 600°F (316°C) fluid and 800°F (427°C) ambient air along with trouble-free service at room temperature in the prototype actuator, it is recommended that the lip type seal, with a material alloy of teflon and Ekonol, and the circumferential type seal, with polyimide resin sealing ring material be considered for other similar rotary, high temperature applications. This recommendation is mainly based on low torque loss and cost impact compared with the radial face type seal using pressure loaded bellows and metallic sealing surfaces. With the low shaft speeds (15 rpm maximum), typical of a flight control actuator, sealing surface velocities are insufficient to develop hydrodynamic lubrication and low torque loss. The high temperature performance of the radial face type was not any better, based on leakage data, than the less costly lip type seal.

4. STIFFNESS/WEIGHT

To obtain a better comparison of the weight and stiffness characteristics between the Dynavector and a Linear Actuator, the following is recommended:

. A design study should be conducted to determine the impact of incorporating servovalve and input/feedback mechanisms in the Dynavector. The study should include considerations for both state-of-the-art servoactuators and fly-by-wire servoactuators.

. A Dynavector installation study should be undertaken to determine realistic airframe weight savings to be attained. The study could be simplified and a more accurate comparison achieved if the installation selected is an existing one using a Linear Actuator. Furthermore, the selected installation should be one with stringent stiffness and weight requirements.

. Consideration should be given to dynamic stiffness testing of a Dynavector and Linear Actuator that were designed to the same requirements for a given installation.

SECTION IX

REFERENCES

1. Verge, K. W. et al
   Investigation of Rotary Actuator Techniques
   AFAPL-TR-70-52
   Bendix Research Laboratories, Bendix Corp.
   September, 1970

2. Van Ausdal, R. K.
   Seal Survey Report
   Report 7-3133
   Bendix Electrodynamics Division, Bendix Corp.
   July, 1972

3. Lee, J.
   Development of High Temperature Polyimide Rod Seals
   NASA CR-72563
   N70-10905
   Republic Aviation Division, Fairchild-Hiller
   August, 1969

4. Findlay, J.A. et al
   "Study of Dynamic and Static Seals for Liquid Rocket Engines", Seals Design Guide
   N70-26148
   Research and Development Center, General Electric Co.
   January, 1970

5. Povinelli, V. P. et al
   Development of Main Shaft Seals for Advanced Air Breathing Systems
   Report No. 3933
   N71-12035-039
   Pratt and Whitney Aircraft
   June, 1970

6. Bayer, P.
   Investigation of Leakage and Sealing Parameters
   AFRPL-TR-65-153
   AD 470462
   ITT Research Institute
   August, 1965

7. Lee, J.
High Temperature Hydraulic System Actuator Seals for Use in Advanced Supersonic Aircraft
NASA CR-72354
N69-22222
Republic Aviation Division, Fairchild-Hiller
September, 1967

8. Mayer, L. F.
An Electrohydraulic Stepper Actuator for Missile Applications
Report No. BASD-M 6561
Bendix Aerospace Systems Division, Bendix Corp.
October, 1976

APPENDIX

HIGH TEMPERATURE DYNAVECTOR®

TORQUE RIPPLE ANALYSIS

A 1.0 SUMMARY

The analysis presented herein shows the vector summation of the periodic (as a function of orbit velocity) oscillation of the hydraulic forces generated by the torque motor and hold-in motor causes a saw-tooth (assuming perfectly located, sharp-edged commutation ports) form of the output torque versus angular displacement relationship. The magnitude of the torque variation is 40 percent of the nominal maximum output torque when the hold-in motor inlet pressure (P_H) is the same value as system supply pressure. With the hold-in motor inlet pressure maintained at the same value as the higher pressure of the torque motor, the magnitude of the torque variation is reduced to approximately 40 percent of the load differential pressure required, i.e., it will vary theoretically from about 0 to 40 percent of maximum as the load varies from 0 to maximum.

A 2.0 CONCLUSION

The impact on output torque developed by the force output of the hold-in motor is considered excessive. When the hold-in motor inlet pressure is maintained at system supply pressure magnitude, the impact is such that a saw-tooth non-linearity is imposed on the torque (or torque motor differential pressure) versus load displacement characteristic curve with a magnitude of 40 percent of the maximum load (or maximum ΔP). Supplying the hold-in motor with the higher of the two torque motor chamber pressures, rather than the system supply pressure, will reduce the amplitude of the saw-tooth non-linearity to 40 percent of the load torque at any given point, rather than the maximum value, only.

A 3.0 ANALYSIS

Based on the Dynavector parameters shown in Table A-1, the considerations necessary to delineate the factors involved in the forces developed by the two motors and the impact on output torque are as follows:

From the free body diaphragm of the ring gear in Figure A-1, the summation of horizontal forces is zero for equilibrium, or

$$\Sigma F_{horizontal} = 0$$

specifically,

$$F_R \cos\phi - F_D \cos \beta = 0$$

So that $F_R \cos\phi P = F_D \cos \beta$ A-1

The output torque developed by the actuator is

$$T_o = F_R \cos\phi \, R_o \quad \text{lb-in} \qquad \text{A-2}$$

So by substituting (A-1) into (A-2)

$$T_o = F_D \cos\beta \, R_o \quad \text{lb-in} \qquad \text{A-3}$$

The force F_D is the resultant of the hydraulic force, F_M, developed by the torque motor and F_H developed by the hold-in motor.

F_M and F_H are summations of the forces developed by the individual chambers in each motor. These individual forces can be shown from Figure A2 to be,

$$F_{mi} = A_{mi} \, \Delta P_m \quad \text{lbs} \qquad \text{A-4}$$

and

$$A_{mi} = 2b \, R_v \sin \frac{\gamma_m}{2} \text{ in.}^2$$

so that (4) becomes

$$F_{mi} = 2bR_v \frac{\gamma_m}{2} \Delta P_m \quad \text{lbs} \qquad \text{A-5}$$

TABLE A-1

PARAMETER SYMBOLS AND VALUES

Symbol	Definition	Units	Value
A_{mi}	Cross sectional area of a torque motor chamber normal to the pressure differential	$in.^2$	
b	Width of a motor chamber parallel to the orbiting axis	in.	
e	Orbit eccentricity	in.	0.0625
F_D	Resultant developed force of F_M and F_H	lbs.	
F_H	Summation of hold-in motor chamber forces	lbs.	
F_{hi}	Individual hold-in motor chamber force	lbs.	
F_M	Summation of torque motor chamber forces	lbs.	
F_{mi}	Individual torque motor chamber force	lbs.	
F_R	Output gear pitch line reaction force	lbs.	
K	Maximum ratio of F_M to F_H	-	.69935
N	Number of chambers in each motor	-	11
R_o	One half of output gear pitch diameter	in.	2.6875
R_v	One half of the vanes sealing diameter	in.	
T_o	Actuator output torque	lb-in.	
α	Angle between application of F_M and F_H	deg.	
β	Angle between F_{MNOM} and F_D	deg.	
$\gamma_{m,h}$	Included angle of torque or hold-in motor chamber	deg.	
E	Difference between R_o and the radius of reaction pins pitch cycle radius	deg.	1.1250
Θ	Angular position of eccentricity	deg.	
ϕ_p	Gear pressure angle	deg.	25

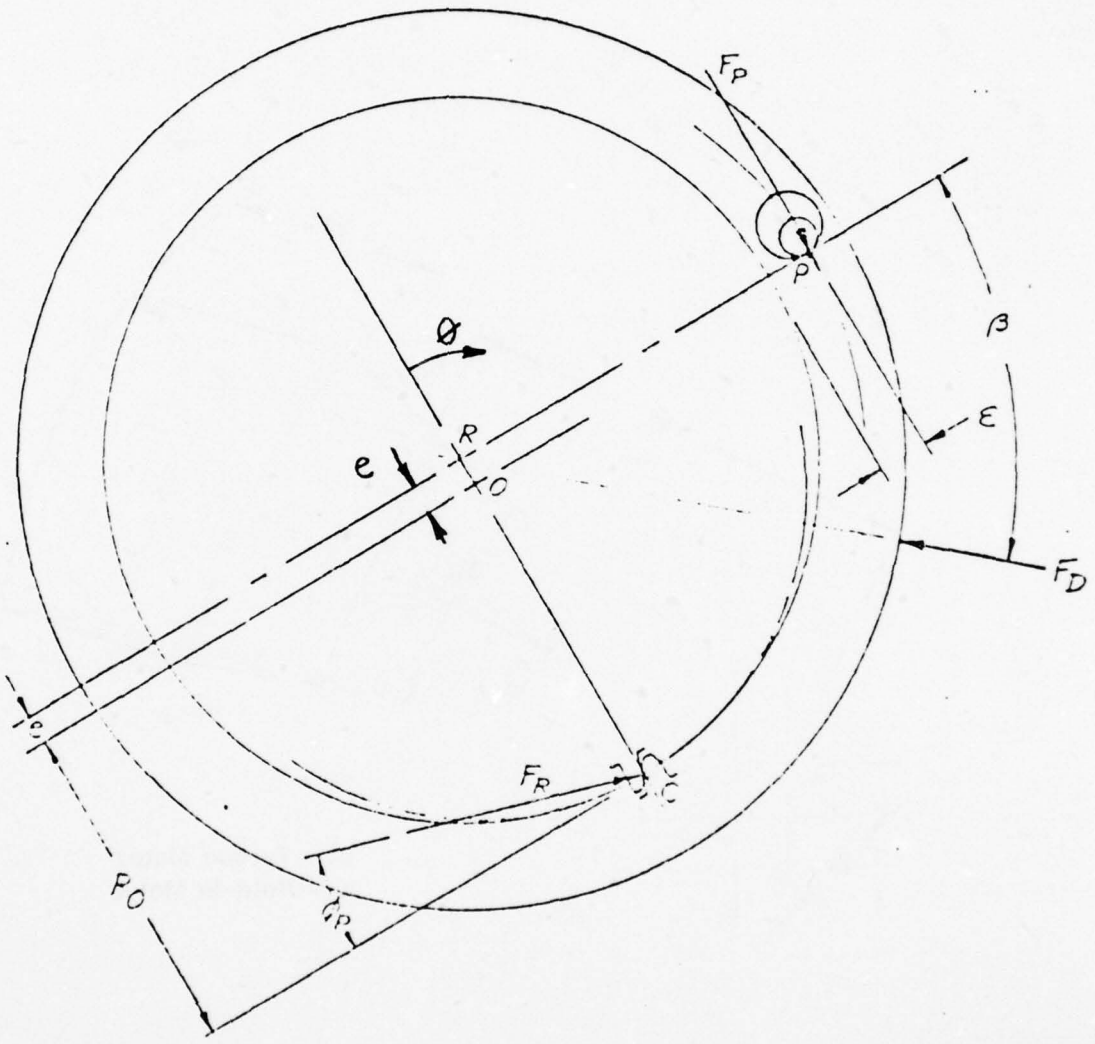

Figure A-1. Free-Body Diagram of Dynavector Ring Gear

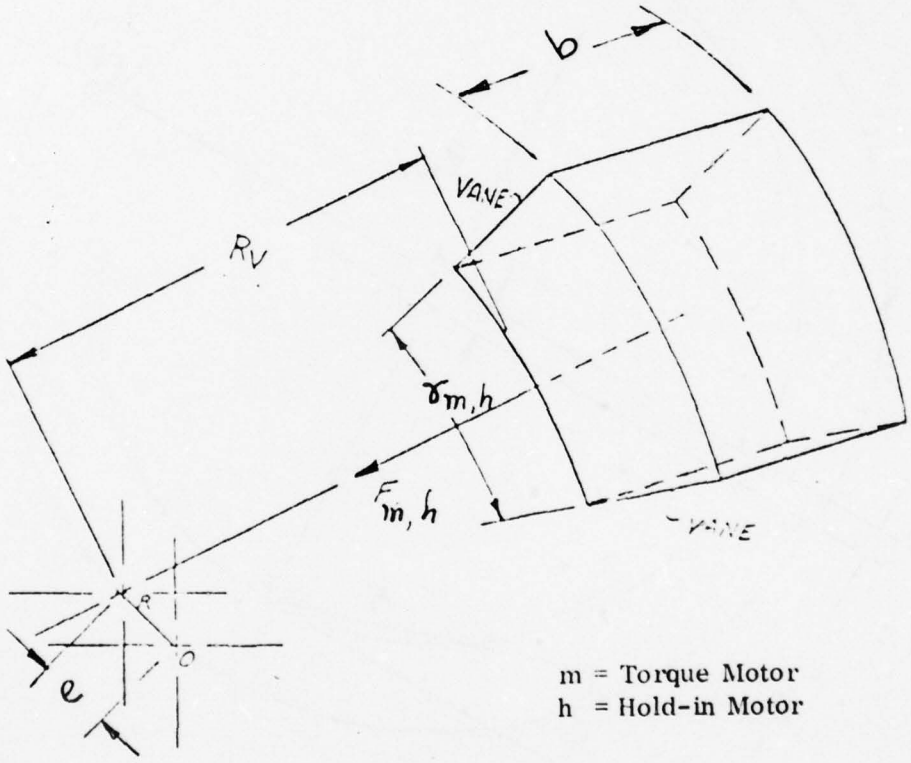

m = Torque Motor
h = Hold-in Motor

Figure A-2. Dynavector Actuator Chamber Geometry

AD-A057 931 BENDIX CORP NORTH HOLLYWOOD CALIF ELECTRODYNAMICS DIV F/G 13/7
DEVELOPMENT OF A HIGH TEMPERATURE ROTARY ACTUATOR FOR AIRCRAFT --ETC(U)
MAY 78 R K VAN AUSDAL F33615-72-C-1187

UNCLASSIFIED AFAPL-TR-78-26 NL

3 OF 3
ADA
057931

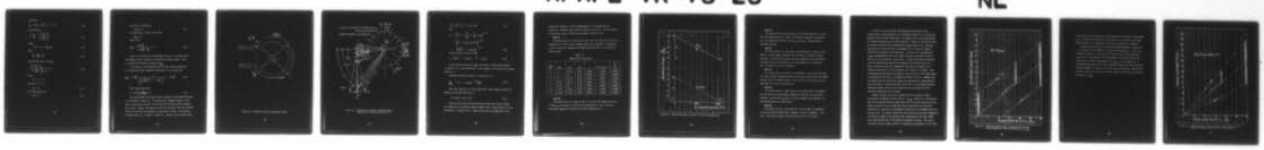

END
DATE
FILMED
10-78
DDC

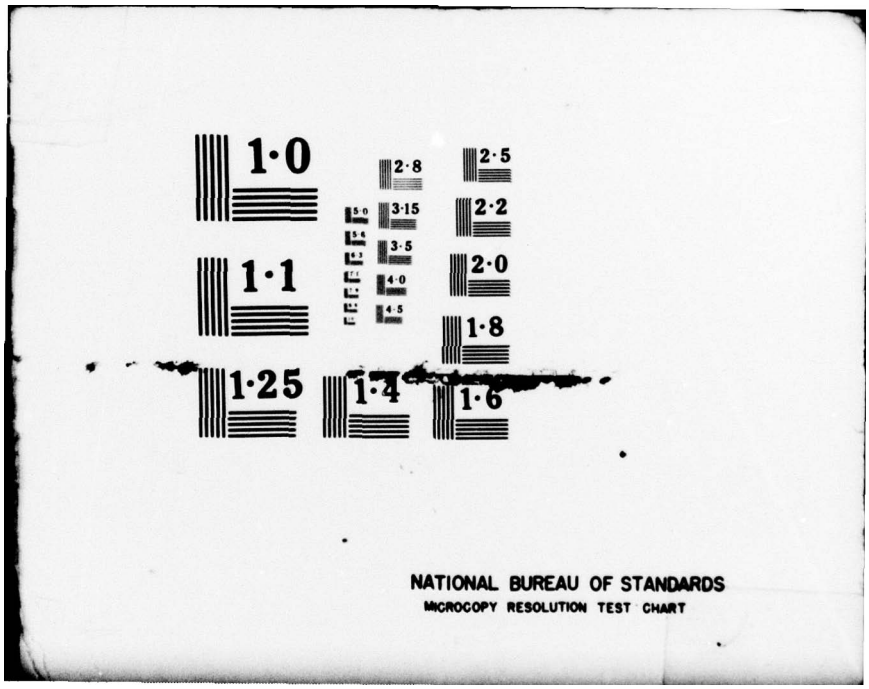
1·0
1·1
1·25
2·8
3·15
3·5
4·0
4·5
1·4
2·5
2·2
2·0
1·8
1·6
NATIONAL BUREAU OF STANDARDS
MICROCOPY RESOLUTION TEST CHART

Similarly,

$$F_{hi} = 2bR_v \sin \frac{\gamma_h}{2} \Delta P_h \quad \text{in.}^2 \qquad \text{A-6}$$

By definition,

$$K \overset{\Delta}{=} \frac{F_M}{F_H} = \frac{\sin \frac{\gamma_m}{2} \Delta P_m}{\sin \frac{\gamma_h}{2} \Delta P_h} \qquad \text{A-7}$$

since,

$$n (\gamma_m + \gamma_h) = 360 \text{ deg.} \qquad \text{A-8}$$

then,

$$\frac{\gamma_h}{2} = \frac{180}{n} - \frac{\gamma_m}{2} \qquad \text{A-9}$$

Substituting (A-9) into (A-8)

$$K = \frac{\sin \frac{\gamma_m}{2} \Delta P_m}{\sin \left(\frac{180}{n} - \frac{\gamma_m}{2}\right) \Delta P_h} \qquad \text{A-10}$$

Since,

$$\Delta P_h = P_s - P_c$$

then with $P_c \lll P_s$

$$\Delta P_h \simeq P_S \qquad \text{A-11}$$

At no-load conditions,

$$\Delta P_{im} \simeq 0 \qquad \text{A-12}$$

and at stall conditions,

$$\Delta P_{in} \simeq P_s \qquad \text{A-13}$$

So from (A-10) - (A-13), at no load

$$K_{min} \simeq 0$$

and at stall

$$K_{MAX} = \frac{\sin \frac{\gamma_m}{2}}{\sin \frac{180}{n} - \frac{\gamma_m}{2}} \qquad \text{A-14}$$

Since, K is the ratio of the two motor forces, it is obvious that the maximum value is necessary to maximize the torque output. Thus, γ_m in design of the motor is based on K_{MAX}.

In an analysis of the required hold-in motor sizing conducted by W. D. MacLennan, Bendix Research Laboratories, it was shown that

$$K_{MAX} = \cos \frac{90}{n} \frac{1}{\left(\frac{R_o + e}{R_o + e + \varepsilon} + \tan\phi_p \right)} - \sin \frac{90}{n} \qquad \text{A-15}$$

Also it was shown that,

$$\beta = \tan^{-1}\left(\frac{\sin\alpha}{K - \cos\alpha} \right) \qquad \text{A-16}$$

The relationship of the motor forces is based on the design philosophy as illustrated in Figure A-3. The torque motor chambers produce a force that is applied over one half of the rotor and the hold-in motor chambers do the same. However, the porting is such for each motor that the resultant forces are nominally at 90 degrees to each other as shown. The resultant of these forces, F_D, is shown in Figure A-4. Based on the triangles shown,

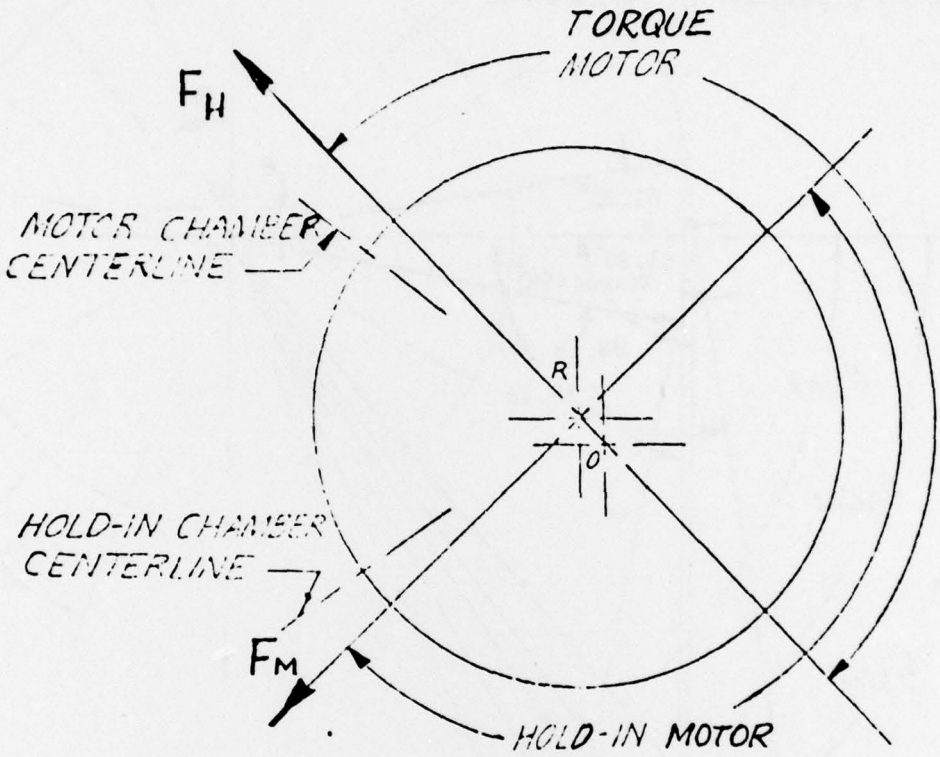

Figure A-3. Dynavector Actuator Commutation Sector

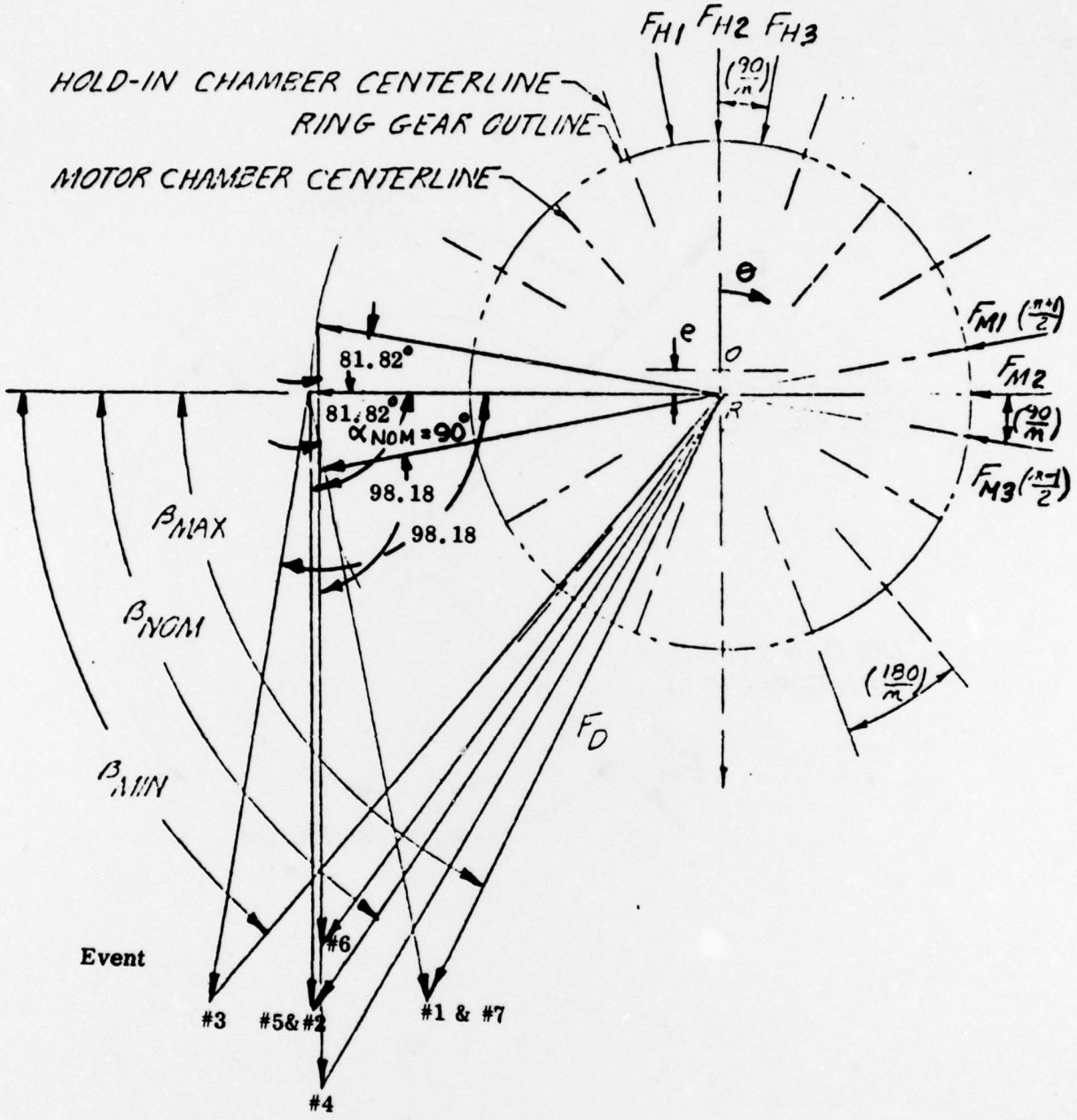

Figure A-4. Orientation of Hold-in and Motor Forces Relative to a Fixed Eccentricity Axis

$$F_D^2 = F_M^2 + F_H^2 - 2 F_m F_H \cos\alpha \qquad \text{A-17}$$

and

$$F_D = \left[F_M^2 \left(1 + \frac{F_H^2}{F_M^2} - 2\frac{F_H}{F_M}\cos\alpha\right)\right]^{1/2}$$

$$= \left[F_M^2 \left(1 + \frac{1}{K^2} - \frac{2}{K}\cos\alpha\right)\right]^{1/2}$$

$$= \frac{F_M}{K}\left[(K^2 + 1 - 2K\cos\alpha)\right]^{1/2} \qquad \text{A-18}$$

Therefore from (A-3) and (A-18)

$$T_o = \frac{F_M}{K}(K^2 + 1 - 2K\cos\alpha)^{1/2} \cos\beta\, R_o \qquad \text{A-19}$$

By dividing the equation by $F_M R_o$ the torque is normalized, because K is constant for a given design and α and β depend on the eccentricity angular position, θ.

Therefore normalized torque as a function of θ is.

$$\frac{T_o}{F_M R_o} = (K^2 + 1 - 2K\cos\alpha)^{1/2} \frac{\cos\beta}{K} \qquad \text{A-20}$$

Also from Figure A-3, it can be seen that α varies about a nominal 90 degrees by plus and minus 90/n, or

$$= 90 \pm 90/n = 90\left(1 \pm \frac{1}{n}\right) \qquad \text{A-21}$$

Table A-2 and Figure A-5 show the torque ripple that occurs through the commutation of the hold-in motor chambers over a limited range of θ, but nonetheless, a complete cycle. Ripple resulting from commutation of the

torque motor chambers is not included because it is insignificant by comparison. Parameter values used are listed in Table A-1. The significance of the events listed in Table A-2 and noted in Figure A-5 are:

Event #1

This event occurs at Θ very close to but less than zero, or just prior to commutation of a hold-in motor chamber from P_H to P_C pressure. Consequently F_{H1} has a horizontal component that opposes F_M and results in a diminished output torque.

TABLE A-2

TORQUE RIPPLE CALCULATION

Event No.	Θ deg	α deg	β deg	K	$K^2+1-2K\cos\alpha$	$\frac{T_o}{F_M R_o}$
1	0^-	81.82	60.63	.69935	1.13582	0.79654
2	0	90	55.03	.69935	1.22028	1.00000
3	0^+	98.18	49.63	.69935	1.29927	1.20345
4	8.18^-	98.18	57.81	.69935	1.29927	1.0094
5	8.18	90	55.03	.69935	1.22028	1.00000
6	8.18^+	81.82	52.45	.69935	1.13582	0.98988
7	16.36^-	81.82	60.63	.69935	1.13582	0.79654

Event #2

This event occurs at Θ equal to zero, or just at the commutation point, so that F_{H2} is directly in line with the eccentricity. Thus, F_{H2} has no horizontal component to diminish the torque produced by F_M.

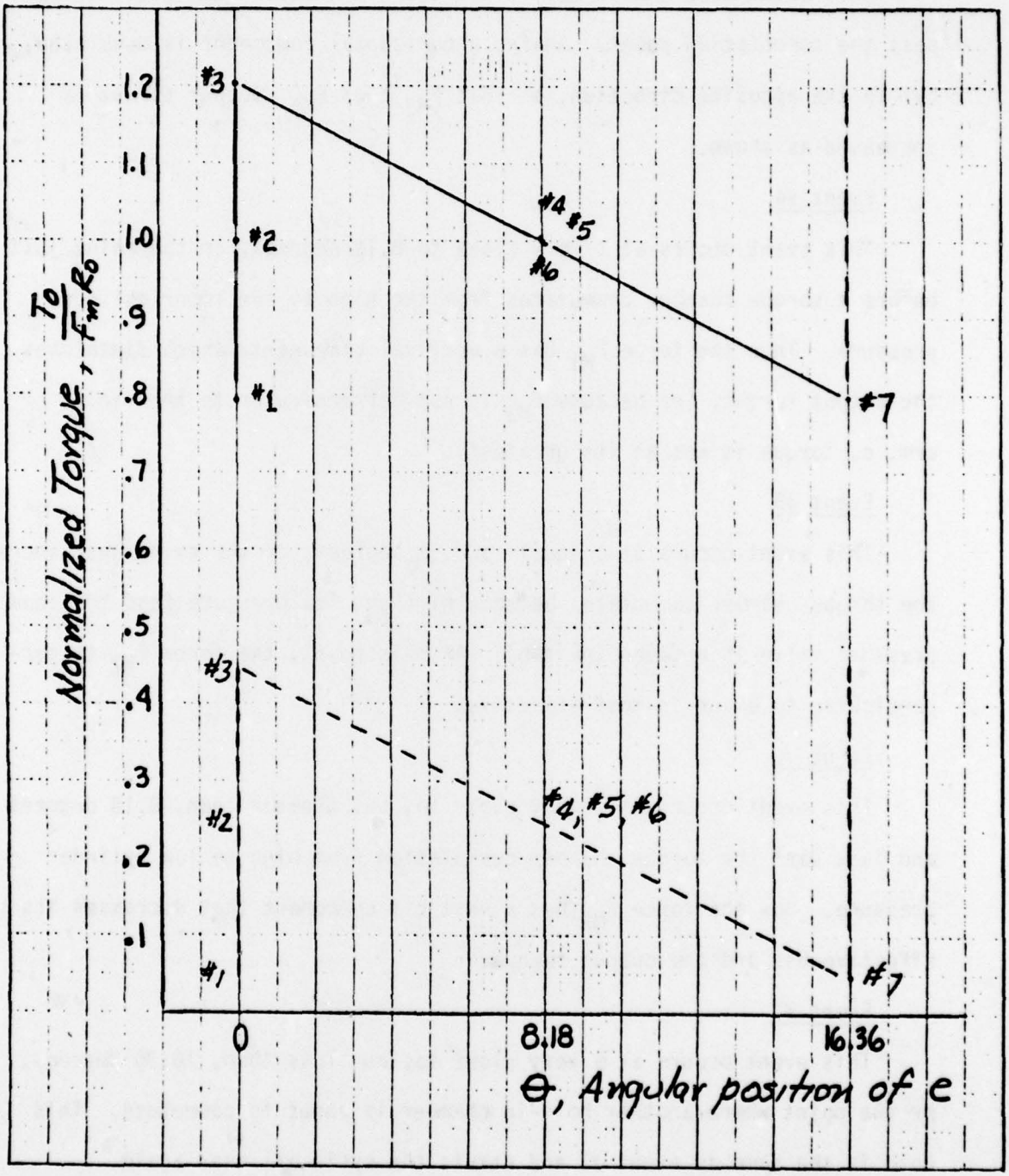

Figure A-5. Normalized Torque vs Angular Position of Eccentricity

Event #3

This event occurs at Θ very close to, but greater than zero, or just past the commutation point. Again, a horizontal component is developed, but in the opposite direction, so that F_{H3} aids F_M. Output torque is increased as shown.

Event #4

This event occurs at Θ very close to 8.18 degrees, or the point just before a torque chamber commutates from the high to the lower cylinder pressure. Thus the force F_{M1} has a vertical component, which diminishes the output torque, (or because F_{M1} is not perpendicular to the radius arm, e, torque is not at its greatest).

Event #5

This event occurs at Θ equal to 8.18 degrees, or the point just where the torque chamber commutates between high and low pressure (and the chamber pressure valve is between the two). At this point, the force F_{M2} is perpendicular to e and is most effective.

Event #6

This event occurs at Θ very close to, but greater than, 8.18 degrees and just past the torque chamber commutation from high to low cylinder pressure. Now the force F_{M3} has a vertical component that decreases its effectiveness and the output torque.

Event #7

This event occurs at Θ very close to, but less than, 16.36 degrees, or the point where another hold-in chamber is about to commutate. This case is the same as event #1 and starts the cycle all over again.

From A-5 it can be seen that the normalized torque varies from a minimum value of approximately 0.8 to a maximum of about 1.2, or ±20 percent, because of hold-in motor commutation. The impact of this can be appreciated by considering operation at no-load conditions. Except for internal friction, the actuator would not have to develop any output torque to run. Assuming approximately 5 percent friction, the dashed cycle in Figure A-5 depicts how events #1 through #7 would take place. As long as P_H is maintained at $P_{S\ MAX}$, the magnitude of the cycle remains the same, but events #1 and #7 drop to the 0.05 normalized torque level, since friction must be overcome. Since the minimum torque required to overcome friction must be met, the excess torque occurring after commutation from event #1 through 2 to #3 produces acceleration of the moving parts until event #7 is reached. Then, the cogging type operation occurs again as long as the ΔP on the torque motor is maintained at the level to overcome the internal friction. Remember that the cogging type action would not appear very noticeable on output position, since the angle θ is ahead of the gear ratio (43:1) so the apparent angular difference between events #1 and #7 would be only 0.38 degrees and the pulsating speed would also be slight.

However, consider the case for operation with an angularly linear spring load, no internal friction, and $P_H = P_{S\ MAX}$, Figure A-6. For displacement with increasing load the torque would have to increase from zero at zero degrees position up to 0.4 normalized torque during which the unit would accelerate to a position of 0.38 degrees (16.36/43) with the minimum torque on the load line. To displace farther the torque would increase after commutation of the hold-in motor to the maximum value, represented by the upper dashed line, then decrease until 0.76 degrees displacement occurred. This cyclic action will occur as long as the ΔP is increased up to maximum, or stall load.

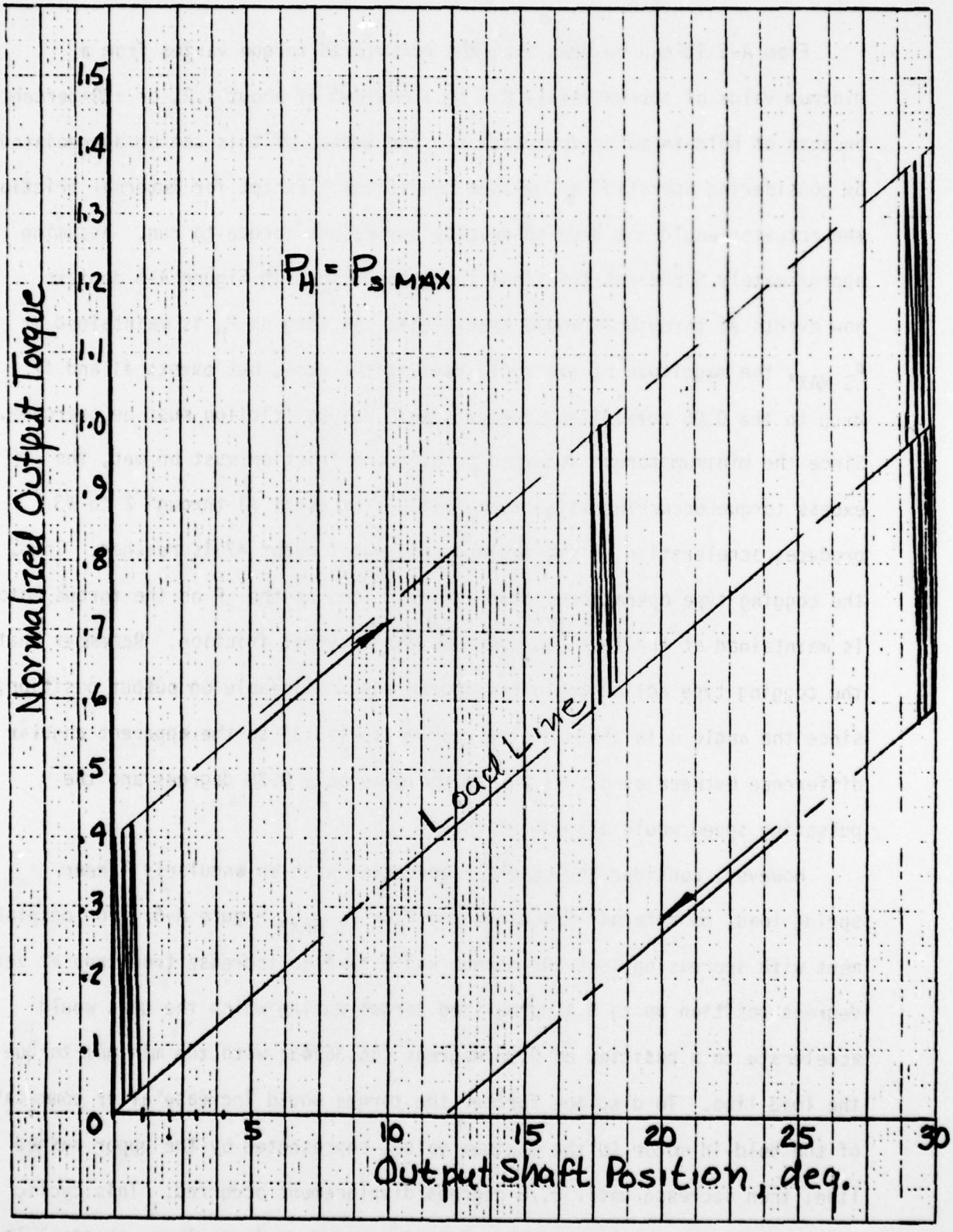

Figure A-6. Normalized Output Torque vs Output Shaft Position with an Angularly Linear Spring Load, $P_H = P_{S\ MAX}$

On decreasing ΔP the torque must be decreased until the maximum instantaneous value is just below the load line, then the cyclic action will occur downward as long as ΔP is decreased, until the zero load point is reached.

Instead of connecting P_H to the constant supply pressure, assume that it is connected to the higher of the two cylinder pressures. In this case, as shown by Figure A-7, the same cyclic action occurs but the amplitude in each case is ±20 percent of the instantaneous ΔP required by the load rather than a constant percentage of the $P_{S\ MAX}$. At low speeds the ΔP is approximately equal to the higher cylinder pressure minus the case drain pressure assumed for Figure A-7. By letting P_H vary with the required load, the unit is better at all loads less than maximum, than when P_H is constant and equal to $P_{S\ MAX}$.

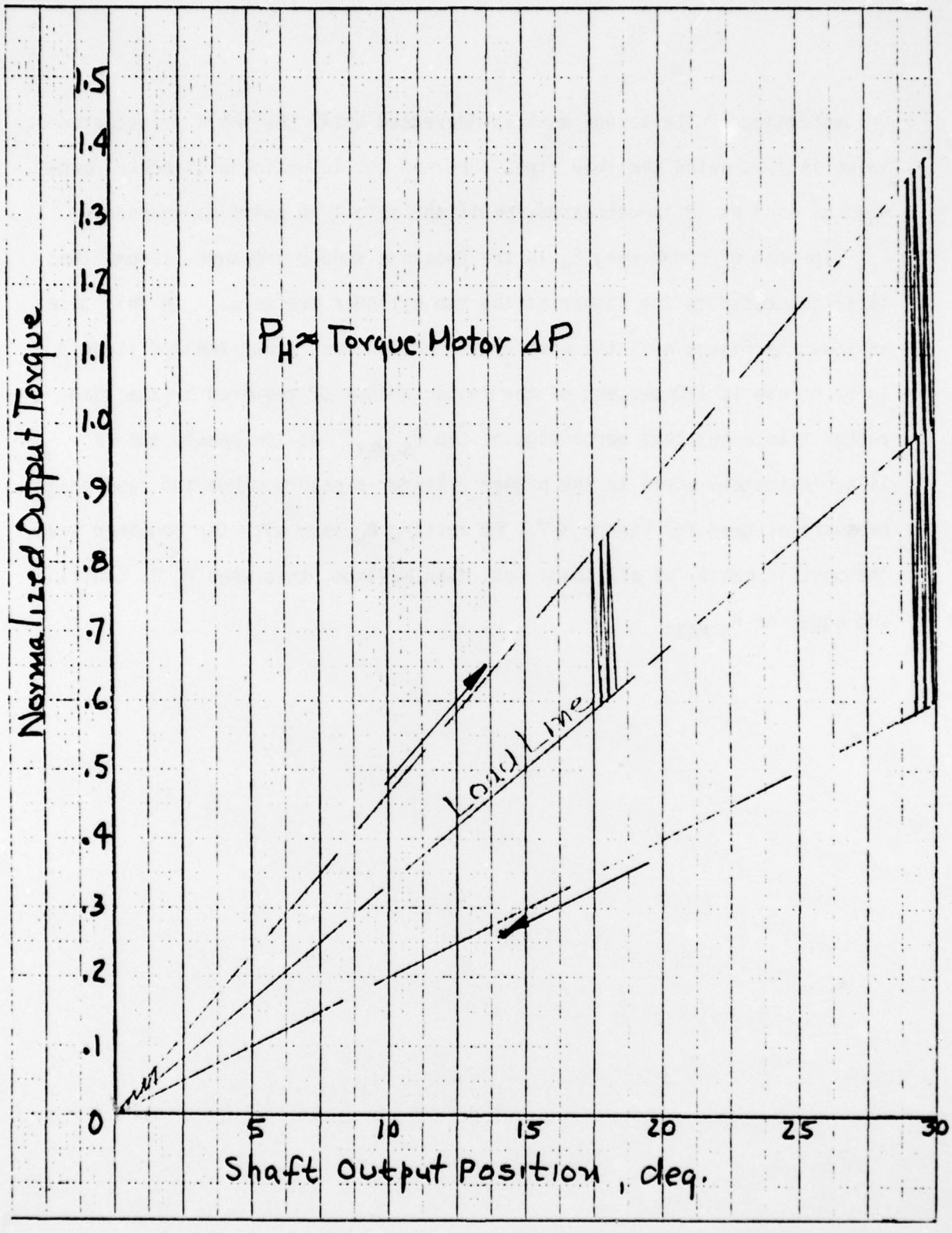

Figure A-7. Normalized Output Torque vs Output Shaft Position with an Angularly Linear Spring Load, P_H = Torque Motor ΔP